The mineralogy and geochemistry of Ni-Cu-PGE sulfide ores and associated biotite from the Totten #2 mine, Worthington offset, Sudbury Igneous Complex, Canada.

by

Michael Roy Warren

A thesis submitted to Saint Mary's University, Halifax, Nova Scotia in partial fulfillment of the requirements for the degree of Master of Science in Applied Science

August 21, 2013, Halifax, Nova Scotia

Approved: Dr. Jacob Hanley
Supervisor
Department of Geology
Saint Mary's University

Approved: Dr. Victor Owen
Supervisory Committee
Department of Geology
Saint Mary's University

Approved: Dr. Doreen Ames
Supervisory Committee
Geological Survey of Canada

Approved: Dr. Sarah Dare
Supervisory Committee
Université du Québec à Chicoutimi

Approved: Dr. Kevin Vessey
Faculty of Graduate Studies Representative
Saint Mary's University

Abstract

The mineralogy and geochemistry of Ni-Cu-PGE sulfide ores and associated biotite from the Totten #2 mine, Worthington offset, Sudbury Igneous Complex, Canada.

The Sudbury Igneous Complex (SIC), Canada, contains a variety of sulfide ore deposits that represent a significant resource of nickel, copper, and platinum-group elements (PGE). Deposits hosted within the quartz diorite offsets are of distinct economic interest owing to their elevated base metal and PGE contents, therefore the detailed characterization of both mineralogical and geochemical features of these deposits is crucial to the exploration, and development of Sudbury ore. The Totten #2 mine located within the Worthington offset was studied in order to: (i) characterize the major/accessory minerals and paragenesis within the sulfide ores; (ii) identify the specific mineralogical domains of the chalcophile metals and their distribution; and (iii) investigate the potential of biotite chemistry as a pathfinder for Ni-Cu-PGE deposits. Key findings are presented and discussed with respect to their applications to exploration, ore processing, and our understanding of mafic to ultra-mafic Ni-Cu-PGE deposits.

August 21, 2013

Acknowledgments

Financial support for this thesis was provided by Vale and the Geological Survey of Canada. Invaluable advice and assistance throughout this project was given by Vale staff in Sudbury: Chris Davis, John Townend, Lance Howland, Caitlin Blackadder, Enrick Tremblay, Clarence Pickett, Sherri Digout, and Breanne Pilon. I would also like to thank Simon Jackson (Geological Survey of Canada), and Xiang Yang (Saint Mary's University) whose technical expertise was instrumental to the success of this research.

This project benifited from the knowledge and direction of my supervisor, Jacob Hanley (Saint Mary's University); other thesis committee members: Victor Owen (Saint Mary's University), Doreen Ames (Geological Survey of Canada), Sarah Dare (Université du Québec à Chicoutimi); the staff of the Department of Geology, Saint Mary's University; and the support of my fellow graduate students.

Special thanks go to those who helped keep me balanced on that fine line between sanity and madness that is trekked by all researchers: Jacob Hanley, Heather Bennett, and Nathaniel MacDonald.

Lastly, I would like to thank my parents: Shelia and Keith, and my sister Rachel for all their love and support throughout the years.

Table of Contents

List of Figures

Chapter 2

Chapter 3

List of Tables

Chapter 2

Chapter 3

Chapter 1: Introduction

1.0 Structure of the thesis

This thesis is comprised of two main studies. The first study, found in Chapter 2, involves a detailed petrographic and geochemical investigation of the Ni-Cu-platinum-group element (PGE; Pt, Pd, Ir, Rh, Ru, Os) ores of the Totten #2 mine, with particular attention given to the distribution of metals between major, and acessory phases in the ore assemblage. Chapter 3 investigates changes in biotite chemistry as a function of distance to ore and host rock lithology at the Totten #2 mine. Both of these chapters have been written in the form of separate manuscripts, for the purpose of submission to Economic Geology. As a result, there is a degree of repetition with respect to certain mutual themes (e.g. geological setting, analytical methods). Chapter 4 highlights the key finding of Chapters 2-3, discussing their potential applications to exploration and ore processing, and summarizes future work to address unresolved questions from these studies.

2.0 Primary objective of the thesis

The primary objective of this thesis was to investigate the mineralogical domains for both the economic (e.g., Ni, Cu, PGE) and deleterious (metals which are problematic for ore processing, reducing the economic value of ore; e.g. As, Te, Bi, Pb) metals within the Totten #2 mine, Worthington offset, Sudbury, Ontario. Major and accessory mineral chemistry, spatial distribution, and textural relationships were studied in detail in order to quantify mineralogical domains controlling metal distribution. This study reveals key mineralogical characteristics which enhance our understanding of the genesis of the offset ores, and are also pertinent to mineral processing. This section of the thesis was funded by Vale (Sudbury Operations division) for the purpose of augmenting the development of

the relatively new Totten #2 mine, through the identification of geological indicators which could assist with the recognition of both economic and problematic areas of ore through the study of: (i) drill core, or underground exposures, and (ii) geochemical data, such as bulk rock assays. Similar studies have been done elsewhere within the Sudbury Igneous Complex (e.g. Kelly Lake, Huminicki et al., 2005; Creighton, Dare et al., 2010; and Garson, LeFort, 2012); however this is the first study of its kind to detail the accessory phase mineralogy and chemistry within the Totten ores.

3.0 Secondary objective of the thesis

The secondary objective of this thesis was to investigate the potential of using biotite chemistry as a vector for magmatic Ni-Cu (PGE) deposits, by studying biotite within the Worthington offset dyke and the surrounding Huronian country rocks in the vicinity of the Totten mine. In addition to evaluating biotite chemistry as an exploration tool, this study highlights issues which must be addressed in order to properly implement this exploration technique. This second study was funded by the Geological Survey of Canada (TGI-4 initiative).

4.0 List of abbreviations

The following is a list of abbreviations which are used throughout this thesis:

AAS: atomic absorption spectroscopy
Ag-Pn: argentopentlandite
Alt: altaite
BSE: backscattered electron
CGSS: cobaltite-gersdorffite solid solution series
Cp: chalcopyrite
DISS: disseminated sulfides (blebby, ragged, stringers)
EDS: energy dispersive spectroscopy
El: electrum
EMP: electron microprobe
Frd: froodite

Gn: galena
Hes: hessite
Hol: hollingworthite
ICP-AES: inductively coupled plasma atomic emission spectroscopy
INMS: semi-massive sulfides/inclusion-bearing massive sulfides
IPGE: iridium-group platinum-group elements
IQD: inclusion-rich quartz diorite
Ir: irarsite
ISS: intermediate sulfide solid solution
LA-ICP-MS: laser-ablation inductively coupled plasma mass spectroscopy
MASU: massive sulfides
Mch: michenerite
MLA: mineral liberation analysis
Mo: molybdenite
MSS: monosulfide solid solution
Nic: nickeline
PPL: plane polarized light
PGE: platinum-group elements
PGM: platinum-group minerals
Pn: pentlandite
PPGE: platinum-group platinum-group elements
Po: pyrrhotite
QD: quartz diorite
SEDEX: sedimentary exhalative deposit
SEM: scanning electron microscope
Sg: silicate gangue
SIC: Sudbury Igneous Complex
Sph: sphalerite
Spr: sperrylite
SDD: silicon drift detector
Tel: tellurobismuthite
Tsu: tsumoite
Ung: ungavaite
VMS: volcanogenic massive sulfide deposit
WDS: wavelength dispersive spectroscopy
XRF: X-ray fluorescence

Chapter 2: The mineralogy and distribution of precious, accessory, and deleterious metals from the Totten #2 Ni-Cu-PGE ores, Worthington offset, Sudbury, Canada

Michael R. Warren*[1], Jacob J. Hanley[1], Simon E. Jackson[2], Chris Davis[3], and John Townend[3]

[1]Department of Geology, Saint Mary's University, Halifax, Nova Scotia, Canada

[2]Geological Survey of Canada, Ottawa, Ontario, Canada

[3]Vale, Ontario operations, Sudbury, Canada

*corresponding author email address: michael.warren90@gmail.com

Number of Pages: 134

Number of Figures: 23

Number of Tables: 17

1.0 Abstract

The Ni-Cu-platinum-group element (PGE) sulfide deposits hosted within the quartz diorite offset dykes of the Sudbury Igneous Complex (SIC), are significantly enriched in base and precious metal compared to other SIC deposit types (which are usually enriched in either base metals or PGE), and represents an important resource of those metals. Offset deposits are highly complex owing to (i) their emplacement in, and assimilation of, a variety of country rocks; (ii) significant textural and compositional variability arising from their dynamic emplacement and in-situ fractional/equilibrium crystallization of sulfide melts; and (iii) syn- to post-magmatic modification of the sulfide ores by a series of hydrothermal and metamorphic events. Therefore the detailed characterization of offset deposits is critical to our understanding of the ore-forming processes at Sudbury, as well as to the ongoing exploration and production of Sudbury Ni-Cu-PGE deposits. The Totten #2 mine, is a typical South Range offset deposit, and is one of the largest sulfide occurences in the Worthington offset. Despite this, a comprehensive study of the major and accessory ore mineralogy has not yet been done. The goals of this study were to: (i) identify and describe the spatial distribution of mineralogical domains of the chalcophile elements (e.g. Ni, Pb, As, Co, PGE), using quantified mass balances; (ii) generate a comprehensive mineralogical model to describe the genesis of the Totten ores using detailed petrography and mineral chemistry (obtained using SEM-EDS, and LA-ICP-MS); and (iii) identify and describe mineralogical indicators that can be used by mine geologists to preform more rapid grade assesments either underground, or in the core lab.

In order of decreasing abundance, the major base metal sulfides at Totten are pyrrhotite (FeS), pentlandite [$(Fe,Ni)_9S_8$], and chalcopyrite ($CuFeS_2$). LA-ICP-MS show

enrichments of Ni in pyrrhotite (6530 ppm average), Co and Pd in pentlandite (8839 ppm average, and 1.26 ppm average respectively), as well as Zn and Cd in chalcophyrite (353 ppm, and 23 ppm average respectively). Mass balances confirm that pyrrhotite is a significant carrier of Ni (~10% of the bulk Ni content of the ores), but that pentlandite does not contribute significantly to bulk rock Pd (which is controlled by discrete accessory phases). The base metal sulfides are consistently depleted in deleterious (e.g. As, Pb, Bi, Te, Hg) and precious metals (e.g. Au, Ag, PGE, with the exception of Pd in pentlandite), indicating that they do not contribute significantly to the bulk rock concentrations of these elements.

The main As-carriers identified (by means of quantified mass balance) at Totten are nickeline (NiAs), and cobaltite-gersdorffite-glaucodot solid solution [(Co,Ni,Fe)AsS]. Nickeline is uncommon in massive (≥ 80% sulfides by volume) and semi-massive sulfide ores (50-80% sulfides by volume), but may occur as anhedral-euhedral grains hosted in the base metal sulfides. Nickeline is much more common in disseminated (<50% sulfides by volume, associated with the margins of sulfide ore bodies and surrounding sulfide "halos") ore types, and occurs as anhedral blebs which may be concentrated in As-rich veins or along the contact of silicates and base metal sulfides. Nickeline contains significant Co and Au (899 ppm average and 5.9 ppm average respectively). The cobaltite-gersdorffite-glaucodot solid solution varies in composition from $[(Ni_{0.76}Co_{0.14}Fe_{0.11})_{\Sigma 1.00}As_{0.99}S_{1.01}$-$(Ni_{0.17}Co_{0.68}Fe_{0.15})_{\Sigma 1.00}As_{0.88}S_{1.12}$, likely representing the range of temperatures over which these sulfarsenides equilibrated (300-600°C). Like nickeline, the sulfarsenides are more abundant in disseminated ore types, but occur as small (10-50μm) subhedral-euhedral crystals hosted in pyrrhotite and pentlandite in

massive sulfides. These grains may contain cores of irarsite-hollingworthite [(Ir,Ru,Rh,Pt)AsS-(Rh,Pt,Pd)AsS], which have been shown by experimental work to be stable above the liquidus of the monosulfide solid solution (the precursor to pyrrhotite and pentlandite, liquidus temperature ~1120°C). Sulfarsenides are enriched in Pd and and Sb (752 ppm average and 1070 ppm average respectively), and are important to the distribution of those metals due to both dissolved concentrations and close spatial association with discrete Pd- Sb-carriers. Two models have been proposed for the origin of the sulfarsenides: (i) precipitation from late hydrothermal and metamorphic fluids enriched in chalcophile elements derived from the magmatic sulfide ores, and (ii) early magmatic crystallization from a chalcophile-rich sulfide melt. This study supports the second model based on the following evidence: (i) euhedral crystals fully enclosed by magmatic sulfides, (ii) the enriched precious metal concentration in sulfarsenides and arsenides relative to the base metal sulfides, and (iii) the occurrence of high temperature platinum-group minerals (PGM) at the core of sulfarsenide grains. This study also proposes that these early arsenides and sulfarsenides were concentrated along the margins of the Totten #2 ore bodies through gravitational setteling, which is supported by an increase in both grain size and abundance in these environments. This relationship can also be seen in handsamples and underground by the occurrence of annabergite [$Ni_3(AsO_4)_2.8H_2O$, “nickel bloom"] along the margins of sulfide mineralization.

Quantified mass balance calculations indicate that PGM, rather than base metal sulfides, arsenides, and sulfarsenides are responsible for the distribution of PGE at Totten. Platinum group minerals found at Totten include sperrylite ($PtAs_2$), froodite ($PdBi_2$), palladian michenerite (PdBiTe), ungavaite (Pd_4Sb_3), and irarsite-hollingworthite

(see above). Sperrylite occurs most commonly in massive and semi-massive ores, forming subhedral-anhedral inclusions in pyrrhotite and pentlandite. Therefore, the early magmatic crystallization of sperrylite is proposed to explain the Pt-poor base metal sulfides (this is supported by experimental work which shows sperrylite is stable at temperatures as high as 1400°C). Palladium carriers occur most commonly in disseminated sulfides, principally as anhedral inclusions along silicate-sulfide grain boundaries. The origin of these minerals is less clear, possibly crystallizing from: (i) a late semi-metal enriched residual melt, and/or (ii) late hydrothermal and metamorphic fluids which may have remobilized Pd.

Other accessory phases found at Totten include: galena (Pbs), altaite (PbTe), hessite (Ag_2Te), hedleyite (Bi_7Te_3), pilsenite (Bi_4Te_3), tellurobismuthite (Bi_2Te_3), tsumoite (BiTe), molybdenite (MoS_2), and electrum (Au,Ag). The origin of these phases is ambiguous and may have occurred under the same conditions as the Pd-carriers (with the exception of molybdenite, which may have crystallized as an early magmatic phase).

Binary plots of Co/Ni ratio *versus* As using the Totten and Garson (contact-style deposit) assay databases, reconciled with quantified mass balances show four major trends: i) Co/Ni ratios > 0.06 and As < 0.1wt%, occur when nickeline and sulfarsenide abundances are low (less than 0.3% by volume) and pentlandite controls the distribution of Ni-Co; (ii) Co/Ni ratios > 0.06, and the As > 0.1wt%, results from sulfarsenides controlling the distribution of As, Co, and Ni; (iii) Co/Ni ratios < 0.06, and elevated As concentrations (> 0.1 wt%), occur when nickeline is the dominant carrier of As; and (iv) Co/Ni ratios < 0.06 and low As concentrations (< 0.1 wt%) occur when As is controlled by sperrylite and irarsite-hollingworthite. Similarlly, binary plots of Pd and Pt can be

used to determine the relative abundance of PGM. Samples skewed towards either Pt or Pd indicate that the PGM associated with those metals are dominant, while positive correlations between Pt and Pd occur as a result of the spatial distribution of the PGM (similar hosts).

2.0 Introduction

2.1 Purpose of Study

Mafic-ultramafic magmatic Ni-Cu-PGE sulfide deposits often demonstrate highly complex and variable precious and accessory mineral assemblages on a variety of scales, despite having common and monotonous major base metal sulfide assemblages. The composition, abundance and complexity of accessory mineral assemblages may be partly the result of factors which influence the primary composition of sulfide liquid and sulfide mineral assemblages (i.e., parental silicate magma composition, the efficiency of silicate-sulfide melt interaction, fractional vs. equilibrium crystallization, simple down-temperature cooling/annealing), but are also largely influenced by thermal and chemical interaction with country rocks that can result in extensive contamination and highly variable compositional-textural domains within the ores (Lightfoot et al., 1993; Lesher and Arndt, 1995; Mukasa et al., 1998; Seabrook et al., 2004; Hanley, 2007; Houlé et al., 2012), and post-magmatic processes that modify ore compositions (e.g., hydrothermal alteration involving both magmatic and externally derived volatiles, and metamorphism). The detailed characterization of both mineralogical and geochemical features of these deposits is critical to our understanding of the processes which were responsible for their formation; furthermore an increased knowledge of mafic-ultramafic magmatic Ni-Cu-PGE systems may lead to innovations in the exploration and development of these deposits.

The sulfide ores of the Sudbury Igneous Complex (SIC), Canada, represent a significant resource of nickel, copper, and platinum-group elements (PGE), and occur within three main deposit types: (i) PGE-poor, Ni-rich contact-style deposits hosted in basal norite and quartz diorite, or within embayments along the base of the SIC, (ii) Cu-Ni-PGE rich offset-style deposits hosted in quartz diorite offset dykes occurring within Neoarchean-Paleoproterozoic country rocks, and (iii) Cu-PGE rich footwall-style deposits (that are further subdivided into "high sulfide" and "low sulfide" deposits) hosted within shock brecciated country rocks (Naldrett et al., 1984; Farrow and Lightfoot, 2002; Farrow et al., 2005; Ames and Farrow, 2007). Offset deposits of the SIC, hosted by the dioritic contact sublayer, are of particular economic importance owing to their often highly elevated base metal and PGE contents, relative to other ore types that are either base metal, or PGE dominated (Farrow and Lightfoot, 2002 and others therein). The ore mineralogy of the offset deposits is highly complex due to several factors: (i) they formed in contact with, and through the assimilation of, a wide range of footwall country rocks by a superheated mafic liquid; (ii) they show significant textural and compositional variability due to dynamic emplacement, variable rates of cooling, and fractional/equilibrium crystallization of sulfide melts *in-situ*; and (iii) they show modification/overprinting by a complex array of syn- to post-cumulus hydrothermal and metamorphic events (Zurbrigg et al., 1957; Cochrane, 1984; Grant and Bite, 1984; Lightfoot et al., 1997; Lightfoot and Farrow, 2002; Murphy and Spray, 2002; Tuchscherer and Spray, 2002). Geochemical and textural variability in the ores may be significant within a single offset environment, and between offsets. Consequently, as new offset deposits are developed during the mining process, the opportunity to conduct

detailed mineralogical investigations in order to better understand the ore-forming processes in this giant mining camp presents itself.

The Totten #2 mine is located within the Worthington Offset, along the Southwest margin of the Sudbury Igneous complex (Figure 1). The Worthington Offset Dyke is a typical example of a radial offset, much like the more extensively studied Copper Cliff Offset (Grant and Bite, 1984; Stewart, 1999; Rickard, 2000; Carter et al., 2001; Huminicki et al., 2005; Magyarosi et al., 2002; Szentpéteri et al., 2002). Although some work has been done to describe the ore mineralogy of Totten #2 mine (Lightfoot and Farrow, 2002; Stewart, 2002), a comprehensive investigation of the domains of both precious and deleterious metals has not yet been done. The objectives of this study are to (i) identify the specific mineralogical domains in which the chalcophile elements reside; (ii) determine the spatial distribution of the aforementioned domains, (iii) provide a comprehensive mineralogical model (i.e. characterization of the major and accessory ore minerals) and describe the paragenesis of the Totten Main and 238 ore bodies, and (iv) describe any basic mineralogical indicators for hand samples/thin sections that will assist mine geologists to identify problematic (i.e., contaminated by deleterious metals with a focus on As and Pb), or PGE-Au enriched domains of the deposit and to conduct more rapid grade assessments underground or in the core lab.

2.2 Regional geology of the Sudbury Igneous Complex

The Sudbury Igneous Complex (SIC) hosts a variety of world-class deposits, and has been a major source of base and precious metals for more than a century. The SIC is contained within a large 30x60 km elliptical structure which is a dominant feature of the Sudbury region (Giblin, 1984; Ames et al., 2008, Figure 1). Although there has been

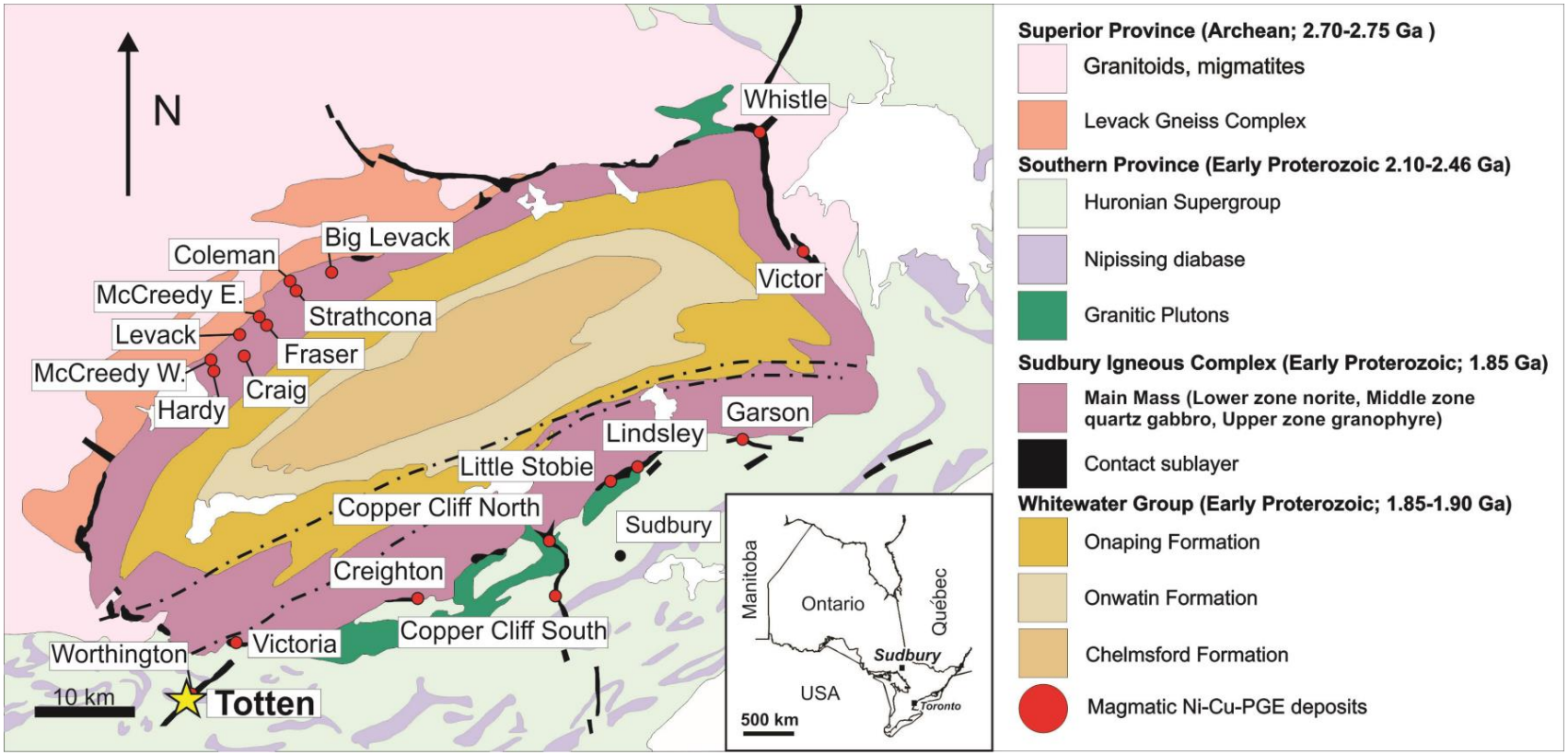

Figure 1. Geological map of the Sudbury Igneous Complex (SIC), and the location of Ni-Cu-PGE deposits, modified from Rousell et al., 2003, ages with major geological units and formations from Ames et al. (2008)

much controversy and debate over the origin of the Sudbury Structure, the recognition of shatter cones in the Sudbury area has led to the widely-accepted theory that the Sudbury Structure is an astrobleme (Dietz, 1964). The age of the SIC (and the timing of the Sudbury impact event) is approximately 1.85 Ga (Krogh et al., 1982).

The regional geology of the Sudbury area is summarized in detail by Card et al. (1984, and references therein). The Sudbury Structure, found in the southern region of the Canadian Shield, occurs along the contact of the Southern Province and the Superior Province (Figure 1). The Superior Province consists of an array of Archean greenstone belts, metasedimentary belts, felsic plutons, and gneissic terrains. Superior Province rocks in contact with the North Range of the SIC are composed of tonalite to granodiorite gneiss that are intruded by the Algoman felsic plutons. The Levack Gneiss Complex (Figure 1) is also found along the northern border of the SIC. The Levack Gneiss Complex is composed of tonalitic gneiss (upper amphibolite to lower granulite facies) with pervasive mafic layers that has been subjected to a variety of intrusives (tonalitic, granodioritic, mafic, anorthositic). It is believed that the Levack Gneiss Complex represents the basement rocks of the Superior Province. The Southern Province rocks along the South Range contact are comprised of the Huronian Supergroup clastic sedimentary units with basal volcanic units. The sedimentary sequences were dominantly sourced from the Superior Province units to the North. The Huronian units were intruded by the Nipissing Diabase and then a series of felsic plutons (e.g. Murray and Creighton).

The Sudbury Structure contains both the SIC and the overlaying Sudbury basin. The Sudbury basin consists of the Whitewater Group (Figure 1), which is divided into the Onaping, Onwatin, and Chelmsford formations (Muir and Peredery, 1984; Rousell,

1984). The Onaping formation consists of a series of breccias which contain clasts of the country rocks as well as glassy fragments. The Onaping formation has been attributed to either pyroclastic flows (Thomson, 1957; Williams, 1957; Stevenson, 1972) or as fall back breccia from the Sudbury impact event (French, 1967; Peredery, 1972). The overlying Onwatin formation consists of pelagic sediments which were followed by the deposition of turbidites of the Chelmsford Formation (Rousell, 1984).

Stratigraphically below the Sudbury Basin is the Sudbury Igneous Complex, which is underlain by shock brecciated, and partially melted basement rocks (referred to as the footwall and Sudbury breccias respectively; Dressler, 1984; Dressler et al., 1992). The SIC has been classified as a lopolith, a differentiated melt sheet generated by a meteorite impact (Dietz, 1964; Naldrett and Hewins, 1984; Therriault et al., 2002). However, there are several characteristics of the SIC that do not conform to conventional models of layered intrusives: (i), geochemical and isotopic signatures consistent with rocks of crustal origin (ii), the large volume of residual granophyre, (iii) an intermediate bulk composition, and (iv) an absence of any fine scale or rhythmic igneous layering (Naldrett and Hewins, 1984; Therriault et al., 2002). Furthermore, the SIC is different from other impact-related melt sheets due to its chemical layering, thickness, and above-average preservation (Therriault et al., 2002). The SIC can be subdivided into two units: the Main Mass, and the Contact Sublayer.

The Main Mass represents the bulk of the SIC, and is divided into the North and South Ranges (Naldrett and Hewins, 1984). The Main Mass consists of noritic and gabbroic cumulates that are overlain by granophyric residue. The Contact Sublayer occurs as a discontinuous unit along the outer margins of the SIC, and as infillings within the offset

dykes that are hosted within the country rocks (Pattison, 1979; Grant and Bite, 1984). In terms of its economic value, the Contact Sublayer is much more important than the Main Mass because it hosts the majority of the Ni-Cu-PGE deposits in Sudbury. Compositionally, the Contact Sublayer ranges from fine to medium grained norite and gabbro, although the offset variety is commonly referred to as quartz diorite (QD). It is not uncommon to find inclusions of foreign rocks within the sublayer (Grant and Bite, 1984). Typically, these inclusions can be attributed to one of two groups: (i) inclusions which were sourced locally from the country rocks, and (ii) mafic-ultramafic inclusions of ambiguous origin (Pattison, 1979). In general, the second group of inclusions tend to be rounded to sub-rounded, whereas inclusions derived from the country rocks are usually more angular. Interestingly, clinopyroxene-rich xenoliths found in the North Range are absent in the South Range sublayer (Scribbins et al., 1984).

There are a variety of deposits hosted within the SIC, however three main types of Ni-Cu-PGE mineralization have been recognized (Farrow and Lightfoot, 2002, and references therein). The offset dykes which host a variety of Ni-Cu-PGE deposits may be categorized as either radial (dykes which extend away from the SIC into the surrounding country rocks) or concentric (dykes with no apparent connection to the SIC, but occur parallel to it; Souch et al., 1969; Grant and Bite, 1984). Offset deposits are typically associated with either an increase in the thickness of the offset dyke, or with structural traps within the dyke (Farrow and Lightfoot, 2002; and references therein). Offset deposits are of particular economic importance, owing to their elevated concentrations of Ni, Cu, and precious metals (Cu/Ni ratios between 1.5-2, Pt+Pd+Au > 2.5 g/t; Farrow and Lightfoot, 2002). However, these deposits are also typically enriched in Pb (Ames and

Farrow, 2007). Spatial variations in major and trace element chemistry occur both between and within offset deposits. The deposits of the Copper Cliff offset and the Worthington offset are examples of these features (Cochrane, 1984; Farrow and Lightfoot, 2002; Lightfoot and Farrow, 2002). Contact-style deposits occur within the Contact Sublayer or footwall breccia at the base of the SIC (Souch et al., 1969; Pattison, 1979; Morrison et al., 1994; Naldrett, 1984a). The Whistle and Murray mines are examples of contact-style deposits. In contrast to offset deposits, contact deposits have lower Cu/Ni ratios, precious metal concentrations (Cu/Ni = 0.7 average, Pt+Pd+Au<1 g/t; Farrow and Lightfoot, 2002), and are relatively poor in Pb (Ames and Farrow, 2007). Footwall style deposits occur exclusively within the footwall breccia and consist of massive sulfide veins ("high sulfide") or blebby disseminated sulfides ("low sulfide"; Farrow and Lightfoot, 2002; Farrow et al., 2005). The McCreedy West and Strathcona mines are typical examples of footwall-type deposits. Footwall-type deposits have high Cu and precious metal contents relative to offset- and contact-style deposits (Cu/Ni ratios> 6, Pt+Pd+Au> 7 g/t; Farrow and Lightfoot, 2002). Although, like offset deposits, footwall deposits are often enriched in Pb (Ames and Farrow, 2007). Additionally, the main Sudbury Ni-Cu-PGE deposits may be distinguished using trace metal chemistry. Deposits occurring within the South Range are typically enriched in As and Sb, whereas Noth Range deposits contain low concentrations of those metals (Ames and Farrow, 2007; Farrow and Watkinson, 1999).

The dominant sulfide phases within the Sudbury ores consist of pyrrhotite, pentlandite, and chalcopyrite (Naldrett, 1984b; and references therein). Pyrrhotite is the dominant sulfide phase found in most Sudbury ores; two distinct species of pyrrhotite

have been reported: (i) ferromagnetic monoclinic pyrrhotite, and (ii) diamagnetic hexagonal pyrrhotite (Hawley and Stanton, 1962; Naldrett, 1984b). Michener & Yates (1944) demonstrated that magnetic pyrrhotite contained greater levels of sulfur than non-magnetic pyrrhotite. Pyrrhotite has a wide range in grain size since it may occur as massive to disseminated sulfides. In massive sulfides, pyrrhotite is typically reported as subrounded, interlocking cumulates (Hawley and Stanton, 1962). Pentlandite may occur as irregular masses (pentlandite "eyes"), as pentlandite stringers between pyrrhotite grains, and as fine exsolution lamellae within pyrrhotite (Hawley and Stanton, 1962). Chalcopyrite is usually much less abundant than pyrrhotite, but may occur in higher concentrations locally (such as within sulfide veins, Hawley and Stanton, 1962). Texturally, chalcopyrite typically occurs interstitial to the other major base metal sulfides, and normally occurs along the margins of veins which contain all the base metal sulfides (Hawley and Stanton, 1962).

Although volumetrically minor, trace minerals are important to the precious (e.g. Au, Ag, PGE) and deleterious (e.g. As, Pb, Sb) metal concentrations in the Sudbury ores, and are well documented in the literature (Hawley and Stanton, 1962; Cabri and Laflamme, 1976; Li and Naldrett, 1993; Farrow and Watkinson, 1999; Rickard, 2000; Carter et al., 2001; Farrow and Lightfoot, 2002; Magyarosi et al., 2002; Stewart, 2002; Szentpéteri et al., 2002; Huminicki et al., 2005; Ames and Farrow, 2007; Dare et al., 2010; LeFort, 2012). Michenerite [(Pd, Pt)BiTe], is usually the main Pd mineral in Sudbury deposits. Platinian michenerite is not typically associated with South Range deposits and is more common in North Range ores. Other reported Pd phases include sudburyite (PdSb), froodite ($PdBi_2$), palladian merenskyite ($PdTe_2$), and kotulskite (PdTe). Sperrylite

($PtAs_2$), is almost exclusive to South Range deposits, and is the primary Pt-phase in all of those deposits whereas moncheite ($PtTe_2$) is more common in North Range deposits. Although elevated Sn has been reported in both North and South Range deposits, niggliite (PtSn) has not been associated with South Range deposits. The PGM may form anhedral inclusions in base metal sulfides, silicates, and arsenide phases (strong associations with chalcopyrite are not uncommon). Arsenide (e.g., nickeline) and sulfarsenide (e.g., cobaltite, gersdorffite) minerals are reported in South Range deposits, but are absent in the North Range. These minerals may form inclusions within the base metal sulfides and silicates. An interesting characteristic of the sulfarsenide phases is chemical variations (variations in Ni, Co, Fe), which are common at all scales (e.g., intragranular, intergranular, between samples, between deposits). Lead typically occurs as galena (PbS) in both North and South Range deposits. Galena usually forms anhedral inclusions, or composite grains with a variety of Bi-Te-Ag alloys hosted in base metal sulfides, sulfarsenides, and silicates.

The formation of the Sudbury ores has been largely attributed to the separation of immiscible sulfide melt from the impact melt sheet, as well as the subsequent migration and fractional crystallization of the sulfide melt (e.g. Keays and Crocket, 1970; Li et al., 1992; Naldrett et al., 1999; Lightfoot et al., 2001; Farrow and Lightfoot, 2002; Lightfoot and Keays, 2002). The chalcophile elements (Cu, Ni, Co, Au, PGE, etc.) are much more compatible with a sulfide melt than a silicate melt (Mungall, 2005, and references therein) and would have been concentrated by this immiscible liquid. The formation of a monosulfide solid solution (MSS) would have occurred around 1120°C (Naldrett, 1984b), forming a cumulate enriched in Fe, Ni, Co, Rh, Ru, Ir, Os, and a residual melt enriched in

elements that are incompatible in the MSS (e.g., Cu, Au, Pt, Pd, Pt, Pd; Naldrett and Kullerud, 1967; Naldrett, 1984b). The residual melt would have crystallized an intermediate sulfide solid solution (ISS), the precursor of chalcopyrite, bornite, and cubanite in the Sudbury ores (Naldrett, 1984b). At lower temperatures (<650°C) the MSS would have exsolved pyrrhotite and pentlandite (Durrazo and Taylor, 1982). Sulfide ores in the offset environment likely represent the earliest stages of sulfide saturation since the greatest (initial, undepleted) availability of base and precious metals to partition into the sulfide melt would have occurred at this stage (Lightfoot and Farrow, 2002). Evidence suggests that this melt containing chalcophile-rich immiscible sulfide liquid and country rock xenoliths was emplaced into the offsets after an initial injection of sulfur-under saturated, inclusion-free quartz diorite (Lightfoot et al., 2001; Farrow and Lightfoot, 2002; Lightfoot and Farrow, 2002). Sulfide saturation continued after the formation of the offsets leading to the concentration of immiscible sulfide liquid, as well as country rock xenoliths, along the base of the melt sheet within embayments, forming the contact-style deposits (Morrison, 1984, Golightly, 1994). Currently, two genetic models have been proposed for the footwall type deposits: (i) foowall ores represent the fractionated (Cu, Pt, Pd enriched) liquid resulting from the crystallization of the MSS in contact environments, which subsequently migrated into the adjacent brecciated country rocks (Keays and Crocket, 1970; Li et al., 1992; Naldrett et al., 1999), and (ii) tectonic/hydrothermal remobilization and concentration of PGE in both high and low sulfide footwall systems (Farrow and Watkinson, 1992, 1997; Molnár et al., 1997, 1999; Hanley et al., 2004, 2005; Ames and Farrow, 2007; Péntek et al., 2008, Hanley et al., 2011).

2.3 Geology of the Worthington offset dyke in the vicinity of the Totten mine

The Worthington offset is a 15 km radial dyke found between the Densen and Drury townships (Figure 2; Lightfoot and Farrow, 2002). It ranges in thickness from 30 to 100m and dips 80 degrees to the southeast (Lightfoot and Farrow, 2002). The dyke has been displaced along two major structures: the Murray and Creighton faults (Lloyd, 2001). The Worthington offset intrudes metasedimentary and metavolcanic units of the Huronian Supergroup, as well as Nipissing amphibolite-metagabbro intrusives (Lightfoot and Farrow, 2002). Late olivine and quartz diabase dykes have intruded the offset and country rocks via the brittle fracture system generated between the region's two main faults (Lloyd, 2001; Stewart, 2002). The contact between the quartz diorite (QD) offset and the surrounding metasedimentary rocks is sharp. Along this contact, the quartz diorite contains spherulitic plagioclase and amphibole which evolves over 1-5m towards medium grained amphibole-biotite quartz diorite. This unit progressively increases in grain size towards the center of the dyke, and may contain minor occurences of sulfides (pyrrhotite, pentlandite, chalcopyrite; Lloyd, 2001; Lightfoot and Farrow, 2002). The sulfide- and inclusion-rich quartz diorite (IQD) typically occurs near, but is not exclusive to, the center of the offset dyke (Lloyd, 2001). The inclusions consist mainly of locally derived metagabbro and amphibolite, supported by a fine-grained QD matrix. Inclusions of Huronian metasediments are rare. Marginal occurrences of IQD occur where the offset dyke is in contact with Nipissing intrusives. These contacts are defined by IQD stockwork in metagabbro, forming a megabreccia (Figure 3, Lloyd, 2001; Lightfoot and Farrow, 2002). In these portions of the dyke, IQD is ubiquitous and shows an increase in the volume of metagabbro xenoliths. Contact between QD and IQD ranges from sharp to diffuse (Lloyd, 2001; Lightfoot and Farrow, 2002). Subangular inclusions of QD within

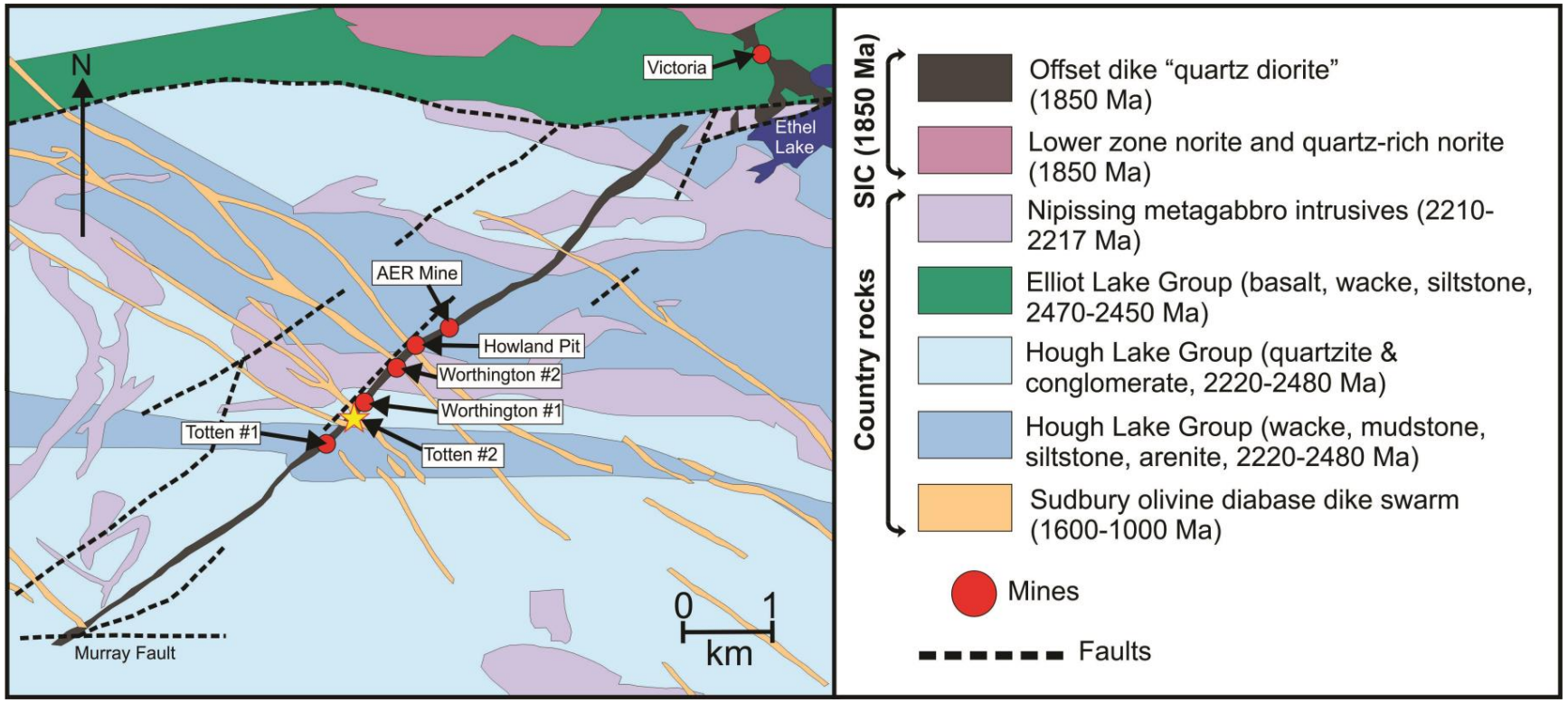

Figure 2. Geological map of the Totten mine area. The Totten #2 mine, which is the focus of this study, is marked by the star. Modified after Lightfoot and Farrow, 2002; and Ames et al., 2008.

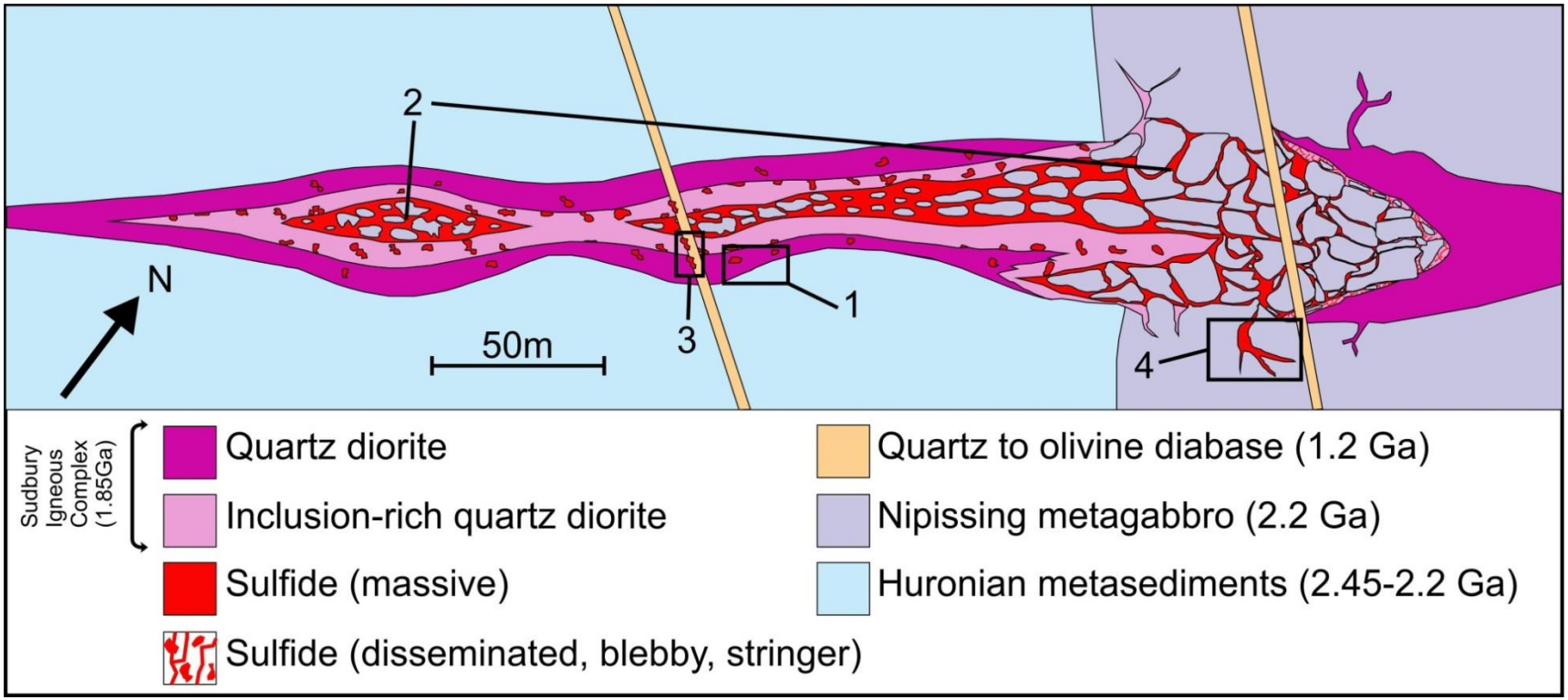

Figure 3. Geological relationships in the Totten mine area, modified after Lloyd (2001): (1) sulfide mineralization in quartz diorite, (2) sulfide mineralization in inclusion-rich quartz diorite (center of the offset dyke and within country rock meggabreccia), (3) structurally controlled sulfides associated with the Sudbury diabase swarm dykes, and (4) structurally controlled sulfides within the offset country rocks.

IQD indicate the possibility of separate events of quartz diorite injection (Lloyd, 2001; Lightfoot and Farrow, 2002).

The Totten (#1 & #2) deposits and Worthington mine host the most economic sulfide occurrences in the Worthington offset (Figure 4). These deposits are located approximately 40 km west of the city of Sudbury (Lloyd, 2001). Several ore styles have been observed at these deposits: (i) massive sulfides (MASU) which are dominantly comprised of sulfides (more than 80% by volume), (ii) semi-massive, or inclusion massive sulfides (INMS), which contain moderate to abundant inclusions (50-80% sulfides by volume), and (iii) sulfide disseminations and veins in silicate rocks (Lloyd, 2001; Stewart, 2002). These ores may occur within one of four different environments (Figure 3): (i) sulfides hosted within offset quartz diorite, (ii) mineralization hosted within inclusion-rich quartz diorite, (iii) structurally controlled mineralization hosted within in the hanging wall and footwall of diabase dykes, and (iv) structurally controlled mineralization within the Worthington offset country rocks. The focus of this study is made on types i-ii since these are the only known Totten environments which host *economic* concentrations of sulfide ore (Lloyd, 2001).

3.0 Methods

3.1 Sampling of the Totten #2 Mine ore bodies

The sampling of the two ore bodies (Main and 238 ore bodies, Figure 4) at the Totten #2 mine was more extensive in the Main ore body. The reason for this bias is due to the fact that the Main ore body represents the focus of the mining activity at the Totten #2 deposit at this time. Approximately 277 samples were obtained to represent the Main and 238 ore bodies. Samples were taken from exploration/definition diamond drill holes (both

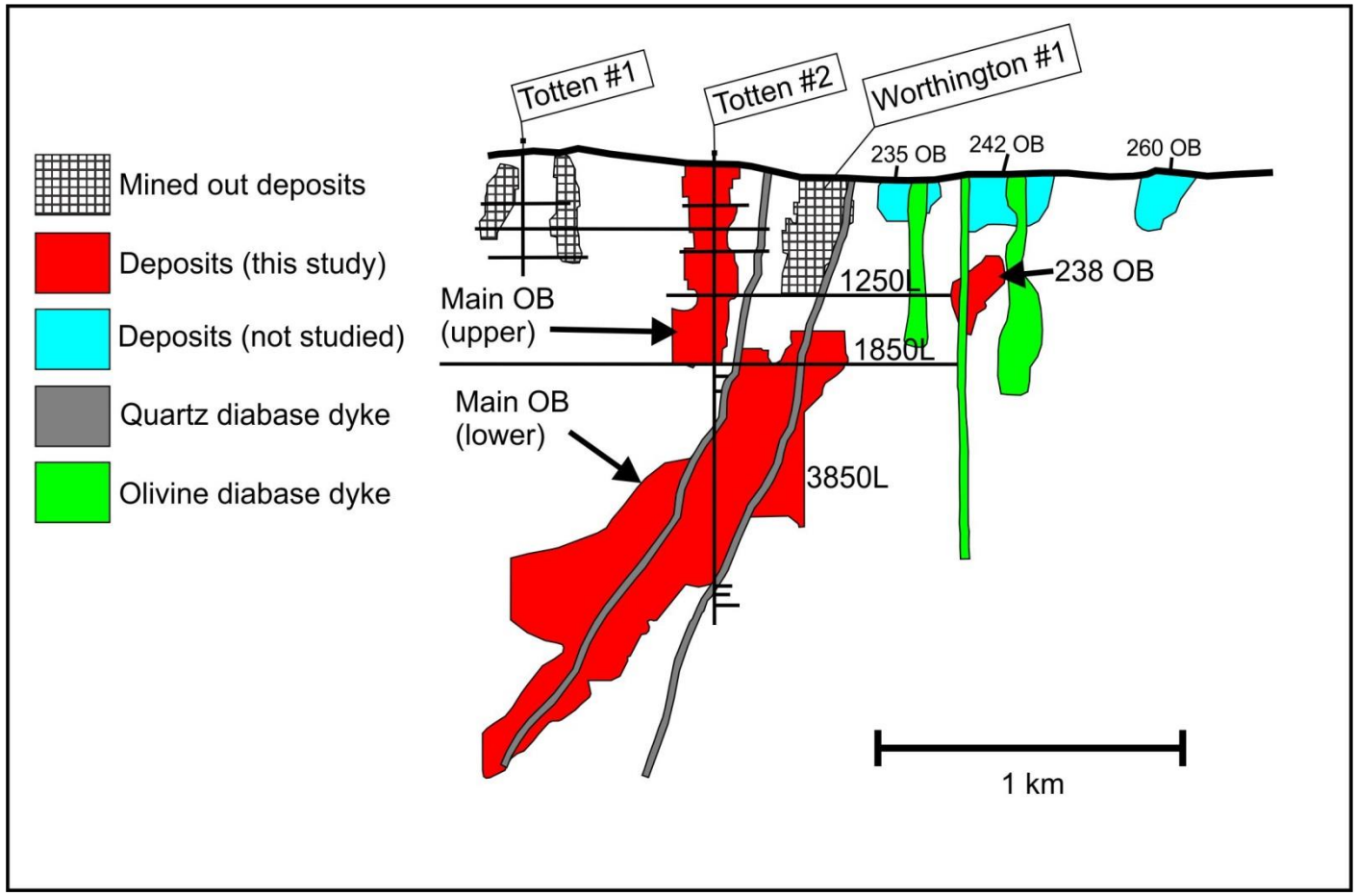

Figure 4. Longitudinal cross section of the Totten mine area, cross section is parallel to offset dyke. Diagram modified after data given by Vale, and Lightfoot and Farrow (2002). Abbreviation (OB) stands for ore body.

past and present), and from active underground mining (where available at the time of sampling) from the 1250, 1850, and 3850 levels (as well as surface exposures; Appendix, A1 and A2). Additionally, 196 thin sections were produced from those same samples in order to study the petrography of both the major and accessory phases of the ore assemblages. Sampling focused mainly on the massive (MASU) and semi-massive (INMS) sulfides since these represent the most economic concentrations of sulfide mineralization. Sampling of peripheral ore (disseminations and veins) was also done in order to observe any variations of the mineralogical domains in the ore environments associated with wall rock contacts and "boulder beds" (areas of complex wall rock-QD interaction).

3.2 Bulk rock analyses of the ores

Samples obtained from drill hole and underground mining were prepared for bulk rock analysis to be performed by ALS minerals, Sudbury, Ontario. Preparation involved cutting the larger hand samples into smaller representative samples. In order to reduce the chance of cross contamination by sulfides, samples were cut in order of increasing sulfide mineralization (by % volume). Once cut, these samples were cleaned in order to remove any surface contamination, packaged, and shipped for assay. Samples were crushed using Boyd crusher-rotary sample divider combo unit, until at least 70% of the material was less than 2mm in diameter. The resulting material was ring pulverized until more than 85% of material was no greater than 74µm in diameter. All samples were analyzed using a standard method combining inductively coupled plasma-atomic emission spectroscopy (ICP-AES) for a range of elements (e.g. Cu, Ni, Co, As, Fe, etc.). In this method, 0.25g of each crushed sample was digested with perchloric, nitric, hydrofluouric, and hydrochloric

acids. The final residue of each sample was again digested in dilute hydrochloric acid before the finished solution was analyzed via ICP-AES, and corrected for spectral interferences. For samples that gave results above upper detection limits for Ag, As, Cu, and Ni, another procedure was used. Once again this method used four-acid digestion, followed by an ICP-AES, or atomic absorption spectroscopy (AAS) finish. For samples which contained levels of S greater than detection limits, a combustion infrared detection technique was used to determine the total sulfur content of the sample. To determine the concentration of precious metals (Au, Pd, Pt) 30g of sample was analyzed by lead fire assay and ICP-MS finish. For Au concentrations greater than detection limits, samples were re-analyzed by lead fire assay with a gravimetric finish.

3.3 Accessory mineral identification and analysis

A scanning electron microscope (SEM) was used in order to study the distribution and textural relationships of the accessory phases present in the Totten samples. The identification of these phases was done using energy dispersive spectroscopy (EDS). The Leo 1450 VL SEM (Saint Mary's University, Nova Scotia) used an accelerating voltage of 20kV, a range in beam current of 5-20nA, and a working distance which ranged from 19-21mm. The backscattered electron images (BSE) produced by the SEM were also used to calculate the modal abundance of each accessory phase by measuring the dimensions of each grain found in thin section. The accessory phase abundance of 44 samples was determined from 270 samples of the Totten sample suite.

3.4 Trace metal content of base metal sulfides, sulfarsenides, and arsenides

The analysis of the trace metal content from major phases (base metal sulfides) and arsenide phases (nickeline, glaucodot, gersdorffite, etc.) was performed by laser ablation

inductively-coupled plasma mass spectroscopy (LA-ICP-MS), at the Geological Survey of Canada, Ottawa. The details of the conditions for the analyses (including beam diameter, standards used, and uncorrected spectral interferences) are summarized in Table 1. Samples were chosen in order to represent the base metal sulfides (pyrrhotite, pentlandite, and chalcopyrite) from both the Main and 238 ore bodies. Due to the limitations of the beam size (which is directly related to the quality of the analysis), As-bearing minerals could only be analyzed in samples that contained grains of sufficient size. In addition to the chalcophile and siderophile elements that are expected in the phases analyzed, some lithophile elements were also measured in order to monitor contamination by silicate phases. Typically, central portions, or regions well removed from grain boundaries, that did not show any visible inclusions of discrete phases, were selected for analysis. Since analysis of As phases required longer washout times due to the greater potential for contamination, the base metal sulfides were analyzed before the As phases. Data reduction of the ICP-MS signal was done using the Glitter^{TM} software package. The program allowed the user to select portions of each signal which showed continuous and consistent count rates, for integration into the final results (thereby eliminating any sources of contamination in the signal). The internal standard for the base metal sulfides and sulfarsenides was Fe, which was based on stoichiometry, and the Fe or Ni content of the arsenides/sulfarsenides was determined by EDS analysis (an average value of used for Fe, since the Fe content of sulfarsenides varies). The calibration standards used were MASS-1 (Co, Ni, Cu, Zn, As, Se, Ag, Cd, Sn, Sb, Te, Hg, Tl, Pb, and Bi in base metal sulfides, arsenides and sulfarsenides), Po726 (Ru, Rh, Pd, Os, Ir, Pt, and Au in base metal sulfides and sulfarsenides), and PGE-B (Ni, Pd, Pt, Ru, Os, Rh, Ir,

Table 1: LA-ICP-MS operating conditions

LA	
Model	Photon Machines Analyte.193
Wavelength	193 nm
Pulse duration (FWHM)	4 ns
Repetition rate	14 Hz
Spot diameter	14-86 µm
Energy density	ca. 4 J/cm^2
Primary (calibration) standards	**Po726** (synthetic, PGE and Au doped pyrrhotite, Sylvester et al., 2005; reference values from certificate) **Mass-1** (synthetic, doped, precipitated sulfide; reference values from Wilson et al., 2002, except Te from Dare et al., 2010b, and Ni (98 ppm) and Pb (73 ppm) determined in house)
Secondary (quality control) standard	**PGE-B** (quenched doped NiS fire assay button, prepared by I. Horn at Memorial University of Newfoundland; reference values from Alard and Lorand, 2001; Gilbert et al., 2012; most probable values from S. Jackson,
ICP-MS	
Model	Agilent 7700x with additional interface rotary pump which approximately doubles instrument sensitivity
Forward power	1550 kW
Shield torch	Used
Sampling depth	7 mm
Gas flows (He carrier mixed downstreamn from cell with Ar make up):	
Carrier (HE)	0.6 L/min
Make up (Ar)	1.08 L/min
ThO^+/Th^+	<0.3%
U^+/Th^+ (NIST 612)	ca. 1.05
Data acquisition parameters	
Data acquisition protocol	Time Resolved Analysis
Scanning mode	Peak hopping, 1 point per blank
Dwell time per isotope	10 ms for all masses (earlier analyses) or as indicated below
Detector mode	Pulse counting except analogue for isotopes in italics below
Isotopes determined (dwell time ms)	^{29}Si(5), ^{34}S(5), ^{42}Ca(5), ^{57}Fe(5), ^{59}Co(10), ^{60}Ni(5), ^{61}Ni(10), ^{65}Cu(10), ^{66}Zn(10), ^{75}As(10), ^{77}Se(10), ^{88}Sr(5), ^{89}Y(5), ^{90}Zr(5), ^{99}Ru(15), ^{101}Ru(15), ^{102}Ru(15), ^{103}Rh(15), ^{105}Pd(15), ^{106}Pd(15), ^{107}Ag(15), ^{108}Pd(15), ^{109}Ag(15), ^{111}Cd(10), ^{118}Sn(15), ^{121}Sb(10), ^{125}Te(10), ^{181}Ta(5), ^{185}Re(15), ^{189}Os(15), ^{193}Ir(15), ^{195}Pt(15), ^{197}Au(15), ^{206}Pb(10), ^{208}Pb(10), ^{209}Bi(10)
Quadrupole settling time	1-5 ms depending upon mass jump
Analysis time	120 s: ~40 s gas blank, up to ~80 s of ablation
Internal standard	Fe (Po, Pn, Cp, CGSS), Ni (Nic)
Uncorrected spectral interferences:	Pyrrhotite: None Pentlandite: ^{61}Ni^{40}Ar on ^{101}Ru, ^{59}Co^{40}Ar on ^{99}Ru Chalcopyrite: ^{65}Cu^{40}Ar on ^{105}Pd, ^{108}Cd^{40}Ar on ^{108}Pd, ^{63}Cu^{40}Ar on ^{103}Rh CGSS: ^{61}Ni^{40}Ar on ^{101}Ru, ^{59}Co^{40}Ar on ^{99}Ru/^{102}Ru Nickeline: ^{61}Ni^{40}Ar on ^{101}Ru

Notes: abbreviation CGSS stands for cobaltite-gersdorffite-glaucodot solid solution

And Au in nickeline). Using MASS-1 on Po726, Po726 on MASS-1, and MASS-1 on PGE-B for concentrations of Au, the accuracy of these calibrations was evaluated by comparison to accepted values, and measured Au concentrations were in agreement with reported values (unfortunately, no other elements could be compared in all three standards). Spectral interferences were avoided where possible by using isotopes for which there are no known interferences (with respect to the mineral species in this study). However, some mineral species proved problematic due to spectral interferences with multiple isotopes of the same element (i.e. Ru in sulfarsenides, uncorrected interferences are given in Table 1). Analyses of sphalerite could not be obtained owing to the size and morphology of the grains.

3.5 Mass balances

Mass balance calculations were used as a means to quantify the mineralogical domains of residence for base, precious, and deleterious metals (Ni, Cu, Pt, Pd, Co, Pb, Bi, and As). In order to perform these calculations, the weight fraction was estimated for both major (base metal sulfides, silicate gangue) and accessory (sulfarsenides, nickeline, PGM, BiTe minerals, etc.) phases. Modal abundance estimates for major phases was done visually using standard reflected and transmitted light microscopy whereas the volume of the accessory phases was calculated by measuring the dimensions of the grains in thin section (via SEM, section 2.3), and compared to the total volume of the same thin section. Furthermore, estimated abundances for base metal sulfides was calculated in massive and semi-massive samples using bulk rock chemistry (assuming 100 percent sulfides, that Cu is contained in chalcopyrite, and that Ni is contained in pentlandite). These estimates could not be performed on disseminated samples due to the significant

increase in the abundance of other Ni carriers (i.e. nickeline and sulfarsenides, see sections 4.2.4 and 4.2.5). These modal percent values were converted to weight fractions using standard mineral specific gravities. In combination with major and trace element data for each phase (which was determined by LA-ICP-MS), the proportion of Ni, As, Pt, Pd, Pb, and Co-hosted in each phase was calculated as a predicted assay value. For samples that did not have LA-ICP-MS data for the base metal sulfides and As-minerals, an average (from the complete data set) value for each metal was used. The predicted assay values were then compared to the analyzed assay results in order to determine the representivity of the thin sections to their corresponding hand samples.

4.0 Results

4.1 Bulk rock analysis

As a means to evaluate the bulk rock geochemical data (Appendix A3) for major metal associations in anticipation of linking ore mineralogy to bulk geochemistry, correlation coefficients were calculated using the Spearman Rank correlation coefficient approach (Table 2). This method was chosen because it does not assume that the data shows a normal distribution, and is more appropriate when dealing with outliers (compared to the more traditional Pearson product-moment method; Rollinson, 1993), which are a common characteristic in complex ore assemblages exhibiting highly localized and irregular metal distribution. Elements (e.g., Th, U, and Tl) which were consistently below routine detection limits were not included in the correlation matrix, because these values artificially inflate the value of the correlation coefficient (assuming a value of zero for samples below detection limits). The lithophile elements (e.g., Li, Mg, K, Ca, etc.) consistently demonstrate weak to strong negative correlation coefficients with the chalcophile elements (e.g., Ag, Cu, As, Bi, Pb, Au, Pt, Pd, Ni, Mo), confirming that the

Table 2: Spearman rank correlation coefficients of representative ore analysis

	Ag	Al	As	Au	Ba	Bi	Ca	Cd	Co	Cr	Cu	Fe	K	La	Mg	Mn	Mo	Na	Ni	P	Pb	Pd	Pt	S	Sc	Sr	Ti	V	Zn
Ag	1																												
Al	-0.38	1																											
As	0.098	0.093	1																										
Au	0.649	-0.047	0.258	1																									
Ba	-0.3	0.837	0.21	0.049	1																								
Bi	0.498	-0.149	0.284	0.573	-0.074	1																							
Ca	-0.35	0.738	0.015	-0.006	0.598	-0.062	1																						
Cd	0.831	0.118	0.266	0.616	0.144	0.551	0.119	1																					
Co	0.369	-0.715	0.204	0.171	-0.656	0.552	-0.701	0.208	1																				
Cr	-0.21	0.166	0.095	-0.145	0.228	-0.056	0.281	0.083	-0.156	1																			
Cu	0.947	-0.293	0.044	0.618	-0.223	0.427	-0.276	0.849	0.28	-0.161	1																		
Fe	0.337	-0.874	-0.016	0.018	-0.791	0.547	-0.799	0.189	0.859	-0.244	0.228	1																	
K	-0.26	0.803	0.19	0.085	0.907	-0.047	0.54	0.169	-0.595	0.26	-0.187	-0.765	1																
La	-0.25	0.757	0.112	-0.009	0.731	-0.028	0.543	0.267	-0.647	0.033	-0.158	-0.795	0.688	1															
Mg	-0.28	0.732	0.058	0.048	0.683	-0.056	0.82	0.158	-0.632	0.507	-0.213	-0.792	0.699	0.48	1														
Mn	-0.35	0.723	0.022	-0.019	0.66	-0.068	0.918	0.131	-0.683	0.342	-0.274	-0.757	0.619	0.508	0.849	1													
Mo	-0.03	0.119	0.412	-0.073	0.15	0.141	-0.025	0.277	0.046	0.171	-0.001	-0.013	0.086	0.329	-0.06	-0.052	1												
Na	-0.21	0.839	0.143	0.098	0.682	-0.045	0.653	0.199	-0.526	0.041	-0.131	-0.72	0.645	0.74	0.536	0.521	0.184	1											
Ni	0.436	-0.735	0.206	0.232	-0.626	0.559	-0.742	0.238	0.916	-0.219	0.32	0.845	-0.556	-0.645	-0.682	-0.73	0.035	-0.505	1										
P	-0.25	0.826	0.058	0.021	0.773	-0.073	0.632	0.182	-0.617	0.02	-0.148	-0.756	0.721	0.81	0.57	0.617	0.174	0.791	-0.613	1									
Pb	0.466	0.019	0.115	0.512	-0.009	0.496	-0.068	0.528	0.129	-0.159	0.421	0.017	0.06	0.086	-0.037	-0.114	-0.07	0.226	0.2	0.037	1								
Pd	0.504	-0.223	0.423	0.758	-0.122	0.545	-0.19	0.436	0.439	-0.121	0.444	0.24	-0.091	-0.188	-0.186	-0.176	0.085	-0.091	0.486	-0.145	0.401	1							
Pt	0.51	-0.492	0.102	0.499	-0.368	0.658	-0.455	0.412	0.549	-0.25	0.439	0.582	-0.329	-0.377	-0.468	-0.463	-0.042	-0.267	0.632	-0.401	0.384	0.589	1						
S	0.487	-0.856	0.042	0.134	-0.777	0.572	-0.815	0.319	0.85	-0.283	0.387	0.957	-0.759	-0.713	-0.831	-0.818	0.065	-0.63	0.869	-0.705	0.147	0.323	0.641	1					
Sc	-0.31	0.791	0.011	0.029	0.678	-0.049	0.883	0.167	-0.723	0.341	-0.235	-0.846	0.676	0.601	0.893	0.872	-0.005	0.649	-0.755	0.656	0.009	-0.198	-0.471	-0.863	1				
Sr	-0.22	0.859	0.104	0.067	0.71	-0.087	0.656	0.193	-0.564	0.063	-0.14	-0.746	0.662	0.753	0.557	0.529	0.184	0.967	-0.549	0.808	0.184	-0.132	-0.329	-0.659	0.657	1			
Ti	-0.31	0.913	0.089	0.021	0.805	-0.094	0.701	0.152	-0.662	0.057	-0.223	-0.801	0.793	0.777	0.667	0.698	0.147	0.82	-0.662	0.901	0.051	-0.134	-0.43	-0.788	0.767	0.827	1		
V	-0.41	0.748	0.064	-0.078	0.661	-0.09	0.741	0.036	-0.604	0.41	-0.363	-0.715	0.655	0.504	0.796	0.767	0.049	0.587	-0.625	0.567	-0.009	-0.22	-0.458	-0.762	0.852	0.59	0.72	1	
Zn	0.689	0.069	-0.001	0.455	0.098	0.259	0.081	0.872	-0.137	-0.078	0.768	-0.171	0.119	0.116	0.121	0.147	-0.03	0.096	-0.138	0.137	0.375	0.239	0.146	-0.044	0.137	0.082	0.112	-0.025	1

Notes: Values listed are Spearman rank correlation coefficients (r_s), n=174

ore metals are consistently associated with non-silicate host assemblages (e.g., sulfides, alloys, arsenides, sulfarsenides). The most significant findings of this exercise are: (i) Ni exhibits strong positive correlations to Fe, Pt, and S, and also shows a near perfect (r_s=0.916, n=174; Table 2) correlation to Co (similar correlations can be found by analysing the Vale Totten assay database); (ii) Cu shows strong positive correlations to Ag, Au, Cd, Zn, but no correlation to As; (iii) Pd exhibits strong positive correlations to Au, Co, and Pt; (iv) Pt shows strong positive correlations to Bi and Co; (vi) Au demonstrates a strong positive correlation to Cd; and (vii) with the exception of As, Mo exhibits very little correlation to the chalcophile/siderophile elements.4.2 Mineralogy and chemistry of the base metal sulfides, arsenides, and sulfarsenides

4.2 Mineralogy and chemistry of the base metal sulfides, arsenides, and sulfarsenides

4.2.1 Pyrrhotite

In both the MASU and INMS ore styles, pyrrhotite is typically the dominant (80-90% by volume) sulfide phase, with lesser amounts of pentlandite (10-15% by volume) and chalcopyrite (0.1-5% by volume, although chalcopyrite dominant massive and semi-massive sulfides are less common). In these samples, pyrrhotite occurs as a massive crystal composite with poorly defined grain boundaries (Figure 5A). Pyrrhotite may contain inclusions of pentlandite, chalcopyrite, silicates, nickeline, magnetite, sulfarsenides, sphalerite, as well as a variety of accessory phases. Massive pyrrhotite may contain lathes of additional pyrrhotite grains that exhibit box work texture. These lathes are easily identified via changes in pleochroism relative to the host grain. In sulfide veins and disseminations (DISS), pyrrhotite may form anhedral inclusions in silicates which indicate open space-filling textures or as inclusions in other sulfides. The abundance of pyrrhotite in DISS samples is variable. Pyrrhotite shows a significant concentration of

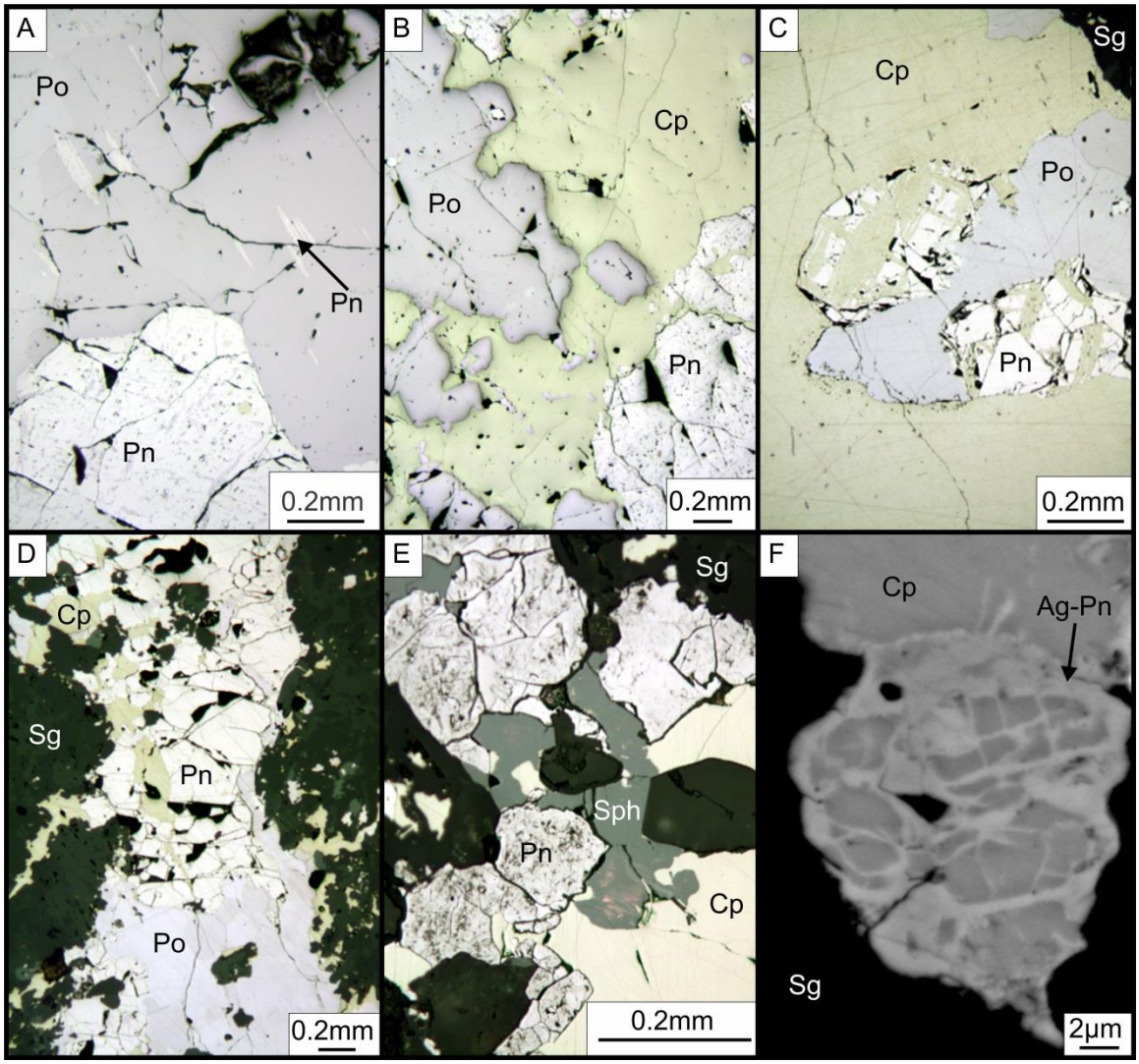

Figure 5. Photomicrographs of the base metal sulfides: (A) massive pyrrhotite (Po) with a pentlandite porphyroblast and exsolution lamellae (Pn); (B) chalcopyrite (Cp) interstitial to pyrrhotite (Po) and pentlandite (Pn); (C) resorption of pentlandite (Pn) by chalcopyrite (Cp); (D) vein consisting of the base metal sulfides with adjacent sulfide blebs; (E) an inclusion of sphalerite (Sph) in chalcopyrite (Cp) in contact with pentlandite (Pn) grains; and (F) a backscattered electron image of argentopentlandite (Ag-Pn) in chalcopyrite (Cp) hosted in silicate gangue (Sg).

Ni (2674-12031 ppm, 6530 ppm average; Table 3) and is a minor carrier of Se (97-432 ppm, 160 ppm average), and Co (25.3-133.6 ppm, 81.1 ppm average). With the exception of Ru (bdl-0.7 ppm, 0.2 ppm average), the PGE concentrations in pyrrhotite are consistently low or below detection limits. Slightly elevated and variable concentrations of Ag-Te-Bi in pyrrhotite are likely the result of small inclusions which consist of minerals such as hessite and a variety of Bi-Te phases. The Ni content of pyrrhotite was also independently evaluated using SEM-EDS in order to confirm the accuracy of the standards used for LA-ICP-MS analyses (in sample T2: SEM analyses give 0.1-0.13 wt% Ni, 0.11 wt% Ni average, n=4; LA-ICP-MS analyses give 0.9-1.2 wt% Ni, 1.1 wt% Ni average). The results of this evaluation show that MASS-1 may not have been an appropriate standard for Ni. However, mass balance calculations for bulk rock Ni are in strong agreement with bulk rock assays suggesting that the discrepancy is minor (section 4.4). The concentrations of the other metals analyzed by LA-ICP-MS (most importantly deleterious metals such as As) are low and typically fall below detection limits. It is therefore unlikely that pyrrhotite would contribute any significant levels of Pt, Pd, or deleterious metals to the bulk rock geochemistry. The complete results of the LA-ICP-MS analyses of pyrrhotite are given in Appendix A4.

4.2.2 Pentlandite

Pentlandite is the dominant Ni mineral in the Totten ore assemblage. In the MASU and INMS ore types, pentlandite may form stringers which occur along pyrrhotite grain boundaries that range from mm to µm in size. Pentlandite can also occur as medium-coarse grained porphyroblasts (pentlandite "eyes") which are often joined to the pentlandite stringers occurring along the edge of pyrrhotite grains (Figure 5A).

Table 3: Summary of LA-ICP-MS results for trace element chemistry of base metal sulfides, arsenides, and sulfarsenides in the Totten #2 mine

Sample no. (mineral)	T9 (Po)		T12 (Po)		TU1 (Po)		T7 (Po)		T10 (Po)		T8 (Po)		T17 (Po)		T26 (Po)		TU18B (Po)	
Ore body	238		238		238		238		Main		238		Main		238		Main	
Sulfide texture	MASU		MASU		MASU		MASU		MASU		MASU		MASU		DISS		MASU	
Isotope	Range	Average (n)	Range	Average (n)	Range	Average (n)	Range	Average (n)	Range	Average (n)	Range	Average (n)	Range	Average (n)	Range	Average (n)	Range	Average (n)
^{59}Co (ppm)	117.5-132.9	127 (6)	99.3-115.6	107.3 (5)	35.8-46.2	39.6 (4)	98.9-133.6	117.1 (4)	59.8-63.3	61.5 (4)	105-106.8	105.9 (4)	79.7-93.6	83.9 (4)	66.4-93.2	81.7 (5)	65.8-93.2	74.4 (7)
^{60}Ni	3380.1-5049.9	4364.9 (6)	4481-5437.3	5099 (5)	7357.2-9052.1	8430.2 (4)	3609.8-5010	4485.9 (4)	7437.1-8700.9	8340.4 (4)	4193-5634.9	5227.4 (4)	2674.7-4348.9	3532 (4)	6466-8570	7396 (5)	6686-8702	8122 (7)
^{65}Cu	0.06-0.15	0.1 (6)	0.78-0.13	0.11 (5)	0.044-0.37	0.18 (4)	0.041-0.151	0.078 (4)	0.89-1.85	1.31 (4)	0.052-0.14	0.1 (4)	BDL-0.58	0.35 (3)	0.07-0.15	0.1 (5)	BDL-0.68	0.26 (5)
^{66}Zn	BDL	-	BDL	-	BDL-0.45	0.32 (2)	BDL-0.51	0.28 (3)	BDL	-	BDL	-	BDL	-	BDL	-	BDL	-
^{75}As	0.019-0.075	0.031 (6)	BDL-0.041	0.029 (4)	BDL-0.19	0.065 (4)	BDL-0.042	0.023 (3)	BDL-0.063	0.061 (2)	BDL-0.04	0.033 (3)	BDL	-	BDL-0.072	0.072 (1)	BDL-0.087	0.046 (5)
^{77}Se	110.6-124.5	116.5 (6)	110.4-116.2	112.6 (5)	104.8-138.9	118.6 (4)	117.8-123	120.1 (4)	198.8-205	202.2 (4)	113.7-116.7	115.2 (4)	149.3-169.2	162.4 (4)	96.8-107.9	102.68 (5)	182.1-251.7	213.8
^{99}Ru	0.21-0.28	0.24 (6)	0.55-0.6	0.57 (5)	0.0097-0.7	0.2 (4)	0.12-0.14	0.13 (4)	0.02-0.061	0.032 (4)	0.44-0.46	0.44 (4)	0.018-0.063	0.032 (4)	0.075-0.32	0.2 (5)	0.013-0.037	0.023 (7)
^{103}Rh	BDL-0.00039	0.00034 (2)	BDL-0.00054	0.00041 (3)	BDL-0.0011	0.00062 (3)	BDL-0.032	0.011 (3)	BDL	-	BDL	-	BDL-0.0016	0.0016 (1)	BDL	-	BDL	-
^{106}Pd	BDL-0.0081	0.0015 (4)	BDL-0.009	0.0033 (3)	BDL-0.016	0.0067 (3)	BDL-0.0013	0.0012 (2)	BDL-0.0022	0.0022 (1)	BDL	-	BDL	-	BDL	-	BDL-0.003	0.023 (2)
^{107}Ag	0.32-1.5	0.65 (6)	0.25-0.52	0.32 (5)	0.3-0.72	0.47 (4)	0.19-0.22	0.21 (4)	0.14-0.24	0.2 (4)	0.16-0.3	0.23 (4)	0.14-0.45	0.28 (4)	0.29-1	0.53 (5)	0.16-0.5	0.27 (7)
^{111}Cd	BDL-0.053	0.032 (3)	BDL-0.029	0.019 (3)	0.0035-0.043	0.022 (4)	BDL-0.048	0.048 (1)	BDL	-	BDL-0.03	0.03 (1)	BDL	-	BDL-0.059	0.059 (1)	BDL-0.049	0.048 (2)
^{118}Sn	BDL-0.078	0.065 (4)	0.062-0.096	0.077 (5)	0.084-0.12	0.1 (4)	0.042-0.062	0.053 (4)	0.063-0.15	0.097 (4)	0.054-0.071	0.064 (4)	0.09-0.67	0.27 (4)	0.039-0.068	0.049 (5)	0.032-0.053	0.044 (7)
^{121}Sb	BDL-0.0043	0.0022 (4)	BDL-0.0026	0.0024 (2)	BDL-0.0054	0.0029 (2)	BDL-0.0025	0.0024 (2)	BDL	-	BDL	-	BDL-0.023	0.019 (2)	BDL-0.012	0.0081 (2)	BDL-0.053	0.044 (7)
^{125}Te	0.097-0.31	0.23 (6)	0.15-0.28	0.21 (5)	0.015-0.49	0.16 (4)	0.27-0.4	0.35 (4)	0.13-0.28	0.23 (4)	0.23-0.58	0.41 (4)	BDL-0.52	0.35 (3)	0.21-1	0.55 (5)	0.098-0.23	0.15 (7)
^{189}Os	BDL-0.0081	0.004 (5)	0.026-0.032	0.029 (5)	0.0018-0.0078	0.0042 (4)	0.0022-0.0042	0.0031 (4)	BDL-0.0085	0.0085 (1)	0.019-0.04	0.028 (4)	BDL	-	BDL	-	BDL	-
^{193}Ir	BDL-0.0021	0.0009 (4)	BDL-0.0028	0.0016 (2)	BDL-0.00097	0.00056 (2)	BDL-0.00067	0.00067 (1)	BDL	-	BDL	-	BDL	-	BDL	-	BDL-0.0016	0.0016 (1)
^{195}Pt	BDL-0.0016	0.0013 (3)	BDL-0.0027	0.0019 (3)	BDL-0.0025	0.0015 (2)	BDL-0.0019	0.0017 (3)	BDL	-	BDL-0.0033	0.0033 (1)	BDL	-	BDL	-	BDL	-
^{197}Au	BDL-0.0064	0.0027 (5)	BDL-0.00068	0.00068 (1)	0.00077-0.0022	0.0014 (4)	BDL-0.0018	0.0018 (2)	BDL	-	BDL	-	BDL-0.099	0.099 (1)	BDL	-	BDL	-
^{202}Hg	BDL-0.11	0.082 (5)	0.016-0.076	0.046 (5)	0.036-0.1	0.071 (4)	BDL-0.077	0.066 (2)	0.064-0.1	0.084 (4)	BDL-0.062	0.062 (1)	BDL-0.29	0.29 (1)	BDL-0.074	0.094 (2)	BDL-0.073	0.076 (2)
^{205}Tl	BDL-0.011	0.0056 (2)	BDL-0.0012	0.001 (3)	BDL-0.011	0.0045 (3)	BDL-0.0033	0.0013 (3)	BDL-0.0018	0.0018 (1)	BDL-0.0052	0.0028 (3)	BDL	-	BDL-0.0086	0.0086 (1)	BDL-0.0013	0.0014 (2)
^{206}Pb	0.39-0.93	0.6 (6)	0.26-0.74	0.48 (5)	0.29-1.6	1 (4)	0.29-1.13	0.6 (4)	0.073-0.4	0.21 (4)	0.22-0.44	0.31 (4)	0.17-0.6	0.45 (4)	0.28-4.6	1.5 (5)	0.14-2.2	0.51 (7)
^{209}Bi	0.49-1.13	0.87	0.28-0.73	0.49 (5)	0.371-1.14	0.673 (4)	0.3-0.83	0.48 (4)	0.14-0.83	0.41 (4)	0.14-0.28	0.22 (4)	1-3.3	2.3 (4)	0.55-3.8	1.6 (5)	0.64-2.2	1.2 (7)
Sample no. (mineral)	TU16B (Po)		TU13 (Po)		TU7 (Po)		T34 (Po)		T44 (Po)		T3 (Po)		T2 (Po)		TU8 (Po)		T6 (Po)	
Ore body	Main		238		238		Main		Main		238		238		238		238	
Sulfide texture	DISS		MASU		MASU		DISS		DISS		MASU		MASU		MASU		MASU	
Isotope	Range	Average (n)	Range	Average (n)	Range	Average (n)	Range	Average (n)	Range	Average (n)	Range	Average (n)	Range	Average (n)	Range	Average (n)	Range	Average (n)
^{59}Co (ppm)	86.6-104.5	92 (6)	45.4-57.2	52 (4)	96.2-110	100.5 (4)	63.3-75.9	68.1 (5)	79.2-102.7	92.5 (4)	41.4-54.8	49.6 (5)	25.3-31.3	28.2 (6)	96.2-130.6	117.7 (6)	54.2-75.4	66.9 (6)
^{60}Ni	8558.6-9936.6	9234 (6)	7422.6-9083.8	8105.2 (4)	4894-5348	5132 (4)	5538.2-6846.9	6042.6 (5)	4781.7-6472.3	5645.9 (4)	4451-6715	5496 (5)	8819-12031	10945 (6)	3246-5582	4500 (6)	4629-8808	6018 (6)
^{65}Cu	BDL-0.3	0.24 (2)	BDL-2.5	1.3 (2)	BDL-0.33	0.21 (2)	0.17-0.57	0.38 (5)	0.13-0.79	0.39 (4)	0.1-0.76	0.3 (5)	BDL-0.15	0.082 (5)	BDL-0.1	0.07 (5)	BDL-0.7	0.22 (5)
^{66}Zn	BDL-0.72	0.72 (1)	BDL-0.64	0.54 (3)	BDL-0.48	0.35 (3)	BDL	-	BDL	-	BDL-0.83	0.83 (1)	BDL-0.3	0.3 (1)	BDL-0.42	0.3	BDL-5.5	2.5 (3)
^{75}As	BDL-0.048	0.048 (1)	BDL-0.062	0.062 (1)	BDL-0.65	0.39 (3)	BDL-0.08	0.078 (2)	BDL-0.026	0.026 (1)	BDL-0.058	0.051 (3)	BDL-0.165	0.067 (5)	BDL-0.064	0.035 (4)	0.03-0.06	0.04 (6)
^{77}Se	150.6-162.8	156.3 (6)	246-276	262 (4)	128.3-135.7	131.6 (4)	115.8-179.2	145.8 (5)	109-137	128 (4)	342.3-431.6	374.5 (5)	128.2-151.6	137.2 (6)	119.1-134	124.3 (6)	115.9-133.9	127.5 (6)
^{99}Ru	0.011-0.025	0.016 (6)	BDL	-	0.5-0.6	0.54 (4)	BDL-0.1	0.05 (4)	0.073-0.15	0.11 (4)	BDL-0.011	0.0089 (3)	0.012-0.52	0.38 (6)	0.22-0.29	0.24 (6)	0.23-0.29	0.25 (6)
^{103}Rh	BDL-0.043	0.043 (1)	BDL	-	BDL-0.0068	0.0047 (3)	BDL	-	BDL-0.091	0.091 (1)	BDL	-	BDL	-	BDL-0.0013	0.00099 (3)	BDL	-
^{106}Pd	BDL	-	0.0046-0.013	0.0081 (4)	BDL	-	BDL-0.039	0.039 (1)	BDL-0.015	0.0094 (2)	BDL-0.002	0.002 (1)	BDL-0.0099	0.0059 (4)	BDL-0.011	0.011 (1)	BDL-0.0021	0.0017 (2)
^{107}Ag	0.049-1.2	0.34 (6)	0.29-3.6	1.2 (4)	0.1-0.18	0.14 (4)	0.12-0.37	0.21 (5)	0.12-0.14	0.13 (4)	0.632-1.1	0.84 (5)	0.18-0.5	0.31 (6)	0.22-0.79	0.46 (6)	0.2-0.4	0.22 (6)
^{111}Cd	BDL-0.11	0.075 (2)	BDL-0.1	0.078 (3)	BDL	-	BDL-0.091	0.091 (1)	BDL-0.032	0.032 (1)	BDL-0.075	0.075 (1)	BDL-0.04	0.039 (2)	BDL-0.028	0.025 (2)	BDL-0.049	0.039 (3)
^{118}Sn	0.044-0.062	0.052 (6)	0.037-0.082	0.058 (4)	0.072-0.11	0.09 (4)	BDL-0.077	0.063 (4)	0.025-0.049	0.038 (4)	0.047-0.073	0.057 (5)	0.03-0.064	0.049 (6)	0.025-0.073	0.05 (6)	0.035-0.07	0.05 (6)
^{121}Sb	BDL-0.006	0.006 (1)	BDL-0.0063	0.005 (2)	BDL-0.0043	0.0043 (1)	BDL-0.02	0.02 (1)	BDL-0.0033	0.0033 (1)	BDL-0.0086	0.0051 (2)	BDL-0.011	0.0068 (2)	BDL-0.0051	0.0039 (2)	BDL-0.005	0.004 (2)
^{125}Te	0.11-0.61	0.28 (6)	BDL-2.9	1.1 (3)	0.17-0.31	0.26 (4)	BDL-0.36	0.24 (3)	BDL-0.12	0.1 (3)	0.16-0.3	0.22 (5)	BDL-0.11	0.088 (5)	0.13-0.3	0.21 (6)	0.15-0.6	0.31 (6)
^{189}Os	BDL	-	BDL-0.0075	0.0075 (1)	BDL-0.029	0.02 (3)	BDL	-	BDL-0.016	0.015 (2)	BDL	-	BDL-0.052	0.029 (5)	BDL-0.011	0.0084 (2)	BDL-0.0099	0.0084 (2)
^{193}Ir	BDL	-	BDL-0.0045	0.0045 (1)	BDL	-	BDL-0.00083	0.00083 (1)	BDL	-	BDL	-	BDL	-	BDL	-	BDL-0.003	0.0021 (2)
^{195}Pt	BDL-0.0057	0.0049 (2)	BDL	-	BDL	-	BDL	-	BDL-0.0027	0.0027 (1)	BDL	-	BDL	-	BDL-0.0049	0.0049 (1)	BDL	-
^{197}Au	BDL-0.066	0.066 (1)	BDL-0.011	0.0063 (2)	BDL	-	BDL-0.0073	0.0073 (1)	BDL	-	BDL-0.0049	0.0032 (2)	BDL-0.0019	0.0018 (2)	BDL-0.0049	0.0043 (2)	BDL-0.0012	0.0012 (1)
^{202}Hg	BDL-0.16	0.15 (2)	BDL-0.1	0.081 (2)	BDL-0.11	0.088 (2)	BDL-0.59	0.59 (1)	BDL-0.075	0.068 (3)	BDL-0.18	0.14 (2)	0.058-0.11	0.086 (6)	BDL-0.1	0.081 (3)	BDL-0.11	0.09 (3)
^{205}Tl	BDL-0.0098	0.0098 (1)	BDL-0.034	0.019 (2)	BDL	-	BDL-0.012	0.0072 (2)	BDL-0.0014	0.0014 (1)	BDL-0.0044	0.0044 (1)	BDL-0.0086	0.0049 (2)	BDL-0.003	0.0024 (2)	BDL-0.004	0.0022 (3)
^{206}Pb	0.088-0.54	0.26 (6)	1-5.1	2.9 (4)	0.2-0.39	0.27 (4)	0.32-3.4	1.12 (5)	0.36-0.74	0.55 (4)	0.31-2.3	1 (5)	0.26-3.2	1.1 (6)	0.12-1	0.49 (6)	0.19-1.4	0.49 (6)
^{209}Bi	0.38-1.31	0.92 (6)	1.1-2.8	1.6 (4)	0.16-0.46	0.24 (4)	0.29-2.7	0.98 (5)	0.58-0.79	0.66 (4)	1.9-5.1	3.2 (5)	0.32-4.2	1.4 (6)	0.22-0.92	0.6 (6)	0.15-0.63	0.27 (6)

Notes: Average values were calculated using measurements within detection limits, the number of samples ("n") used for each calculation are given. Abbreviations: below detection limit (BDL), pyrrhotite (Po), pentlandite (Pn), chalcopyrite (Cp), sulfarsenide solid solution (CGSS), nickeline (Nic), massive sulfides (MASU), intermediate massive sulfide (INMS), and disseminated sulfide (DISS).

Table 3 (continued) : Summary of LA-ICP-MS results for trace element chemistry of base metal sulfides, arsenides, and sulfarsenides in the Totten #2 mine

Sample no.	T9 (Pn)		T12 (Pn)		TU1 (Pn)		T7 (Pn)		T10 (Pn)		T8 (Pn)		T17 (Pn)		T26 (Pn)		TU18B (Pn)	
Ore body	238		238		238		238		Main		238		Main		238		Main	
Sulfide texture	MASU		MASU		MASU		MASU		MASU		MASU		MASU		DISS		MASU	
Isotope	Range	Average (n)	Range	Average (n)	Range	Average (n)	Range	Average (n)	Range	Average (n)	Range	Average (n)	Range	Average (n)	Range	Average (n)	Range	Average (n)
^{59}Co (ppm)	11872-13308	12874 (6)	5176-15175	11731 (6)	4589-5473	5117 (5)	13060-13755	13290 (4)	6910-7326	7115 (4)	100630-14621	13346 (4)	7304-7839	7528 (5)	9403-9815	9582 (4)	5278-6496	5752 (6)
^{65}Cu	1.8-10.8	6.5 (6)	0.29-7.3	1.9 (6)	2.5-7.3	5.1 (5)	0.0089-0.4	0.2 (4)	0.32-0.37	0.35 (4)	0.13-0.38	0.23 (4)	BDL-0.15	0.21 (2)	0.13-0.24	0.17 (4)	BDL-6.1	3.9 (5)
^{66}Zn	BDL-3	3 (1)	BDL-0.32	0.32 (1)	BDL-2.1	1.2 (3)	BDL-0.13	0.13 (1)	BDL	-	BDL	-	BDL	-	BDL	-	BDL	-
^{75}As	00.013-0.7	0.2 (6)	BDL-11	2.2 (5)	7.1-33.5	13.4 (5)	0.019-4	1.2 (4)	BDL-0.08	0.065 (3)	BDL-0.07	0.064 (2)	BDL-6.4	3.2 (4)	BDL	-	BDL-0.52	0.29 (4)
^{77}Se	101-121	108 (6)	96.1-129.4	105.2 (6)	100-126.9	110.5 (5)	103.8-142.9	116.1 (4)	178.4-191.7	182.7 (4)	98.9-105.6	103.6 (4)	146.3-229.1	181.1 (5)	90-101	95 (4)	151-206	178 (6)
^{101}Ru	1.1-1.4	1.3 (6)	1.3-1.6	1.4 (6)	1.1-2	1.4 (5)	1-1.5	1.2 (4)	1.1-1.12	1.1 (4)	1.38-1.44	1.42 (4)	1-1.1	1.1 (5)	1.2-1.5	1.3 (4)	0.8-1.2	1 (6)
^{103}Rh	BDL-0.0015	0.001 (5)	BDL-5	1.3 (4)	0.03-5	1.1 (5)	0.00031-0.0038	0.0017 (4)	BDL	-	BDL-0.0018	0.0018 (1)	BDL-0.014	0.01 (3)	BDL-0.0011	0.0011 (1)	BDL-0.014	0.0092 (2)
^{106}Pd	1.3-1.8	1.5 (6)	0.02-3.1	0.78 (6)	2.7-3.8	3.1 (5)	0.3-1.1	0.51 (4)	0.11-0.28	0.2 (4)	0.037-1	0.62 (4)	1.2-1.8	1.4 (5)	0.1-0.36	0.21 (4)	0.056-0.23	0.14 (6)
^{107}Ag	4.4-11.7	8.6 (6)	0.35-17	4.1 (6)	7.8-20	16.1 (5)	0.24-1.2	0.51 (4)	0.74-1.4	1.1 (4)	0.23-0.42	0.33 (4)	0.7-1.5	1.1 (5)	0.24-0.45	0.34 (4)	1.2-38.4	19.5 (6)
^{111}Cd	BDL-0.04	0.03 (3)	BDL-0.013	0.07 (5)	0.04-0.2	0.14 (5)	BDL-0.04	0.04 (1)	BDL	-	BDL	-	BDL-0.12	0.12 (1)	BDL	-	BDL-0.65	0.37 (2)
^{118}Sn	0.05-0.07	0.06 (6)	0.06-0.29	0.14 (6)	0.086-0.4	0.21 (5)	0.032-0.06	0.047 (4)	0.06-0.17	0.09 (4)	0.052-0.11	0.076 (4)	0.032-0.15	0.091 (4)	0.054-0.074	0.063 (4)	0.044-0.29	0.13 (6)
^{121}Sb	0.09-0.5	0.2 (6)	BDL-1	0.23 (5)	0.9-1.5	1.2 (5)	0.018-0.23	0.1 (4)	0.0093-0.088	0.038 (4)	0.014-0.39	0.16 (4)	BDL-0.43	0.34 (5)	0.036-0.12	0.079 (4)	0.035-0.32	0.15 (6)
^{125}Te	0.6-27.4	7 (6)	0.2-34	6.2 (6)	25.7-58.8	38.5 (5)	4.2-72.8	24.5 (4)	0.131-0.57	0.36 (4)	0.14-2.1	0.76 (4)	2.6-45.4	28.2 (5)	0.39-2.7	1 (4)	BDL-48.2	13.1 (5)
^{189}Os	BDL-0.016	0.0072 (3)	0.014-0.12	0.038 (6)	BDL-0.12	0.047 (4)	0.0018-0.02	0.0092 (4)	BDL	-	0.024-0.051	0.033 (4)	BDL-0.013	0.013 (1)	BDL	-	BDL-0.03	0.03 (1)
^{193}Ir	BDL-0.00045	0.00032 (3)	BDL-0.13	0.13 (1)	0.0032-0.13	0.031 (5)	BDL-0.0013	0.0009 (2)	BDL-0.01	0.01 (1)	BDL	-	BDL	-	BDL-0.0025	0.0025 (1)	BDL	-
^{195}Pt	0.0011-0.0057	0.0026 (6)	BDL-0.18	0.046 (4)	BDL-0.18	0.046 (4)	BDL-0.0073	0.0032 (3)	BDL	-	BDL	-	BDL	-	BDL	-	BDL	-
^{197}Au	0.0017-0.0094	0.0059 (6)	BDL-0.03	0.015 (2)	0.007-0.035	0.02 (5)	BDL-0.072	0.038 (4)	BDL-0.003	0.0028 (2)	BDL	-	BDL-0.06	0.036 (4)	BDL-0.003	0.003 (1)	BDL-0.015	0.022 (2)
^{202}Hg	BDL-0.12	0.06 (4)	BDL-0.07	0.05 (5)	0.032-0.13	0.08 (5)	0.0089-0.072	0.038 (4)	BDL-0.081	0.081 (1)	BDL-0.093	0.083 (2)	BDL	-	BDL	-	BDL-0.097	0.097 (1)
^{205}Tl	0.0056-0.71	0.22 (6)	BDL-6	1.4 (5)	1.6-6.9	3.9 (5)	0.015-0.28	0.18 (4)	0.0032-0.16	0.044 (4)	0.0018-1.4	0.35 (4)	BDL-0.0094	0.0094 (1)	0.043-0.38	0.15 (4)	0.019-3.8	1.7 (6)
^{206}Pb	0.16-4.9	2.5 (6)	0.08-40.6	12.4 (6)	13.9-47.3	27.2 (5)	0.37-3.6	1.6 (4)	0.23-8	3.8 (4)	0.015-8.2	2.2 (4)	0.34-0.78	0.54 (5)	0.02-1.7	0.5 (4)	2.4-625	111 (6)
^{209}Bi	0.058-1.8	0.71 (6)	0.09-8.1	2.1 (6)	2.1-15.1	6.6 (5)	0.037-1.2	0.42 (4)	0.02-2.6	1.1 (4)	0.0035-0.93	0.34 (4)	0.62-1.5	0.93 (5)	0.0028-0.4	0.25 (4)	0.34-46.2	12.3 (6)
Sample no.	TU16B (Pn)		TU13 (Pn)		TU7 (Pn)		T34 (Pn)		T44 (Pn)		T3 (Pn)		T2 (Pn)		TU8 (Pn)		T6 (Pn)	
Ore body	Main		238		238		Main		Main		238		238		239		240	
Sulfide texture	DISS		MASU		MASU		DISS		DISS		MASU		MASU		MASU		MASU	
Isotope	Range	Average (n)	Range	Average (n)	Range	Average (n)	Range	Average (n)	Range	Average (n)	Range	Average (n)	Range	Average (n)	Range	Average (n)	Range	Average (n)
^{59}Co (ppm)	5949-6881	6500 (5)	5800-7012	6409 (4)	12299-15352	14384 (6)	4673-5211	4958 (4)	6988-7987	7552 (4)	3693-4219	4035 (6)	5338-6315	5849 (6)	12363-13052	12792 (5)	9772-11412	10681 (6)
^{65}Cu	BDL-1.6	0.76 (4)	2.1-116.7	53.7 (4)	0.11-12.8	4.3 (6)	BDL-2.3	1.3 (2)	0.24-0.4	0.32 (4)	2.4-7.8	5.8 (6)	2.2-57.8	19 (6)	1.3-4.6	2.8 (5)	0.16-0.34	0.24 (6)
^{66}Zn	BDL	-	BDL-4.9	4.9 (2)	BDL-11	4.3 (4)	BDL-10.9	10.9 (1)	BDL	-	BDL	-	0.53-1.5	1 (2)	BDL-1.6	1 (2)	BDL	-
^{75}As	BDL-0.35	0.24 (3)	0.5-5.4	3 (4)	BDL-27.7	6.8 (5)	2.7-34.9	18.6 (4)	1.5-11.4	6.9 (4)	2.1-27	9.3 (6)	2.3-50.8	18.5 (6)	BDL-0.26	0.13 (4)	BDL-0.06	0.052 (2)
^{77}Se	127.6-182.9	155.6 (5)	190.1-394.8	283 (4)	117.8-126.3	121.4 (6)	115.6-144.8	127.2 (4)	114.5-133.6	123.3 (4)	294-428	346 (6)	81.7-182.2	140.6 (6)	96.7-124.4	109 (5)	111.8-152	125.9 (6)
^{101}Ru	1-1.2	1.1 (5)	0.85-1.1	0.95 (4)	1.2-1.7	1.5 (6)	0.95-1.2	1.1 (4)	1.1-1.2	1.1 (4)	0.85-1	0.92 (6)	0.99-1.9	1.4 (6)	1-1.3	1.2 (5)	1-1.3	1.2 (6)
^{103}Rh	BDL-0.0053	0.0053 (1)	BDL	-	BDL-1	0.34 (4)	BDL-0.0074	0.0074 (1)	0.0086-0.061	0.026 (4)	BDL-0.0032	0.0023 (4)	BDL-0.012	0.012 (1)	BDL	-	BDL-0.012	0.0066 (2)
^{106}Pd	1.5-1.8	1.6 (5)	0.45-2.3	1.3 (4)	0.072-1.4	0.82 (6)	0.99-1.9	1.29 (4)	2.9-4.3	3.5 (4)	1-2.3	1.7 (6)	1.2-3.1	2.2 (6)	0.4-2.3	1.1 (5)	0.0057-0.67	0.3 (6)
^{107}Ag	0.8-12.3	3.5 (5)	3.8-150.6	47.4 (4)	0.18-2.6	1.6 (6)	1.4-3.3	2 (4)	0.77-1.7	1.2 (4)	14.4-47.1	33 (6)	18.3-34.1	26.7 (6)	4.9-17	10.3 (5)	0.28-0.74	0.49 (6)
^{111}Cd	BDL	-	BDL-0.45	0.41 (3)	BDL	-	BDL-0.26	0.26 (1)	BDL-0.054	0.054 (1)	0.023-0.06	0.04 (6)	0.05-0.2	0.14 (3)	BDL-0.05	0.038 (2)	BDL-0.017-0.05	0.034 (4)
^{118}Sn	0.037-0.074	0.056 (2)	0.3-3.8	1.2 (4)	0.05-0.1	0.08 (6)	BDL-0.1	0.1 (3)	0.022-0.087	0.051 (4)	0.23-0.7	0.43 (6)	0.06-0.1	0.075 (4)	0.0.048-0.081	0.061 (5)	0.048-0.075	0.065 (6)
^{121}Sb	BDL-0.16	0.1 (4)	0.2-1.4	0.82 (4)	0.025-0.1	0.06 (6)	0.33-0.45	0.4 (4)	0.73-1.1	0.88 (4)	0.8-2.9	1.3 (6)	0.3-0.66	0.4 (6)	0.11-0.54	0.31 (5)	0.0051-0.14	0.045 (6)
^{125}Te	0.25-9.5	3.4 (5)	4-131.5	55.4 (4)	0.22-1.9	0.76 (6)	23.3-56.6	38.1 (4)	4.2-40.3	27.7 (4)	10.1-49.1	20 (6)	3.4-40	30.3 (6)	0.8-20.9	8.7 (5)	0.31-11.8	3.6 (6)
^{189}Os	BDL	-	BDL-0.021	0.02 (1)	BDL-0.13	0.055 (4)	BDL-0.043	0.043 (1)	BDL-0.025	0.018 (2)	BDL	-	BDL-0.12	0.072 (4)	BDL-0.013	0.013 (1)	BDL	-
^{193}Ir	BDL	-	BDL-0.01	0.01 (1)	BDL-0.048	0.014 (4)	BDL-0.0077	0.0077 (1)	BDL	-	BDL	-	BDL-0.0047	0.0047 (1)	BDL-0.005	0.003 (2)	BDL-0.032	0.012 (3)
^{195}Pt	BDL	-	BDL	-	BDL-0.01	0.009 (2)	BDL-0.017	0.017 (1)	BDL	-	BDL	-	BDL-0.016	0.016 (1)	BDL	-	BDL-0.0037	0.0037 (1)
^{197}Au	BDL-0.027	0.019 (4)	BDL-0.046	0.037 (3)	BDL-0.11	0.06 (2)	BDL-0.015	0.015 (1)	BDL-0.0083	0.0083 (1)	0.032-0.12	0.058 (6)	BDL-0.02	0.014 (3)	BDL-0.0082	0.0052 (3)	BDL-0.0022	0.0022 (1)
^{202}Hg	BDL-0.18	0.15 (2)	0.36-1.2	0.77 (3)	BDL-0.11	0.081 (3)	BDL	-	BDL	-	BDL-0.14	0.098 (5)	BDL-0.65	0.34 (3)	BDL-0.18	0.14 (3)	BDL-0.079	0.075 (3)
^{205}Tl	0.006-0.18	0.055 (5)	0.91-4.8	2.8 (4)	BDL-0.33	0.077 (5)	0.015-0.44	0.13 (4)	0.0089-0.096	0.034 (4)	8-18.2	14.3 (6)	0.42-5.3	3.1 (6)	0.007-0.13	0.061 (5)	BDL-0.29	0.072 (5)
^{206}Pb	0.21-8.5	2 (5)	21-48.5	32.4 (4)	0.074-5.3	1.3 (6)	0.06-1.4	0.13 (4)	0.19-0.4	0.29 (4)	60.8-108.9	86 (6)	9.5-46.4	22.3 (6)	0.063-1	0.6 (5)	0.046-6.8	1.7 (6)
^{209}Bi	0.054-2.8	0.91 (5)	5.8-23.2	13.5 (4)	0.028-1.5	0.48 (6)	0.083-1.2	0.42 (4)	0.065-0.48	0.28 (4)	29-71.9	54.9 (6)	1.9-22.8	13.3 (6)	0.16-0.6	0.31 (5)	0.009-1	0.29 (6)

Notes: Average values were calculated using measurements within detection limits, the number of samples ("n") used for each calculation are given. Abbreviations: below detection limit (BDL), pyrrhotite (Po), pentlandite (Pn), chalcopyrite (Cp), sulfarsenide solid solution (CGSS), nickeline (Nic), massive sulfides (MASU), intermediate massive sulfide (INMS), and disseminated sulfide (DISS).

Table 3 (continued) : Summary of LA-ICP-MS results for trace element chemistry of base metal sulfides, arsenides, and sulfarsenides in the Totten #2 mine

Sample no.	T9		T12		TU1		T7		T10		T8		T17		T26		TU18B	
Ore body	238		238		238		238		Main		238		Main		238		Main	
Sulfide texture	MASU		MASU		MASU		MASU		MASU		MASU		MASU		DISS		MASU	
Isotope	Range	Average (n)	Range	Average (n)	Range	Average (n)	Range	Average (n)	Range	Average (n)	Range	Average (n)	Range	Average (n)	Range	Average (n)	Range	Average (n)
^{59}Co (ppm)	0.17-62	18.2 (4)	0.15-1.6	0.57 (5)	0.13-0.25	0.21 (5)	0.23-1.3	0.75 (4)	0.058-0.086	0.071 (4)	0.18-3.8	1.3 (4)	0.068-0.11	0.087 (4)	0.091-0.78	0.44 (5)	0.078-2	1 (2)
^{60}Ni	22.6-271	86.7 (4)	31.4-183.3	71.6 (5)	51.1-64.3	58 (5)	29.4-72.3	46.4 (4)	19.2-24.6	21.2 (4)	29.1-211	83.9 (4)	25.9-32.9	28.9 (4)	9.6-32	23.1 (5)	24.1-176	100 (2)
^{66}Zn	228-366.2	305.1 (4)	250.4-300.2	267.3 (5)	347.5-682.4	441.9 (5)	254.2-325.5	283.3 (4)	266.6-339.6	296.4 (4)	224.1-470.6	334.2 (4)	282.4-368.7	320.3 (4)	258.9-395.1	346.9 (5)	232.3-417.2	324,8 (2)
^{75}As	0.0028-0.18	0.071 (4)	BDL-0.066	0.028 (3)	BDL-0.026	0.021 (3)	BDL-0.056	0.056 (1)	BDL-0.44	0.31 (2)	BDL-0.034	0.034 (1)	BDL-0.2	0.2 (1)	BDL-0.048	0.048 (1)	BDL	-
^{77}Se	83.3-138	104.9 (4)	99.3-128.6	110 (5)	90.1-103.4	98.4 (5)	111-146.9	120.3 (4)	94.9-238.2	174.5 (4)	105.8-129.5	116.4 (4)	102.3-184.4	142 (4)	88.4-99.8	96.5 (5)	156.3-235.5	196 (2)
^{99}Ru	0.18-0.29	0.22 (4)	0.18-0.2	0.19 (5)	0.18-0.2	0.19 (5)	0.2-0.23	0.21 (4)	0.22-0.28	0.23 (4)	0.2-0.23	0.21 (4)	0.16-0.29	0.23 (4)	0.17-0.44	0.3 (5)	0.1-0.24	0.17 (2)
^{106}Pd	0.11-0.15	0.13 (4)	0.14-0.18	0.15 (5)	0.62-0.91	0.73 (5)	0.09-0.11	0.1 (4)	0.39-0.55	0.47 (4)	0.1-0.27	0.17 (4)	0.45-0.61	0.53 (4)	0.2-0.44	0.3 (5)	0.18-0.46	0.32 (2)
^{107}Ag	3-5.4	4.3 (4)	0.86-1.6	1.2 (5)	3.9-13.4	8.9 (5)	1.9-2.7	2.2 (4)	0.94-2.2	1.5 (4)	0.92-2.4	1.6 (4)	1.6-2.3	1.9 (4)	10.9-17.3	14.1 (5)	1.3-1.5	1.4 (2)
^{111}Cd	4.2-7.1	5.7 (4)	6.7-8.9	7.9 (5)	31.2-51	39.1 (5)	4.2-4.5	4.3 (4)	23.9-36.2	28.8 (4)	6.1-12.9	9.5 (4)	18.8-25.3	22.1 (4)	10-23.4	16 (5)	15.3-32.5	23.9
^{118}Sn	2.6-17.1	8.3 (4)	2.9-13.4	8.1 (5)	29.7-56.5	43.1 (5)	1.2-1.4	1.3 (4)	6.8-22.1	14.7 (4)	4.4-10.5	6.8 (4)	33.3-65.8	52.3 (4)	5.5-19.4	12.4 (5)	0.77-1.1	0.95 (2)
^{121}Sb	0.3-0.94	0.6 (4)	0.034-0.11	0.072 (5)	0.0075-0.022	0.018 (5)	0.076-0.17	0.11 (4)	0.024-0.44	0.21 (4)	0.037-0.18	0.12 (4)	0.25-1.2	0.7 (4)	0.018-0.37	0.1 (5)	0.17-0.26	0.21 (2)
^{125}Te	0.9-3.5	1.9 (4)	2.1-4.5	3 (5)	2.3-7.2	4.8 (5)	3-6.3	4.9 (4)	0.2-5	2.2 (4)	2-4.2	2.8 (4)	0.8-3.1	1.6 (4)	0.38-10	5.7 (5)	BDL-0.66	0.66 (1)
^{189}Os	BDL	-	BDL-0.0011	0.0011 (1)	BDL-0.0029	0.0021 (4)	BDL-0.009	0.006 (3)	BDL	-	BDL	-	BDL-0.024	0.024 (1)	BDL-0.014	0.0089 (2)	BDL	-
^{193}Ir	BDL-0.18	0.059 (3)	BDL-0.00084	0.00048 (2)	BDL-0.00042	0.00034 (2)	BDL-0.00029	0.00029 (1)	BDL	-	BDL	-	BDL	-	BDL	-	BDL	-
^{195}Pt	BDL-0.02	0.008 (3)	BDL-0.00046	0.00046 (1)	BDL-0.0031	0.0022 (3)	BDL-0.00053	0.00048 (2)	BDL	-	BDL	-	BDL-0.049	0.049 (1)	BDL	-	BDL	-
^{197}Au	0.01-0.03	0.017 (4)	0.0094-0.13	0.051 (5)	0.013-0.0031	0.035 (5)	0.004-0.082	0.027 (4)	BDL-0.03	0.016 (2)	0.01-0.063	0.039 (4)	BDL-0.06	0.033 (3)	0.022-0.047	0.032 (5)	0.04-0.41	0.23 (2)
^{202}Hg	BDL-0.04	0.04 (1)	0.031-0.044	0.036 (5)	0.041-0.082	0.062 (5)	BDL-0.049	0.039 (2)	BDL	-	BDL-0.092	0.087 (2)	BDL	-	BDL-0.085	0.067 (2)	BDL	-
^{205}Tl	0.023-0.24	0.086 (4)	BDL-0.025	0.0075 (4)	BDL-0.0045	0.0016 (4)	BDL-0.0013	0.00083 (3)	BDL-0.006	0.006 (1)	BDL-0.16	0.056 (3)	0.0098-0.041	0.021 (4)	BDL-0.042	0.015 (3)	BDL-0.026	0.026 (1)
^{206}Pb	13.8-46.5	27.1 (4)	4.6-13.2	7.4 (5)	1.4-6.9	3.3 (5)	3-9.7	7.1 (4)	0.88-7.7	4.7 (4)	4.7-14.5	9 (4)	8.1-30.8	16.8 (4)	1-12.1	3.6 (5)	9.4-9.5	9.5 (2)
^{209}Bi	2.8-8.9	4.5 (4)	1-2.2	1.3 (5)	0.75-2	1.2 (5)	0.74-1.7	1.3 (4)	0.11-1.5	0.77 (4)	0.74-2.7	1.6 (4)	3.6-14.1	7.8 (4)	0.6-3.7	1.4 (5)	5.8-6.3	6.1 (2)
Sample no.	TU16B		TU13		TU7		T34		T44		T3		T2		TU8		T6	
Ore body	Main		238		238		Main		Main		238		238		239		240	
Sulfide texture	DISS		MASU		MASU		DISS		DISS		MASU		MASU		MASU		MASU	
Isotope	Range	Average (n)	Range	Average (n)	Range	Average (n)	Range	Average (n)	Range	Average (n)	Range	Average (n)	Range	Average (n)	Range	Average (n)	Range	Average (n)
^{59}Co (ppm)	0.03-0.54	0.25 (6)	0.14-0.42	0.27 (4)	0.12-0.66	0.3 (4)	0.092-0.4	0.25 (4)	0.13-0.17	0.15 (4)	0.098-4.5	0.93 (6)	0.13-0.24	0.18 (6)	0.23-1	0.53 (4)	0.12-5.4	1 (6)
^{60}Ni	22.5-44	35.9 (6)	43-162.8	77.3 (4)	23.8-59.5	36.4 (4)	31.2-42.9	37.6 (4)	28-50.6	37.5 (4)	39.5-814.4	178.8 (6)	40-60.2	53.6 (6)	27.9-63.5	45.7 (4)	9.7-23.5	15.7 (6)
^{66}Zn	221-449	364 (6)	324.5-693.5	477.9 (4)	270.5-444.2	349 (4)	355-482	394 (4)	337-437	386 (4)	243.7-590	393.1 (6)	280.3-466.9	348.2 (6)	277.6-414	328.1 (4)	273-515.5	416.5 (6)
^{75}As	BDL	-	BDL-0.021	0.017 (2)	BDL-0.021	0.021 (1)	BDL	-	BDL-0.029	0.029 (1)	BDL-2.4	0.08 (4)	BDL-0.03	0.021 (3)	0.018-0.051	0.03 (4)	BDL-0.09	0.09 (1)
^{77}Se	138.6-156.4	144.7 (6)	219.3-233.5	226.6 (4)	122-164	139.6 (4)	95.8-106	102.8 (4)	101.7-113.2	105.7 (4)	319.5-340	330.6 (6)	97.4-137.7	114.8 (6)	110.2-125.4	118 (4)	114-218.8	155.5 (6)
^{99}Ru	0.18-0.23	0.21 (6)	0.12-0.21	0.17 (4)	0.16-0.21	0.2 (4)	0.2-0.21	0.21 (4)	0.17-0.21	0.19 (4)	0.18-0.22	0.2 (6)	0.17-0.2	0.19 (6)	0.16-0.22	0.2 (4)	0.19-0.31	0.24 (6)
^{106}Pd	0.2-0.29	0.26 (6)	0.65-1.2	0.1 (4)	0.17-0.25	0.21 (4)	0.56-0.69	0.61 (4)	0.3-0.39	0.34 (4)	0.34-1.1	0.69 (6)	0.44-0.71	0.59 (6)	0.12-2	0.15 (4)	0.18-0.39	0.3 (6)
^{107}Ag	0.49-0.9	0.7 (6)	9.4-17.4	13.1 (4)	0.78-1.3	1.1 (4)	3.5-10.5	7.3 (4)	2-5.7	4 (4)	5.1-10.3	7.6 (6)	2.9-6.9	4.5 (6)	2.1-12.2	5.2 (4)	5.3-10	6.6 (6)
^{111}Cd	13.3-17.6	15.8 (6)	42.9-75.4	61.8 (4)	12.3-15.9	13.8 (4)	32.6-38.6	35 (4)	15.7-20.3	18.2 (4)	15.9-68.8	40.7 (6)	23.2-41.6	32.7 (6)	6.9-12.7	9.4 (4)	14.2-22.9	19.1 (6)
^{118}Sn	0.6-2	1.2 (6)	20.9-26.7	22.8 (4)	5.1-17.7	11.9 (4)	19.1-23.4	21.4 (4)	5.1-7.2	6 (4)	40.1-119.4	81.3 (6)	2.5-2.9	2.8 (6)	4.2-9.5	6.5 (4)	0.66-1.2	0.98 (6)
^{121}Sb	0.09-0.51	0.27 (6)	0.012-0.033	0.023 (4)	0.044-0.16	0.094 (4)	0.014-0.064	0.031 (4)	0.021-0.054	0.03 (4)	0.087-0.21	0.16 (6)	BDL-0.0084	0.0052 (5)	0.14-0.28	0.22 (4)	0.04-0.11	0.077 (6)
^{125}Te	0.26-1.5	0.88 (6)	4.4-17	10.4 (4)	1.3-4.5	2.6 (4)	5.6-13.7	9.8 (4)	3.1-8	5.4 (4)	0.53-10	4.3 (6)	1.5-7.4	3.2 (6)	1.2-7.3	4.2 (4)	1.4-15.4	4.6 (6)
^{189}Os	BDL-0.0059	0.0059 (1)	BDL-0.005	0.005 (1)	BDL	-	BDL	-	BDL	-	BDL	-	BDL	-	BDL	-	BDL	-
^{193}Ir	BDL-0.0015	0.0015 (1)	BDL-0.00094	0.00094 (1)	BDL	-	BDL	-	BDL-0.18	0.18 (1)	BDL-0.0017	0.0017 (1)	BDL	-	BDL-0.0011	0.0011 (1)	BDL	-
^{195}Pt	BDL	-	BDL	-	BDL	-	BDL	-	BDL	-	BDL	-	BDL	-	BDL	-	BDL	-
^{197}Au	0.0082-0.025	0.017 (6)	0.024-0.067	0.042 (4)	BDL-0.13	0.059 (3)	0.0088-0.14	0.062 (4)	0.0092-0.067	0.033 (4)	0.11-0.25	0.18 (6)	BDL-0.0076	0.0038 (4)	0.02-0.07	0.05 (4)	BDL-0.034	0.03 (2)
^{202}Hg	BDL-0.33	0.19 (2)	BDL-0.067	0.056 (2)	BDL-0.07	0.07 (1)	BDL-0.068	0.068 (1)	BDL-0.06	0.06 (1)	BDL-0.16	0.078 (5)	BDL-0.18	0.11 (5)	BDL-0.093	0.093 (1)	0.09-0.72	0.4 (2)
^{205}Tl	0.002-0.042	0.011 (6)	BDL-0.0022	0.0021 (2)	BDL-0.0023	0.0023 (1)	BDL-0.0027	0.0016 (3)	0.0016-0.0033	0.002 (4)	0.00088-0.025	0.0067 (6)	BDL	-	BDL-0.026	0.012 (4)	BDL-0.021	0.015 (2)
^{206}Pb	3.6-9.3	5.9 (6)	1-3.5	2.3 (4)	4.1-12.8	8.1 (4)	1.2-3.8	2.1 (4)	2.1-14.7	6.9 (4)	7-15.9	11 (6)	2-3.2	2.4 (6)	5.9-11.8	9.9 (4)	6.1-16.7	11.6 (6)
^{209}Bi	1.3-5.9	3.1 (6)	1.2-2.9	2 (4)	0.9-1.6	1.3 (4)	0.27-1.5	0.7 (4)	0.77-1.2	0.93 (4)	6.4-16.8	10.6 (6)	1.3-3.3	2 (6)	0.9-1.6	1.3 (4)	0.56-2.4	1.6 (6)

Notes: Average values were calculated using measurements within detection limits, the number of samples ("n") used for each calculation are given. Abbreviations: below detection limit (BDL), pyrrhotite (Po), pentlandite (Pn), chalcopyrite (Cp), sulfarsenide solid solution (CGSS), nickeline (Nic), massive sulfides (MASU), intermediate massive sulfide (INMS), and disseminated sulfide (DISS).

Table 3 (continued) : Summary of LA-ICP-MS results for trace element chemistry of base metal sulfides, arsenides, and sulfarsenides in the Totten #2 mine

Sample no.	T10 (CGSS)		T131 (CGSS)		T34 (CGSS)		TU4B (CGSS)		T131 (Nic)		T34 (Nic)		TU11 (Nic)		MASS-1 (n=71)			Po726 (n=71)			PGE-B (n=4)		
Ore body	Main		N/A		Main		238		N/A		Main		238		Average	1σ	Accepted values	Average	1σ	Accepted values	Average	1σ	Accepted values
Sulfide texture	MASU						DISS						DISS										
Isotope	Range	Average (n)	Range	Average (n)	Range	Average (n)	Range	Average (n)	Range	Average (n)	Range	Average (n)	Range	Average (n)									
^{34}S (ppm)		-		-		-		-	1678-5498	2698 (11)	628.8-11925	2216 (10)	-	1561 (1)									
^{57}Fe		-		-		-		-	BDL-159.6	75 (6)	73.2-127.2	103.2 (10)	-	125.5 (1)									
^{59}Co		-		-		-		-	569-926	737 (11)	643.3-895.7	760.3 (10)	-	1139.4 (1)									
^{65}Cu	0.41-0.74	0.56 (4)	89.9-3404	1206 (3)	0.14-916	143 (13)	0.12-915.7	176.3 (6)	0.23-2.2	0.75	BDL-1.8	0.64 (7)	-	0.69 (1)									
^{66}Zn	BDL-0.32	0.31 (2)	BDL-22.4	11.5 (2)	0.15-3.3	0.81 (11)	BDL-2.4	1.1 (4)	BDL-0.17	0.17 (1)	BDL-6.6	4.2 (3)	-	0.74 (1)									
^{77}Se	282.9-687.2	524.8 (4)	578.5-854.3	746.3 (3)	242.4-584.4	422.3 (16)	222.2-320.7	267.5 (6)	87.1-226	132.3 (11)	31.3-46.9	36.6 (10)	-	38.4 (1)									
$^{101/99}$Ru*	0.86-2.2	1.2 (4)	0.83-0.9	0.86 (3)	0.82-11.6	5 (16)	0.42-0.72	0.58 (6)	0.45-3.5	2 (11)	0.5-1.2	0.89 (10)	-	0.23 (1)									
^{103}Rh	0.11-8.6	3.4 (4)	0.035-0.28	0.16 (3)	0.017-63.1	11.2 (16)	0.0023-0.051	0.022 (6)	BDL-0.59	0.31 (10)	0.0056-0.42	0.15 (10)	-	0.011 (1)									
^{106}Pd	415.6-1226.5	812.8 (4)	39.4-118.3	66.3 (3)	243.7-1029	675.1 (16)	732.8-1960	1354 (6)	4.7-18.3	8.6 (11)	1.3-2.6	1.7 (10)	-	0.72 (1)									
^{107}Ag	0.73-0.43	0.23 (4)	145.7-1215.2	535.4 (3)	BDL-6	0.96 (15)	0.45-450.1	81.2 (6)	BDL-0.27	0.13 (10)	0.064-0.13	0.097 (10)	-	0.31 (1)									
^{111}Cd	0.052-0.069	0.061 (2)	0.23-1.2	0.71 (3)	BDL-0.2	0.11 (13)	BDL-0.47	0.19 (5)	BDL-0.52	0.17 (7)	BDL-0.053	0.036 (5)	-	0.1 (1)									
^{118}Sn	0.059-0.15	0.096 (4)	0.083-0.4	0.27 (3)	0.019-0.23	0.11 (16)	0.041-0.12	0.079 (6)	BDL-0.24	0.16 (8)	0.074-0.15	0.098 (10)	-	0.051 (1)									
^{121}Sb	492.5-2860	1858.3 (4)	866.7-1424.3	1140.2 (3)	439.2-1698	986.3 (16)	538.1-923.1	732.7 (6)	4228-6429	4970.7 (11)	4573-6595	5127 (10)	-	4287.4 (1)									
^{125}Te	19.3-78	54.4 (4)	189.8-3070.6	1328.7 (3)	15.9-132.5	52.1 (16)	43.8-1030	393.3 (6)	252.5-793	401 (11)	268.8-575	365.6 (10)	-	284 (1)									
^{189}Os	BDL-0.9	0.9 (1)	BDL-0.13	0.13 (1)	0.07-2.6	0.89 (16)	BDL	-	0.088-0.73	0.48 (11)	0.056-1	0.22 (10)	-	BDL									
^{193}Ir	BDL-11.3	11.3 (1)	BDL-0.022	0.022 (1)	0.055-3.4	12.8 (16)	BDL	-	0.04-0.86	0.23 (11)	0.062-1.2	0.23 (10)	-	BDL	64.4	2.9	63.5						
^{195}Pt	1.6-27.8	13.9 (4)	0.18-0.88	0.63 (3)	0.2-33.6	12.8 (16)	BDL-17.7	16.5 (6)	BDL-0.073	0.032 (5)	BDL-0.013	0.01 (2)	-	BDL	54.3	3.8	61.8						
^{197}Au	BDL-4	1.4 (3)	2.5-325.5	119.7 (3)	BDL-0.32	0.051 (13)	0.082-61.6	16.5 (6)	4.5-10	7 (11)	3.7-6.8	4.9 (10)	-	3.5 (1)	51.6	4.4	48.4	40.4	3.9	45.8	242.9	21.4	212-274
^{202}Hg	BDL-0.18	0.18 (1)	BDL-0.72	0.72 (1)	BDL-0.34	0.21 (10)	BDL-0.15	0.11 (3)	BDL-0.19	0.19 (1)	BDL-0.21	0.11 (7)	-	0.18 (1)									
^{205}Tl	BDL-0.0021	0.0021 (2)	BDL-0.35	0.19 (2)	BDL-0.12	0.03 (7)	BDL-0.057	0.023 (5)	BDL-0.026	0.026 (1)	BDL-0.0064	0.0051 (2)	-	BDL									
^{206}Pb	0.11-2	0.7 (4)	26.6-3095	1059 (3)	0.01-375.3	32.8 (16)	0.97-21.4	10 (6)	BDL-0.32	0.11 (8)	BDL-0.038	0.021 (7)	-	0.2 (1)									
^{209}Bi	2.9-52.1	26 (4)	231.8-2381	1645 (3)	2-170.8	32 (16)	9.2-2871	601.6 (6)	2.6-15.3	7.3 (11)	4.5-21.2	10.5 (10)	-	8.7 (1)									

Notes: Average values were calculated using measurements within detection limits, the number of samples ("n") used for each calculation are given. Abbreviations: below detection limit (BDL), pyrrhotite (Po), pentlandite (Pn), chalcopyrite (Cp), sulfarsenide solid solution (CGSS), nickeline (Nic), massive sulfides (MASU), intermediate massive sulfide (INMS), and disseminated sulfide (DISS). *^{101}Ru used for CGSS due to Co interference on ^{99}Ru. MASS-1, Po726, PGE-B are calibration standards used in this study.

Less common are minute (μm scale) pentlandite exsolution lamellae (pentlandite "flames"), which typically occur in pyrrhotite along fractures and grain boundaries with pentlandite. Grains of pentlandite in DISS ore types are typically anhedral and occur within sulfide blebs or veins. Argentopentlandite was also observed as narrow (μm) veins in chalcopyrite (Figure 5F). Similar to pyrrhotite, pentlandite may also host inclusions of chalcopyrite, pyrrhotite, and a variety of accessory phases. The key findings of the LA-ICP-MS analysis of pentlandite are summarized here, however the complete results of the analyses can be found in the Appendix A5. Pentlandite contains significant levels of Co (3693-15352 ppm, 8839 ppm average; Table 3), Se (82-428 ppm, 152 ppm average), as well as elevated Pd (0.04-4.26 ppm, 1.26 ppm average), and Ru (0.8-4.6 ppm, 2.3 ppm average). It is important to note that the elevated concentrations of Co and Pd in pentlandite are the result of the incorporation of these metals into its structure (through substitution), and not by the occurrence of micro-inclusions within pentlandite (which is indicated by the consistency of the analyses). The Co content of pentlandite was also independently evaluated using SEM-EDS in order to ensure the accuracy of the calibration standards (in sample T2: SEM analyses give 0.4-0.6 wt% Co, 0.5 wt% Co average, n= 4; LA-ICP-MS analyses give 0.5-0.6 wt% Co, 0.58 wt% Co average, n=6). The SEM-EDS values agree with those measured using the MASS-1 calibration. The concentrations of Te, Bi, Pb, and Ag in pentlandite (as measured by LA-ICP-MS) vary widely in both ore bodies. This range can be contributed to micro-inclusions in pentlandite which were characterized by SEM (hessite, galena, and Bi-Te phases). The concentrations of the other metals (including Au, Pt, As, Hg, and Cd) are low and are typically below detection limits.

4.2.3 Chalcopyrite

Chalcopyrite is the dominant Cu mineral found at Totten. Although typically less abundant in most MASU and INMS ore samples than pentlandite and pyrrhotite, chalcopyrite-rich (>30% by volume) samples of all ore types can occur in the periphery of the Ni ores (near the contact with the silicate host rocks). Chalcopyrite typically occurs interstitial to pyrrhotite and pentlandite (by infilling fractures or cavities, Figure 5B, D, and E) and is inferred to post-date the crystallization of pyrrhotite and pentlandite. In fact, examples of the resorption of pentlandite by chalcopyrite have been observed (Figure 5C). Sphalerite is primarily hosted in chalcopyrite as anhedral inclusions, but may also occur in fractures and vacancies formed in the pyrrhotite and pentlandite phases. Sphalerite is enriched in Cd (concentrations in sphalerite were detectable via EDS). Inclusions of pyrrhotite, pentlandite, sulfides, silicates, and the other accessory phases are common in chalcopyrite. Chalcopyrite contains significant levels of Zn (28-693 ppm, 353 ppm average; Table 3) as well as Se (83-507 ppm, 150 ppm average), Cd (bdl-75.4 ppm, 23 ppm average) and Sn (0.55-119.4 ppm, 18 ppm average). Elevated and sometimes variable concentrations of Ni, Ag, Te, Bi, and Pb are likely not present as solid state substitutions, but are caused by micro-inclusions (of pentlandite, hessite, galena, etc.). Other analyzed metals (including PGE and As) often show concentrations that are low or below detection limits. Although still low, the average concentration of Au is slightly higher in chalcopyrite than in the other sulfides (0.05 ppm average). For the complete results of the LA-ICP-MS analysis of chalcopyrite, please refer to Appendix A6.

4.2.4 Nickeline

Nickeline (NiAs) is typically rare to absent in MASU and INMS ore types, where it occurs as anhedral inclusions within the base metal sulfides, (predominantly in pyrrhotite,

see Tables 4 and 5) as well as the sulfarsenides (cobaltite- gersdorffite-glaucodot solid solution). Euhedral inclusions of nickeline within pyrrhotite and pentlandite are rare but have been observed (Figure 6B). In DISS ore types, nickeline may be more abundant (with respect to modal abundance) and forms anhedral blebs in the silicate host rocks, or within the base metal sulfides (Figure 6A and C). Nickeline may also form anhedral grains within sulfide veins and may in some cases represent the dominant mineral present in such veins (Figure 6F). The dominant host for nickeline in DISS ore types is silicate gangue, typically immediately adjacent to sulfide veins/blebs (see Table 6). Nickeline typically occupies the margins of sulfide blebs and veins. In one instance, nickeline blebs in a sulfide vein have rims of euhedral sulfarsenide aggregates (Figure 6C). Graphic intergrowth of nickeline with chalcopyrite has been observed within South Range sulfarsenides (Hawley and Stanton, 1962). This form of graphic texture has been reported in the Worthington area before by Lausen (1930), however it was also observed within the sulfarsenides in this study (Figure 6E). Nickeline contains significant Co (569-3820 ppm, 899 ppm average; Table 3), Sb (2118-6195 ppm, 4885 ppm average), Te (252-793 ppm, 374 ppm average), as well as elevated Se, Ru, Pd, and Au. Deleterious metals (with the exception of As) and Pt are present only in low concentrations. The Sb content of nickeline was also independently evaluated using SEM-EDS in order to test the accuracy of the calibration standard (in sample TU11: SEM-EDS analyses give 0.62-0.8 wt% Sb, 0.71 wt% Sb average, n=4; LA-ICP-MS analysis gives 0.43 wt% Sb, n=1). The evaluation shows that the MASS-1 calibration is in agreement with the SEM-EDS results. Some studies on the Worthington area have reported maucherite ($Ni_{11}As_8$: Lausen, 1930;

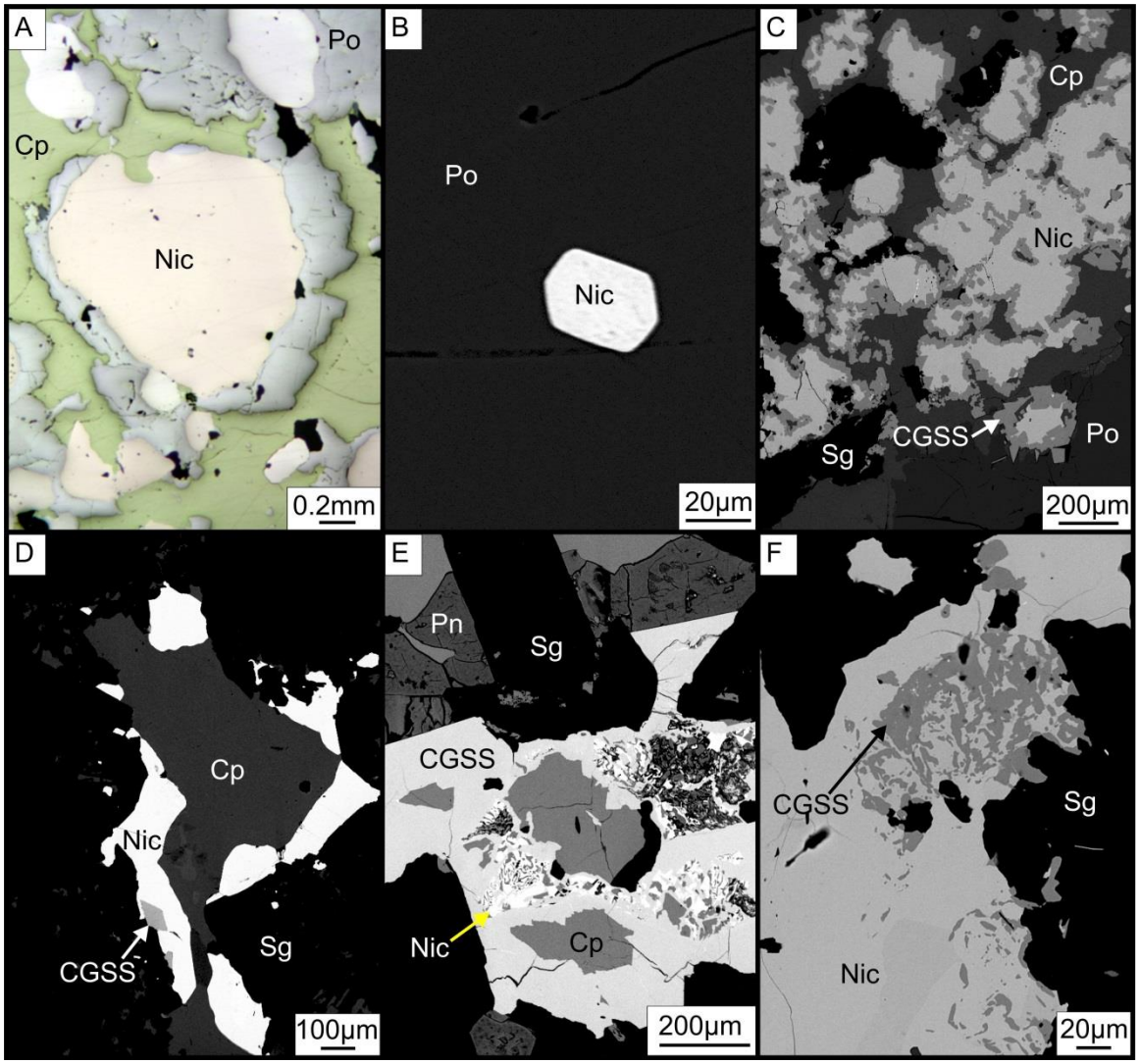

Figure 6. Photomicrographs of nickeline: (A) nickeline (Nic) blebs in base metal sulfides; (B) euhedral nickeline (Nic) hosted in pyrrhotite (Po); (C) nickeline blebs (Nic) in base metal sulfides mantled by small euhedral-subhedral sulfarsenide crystals (CGSS), possibly grown by reactions along the nickeline-sulfide interface; (D) a sulfide bleb with nickeline (Nic) and sulfarsenides (CGSS) occurring exclusively along its margins hosted in silicate gangue (Sg); (E) graphic intergrowth of chalcopyrite (Cp) and nickeline (Nic) within a sulfarsenide grain (CGSS) hosted in silicate gangue (Sg); and (F) reabsorption of sulfarsenides (CGSS) by nickeline (Nic) hosted in silicate gangue (Sg).

Table 4: Accessory phase host mineral associations shown as volume percent of the total area of "n" grains in massive sulfides

Mineral	altaite	CGSS	electrum	froodite	galena	hedleyite	hessite	hollingworthite-irarsite	michenerite	molybdenite	nickeline	pilsenite	sperrylite	tarkianite	tellurobismuthite	tsumoite	ungavaite
(number of grains)	21*	272*	1*	10*	535*	1*	147*	81*	12*	16*	10*	19*	7*	8*	152*	161*	1*
CGSS					0.4			59.2					17.4		0.1		
CGSS/Cp								7							0.2		
CGSS/Pn								9.4									
Cp	24.8	31.2		41.9	22.1		18.1	1.5	50	19.9		25		61.7	15.1	4.1	
Cp/Pn		0.1													1.3		
Cp/Po		0.3			0.6		0.1								1.2		
Cp/Sg					7.9		0.3									0.2	
Cp/Sph					0.9												
Mo/Cp															5.8		
Pn	16.7	6			12.5		14.7	2.1	1.4	7.3					20.2	13.6	
Pn/Po	5.2	0.4			3.5		7.8					25				1.9	
Pn/Sg							6.6			20					2.8		
Po	53.3	59.4		24.8	47		52.4	20.8	48.6	35.6	66.7	42.8	62.6	38.3	51	70.8	100
Po/CGSS															2.3	0.1	
Po/Sg		2.6								17.2	33.3	3.7				3.4	
Sg			100	33.3	2.1	100						3.5	20			5.9	
Sph					3												
Total	100	100	100	100	100	100	100	100	100	100	100	100	100	100	100	100	100

Notes: abbreviations stand for sulfarsenide solid solution (Cgss), chalcopyrite (Cp), pentlandite (Pn), pyrrhotite (Po), chalcopyrite (Cp), silicate gangue (Sg), sphalerite (Sph), and molybdenite (Mo). Accessory grains which have host associations in the form of A/B occur along a mutual grain boundary between these minerals. Numeric values represent the % of the total volume of an accessory phase in a specific host association.

Table 5: Accessory phase host mineral associations shown as volume percent of the total area of "n" grains in semi massive sulfides

Mineral (number of grains)	altaite 7*	CGSS 200*	electrum 2*	froodite 23*	galena 405*	hedleyite 5*	hessite 149*	hollingworthite-irarsite 19*	michenerite 6*	molybdenite 9*	nickeline 70*	pilsenite 163*	sperrylite 34*	tellurobismuthite 151*	tsumoite 199*
CGSS					15.7			66.6			28.2	0.5		6	0.2
Cp	33.3	8.2			2.5		19.4		33.3		0.3		0.4	6.4	19.4
Cp/Cgss															
Cp/Po					0.1		1.1							2.4	
Cp/Sg		0.1			6.1		3.1				0.9	2.8	4.1	6.1	6.3
Cp/Sph															
Cp/telluro															
Pn		35.4		47.4	9		31.1	2.9	44.5	20.2		1.8	21	11.4	18.5
Pn/Cp		0.9												0.2	
Pn/Sg		2.3								33.3	0.1	2.5		2.5	1.3
Po	33.3	41	50		28.2	33.3	39	25.9		29.8	66.7	62.2	50.6	37.4	18.6
Po/CGSS							0.3						1.2		1.7
Po/Pn		1.7					3.1	4.6						1.6	0.9
Po/Pn/Cgss													0.7		
Po/Sg		9.5			8		2.5			16.7		3		19.7	14.1
Po/Sperry		0.1													
Po/Sph							0.4								
Sg	33.4	0.8	50	52.6	30.4	66.7			22.2		3.8	27.2	22	6.3	19
Total	100	100	100	100	100	100	100	100	100	100	100	100	100	100	100

Notes: abbreviations stand for sulfarsenide solid solution (Cgss), chalcopyrite (Cp), pentlandite (Pn), pyrrhotite (Po), chalcopyrite (Cp), silicate gangue (Sg), sphalerite (Sph), and molybdenite (Mo). Accessory grains which have host associations in the form of A/B occur along a mutual grain boundary between these minerals. Numeric values represent the % of the total volume of an accessory phase in a specific host association.

Table 6: Accessory phase host mineral associations shown as volume percent of the total area of "n" grains in disseminated sulfides

Mineral (number of grains)	altaite 16*	CGSS 2885*	electrum 47*	froodite 53*	galena 625*	hedleyite 14*	hessite 201*	hollingworthite-irarsite 4*	michenerite 33*	nickeline 638*	pilsenite 58*	sperrylite 4*	tellurobismuthite 321*	tsumoite 309*	ungavaite 65*
CGSS	25		11.7	20.8	5.6	50	16.7	65.3	28.6	14.5	50		12.5	14	58.6
CGSS/Nic															0.3
CGSS/Sg															
Cp	9.7	12.8	13.3	10.2	12		0.3	23.8		6.5			1.7		
Cp/CGSS			0.9	3.7			0.1	10.9		0.4				0.2	3.4
Cp/Nic	7.4	1.5	0.1				8.5								4.3
Cp/Po/Sg									1.4	1.9					
Cp/Sg	40.3	4.3	5.3		2		7.7		8.3	5.6		33.3	15.5	7.2	
Nic	17.6	16.6	13.7		22.7		29						13	0.4	31.9
Nic/Sg		2.2	2.1				0.3								0.7
Pn		7	8.1		1		2.6					0.9	0.9		
Pn/CGSS															
Pn/Cp					0.1										
Pn/Nic															0.4
Pn/Sg					0.1								0.2		
Po		15.6		2.9	9.5		11.2			4.2	45.8		6.1	1.7	
Po/CGSS							0.3						3.3		
Po/Cp		4.8	12.5		0.1		3			12.2			4	20.9	
Po/Cp/Nic		0.6													
Po/Nic		2.4			1.8		1.5								0.4
Po/Pn/CGSS/Sg										0.1					
Po/Pn/Sg															
Po/Sg		8.8			1					23.6	3.7		3.4	4.9	
Sg		23.4	32.3	57.2	44	50	18.8		61.7	31	0.5	65.8	39.4	50.7	
Po/Pn				5.2	0.1										
Total	100	100	100	100	100	100	100	100	100	100	100	100	100	100	100

Notes: abbreviations stand for sulfarsenide solid solution (Cgss), chalcopyrite (Cp), pentlandite (Pn), pyrrhotite (Po), chalcopyrite (Cp), silicate gangue (Sg), sphalerite (Sph), and molybdenite (Mo). Accessory grains which have host associations in the form of A/B occur along a mutual grain boundary between these minerals. Numeric values represent the % of the total volume of an accessory phase in a specific host association.

4.2.5 Cobaltite-gersdorffite-glaucodot solid solution

Sulfarsenide phases, which occur in all ore types, have compositions (see Appendix A7) that vary between endmembers cobaltite (CoAsS), gersdorffite (NiAsS), and glaucodot [(Co,Fe)AsS]. Furthermore crystals with similar chemical properties can exhibit different sulfarsenide crystal forms (the most common seen in this study are those of gersdorffite and glaucodot, see Figure 7A-F). In both MASU and INMS ore types, pyrrhotite is the dominant host of sulfarsenides, whereas chalcopyrite and pentlandite are also important host phases (see Tables 4 and 5). In these samples, sulfarsenides typically occur as small (µm scale) euhedral inclusions, but in rare cases can be much larger (mm-cm scale) and are typically fully enclosed within BMS (Figure 7A-C, E, and F). These features indicate that the sulfarsenides crystallized either pre- or synchronous to the base metal sulfides. It is also not uncommon to find PGE-zoned sulfarsenide crystals, these zones consist of PGM cores of irarsite-hollingworthite [(Ir,Ru,Rh,Pt)AsS-(Rh,Pt,Pd)AsS, Figure 7B, C, and F]. Galena, hessite, and Bi-Te phases may infill fractures in, or rim sulfarsenide crystals (Figure 7A and E). Larger (mm-cm scale) sulfarsenide grains may exhibit inclusions of base metal sulfides and nickeline that appear to be open space infillings. Other chemical zoning (specifically the proportion of Ni:Co) was observed on rare occasion. Although PGE-zonation is typically concentric in nature, Ni-Co zonation is not. In DISS ore types, sulfarsenides may demonstrate an increase in both size and abundance (Table 6, also Appendix A10). Sulfarsenides tend to occur along the margins of sulfide blebs and veins (Figure 6C-F, and Figure 7D). In nickeline-rich DISS ore samples, there is a strong association between the sulfarsenide and arsenide phases. In some cases, sulfarsenides hosted within nickeline appear to have been resorbed (Figure 6F). Irarsite-hollingworthite cores have been observed in sulfarsenides from DISS ore

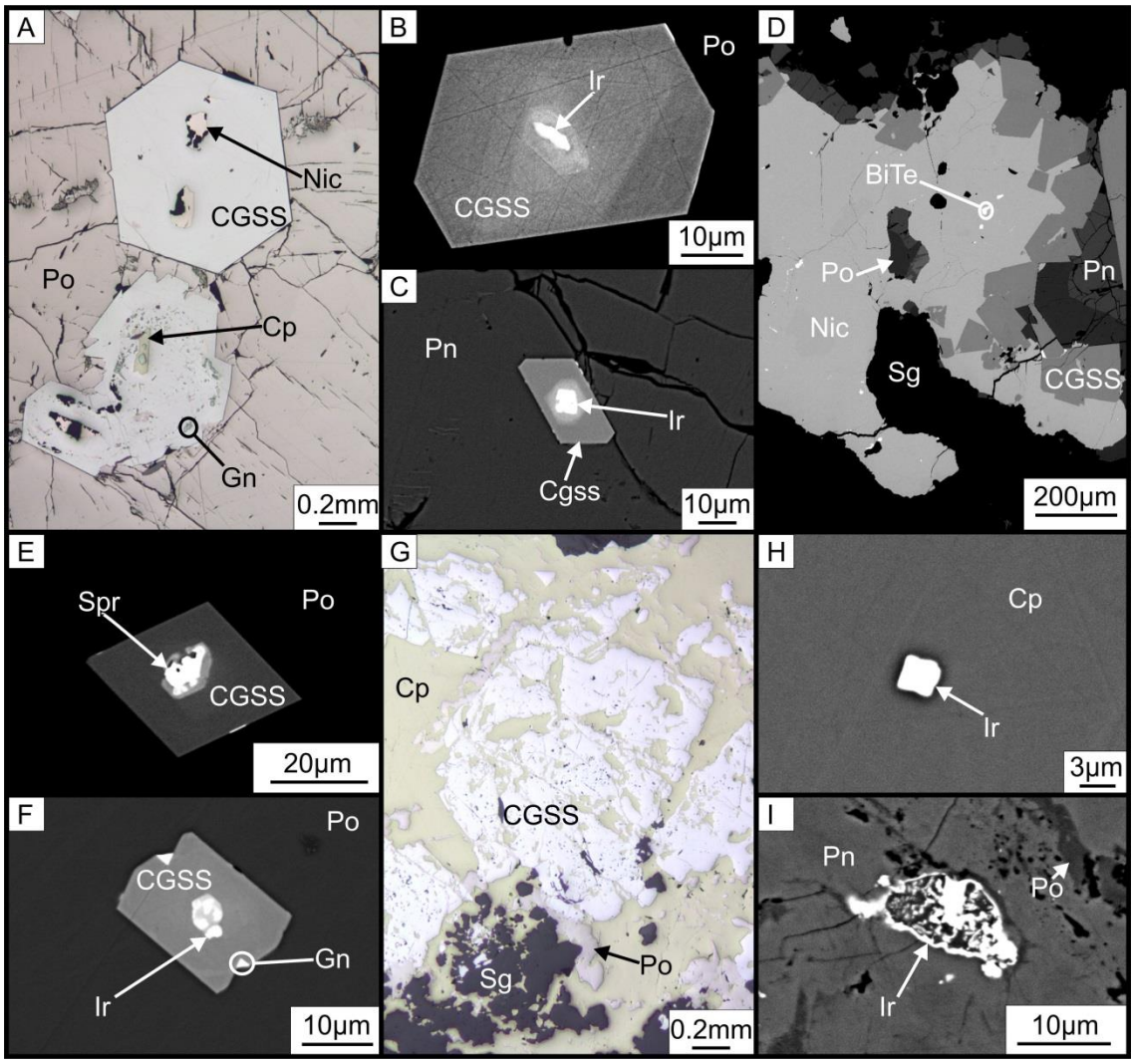

Figure 7. Photomicrographs of sulfarsenide phases: (A) euhedral-subhedral sulfarsenide solid solution (CGSS) hosted in pyrrhotite (Po) with sieve infill by nickeline (Nic), the euhedral crystal demonstrates the same form as cobaltite; (B) euhedral sulfarsenide (CGSS) in pyrrhotite (Po) with irarsite-hollingworthite (Ir) core; (C) euhedral sulfarsenide (CGSS) showing the form of glaucodot with an irarsite-hollingworthite (Ir) core; (D) euhedral-subhedral sulfarsenide cumulates (CGSS) within a nickeline-rich (Nic) vein, the forms of the sulfarsenides range from the irregular hexagon faces of gersdorffite to the orthorhombic forms of glaucodot, other inclusions in nickeline consist of a variety of Bi-Te phases (BiTe), sulfide vein hosted in silicate gangue (Sg); (E) sulfarsenide (CGSS) with a core of sperrylite (Spr), it is not clear which sulfarsenide form the crystal represents; (F) subhedral sulfarsenide (CGSS) in pyrrhotite (Po) with an irarsite-hollingworthite core (Ir) and minor galena rims (Gn); (G) an anhedral sulfarsenide crystal (CGSS) within a chalcopyrite vein (Cp), sieves within the sulfarsenide are infilled mainly by chalcopyrite, inclusions of silicate minerals (Sg) are also present; (H) subhedral cubic crystal of irarsite (Ir) in chalcopyrite (Cp); and (I) resorbed irarsite-hollingworthite (Ir) hosted within pentlandite (Pn).

types, but do not occur in larger (mm-cm scale) grains. Large sulfarsenide grains are often characterized by their subhedral-anhedral nature and abundant sieve texture with infill by base metal sulfides, nickeline, PGM, and other accessory phases (Figure 7G). As previously mentioned, graphic intergrowth between nickeline and chalcopyrite has been observed in sulfarsenide sieves (Figure 6E). The sulfarsenide solid solution series is enriched in Pd (39-1880 ppm, 752 ppm average; Table 3), Sb (439-2860 ppm, 1070 ppm average), Te (15.9-3070 ppm, 255 ppm average) Pt (0.18-33.6 ppm, 11 ppm average) and Ru (19-91ppm, 45 ppm average). Precious metals such as Ag and Au are typically low; outliers in Bi, Te, Pb, and Ag are likely the result of discrete inclusions within the sulfarsenides. The complete results of the LA-ICP-MS analyses of sulfarsenides are given in Appendix A7.

4.3 Mineralogy of other accessory phases

4.3.1 Platinum group minerals

A variety of platinum group minerals (PGM) was observed in this study, however sperrylite ($PtAs_2$, Table 7) was the only discrete Pt mineral found within the Totten ores. In MASU and INMS ore types, sperrylite forms anhedral-euhedral grains which are predominantly hosted within pyrrhotite (Table 4 and 5). In DISS ore samples, sperrylite typically occurs as anhedral grains mainly hosted in silicates immediately adjacent to sulfide veins and blebs, or along the margins of those same features (Table 6; Figure 8E). Sperrylite is also more common in MASU and INMS ore types than in DISS samples (Tables 4-6). In all ores types, sperrylite may be rimmed by hessite, galena, and Bi-Te minerals. The mineralogy of Pd is more complex than that of Pt, several PGM were observed (in order of most common to least): froodite ($PdBi_2$), palladian michenerite (PdBiTe), and ungavaite (Pd_4Sb_3). In MASU and INMS ore types, michenerite and

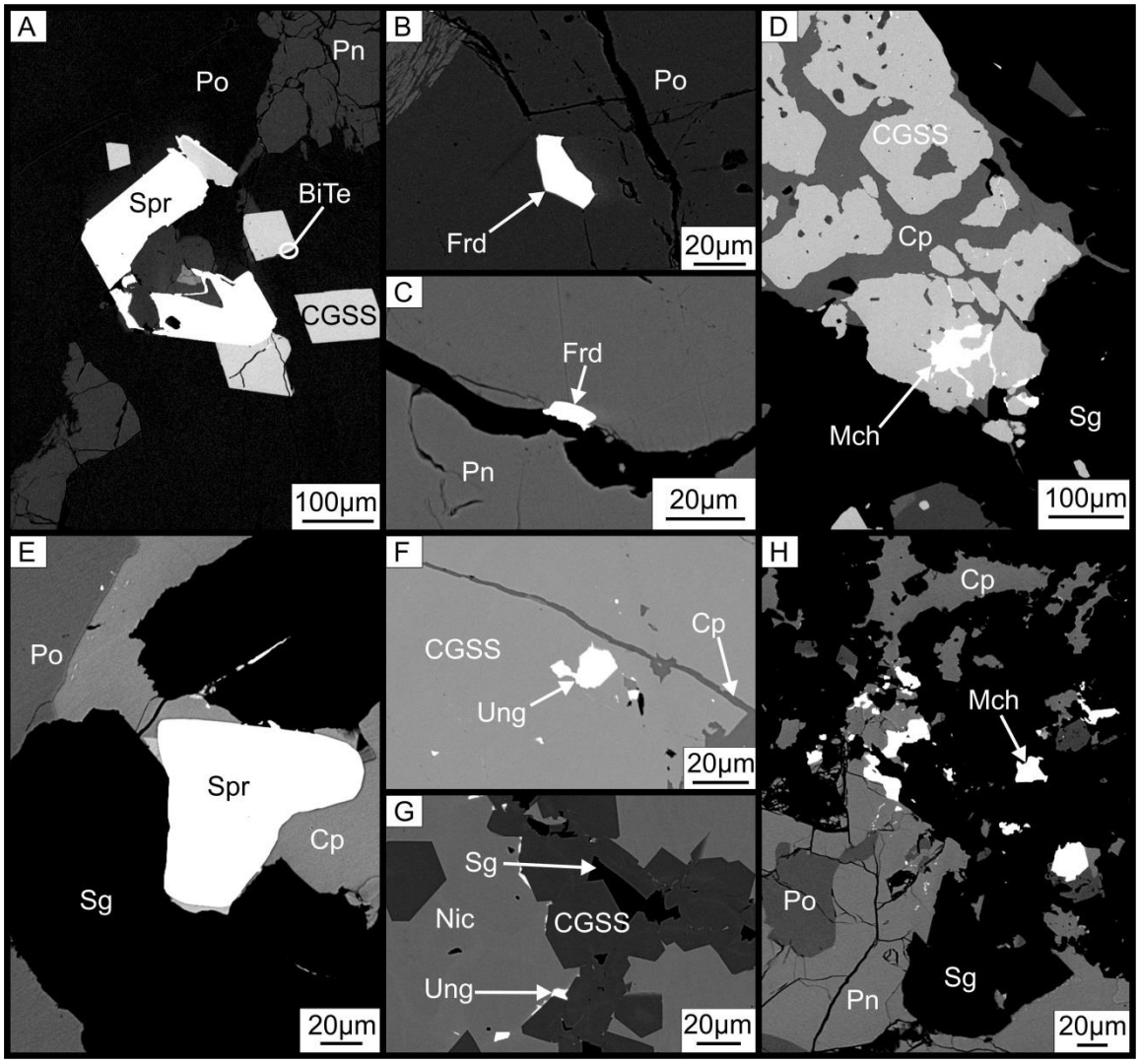

Figure 8. Photomicrographs of platinum-group minerals (PGM): (A) Sperrylite (Spr) hosted in pyrrhotite (Po) with riming by Bi-Te phases and sulfarsenides (CGSS); (B) Anhedral froodite inclusion (Frd) in pyrrhotite (Po); (C) anhedral froodite (Frd) infilling a fracture in pentlandite (Pn); (D) michenerite (Mch) infilling fractures in sulfarsenides (GGSS); (E) anhedral inclusion of sperrylite (Spr) along the sulfide-silicate gangue (Sg) interface; (F) Vug infill of ungavaite (Ung) within a sulfarsenide sieve (CGSS); (G) anhedral inclusions of ungavaite (Ung) in nickeline (Nic) along the contact with sulfarsenide (CGSS) cumulates; and (H) michenerite inclusions (Mch) along the margins

Table 7: Representative analysis (SEM-EDS) of accessory minerals from the Totten #2 Mine

Analysis #	Ag (wt%)	As	Au	Bi	Ir	Mo	Ni	Pb	Pd	Pt	Rh	S	Sb	Te	Co	Fe	Total	Atomic formula
1								62.1						37.9			100	$Pb_{1.00}Te_{1.00}$
2								62.0						38.0			100	$Pb_{1.00}Te_{1.00}$
3								61.7						38.4			100	$Pb_{0.99}Te_{1.01}$
4	21.9		78.1														100	$Au_{1.32}Ag_{0.68}$
5	35.3		64.7														100	$Au_{1.00}Ag_{1.00}$
6	41.2		58.8														100	$Au_{0.88}Ag_{1.12}$
7	12.4		87.6														100	$Au_{1.59}Ag_{0.41}$
8				79.4					20.6								100	$Pd_{1.01}Bi_{1.99}$
9				80.3					19.7								100	$Pd_{0.98}Bi_{2.02}$
10				80.7					19.3								100	$Pd_{0.96}Bi_{2.04}$
11				79.6										20.4			100	$Bi_{7.04}Te_{2.96}$
12				80.6										19.4			100	$Bi_{7.17}Te_{2.83}$
13	62.7													37.4			100	$Ag_{1.99}Te_{1.01}$
14	62.7													37.3			100	$Ag_{2.00}Te_{1.00}$
15	62.5													37.5			100	$Ag_{1.99}Te_{1.01}$
16		35.1			28.0						19.1	17.8					100	$(Ir_{0.44}Rh_{0.56})_{\Sigma 1.00}As_{0.92}S_{1.08}$
17		36.9			22.7						21.7	18.8					100	$(Ir_{0.36}Rh_{0.64})_{\Sigma 1.00}As_{0.91}S_{1.09}$
18		29.8			48.5						6.7	15.1					100	$(Ir_{0.80}Rh_{0.20})_{\Sigma 1.00}As_{0.92}S_{1.08}$
19		39.4			10.3						31.6	18.6					100	$(Ir_{0.15}Rh_{0.85})_{\Sigma 1.00}As_{0.95}S_{1.05}$
20		38.9			12.8						28.7	19.7					100	$(Ir_{0.19}Rh_{0.81})_{\Sigma 1.00}As_{0.92}S_{1.08}$
21		36.9			15.0						29.8	18.3					100	$(Ir_{0.21}Rh_{0.79})_{\Sigma 1.00}As_{0.93}S_{1.07}$
22				44.5					25.9					29.6			100	$Pd_{1.06}Bi_{0.93}Te_{1.01}$
23				44.9					27.2					27.9			100	$Pd_{1.11}Bi_{0.94}Te_{0.95}$
24				45.2					25.7					29.0			100	$Pd_{1.06}Bi_{0.95}Te_{0.99}$
25		56.6					43.4										100	$Ni_{1.01}As_{0.99}$
26		55.8					44.2										100	$Ni_{1.00}As_{1.00}$
27		56.6					43.4										100	$Ni_{1.01}As_{0.99}$
28				68.5										31.6			100	$Bi_{3.99}Te_{3.01}$
29				68.7										31.4			100	$Bi_{4.00}Te_{3.00}$
30		43.8								56.2							100	$Pt_{0.99}As_{2.01}$
31		43.1								56.9							100	$Pt_{1.01}As_{1.99}$
32		43.8								56.2							100	$Pt_{0.99}As_{2.01}$
33				52.2										47.8			100	$Bi_{2.00}Te_{3.00}$
34				52.9										47.1			100	$Bi_{2.03}Te_{2.97}$
35				62.4										37.6			100	$Bi_{1.01}Te_{0.99}$
36				61.7										38.3			100	$Bi_{0.99}Te_{1.01}$
37									54.5				45.5				100	$Pd_{4.05}Sb_{2.95}$
38									55.2				44.9				100	$Pd_{4.09}Sb_{2.91}$
39									55.0				45.0				100	$Pd_{4.08}Sb_{2.92}$
40		47.9					23.9					20.7			4.3	3.2	100	$(Ni_{0.76}Co_{0.13}Fe_{0.11})_{\Sigma 1.00}As_{0.99}S_{1.01}$
41		41.8					7.2					23.2			23.5	4.3	100	$(Ni_{0.21}Co_{0.67}Fe_{0.13})_{\Sigma 1.00}As_{0.87}S_{1.13}$
42		48.1					11.8					21.5			13.9	4.7	100	$(Ni_{0.39}Co_{0.45}Fe_{0.16})_{\Sigma 1.00}As_{0.98}S_{1.02}$
43		45.5					14.7					22.3			9.9	7.6	100	$(Ni_{0.45}Co_{0.30}Fe_{0.25})_{\Sigma 1.00}As_{0.93}S_{1.07}$
44		41.3					10.4					24.1			18.2	6.0	100	$(Ni_{0.30}Co_{0.52}Fe_{0.18})_{\Sigma 1.00}As_{0.85}S_{1.15}$
45						58				2.9		39.1					100	$(Mo_{0.99}Pt_{0.02})_{\Sigma 1.01}S_{1.99}$
46						60.7				2.2		37.1					100	$(Mo_{1.05}Pt_{0.02})_{\Sigma 1.07}S_{1.93}$
47						59.5				2.5		38.1					100	$(Mo_{1.03}Pt_{0.02})_{\Sigma 1.04}S_{1.96}$

Notes: Analyses are for altaite (1-3), electrum (4-7), froodite (8-10), hedleyite (11-12), hessite (13-15), hollingworthite-irarsite (16-21), michenerite (22-24), nickeline (25-27), pilsenite (28-29), sperrylite (30-32), tellurobismuthite (33-34), tsumoite (35-36), ungavaite (37-39), cobaltite-gersdorffite solid solution (40-44), and molybdenite (45-47). Atomic formula calculated based on 2 atoms (altaite, electrum, tsumoite), 3 atoms (sulfarsenides, irarsite-hollingworthite, sperrylite, michenerite, froodite, hessite, molybdenite), 5 atoms (tellurobismuthite), 7 atoms (pilsenite), and 10 atoms (hedleyite).

froodite (representative EDS analysis for both minerals can be found in Table 7) occur as anhedral inclusions within the base metal sulfides, which in some cases appear to be open space infillings (Figure 8B-C). They may also occur within silicate inclusions immediately adjacent to sulfides (Figure 8H). The base metal sulfides and silicate gangue are often dominant host phases for michenerite and froodite. In DISS ore samples, both michenerite and froodite are primarily hosted along the boundary of sulfides and silicate gangue, or within silicate gangue dispersed around the sulfides (Table 6). These minerals may also occur as open space infillings within the sieves of sulfarsenide grains. Ungavaite was observed in one MASU ore sample, but was absent in INMS ore samples. Ungavaite occurred as an anhedral inclusion in pyrrhotite hosted along a fracture. Ungavaite more commonly forms anhedral inclusions which occur in sulfarsenide sieves, or between the boundaries of nickeline grains in DISS ore samples (Table 6). Irarsite-hollingworthite [(Ir,Ru,Rh,Pt)AsS-(Rh,Pt,Pd)AsS; Table 7) predominantly occurs within PGE-zoned sulfarsenides in all ore types. However, irarsite may also occur as euhedral-subhedral grains hosted within the base metal sulfides. In some cases, these grains appear to be resorbed by the base metal sulfides (Figure 7H and I). Tarkianite [(Cu,Fe)Re_4S_8], is a rare PGM, which typically forms anhedral inclusions in chalcopyrite and pyrrhotite.

4.3.2 Ag-Te-Bi-Pb minerals

Another group of minerals that show common associations are: altaite (PbTe), galena (PbS), hessite (Ag_2Te), hedleyite (Bi_7Te_3), pilsenite (Bi_4Te_3), tellurobismuthite (Bi_2Te_3), and tsumoite (BiTe, Table 7). These minerals typically occur as anhedral inclusions in the base metal sulfides, sulfarsenides, nickeline, and within silicate gangue dispersed near the

sulfides and arsenides (Figure 9). Inclusions demonstrate open space infilling textures (occurring within vugs, fractures, and sieves) and likely postdate host phases. As previously mentioned, these phases are also known to rim sulfarsenides and PGM. On occasion, these minerals will be intergrown with each other. Galena, tellurobismuthite, and tsumoite are by far the most common members of this group of minerals at Totten.

4.3.3 Molybdenite

Molybdenite (MoS_2) forms anhedral-subhedral lathe inclusions which occur in base metal sulfides (Figure 9A). Molybdenite was not observed within the DISS ore samples studied, however, in MASU and INMS ore types, the primary host of molybdenite was found to be pyrrhotite and pentlandite (Tables 4 and 5). Fractures in molybdenite are commonly infilled by galena, hessite, and Bi-Te phases. Results of the EDS analysis of molybdenite sometimes indicated elevated (wt%, Table 7) concentrations of Pt.

4.3.4 Electrum

Electrum (AuAg, Table 7) is an uncommon accessory phase at Totten, and typically forms anhedral inclusions that show open space infilling textures (occurring in fractures and vugs, Figure 9H and K). The most common host of electrum is silicate gangue dispersed around sulfides (Tables 4-6).

4.4 Quantitative mass balance of the Totten ores

The quantitative mass balances of Totten ores, from both ore bodies, are given in Appendix A10, and summarized in figure 10. Mass balances were based on calculated bulk rock concentrations derived from the modal abundance of major (visual estimation in thin section, verified for massive and semi massive samples by comparison to calculated abundances from bulk rock assays) and accessory phases (abundance

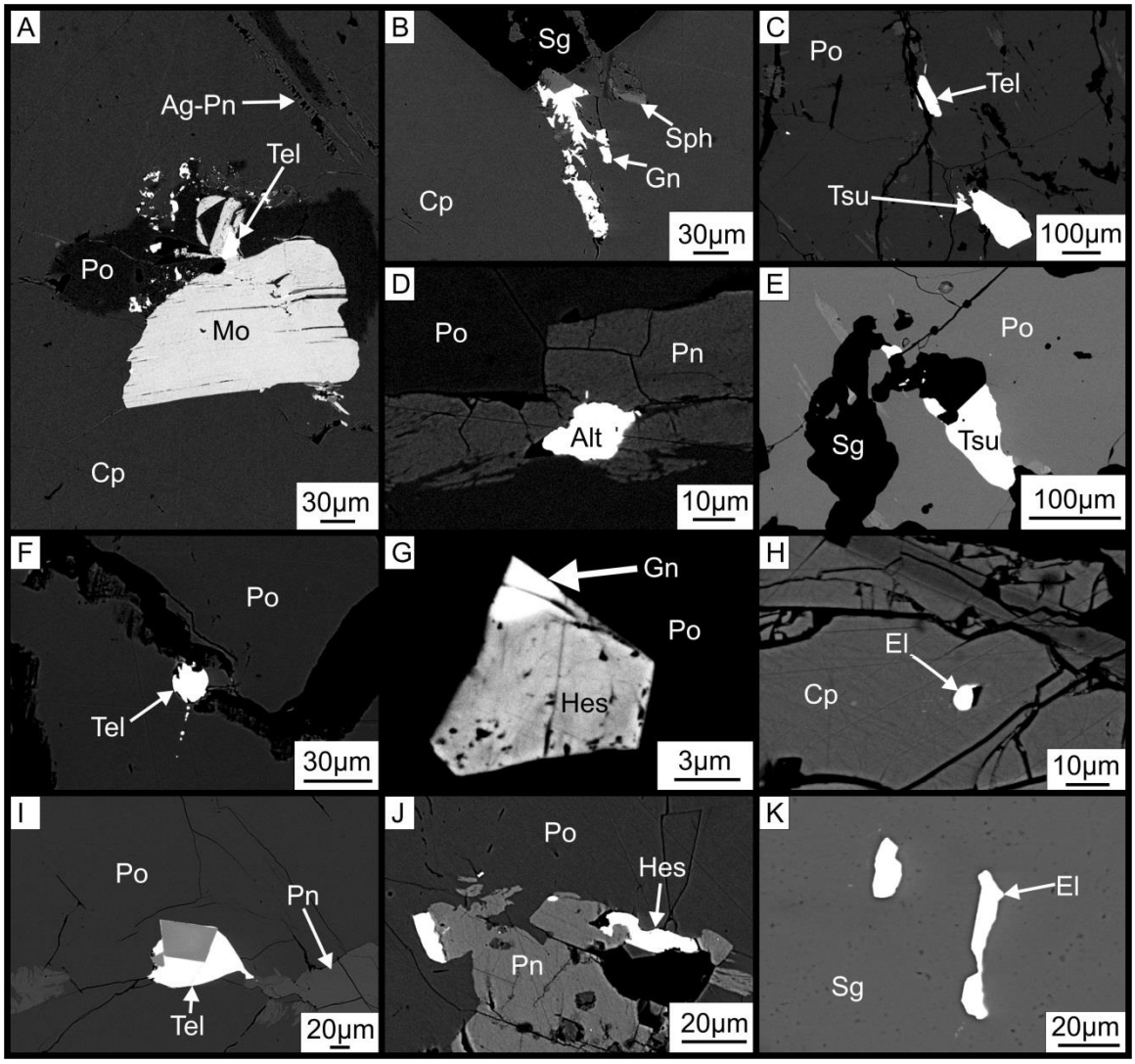

Figure 9. Photomicrographs of other accessory phases: (A) Subhedral lathe of molybdenite (Mo) with inclusions of tellurobismuthite (Tel), also argentopentlandite (Ag-Pn) stringers in chalcopyrite (Cp); (B) anhedral inclusions of galena (Gn) and silicate gangue (Sg) infilling fractures in chalcopyrite (Cp); (C) tsumoite (Tsu) and tellurobismuthite (Tel) inclusions in fractures within pyrrhotite (Po); (D) altaite (Alt) inclusion in pentlandite (Pn); (E) tsumoite (Tsu) infilling a fracture in pyrrhotite; (F) tellurobismuthite (Tel) inclusion within a fracture in pyrrhotite (Po); (G) composite grain of hessite (Hes) and galena (Gn) in pyrrhotite; (H) electrum (El) infilling a vug within chalcopyrite (Cp); (I) tellurobismuthite (Tel) riming sulfarsenide grains in pyrrhotite (Po); (J) hessite (Hes) rimming pentlandite (Pn); and (K) anhedral electrum (El) inclusions within silicate gangue (Sg)

quantified by SEM). Scatter plots which compare calculated assays to actual bulk rock analyses are given in Figure 11.

4.4.1 Nickel

In massive sulfides (MASU) from both Totten ore bodies, pentlandite is the only major (≥1% by volume) Ni-bearing phase. It is therefore logical that the mass balance calculations demonstrate that pentlandite is the dominant carrier of nickel in that ore type (~80%, Figure 10A and B). Interestingly, pyrrhotite is responsible for a significant amount (10%, Figure 10A) of the bulk nickel content of massive sulfides (MASU). Semi-massive sulfides (INMS) differ from MASU samples only in that arsenides and sulfarsenides represent minor carriers of nickel (5% and 2% respectively, Figure 10B). In disseminated sulfides (DISS) from both ore bodies, pentlandite is still the dominant carrier of nickel (52%, Figure 10C); however, due to low abundances relative to MASU samples, and variable modal abundances between samples, pentlandite contributes less to the overall nickel budget than in MASU-INMS ore samples. Due to their increased modal abundances in DISS ore samples, nickeline and the sulfarsenides represent important carriers of nickel (30% and 15% respectively, Figure 10C). Pyrrhotite still contributes to the nickel budget in DISS ore types, however the proportion of nickel attributed to pyrrhotite is typically half that of MASU ore samples. Scatter plots of estimated (via quantitative mass balance) versus actual bulk rock analysis show a high positive correlation (Figure 11), meaning that the distribution shown by the mass balances is representative of the distribution within the sample.

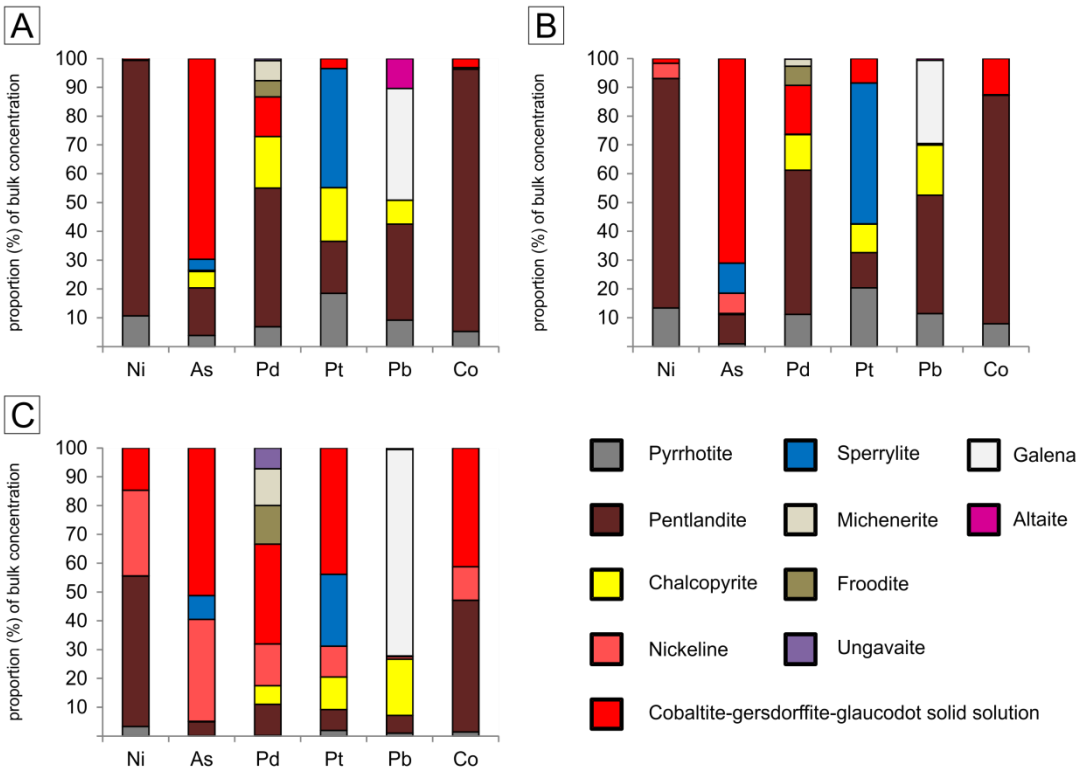

Figure 10. Summary of the mass balance results: calculated for Ni, As, Pd, Pt, Pb, and Co from: (A) massive, (B) semi-massive, and (C) disseminated sulfides in both the Main and 238 orebodies. Graphs plotted as the proportions of the total calculated bulk rock concentration of each element (%) contained with each mineralogical domain. Full results of the Totten mass balances are given in Appendix A10.

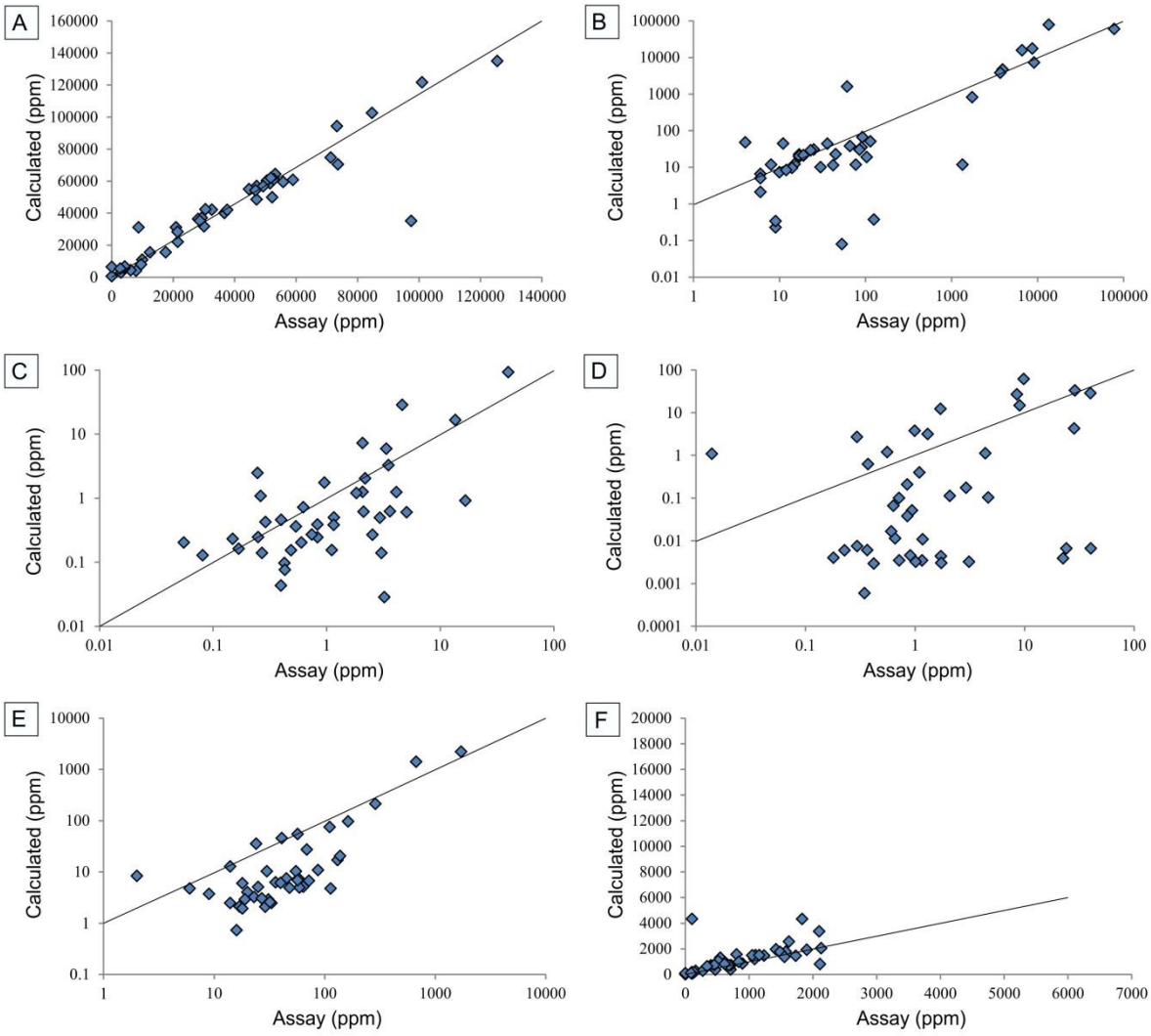

Figure 11. Scatter plot diagrams of the calculated vs. actual bulk rock assays of each element in the quantitative mass balance: (A) Ni, (B) As, (C) Pd, (D) Pt, (E) Pb, and (F) Co. A line showing perfect correlation (predicted assay=actual assay) between each parameter has been added to each to demonstrate the extent of over or under estimation of values.

4.4.2 Arsenic

The dominant carrier of arsenic in massive and semi-massive sulfides from both ore bodies is the sulfarsenide solid solution (70% of the total As budget, Figure 10A and B). The base metal sulfides and sperrylite contribute only minor amounts of bulk rock arsenic (<30% combined, Figure 10A and B). The sulfarsenides are also a major carrier of arsenic in disseminated ore from both ore bodies; however, nickeline is also a major carrier due to an increased average modal abundance in this ore type (35%, Figure 10C). Sperrylite and pentlandite are shown as minor contributors of As in disseminated ore (8% and 5% respectively, Figure 10C). Although the calculated versus actual assay scatter plot for arsenic shows an overall positive correlation, many samples are under reported (Figure 11). Discrepancy occurs when the relative abundances of minerals in thin section are not completely representative of those found on the hand sample-scale. The result is an under (or over) reported concentration of arsenic in the sample. In samples that were under reported, a greater proportion of arsenic is attributed to minor carriers (such as the base metal sulfides, which we know from LA-ICP-MS to be depleted in As) than the actual major carriers that control the bulk rock assays. This is likely the case for samples which attribute a major proportion of the calculated As to the base metal sulfides and sperrylite (in which case these samples typically show greatly underreported As relative to the bulk rock analysis).

4.4.3 Platinum

In MASU and INMS samples, sperrylite is the dominant domain of residence for platinum (40% and 50% respectively, Figure 10A and B). The sulfarsenide solid solution, which demonstrates a significant control on the Pt content in massive and semi massive

sulfides from both ore bodies (3-9%, Figure 10A and B), increases its overall contribution (43%, Figure 10C) to the Pt budget in disseminated ore (where sperrylite is less abundant, Tables 4-6). In all ore types from both ore bodies, the base metal sulfides are shown to be minor to major carriers of Pt. However, when calculated assays are compared with actual bulk rock analysis, the majority of the predicted assays are under reported (since the base metal sulfides only contribute small amounts of Pt to bulk rock concentration, Figure 11). This is likely the cause of highly localized grains of sperrylite occurring in hand sample, which were not represented in thin section.

4.4.4 Palladium

Quantitative mass balances of massive and semi-massive sulfide samples from both ore bodies, suggest that pentlandite is the major carrier of Pd rather than discrete PGM (~50% of the total Pd budget, Figure 10A and B). Sulfarsenides are only minor carriers of Pd in massive and semi-massive sulfides from both ore bodies (~15%, Figure 10A and B), but supplies a greater proportion of Pd in disseminated ore types (35%, Figure 10C). Discrete PGM, which are more abundant in disseminated ore samples than massive or semi-massive ore types, represent more important domains for Pd in those samples (Figure 10A, B, and C). Scatter plots of calculated and actual bulk rock analysis for Pd, show a weak positive correlation. Many samples are under reported (compared to bulk rock assays) Pd concentrations from mass balance calculations, suggesting that the distribution and relative proportions of discrete phases seen in thin section do not represent those in the assay sample (Figure 11). Therefore, in disseminated samples where discrete Pd-carriers (Pd-Bit-Te-Sb minerals) are more abundant (Tables 4-6), a

greater proportion of Pd is attributed to these phases (whereas Pd is attributed to Pn in under reported massive and semi-massive samples).

4.4.5 Cobalt

In massive and semi-massive sulfides from both ore bodies, pentlandite is the dominant host for Co (80-90% of the total Co budget, Figure 10A and B). Though Co is a major constituent of the sulfarsenides, these phases only account for a minor amount of Co seen in massive and semi-massive sulfides (3-12%, Figure 10A and B). In disseminated samples, where the sulfarsenides occur in greater abundance (with respect to volume % and grain abundance, Tables 4-6), they represent a major host for Co (43%, Figure 10C; however pentlandite remains a major contributor). The scatter plot of calculated and actual Co assay values shows a strong positive correlation. This implies that the distribution of Co seen in thin section is representative of the distribution in the hand sample (Figure 11).

4.4.6 Lead

The dominant host of Pb in massive and disseminated sulfide ores is galena (40% and 70% respectively, Figure 10A and C). However, galena is attributed less of the overall Pb budget in semi massive samples (~30%, Figure 10B). Altaite, another Pb-phase found at Totten, is a minor contributor to bulk rock Pb by comparison (0.5-10%, Figure 10). Although the Pb content is typically low, the base metal sulfides are assigned a significant proportion of the Pb budget (especially pentlandite in massive and semi-massive samples, Figure 10). The scatter plot of estimated versus actual bulk rock analysis for Pb shows a moderate positive correlation, however, values of Pb are often under reported, suggesting that proportions assigned to base metal sulfides are inflated

due to the difference in the distribution of galena in thin section compared to the corresponding hand sample (Figure 11).

5.0 Discussion

5.1 Comparison of the mineralogy of Totten ores to other Sudbury deposits

Detailed studies of the ore mineralogy and mineral chemistry of major and accessory phases in contact and offset deposits along the South Range are well represented in the literature (e.g., Hawley and Stanton, 1962; Cabri and Laflamme, 1976; Lightfoot et al., 1997; Carter et al., 2002; Lightfoot and Farrow, 2002; Magyarosi et al., 2002; Szentpéteri et al., 2002; Huminicki et al., 2005; Dare et al., 2010; Lefort, 2012). Similar to this study, those investigations have shown that both the PGE and As concentrations of the major base metal sulfides (pyrrhotite, pentlandite, chalcopyrite) are consistently low to below detection limits in both offset dykes and contact-style deposits. However, due to their abundance, the base metal sulfides still represent a minor proportion of the overall concentration of PGE in these systems (c.f. Huminicki et al., 2005).

Sulfarsenide and arsenide phases are present in South range ores, but are absent to rare in North Range systems (Cabri and Laflamme, 1976, Dare et al., 2011). Texturally, the sulfarsenides seen in other deposits are similar to Totten in that they occur as subhedral-anhedral inclusions associated with both the base metal sulfides and silicate host rocks, furthermore these may be chemically zoned with PGM cores (Hawley and Stanton, 1962; Cabri and Laflamme, 1976; Carter et al., 2002; Magyarosi et al., 2002; Szentpéteri et al., 2002; Huminicki et al., 2005; Dare et al., 2010; Lefort, 2012). Laser-ablation studies of the South Range sulfarsenides demonstrate that they contain elevated levels of dissolved PGE, and when combined with their textural associations with PGM, this suggests that

the sulfarsenides and arsenides are important carriers of PGE in South Range ores (Cabri and Laflamme, 1976; Carter et al., 2002; Huminicki et al., 2005; Dare et al., 2010; Lefort, 2012). Figure 12 demonstrates the Ni-Co-Fe compositions of sulfarsenides from Totten (this study), Garson (modified contact-style deposit; LeFort, 2012), Creighton (contact-style deposit; Dare et al., 2010), and various deposits within the Copper Cliff offset (Copper Cliff North Mine, South Mine, and Kelly Lake deposits; Szentpéteri et al., 2002; Rickard, 2000; Magyarosi et al., 2002; Carter, 2000; Stewart, 1999). Although these deposits may be found in different ore environments, the South Range deposits show similar ranges in sulfarsenide (CGSS) composition (Figure 12). In the case of Totten, CGSS grains range in composition from $(Ni_{0.76}Co_{0.14}Fe_{0.11})_{\Sigma 1.00}As_{0.99}S_{1.01}$ to $(Ni_{0.17}Co_{0.68}Fe_{0.15})_{\Sigma 1.00}As_{0.88}S_{1.12}$ (Appendix A9) indicating that they achieved final equilibration compositions over a prolonged history of post magmatic cooling (300°C-600°C, Figure 12). Unlike the trace metal content reported in South Range deposits by other authors (e.g. Cabri and Laflamme, 1976; Lefort, 2012), nickeline from Totten exhibits enrichment in Co (569-1139 ppm, Appendix A8). In these deposits, nickeline is texturally identical to what is seen at Totten. It is reported to occur as anhedral grains associated with sulfarsenides, sulfides, and silicate host rocks, and can also demonstrate graphic intergrowth with chalcopyrite (Hawley and Stanton, 1962; Cabri and Laflamme, 1976; Dare et al. 2010, Lefort, 2012). The principle Pt mineral reported in South Range deposits is sperrylite (Cabri and Laflamme, 1976; Carter et al., 2002; Huminicki et al., 2005; Dare et al., 2010; Lefort, 2012). Although sperrylite is inferred to be the major carrier of Pt, it contributes very little As to bulk rock geochemistry in comparison to sulfarsenides and arsenides (Huminicki et al., 2005). Sperrylite may occur as euhedral-

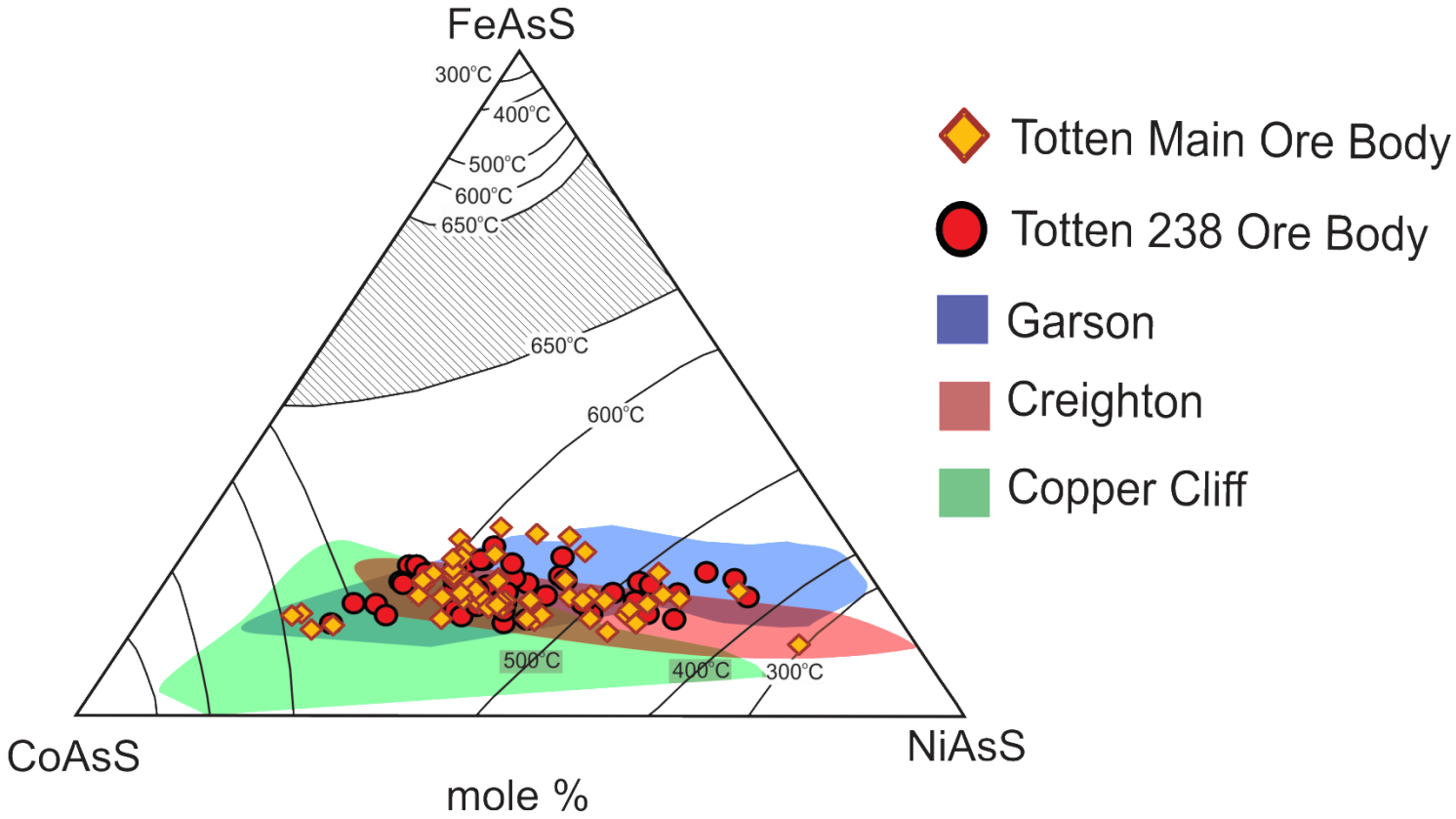

Figure 12. Compositions of the sulfarsenides from the Main and 238 ore bodies, plotted on the ternary diagram of Klemm (1965), with isotherms for various limits of immiscibility as well as an immiscibility gap (hatched field) at 650°C. Additionally, sulfarsenide compositional data is given for other South Range deposits: Garson (LeFort, 2012), Creighton (Dare et al., 2010), as well Copper Cliff North, South, and Kelly Lake deposits (Szentpéteri et al., 2002; Rickard, 2000; Magyarosi et al., 2002; Carter, 2000; Stewart, 1999).

anhedral inclusions in base metal sulfides, sulfarsenides, or in silicate minerals (Cabri and Laflamme, 1976; Carter et al., 2002; Magyarosi, 2002; Szentpéteri et al., 2002; Huminicki et al., 2005; Dare et al., 2010; Lefort, 2012). Michenerite and froodite are the discrete Pd-phases in most South Range ores (Cabri and Laflamme, 1976; Carter et al., 2002; Magyarosi, 2002; Huminicki et al., 2005; Dare et al., 2010; Lefort, 2012). The ideal formula for michenerite allows for substitution between Pt and Pd. Interestingly michenerite from South Range deposits does not contain Pt, whereas Pt is present in North Range michenerite (Cabri and Laflamme, 1976). Palladium minerals usually form anhedral inclusions in association with sulfarsenides and Bi-Te-Ag-Pb carriers (e.g., galena, altaite, hessite, tsumoite, tellurobismuthite).

5.2 Paragenesis of the accessory phases

5.2.1 Arsenide and sulfarsenide phases

The characterization of As-phases is an important task due to their deleterious nature and their close association with many economic metals in magmatic Ni-Cu-PGE sulfide deposits (Skinner et al., 1976; Makovicky et al., 1990; Fleet et al., 1993; Gervilla et al., 1994; Wood, 2003; Hem and Mackovicky, 2004; Hanley, 2007). As shown in section 5.1, arsenide and sulfarsenide phases have been previously reported in South Range deposits. There are currently two theories regarding the origin of these sulfarsenides: (i) direct crystallization from a primary sulfide melt (Szentpéteri et al., 2002; Dare et al., 2010; Lefort, 2012), and (ii) precipitation from a secondary (hydrothermal, metamorphic) fluid (Carter et al., 2001; Magyarosi et al., 2002; Szentpéteri et al., 2002; Stewart, 2002). This study supports a primary magmatic origin for the sulfarsenides, and evidence for this will be presented in this section. At around 1120°C, the MSS will begin to crystallize from the sulfide melt (Naldrett and Kullerud, 1967; Naldrett, 1984b). This phase would have been

enriched in Fe-Ni-Co-IPGE, whereas Ni-Cu-Au-PPGE would have been more compatible in the residual sulfide liquid (e.g., Naldrett and Kullerud, 1967; Naldrett, 1984b; Li et al., 1992; Sinyakova and Kosyakova, 2012). In a recent experimental study, Sinyakova and Kosyakova (2012) demonstrated that IPGE sulfarsenides (such as hollingworthite and irarsite) could have already begun to crystallize from the melt during the formation of the MSS, which would explain why pyrrhotite and pentlandite at Totten are depleted in Ir and Ru (Table 3; Figure 13). Similarly, the enrichment of Pt in sulfarsenides (Table 3) suggests that these crystals may have formed before the Pt-depleted base metal sulfides. There exists very little data in the literature regarding the temperatures at which cobaltite, gersdorffite, and glaucodot could begin to form in magmatic systems, however, Makovicky (2002), showed that cobaltite can be stable at temperatures as high as 850°C. Furthermore, experimental studies of sulfarsenides demonstrate a great deal of compositional variability with regards to Fe, Ni, Co, As, and S at various temperatures (Yund, 1961; Hem and Mackovicky, 2004). Therefore, it is possible that magmatic Ni-Co-Fe-sulfarsenides nucleated on magmatic IPGE sulfarsenides which had already crystallized (Figure 13; which has also been proposed by Dare et al., 2010). This suggests that it is possible that magmatic processes (i.e. *in situ* crystallization from a melt phase) can cause resulting sulfarsenide crystals to become enclosed within the MSS phases during crystallization, and that they will exhibit the same compositional variations seen by this study (Figure 7B, C, and F). This process would explain the euhedral nature of sulfarsenides (both CGSS, and irarsite-hollingworthite) that are found within pyrrhotite and pentlandite, and the lack textural evidence of secondary origin (such as frequent occurrence as vug or fracture infillings in the base metal sulfides). Due to the

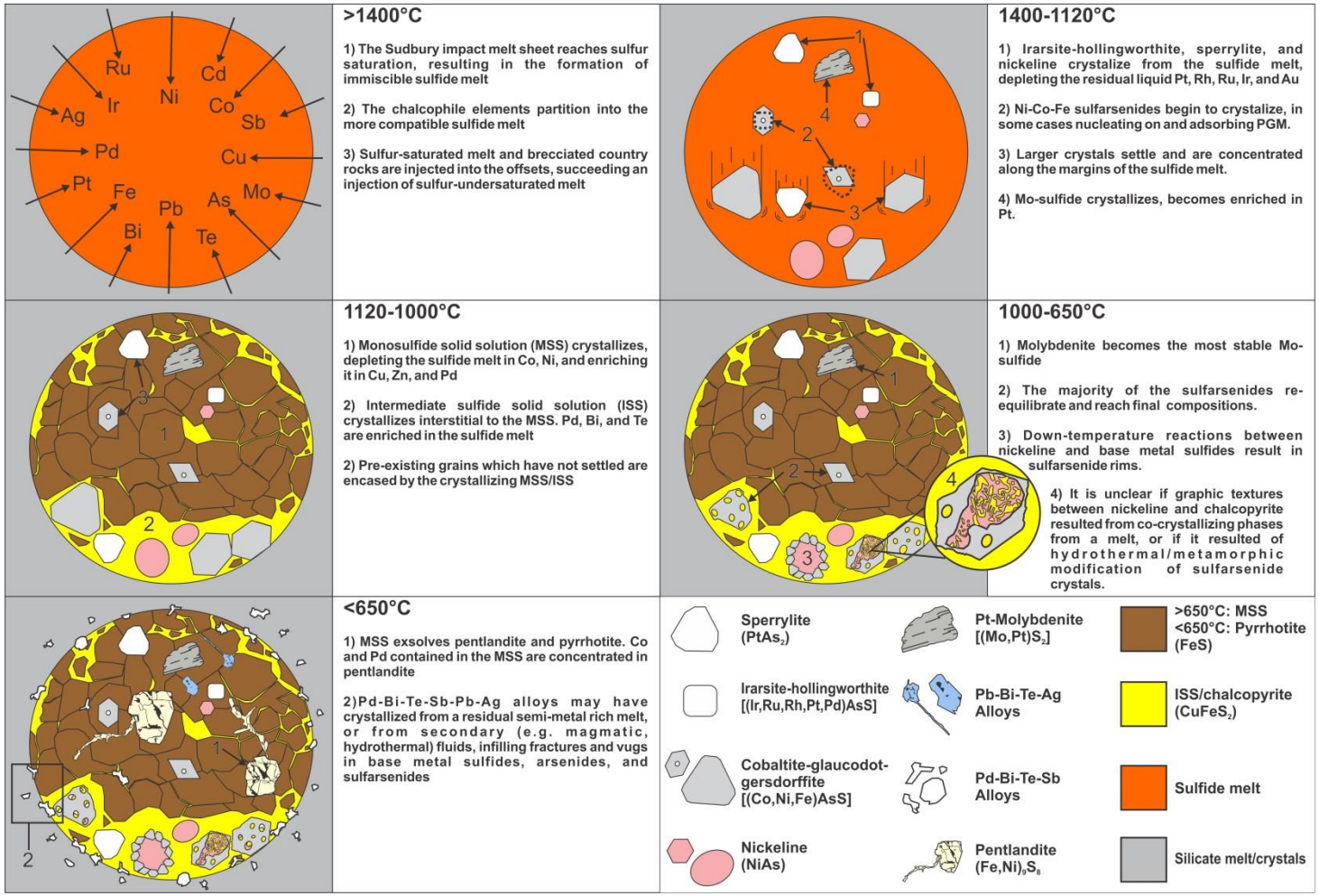

Figure 13. Genetic model of the Totten Ni-Cu-PGE ores. Proposed model is based on textural and chemical evidence provided in this study.

aforementioned compatibility of IPGE with the MSS cumulates; some of the sulfarsenides (specifically irarsite and hollingworthite) hosted within pyrrhotite and pentlandite could have experienced resorption, as shown in the petrographic results of this study (Figure 7I). As described in section 4.2, sulfarsenides typically increase in both abundance and size near the peripheries of sulfide mineralization (disseminated ore types, and samples with increased abundance in chalcopyrite relative to pyrrhotite, Tables 4-6 and also Appendix A10); furthermore, sulfarsenides with IPGE cores are uncommon in these same samples. This study suggests that gravitational differentiation is the mechanism by which the distribution of larger sulfarsenide grains and the distribution of IPGE cores were controlled. Smaller crystals observed in the pyrrhotite and pentlandite were likely able to remain in suspension long enough to be encapsulated by the crystallizing sulfide cumulates, whereas grains which had achieved sufficient mass were not buoyant and sank to the lower regions of the melt. This would explain the increase in the number of sulfarsenide grains and average grain volume (as former accumulations of single grains that have since annealed) in disseminated samples (Appendix A10, Tables 4-6); sulfarsenide grains may have settled along contacts, but may have also nucleated along these contacts. Furthermore, sulfarsenide grains with IPGE cores must have been captured by the forming pyrrhotite and pentlandite before achieving enough mass to lose buoyancy (due to the lack of such features in disseminated ore types). Gravitational settling is also supported by the observation that many sulfarsenides within sulfide and arsenide veins, occur along the margins of those features (and depending on the original orientation of the vein relative to gravity, those grains may preferentially collect along one side of the vein, Figure 7D).

Although nickeline is rare in massive to semi-massive sulfides, it usually forms anhedral-euhedral inclusions in pyrrhotite. Euhedral inclusions of nickeline do not demonstrate open space infill textures and probably represents early magmatic crystals which were enclosed by crystallizing pyrrhotite and pentlandite (Figure 6B). In DISS ore samples, nickeline typically forms anhedral/globular grains associated with the margins of sulfide mineralization (Figure 6A, D). Although experimental work indicates that nickeline is stable at temperatures that are much lower than the liquidus/solidus of the Sudbury ores (Yund, 1961), the enrichment of Au in nickeline and subsequent depletion in chalcopyrite (Table 3), as well as the occurrence of well formed nickeline crystals in massive sulfide ores, indicates that nickeline crystallized before or synchronous to the base metal sulfides. In one sample, anhedral nickeline blebs are rimmed by euhedral sulfarsenides (Figure 6C). Due to the complete enclosure of nickeline blebs by sulfarsenides, it is unlikely that these lenses formed simply by accumulation through gravitational settling, and it is more likely that they crystallized at the nickeline-sulfide melt interface (Figure 13). This is supported by early experimental work by Smith (1961), who demonstrated that at high (750°C) temperatures, gersdorffite may crystallize along the contact of pyrrhotite and nickeline in the presence of H_2S (vapor or liquid). Nickeline does not always appear in textural equilibrium with sulfarsenides and in some cases it seems to have replaced the sulfarsenides (Figure 6F). The graphic intergrowth of nickeline and chalcopyrite (Figure 6E) indicates that at least some of the nickeline present in the Totten ores may have exsolved or crystallized from a sulfide melt at some minimum (i.e. eutectic). However, this texture may have also resulted from post-magmatic modification (hydrothermal, metamorphic) of the ores.

5.2.2 Platinum-group minerals

The only IPGE phases observed in this study consist of the irarsite-hollingworthite solid solution series which form cores at the center of sulfarsenide grains, or subhedral to anhedral inclusions in base metal sulfides (Figure 7B, C, H, and I), and therefore crystallized early as described above. Sperrylite is the only Pt-mineral present at Totten; it occurs in all ore types. Experimental work shows that sperrylite crystallizes at high temperatures (around 1400°C; Hansen and Anderko, 1958; Bennett and Heyding, 1966; Sinyakova and Kosyakova, 2012). Euhedral-anhedral inclusions of sperrylite found within pyrrhotite and pentlandite likely represent a primary magmatic phase that was incorporated into the sulfides when the latter crystallized (Figure 8F). The PGE cores found in some sulfarsenide crystals typically consisted of irarsite-hollingworthite, though in one case magmatic sperrylite occurs at the center of a sulfarsenide grain (Figure 7E), and likely acted as a nucleation "seed" crystal for this later overgrowth. Sperrylite is also found in disseminated ore samples (but is less abundant than in massive and semi-massive samples, Tables 4-6) associated with silicate gangue dispersed around sulfides, and the boundaries between the sulfide and silicate minerals (Figure 8E). Similar to the sulfarsenides, these grains may represent early formed magmatic crystals which settled to the margins of the sulfide melt body along its host rock contacts (Figure 13).

Palladium forms highly stable complexes with Bi and Te (as michenerite, and froodite), and more rarely with Sb (ungavaite; Wood, 2002; McDonald et al., 2005). Unlike sperrylite, these Pd minerals may appear to be secondary (vug or fracture infill) inclusions in base metal sulfides, arsenides, and sulfarsenides (Figure 8B-D, and F), but also occur in association with the grain boundaries of sulfides and silicates. Experimental

work by Hoffman and Maclean (1976), show that michenerite is stable at low temperatures (relative to sperrylite, and hollingworthite-irarsite) up to approximately 550°C. Therefore, it is possible that the Pd-Bi-Te minerals may have formed as a consequence of: (i) late magmatic crystallization from a semi-metal rich melt persisting to low temperatures, which may have migrated to the margins of the sulfide melt (e.g. Cabri and Laflamme, 1976; Tomkins et al., 2006; Dare et al., 2010), and/or (ii) precipitation from hydrothermal/metamorphic fluids (Farrow and Watkinson, 1997; Carter, 2000; Pentek et al., 2008). Textural evidence from the petrographic analysis of Totten ore samples supports both theories; therefore it is possible that both processes were responsible for the formation of Pd-phases. Ungavaite is typically associated with relatively larger volumes of CGSS and nickeline (such as in the disseminated sulfide samples, Figures 8F and G), which are themselves enriched in Sb. There is currently no experimental work which indicates the temperature range at which ungavaite is stable, so it is possible that ungavaite may have formed either by magmatic or post-magmatic processes.

5.2.3 Other accessory phases

Molybdenite inclusions in base metal sulfides are well-formed and do not appear to have formed by secondary processes (e.g., hydrothermal, metamorphic, Figure 9A). Furthermore, the elevated concentration of Pt in molybdenite does not support exsolution from Pt-poor base metal sulfides. Experimental work shows that above temperatures of 650°C, a high temperature mineral (Mo_2S_3) is more stable than molybdenite and breaks down into Mo_2S_3+MoS_2 at temperatures below 650ºC (Morimoto and Kullerud, 1962; Takeno and Moh, 1977). Therefore it seems more likely that molybdenite crystallized as an early magmatic phase that was later encased by the base metal sulfides (Figure 13).

The Bi-Te-Ag-Au-Pb carriers (e.g., bismuth tellurides, hessite, electrum, galena, altaite) are stable at relatively low temperatures below 500ºC (Cabri, 1965; Elliot, 1965; Hoffman and Maclean, 1976). Texturally, these phases appear late (i.e., open space infillings, fracture infillings, vug infilling, rimming sulfarsenides and sperrylite) with regards to the base metal sulfides (Figure 9B-K). However, it is difficult to identify whether these minerals exsolved from a late stage, semi-metal rich melt, or by precipitation from a secondary (hydrothermal, metamorphic) fluid.

5.3 Observations of mineralogical controls in assay data

Figure 14 shows a binary plot of the Co/Ni ratio versus the As concentration of samples from both Totten and Garson (contact-style deposit), using the Vale bulk rock assay databases for these deposits. Immediately, it is clear that both deposits show different geochemical signatures. In the Garson data, a positive correlation occurs between Co-Ni-As above a threshold of approximately 0.1wt% As. LeFort (2012) determined that above this threshold, the sulfarsenide solid solution (cobaltite-gersdorffite) becomes the primary control on both parameters. Below this threshold, the abundance of sulfarsenides is too low to control the Co/Ni ratio, and pentlandite is the dominant contributor. A similar trend was observed at Totten, however a much greater proportion of analyses remain in the pentlandite field, suggesting that the Totten ore bodies do not contain as much arsenic as the Garson deposit. The majority of the Ni and Co in the Totten ores is controlled by the distribution of pentlandite, which explains the near perfect (r_s=0.916, n=174; Table 2) correlation that was observed between Co and Ni. Furthermore, As, which has been shown to be mainly controlled by the distribution of sulfarsenides (section 4.4), shows ambiguous low positive correlations to Ni (r_s=0.206,

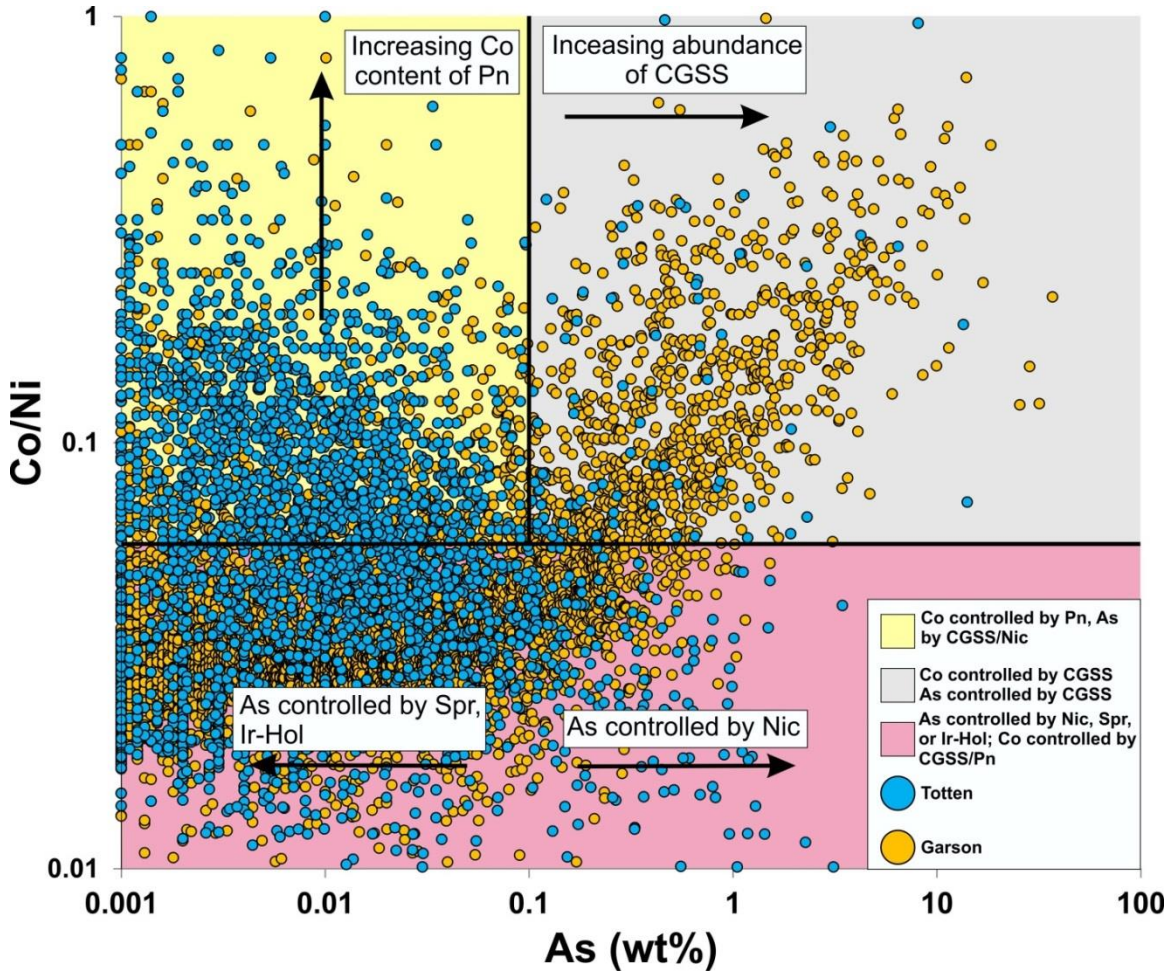

Figure 14. Scatter plot of the Co/Ni ratio versus the As concentration of Totten and Garson ores. Data for comparison in this diagram was used, with permission, from the Vale bulk rock assay databases for Totten and Garson. Abbreviations: sperrylite (Spr), nickeline (Nic), sulfarsenide solid solution (CGSS), irarsite-hollingworthite (Ir-Hol) and pentlandite (Pn)

n=174; Table 2), and Co (r_s=0.204, n=174; Table 2), however these correlations only apply at low concentrations of As (<0.1 wt%, Figure 14).

LeFort (2012) suggested that the high concentration of As in the Garson ores was a result of contamination through the regional assimilation of country rocks into the SIC melt sheet locally. At Totten, the ore-related IQD occurs within the central portions of the offset dyke, or along the margins in contact with Sudbury gabbro. Furthermore, the contact relationships between the mineralized IQD and barren QD suggest that the two may have been emplaced separately (Lloyd, 2001; Farrow et al., 2002; Lightfoot and Farrow, 2002). In the Totten deposits, the sulfide bearing-IQD would have experienced limited contact with the offset country rocks, and as a consequence the level of As (and other metals that can be derived from the country rocks) contamination would have been reduced relative to Garson. Also, inclusions found within the IQD consist mainly of Nipissing intrusive rocks (As-poor), with rare metasedimentary and QD inclusions (Lloyd, 2001; Lightfoot and Farrow, 2002) thereby further limiting the degree of As contamination. The Totten assay data in the pentlandite field appear to have greater Co/Ni ratios than at Garson. This suggests that the overall geochemistry of pentlandite from the Totten deposits is enriched in Co (or depleted in Ni) compared to the contact-style deposit of Garson, possibly reflecting an overall lower abundance of magmatic sulfarsenides that could sequester Co from the sulfide melt prior to the crystallization of the MSS. Another field shown in this diagram represents a group of samples with low to elevated As, but low Co/Ni ratios (the threshold which was determined from the quantitative mass balance was a Co/Ni ratio=0.06). Quantitative mass balance of the Totten samples suggests that it is unlikely that the sulfarsenides are responsible for the

distribution of As in these samples. It is more likely that nickeline, sperrylite, irarsite-hollingworthite, or BMS (other than pentlandite) control the concentration of As in these samples since these minerals do not contribute significantly to bulk rock Co (section 4.4). The quantitative mass balance has also shown that sperrylite does not contribute significantly to As in As-rich samples, but that sperrylite and BMS (other than pentlandite) do represent the major controlling phases for As in samples with low As and Co/Ni ratio. Nickeline controls the concentration of As in samples with high As, and a low Co/Ni ratio. Co in this field, is likely controlled by trace abundances of BMS (i.e. pentlandite) and sulfarsenides.

Similar trends can be found in Figure 15, which shows a Ni-Co-As ternary plot for the Totten bulk rock assay database. In this diagram, the type of ore (e.g., MASU, INMS, or DISS) has been estimated using the bulk rock concentration of S. This dataset is compared with the calculated bulk rock concentrations (as calculated by quantitative mass balance and represented on the diagram as an orange-colored field; Figure 15) from this study. The estimated bulk rock values (based on mineralogy) span a representative cross section of the variations in the proportions of Ni-Co-As observed in the Totten ores, suggesting that the mineralogical controls determined by the mass balance describes the mineralogical controls on bulk rock geochemistry at the scale of the entire Vale database from a subset of samples. In this study it was found that as samples increased in As relative to Ni and Co, there was an increase in the abundance of sulfarsenide and arsenide phases. Samples with higher Ni and Co relative to As are attributed higher modal abundances of pentlandite. Furthermore, the range of Co-Ni proportions in the low As samples is much greater than near the As apex. This can be explained by the variations in

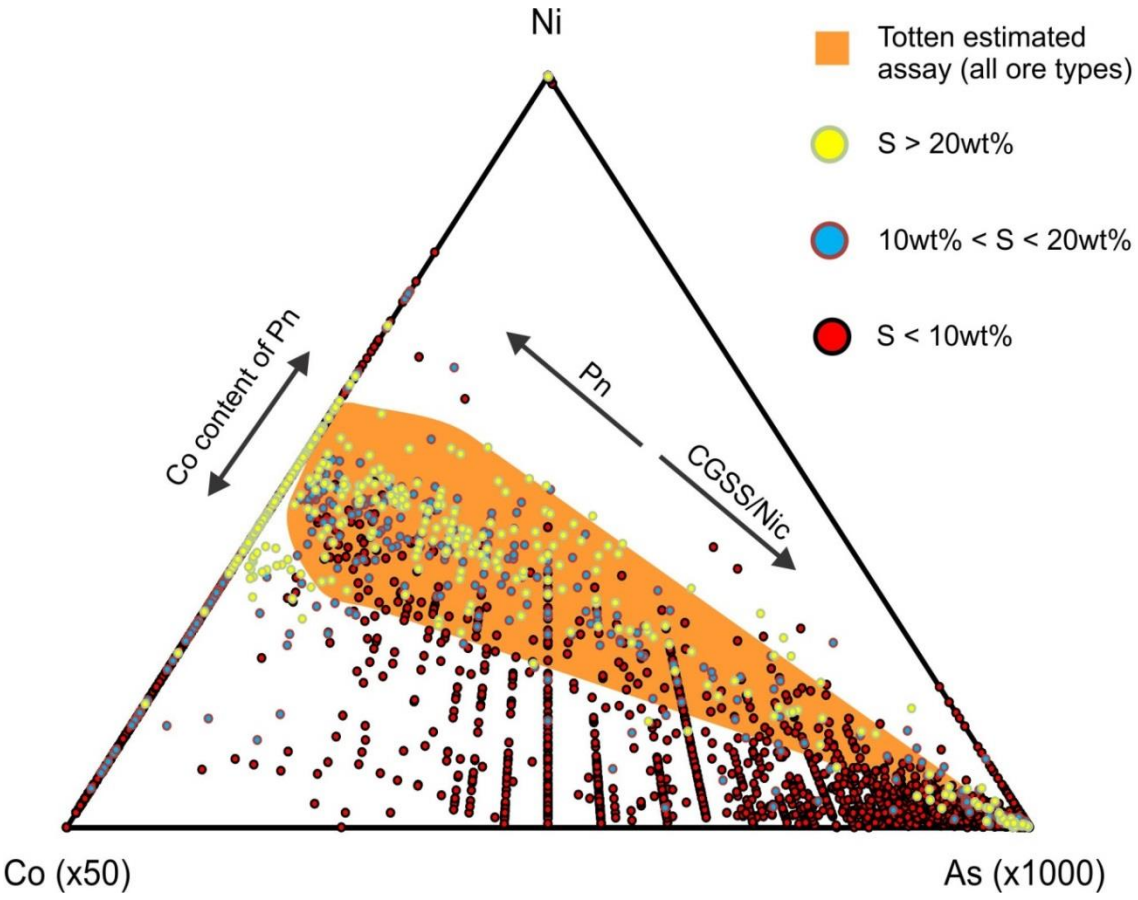

Figure 15. Ni-Co-As ternary diagram of calculated (orange field) and actual bulk rock assays. Data for actual assays from Totten assay database, which was used with the permission of Vale. The color of the Totten assay database points is representative of ore type, which was estimated from the bulk rock concentration of S (S > 20wt% for massive sulfide samples, 10wt% < S <20wt% for semi-massive sulfides, and S < 10wt% for disseminated samples). The chemical trend of the estimated assay appears representative of the range measured in the bulk rock assays, suggesting that the mineralogical controls on Ni-Co-As found in the estimated assays are representative of the bulk rock assays. The mass balance calculations show that with increasing bulk rock As, there is an increase in the proportions of sulfarsenides (CGSS) and nickeline. Whereas high Ni is attributed to the abundance of pentlandite (Pn), the wide spread in data seen with increasing Ni is attributed to variations in the Co content of pentlandite.

the Co content of pentlandite. Not surprisingly, the majority of the massive sulfide and semi-massive sulfide samples are located away from the As apex, which agrees with the observation that sulfarsenides and arsenides are larger/higher in grain size and abundance, respectively in disseminated samples (Appendix A10, Tables 4-6). The location massive and semi-massive samples may also indicate a correlation between As and the abundance of wall rock inclusions, suggesting that these may be the source of As (alternatively, wall rock inclusions may function as a neucleations site for As-carriers). Massive sulfides which sit near the As apex represent rare cases where larger (mm to cm scale) grains of sulfarsenides and arsenides occur in assayed samples. The majority of disseminated samples are located near the As apex of the diagram which is due to the increase in sulfarsenides and arsenides relative to the proportion of pentlandite. Unlike the massive and semi-massive sulfides, the relative proportions of the base metal sulfides in disseminated sulfide samples can be quite variable. Therefore, disseminated sulfides with lower As relative to their Ni and Co content may be attributed to either: (i) low overall abundances of sulfarsenides and arsenides, and/or (ii) high proportions of pentlandite relative to the other base metal sulfides.

A binary plot of Pt versus Pd is shown in Figure 16, showing data from both the Totten and Garson bulk rock assay databases. Both deposits show positive correlations between Pt and Pd. However, the degree of this correlation is stronger in the Totten dataset. There are two possible explanations for the correlation: (i) the distribution of Pt and Pd is controlled by common single mineral phases, or (ii) the spatial distribution of the phases controlling Pt and Pd are the same. The petrographic study and quantitative mass balance of the Totten ores has shown that although the sulfarsenides contain

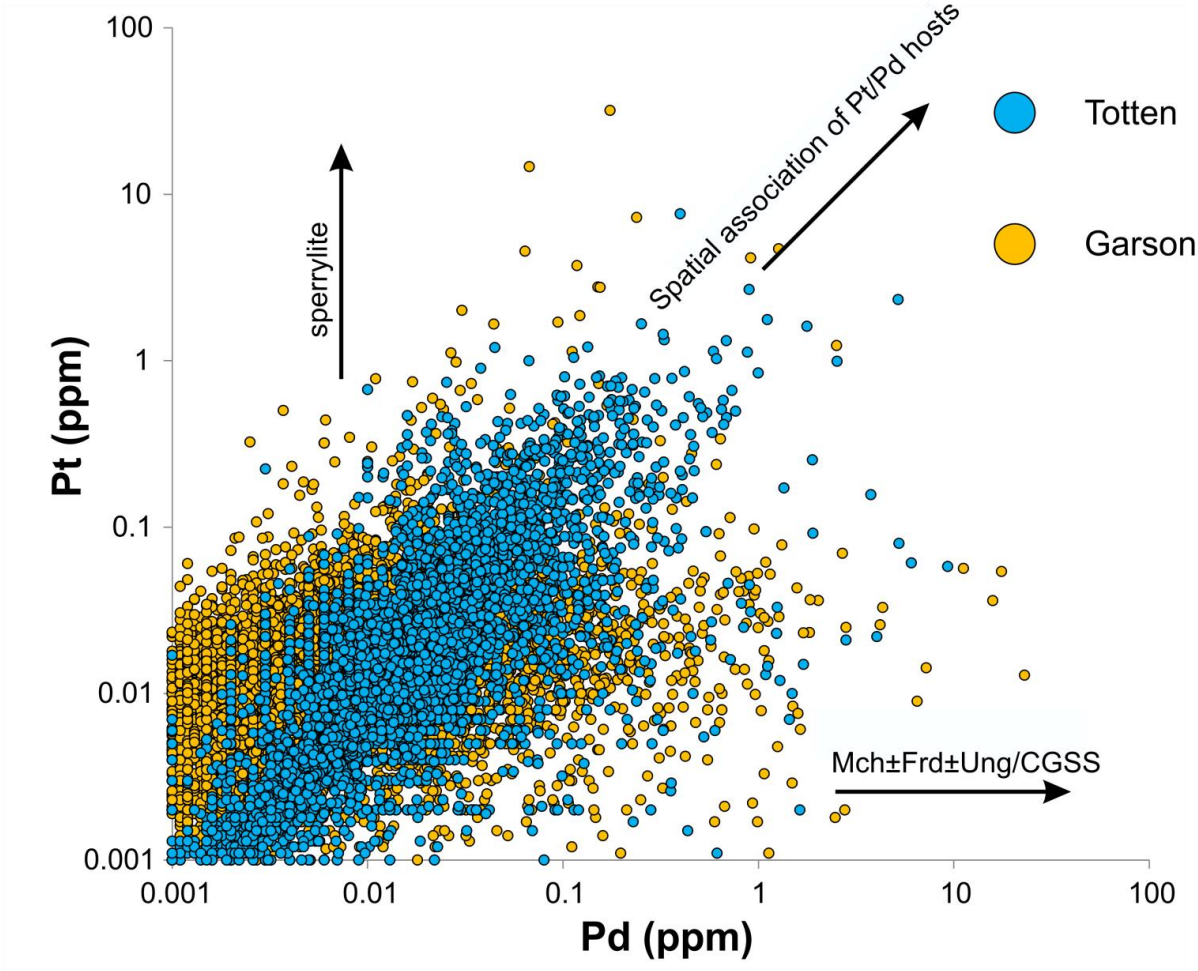

Figure 16. Pd versus Pt scatter plot for the Totten and Garson ores. Data for comparison in this diagram was used, with permission, from the Vale bulk rock assay databases of Totten and Garson. Arrows indicate mineralogical associations. Abbreviations: michenerite (Mch), froodite (Frd), ungavaite (Ung), and sulfarsenide solid solution (CGSS).

elevated PGE in solid solution, they do not account for the bulk of the PGE content of the Totten ores. Rather, discrete PGM (e.g., sperrylite, michenerite, froodite, ungavaite) are responsible for the distribution of most of the PGE (see sections 4.4.3 and 4.4.4) and the vast majority of PGE mineral grains are hosted in base metal sulfides rather than sulfarsenides. This is in contrast to the Garson deposit (Figure 16; Lefort, 2012) where a much larger proportion of the Pd+Pt is hosted in sulfarsenides and arsenides, either as discrete minerals grains/inclusions, or as dissolved Pd. The correlation between Pd and Pt at Totten can be explained through the distribution of PGM. This is supported by observations made in the distribution of Pt and Pd phases at Totten between hosts (Tables 4-6), showing that the main Pd phases (michenerite, froodite) often share a major host phase with associated grins of sperrylite. In disseminated sulfides it was usually observed that the sulfarsenides were an important host of michenerite/froodite, and the dominant host for ungavaite (but not for sperrylite). This explains the moderate positive correlation seen between Pd and As (r_s=0.423, n=174; Table 2), but also the low positive correlation seen between Pt and As (r_s=0.102, n=174; Table 2).

In addition to Pt, Pd also demonstrates strong to moderate positive correlations to Ag (r_s=0.504, n=174; Table 2, also Figure 17), Au (r_s=0.758, n=174; Table 2 as well as Figure 17), and Bi (r_s=0.545, n=174; Table 2). As before, these correlations may be explained through the distribution of the phases responsible for the bulk concentrations of Ag-Au-Bi-Pd (e.g., altaite, galena, hessite, tsumoite, tellurobismuthite, pilsenite, hedleyite, froodite, michenerite, and electrum). In general, these phases appear late and typically occur as open space fillings in the base metal sulfides, or within alteration silicates dispersed within sulfide samples (see section 4.3). Samples which compositions

skewing towards high Pt without corresponding increases in Pd represent samples in which the the abundance of sperrylite increases without an corresponding increase in the abundance of Pd carriers.

The sulfarsenides may not be magmatic in origin (Carter et al., 2001; Magyarosi et al., 2002; Szentpéteri et al., 2002; Stewart, 2002). It is suggested instead that these phases formed through secondary processes (e.g., hydrothermal, or metamorphic). If this were the case then it could be expected that elevated abundances in sulfarsenides (and as a consequence, bulk rock As) would be associated with late (relative to the formation of the sulfide ores), cross cutting veins. In the vicinity of the SIC, neotectonic veins are the only structures that cross cut the ore zones and are characterized by a mineral assemblage of galena, sphalerite, quartz, calcite, and chlorite (Marshall et al., 1999). The occurrence and relative proportions of galena and sphalerite are usually the same within these veins, whereas the quartz, calcite, and chlorite are more irregular. Figure 17 contains a scatter plot of the combined Pb and Zn concentrations plotted against As from the Vale Totten database. The resulting diagram shows no correlation between As and total Pb+Zn (as an indicator metal association for cross cutting structures). Furthermore the bulk rock data of this study does not show any significant correlation between As and Pb (r_s=0.115, n=174) or As and Zn (r_s=-0.001, n=174). This suggests that the sulfarsenides and arsenides (which are a major control on bulk rock As, section 4.4.2) do not show an association (domain) with these late veins, indicating that they may not have formed as a consequence of the late fluids which generated the galena-sphalerite-quartz-chlorite-calcite veins.

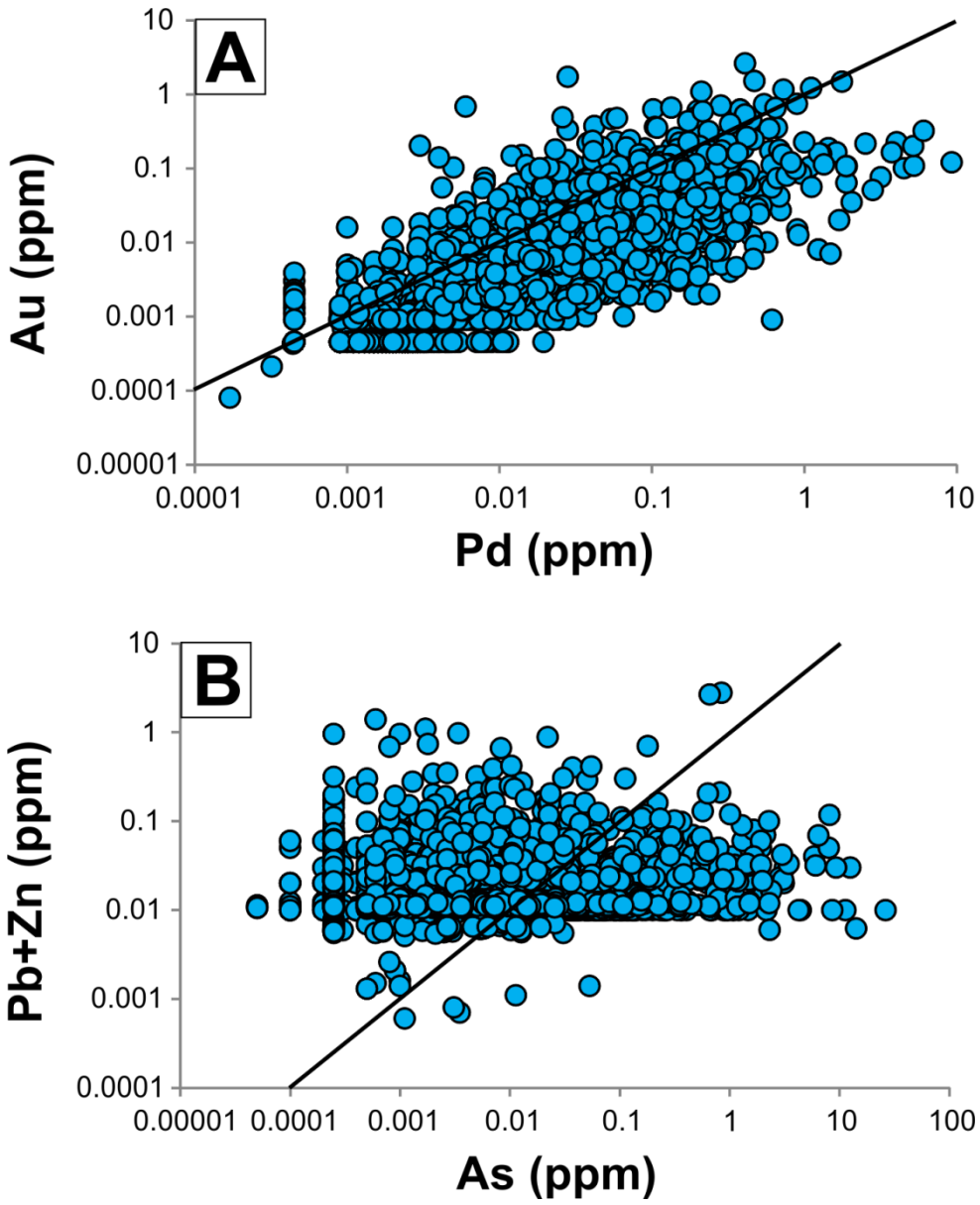

Figure 17. Scatter plots using the Vale Totten bulk rock assay database for Au versus Pd (A), and Pb+Zn versus As (B). A line of perfect correlation has been added to each diagram to establish the nature of the correlation seen in the Totten data. The data was used with the permission of Vale. Although Au and Pd show a positive correlation, no correlation is observed between As and Pb+Zn.

5.4 The spatial distribution of ore metals

The distribution of the accessory phases (in particular, the PGM) has already been shown to be highly variable on the scale of thin sections (Figure 11). In order to observe the distribution of trace phases identified by SEM on a larger scale, the locations of samples quantified by mass balance have been marked on a cross section of a Main ore body drill core (Figures 18 and 19), as well as an underground map for the 1250 level of the 238 ore body (Figures 20 and 21). These diagrams illustrate the stope and orezone-scale distribution of As and Pd as a function of the percent of the total calculated bulk rock concentration contained within each mineral species.

In both Figures 18 and 20, it is clear that the sulfarsenides (CGSS) are largely responsible for the distribution of As, as seen on the scale of thin sections. However, there are localized examples where the abundance of CGSS decreases, which is shown by an increase in the importance of base metal sulfides to the As budget (though it is known that these do not contain significant As, therefore the calculated As content must be low). In both the underground and drill core cross sections, sulfarsenide occurrences do not appear to be related to any host lithological changes. As shown in Figure 18, two different thin sections taken from the same sample demonstrate very different distributions of sulfarsenide phases. As suggested in section 5.2.1, gravitational settling of magmatic sulfarsenide crystals may have caused the concentration of these phases within structural traps, such as the margins of sulfide occurrences. Small localized increases in the abundance of sperrylite are also shown in Figure 18. These are associated with some occurrences of massive and semi-massive sulfides, but not all sulfides show increased abundances in sperrylite. Thus, highly localized variations in

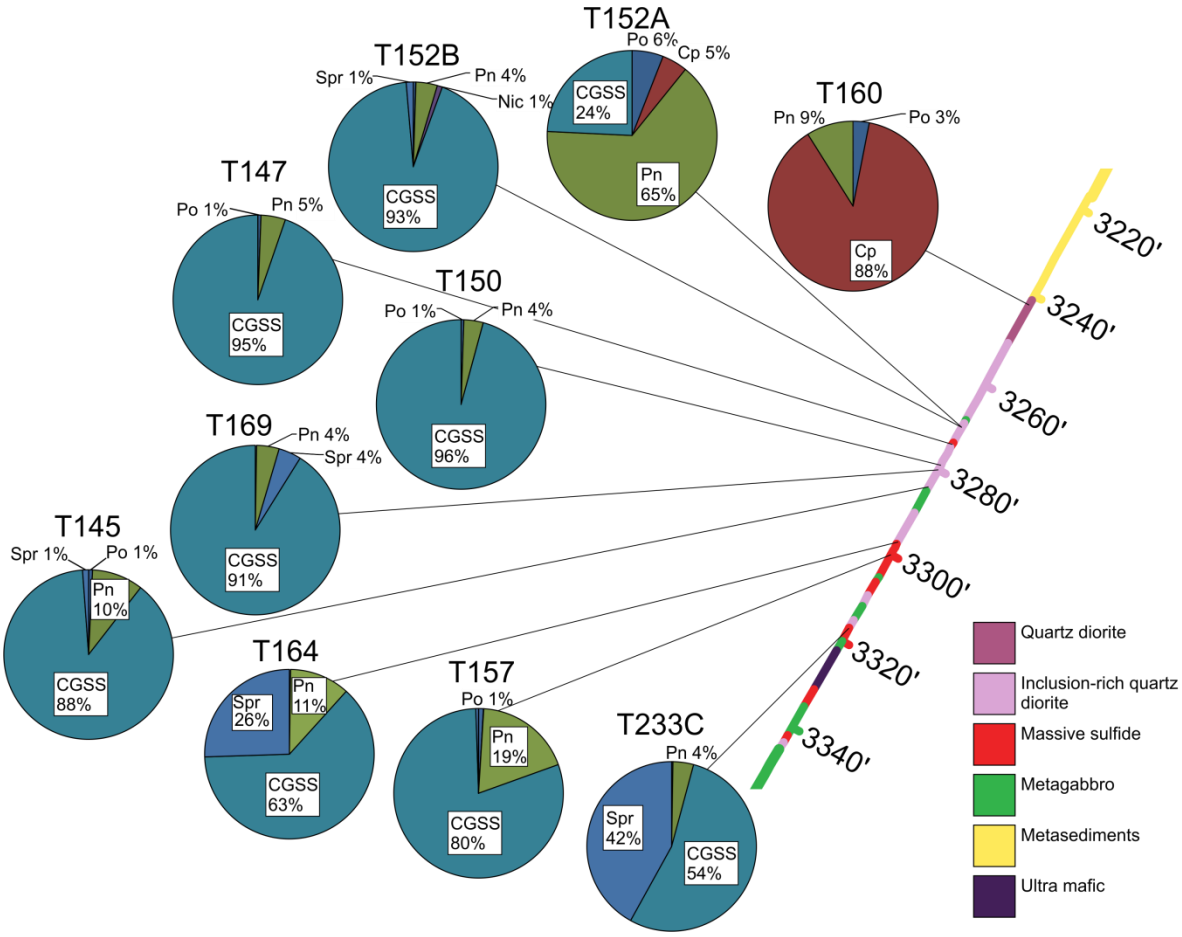

Figure 18. The distribution of As between phases within drill hole 971512 (Main ore body). The lithology of the drill hole was provided by logs given by Vale. Values represent the percentage of the calculated bulk rock concentration hosted within each phase: pyrrhotite (Po), pentlandite (Pn), chalcopyrite (Cp), nickeline (Nic), sulfarsenides (CGSS), and sperrylite (Spr).

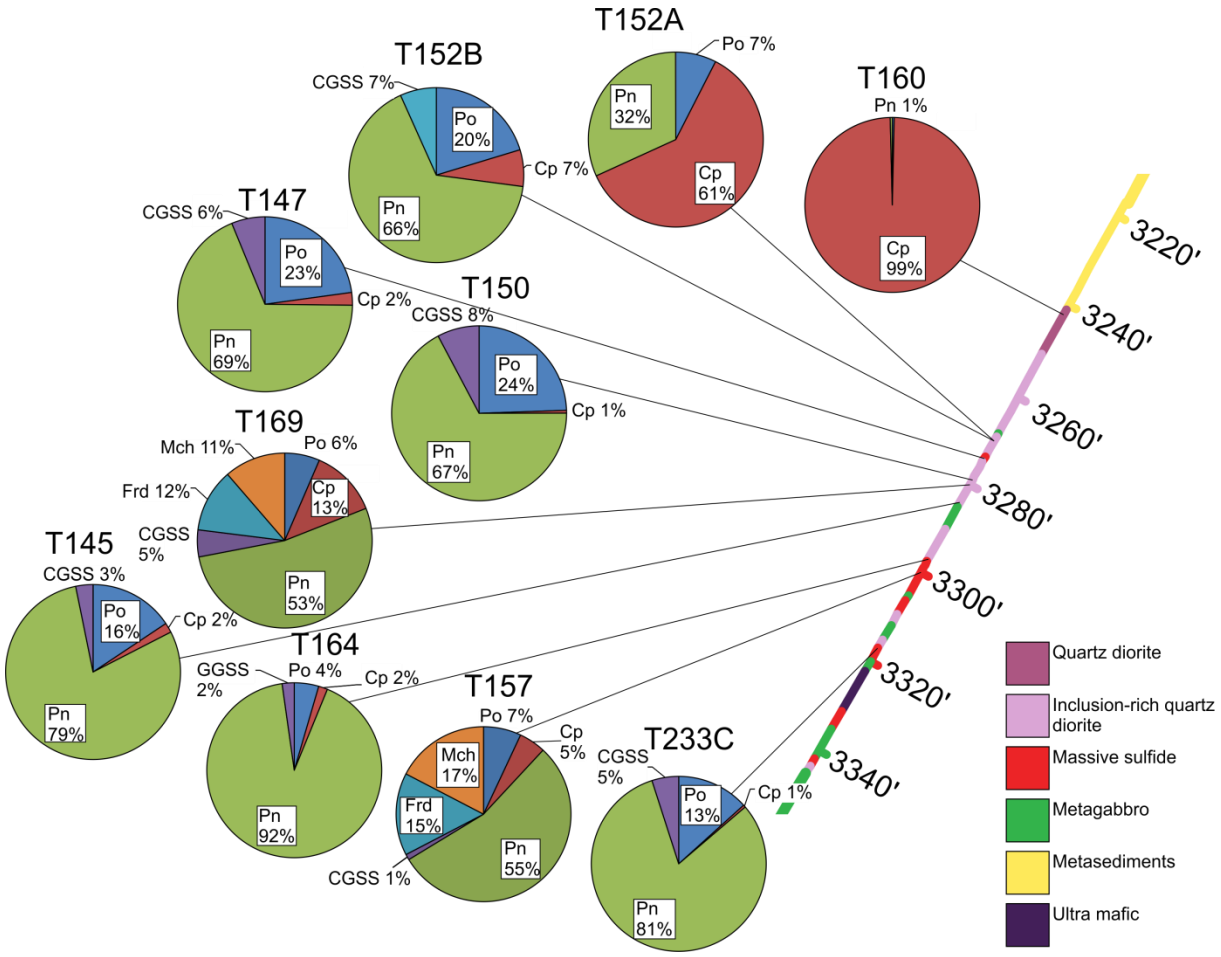

Figure 19. The distribution of Pd between phases within drill hole 971512 (Main ore body). The lithology of the drill hole was provided by logs given by Vale. Values represent the percentage of the calculated bulk rock concentration hosted within each phase: pyrrhotite (Po), pentlandite (Pn), chalcopyrite (Cp), sulfarsenides (CGSS), michenerite (Mch), and froodite (Frd).

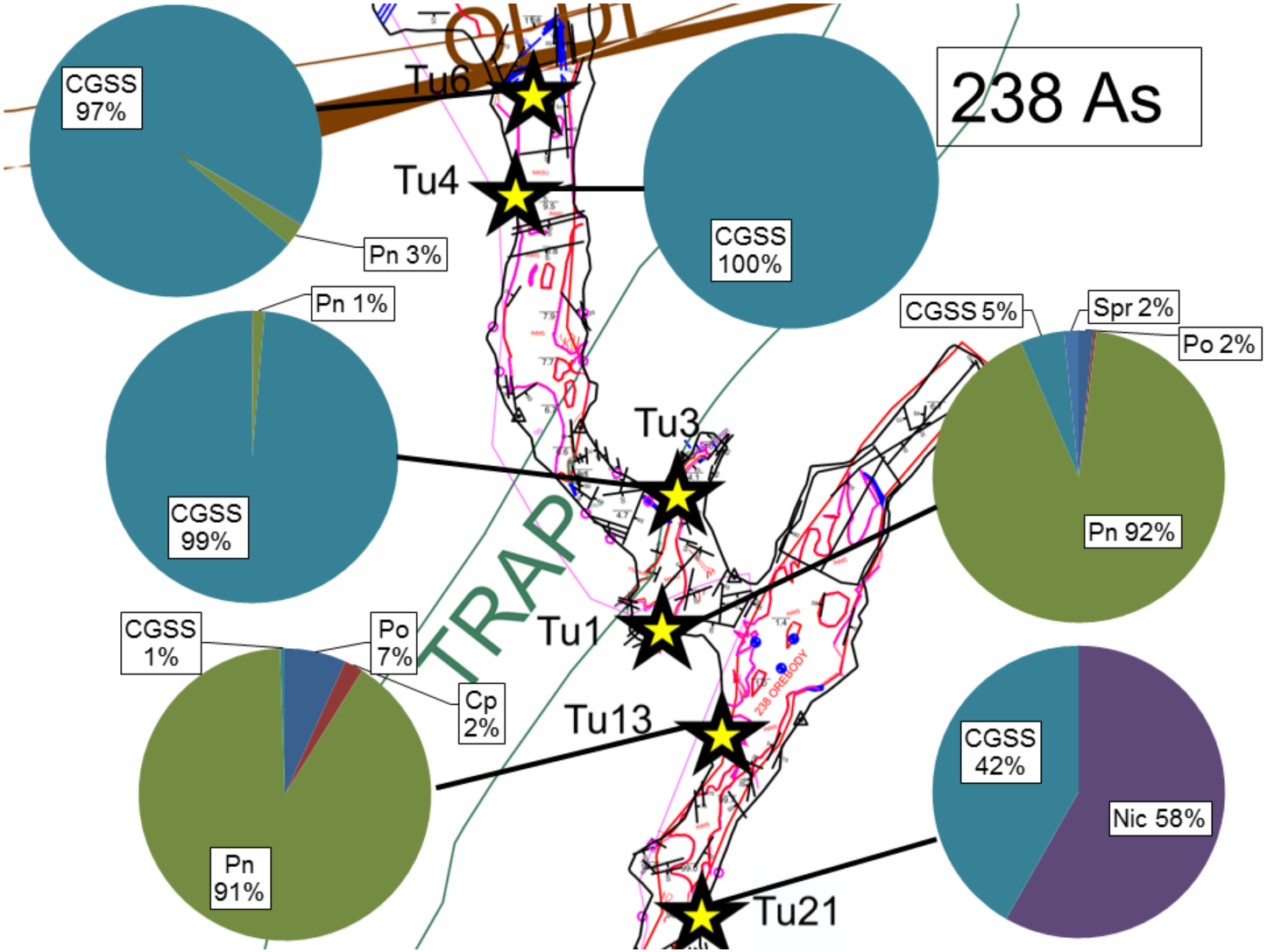
238 As
Tu6
Tu4
Tu3
Tu1
Tu13
Tu21
CGSS 97%
Pn 3%
CGSS 100%
Pn 1%
CGSS 99%
CGSS 5%
Spr 2%
Po 2%
Pn 92%
CGSS 1%
Po 7%
Cp 2%
Pn 91%
CGSS 42%
Nic 58%
TRAP
238 OREBODY

Figure 20 (previous page). The distribution of As between phases within a section of the 1250 level, of the 238 ore body. Values represent the percentage of the calculated bulk rock concentration hosted within each phase: pyrrhotite (Po), pentlandite (Pn), chalcopyrite (Cp), sulfarsenides (CGSS), nickeline (Nic), and sperrylite (Spr). The unit on the Vale map labeled as "Trap" is part of the Sudbury diabase dyke swarm.

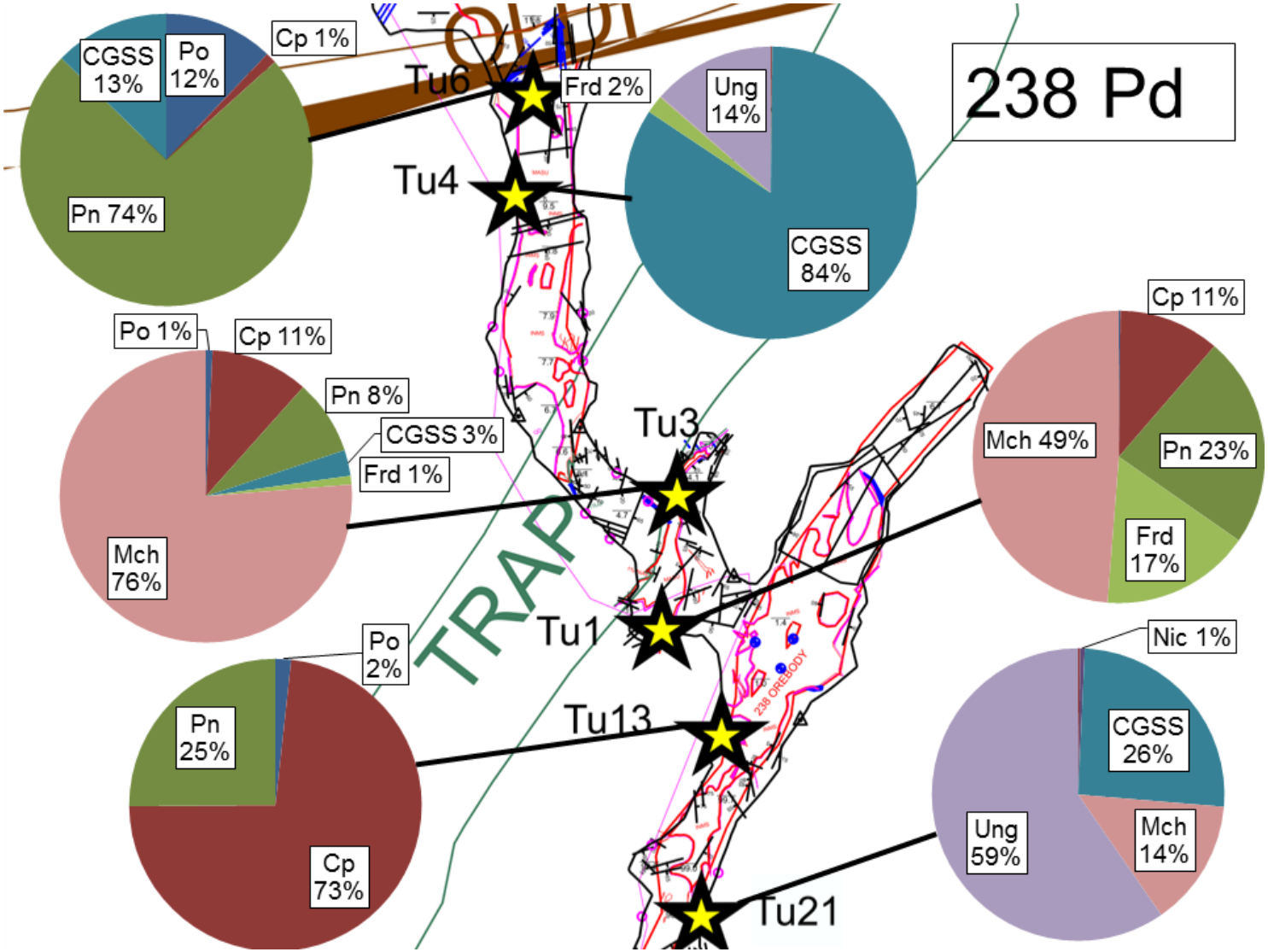
238 Pd
Tu6
Tu4
Tu3
Tu1
Tu13
Tu21
TRAP
Cp 1%
CGSS 13%
Po 12%
Pn 74%
Frd 2%
Ung 14%
CGSS 84%
Po 1%
Cp 11%
Pn 8%
CGSS 3%
Frd 1%
Mch 76%
Cp 11%
Mch 49%
Pn 23%
Frd 17%
Po 2%
Pn 25%
Cp 73%
Nic 1%
CGSS 26%
Ung 59%
Mch 14%

Figure 21 (previous page). The distribution of Pd between phases within a section of the 1250 level, of the 238 ore body. Values represent the percentage of the calculated bulk rock concentration hosted within each phase: pyrrhotite (Po), pentlandite (Pn), chalcopyrite (Cp), sulfarsenides (CGSS), michenerite (Mch), froodite (Frd), and ungavaite (Ung). The unit on the Vale map labeled as "Trap" is part of the Sudbury diabase dyke swarm.

sulfarsenide/sperrylite abundance may reflect variations in temperature in proximity to wall rock inclusions as nucleation sites, wall rock surfaces as setteling sites, or variations in flow dynamics of sulfide melt in which sulfarsenides/sperrylite were entrained.

The distribution of Pd shows much more variability than As (Figures 19 and 21). The calculated concentrations of many samples shown are under reported in terms of Pd, which causes much of the Pd budget to be attributed to pentlandite (Figure 11). In two thin sections taken from the same sample (Figure 19), the intra-sample changes in the relative proportions of the base metal sulfides cause variations in the calculated distribution of Pd between sulfide phases. The 238 underground samples (Figure 21), show a greater proportion of PGM (michenerite, froodite, ungavaite) represented in thin section in some localized areas. It is not clear if this distribution is a function of lithology (the occurrence of michenerite seems greatest adjacent to the trap dyke), or is controlled by the occurrence of structural traps (such as the margins of the ore body). During underground and drill core sampling, it was observed that the margins of some sulfide occurrences were marked by a pale green tarnish (Figure 22). Petrographic analysis of these samples revealed an association of the tarnish with sulfarsenides. This suggests that the tarnish is in fact annabergite [$Ni_3(AsO_4)_2.8H_2O$, also known as "nickel bloom"], an alteration product of Ni-arsenides (Melgarejo and Martin, 2011). In Figure 22, annabergite is located on both margins of the sulfide vein.

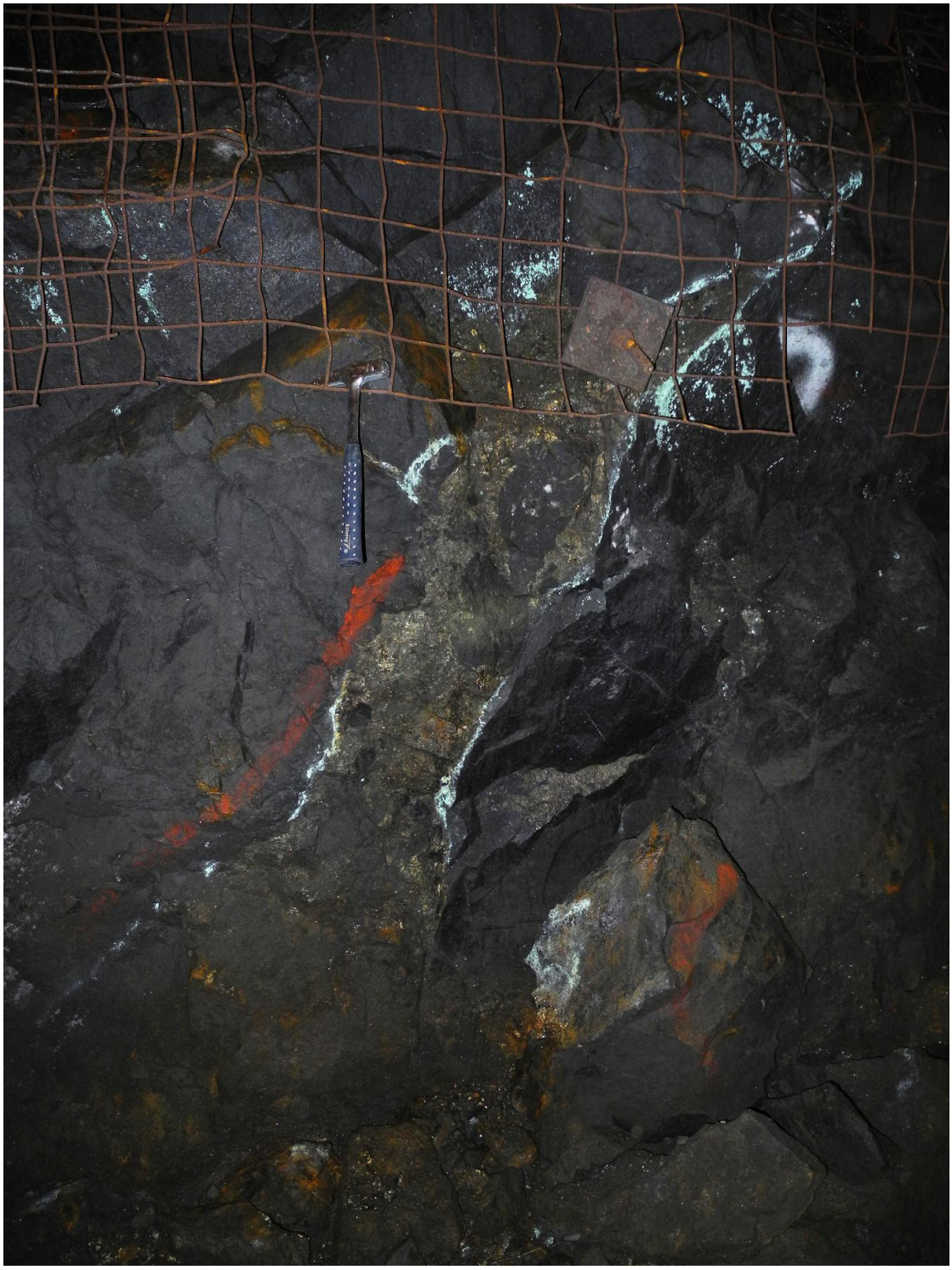

Figure 22. Annabergite [$Ni_3(AsO_4)_2.8H_2O$, green tarnish] occurring along the margins of a near vertical (see rock hammer) sulfide vein. Annabergite is a weathering by-product of the Ni-arsenides concentrated along the edges of the vein. Photo credit: Enrick Tremblay (Vale). Local contamination along the margins of the sulfide vein is unlikely since the host rock (quartz diorite) is As-poor. Furthermore, metamorphic melting is an unlikely source for an As-rich liquid (Tomkins et al., 2006).

Other underground occurrences of annabergite were seen in sulfide veins which run parallel to the horizontal stopes shown in Figure 4 and are contained within a single rock type. In these cases annabergite concentrated *only* along the bottom (sill) contact of the vein with its country rock. This was also observed in some veins seen in drill core during sampling. Since annabergite represents the weathering of Ni-arsenides, it seems that the sulfarsenides (and possibly arsenides) are concentrated along the lower margins of sulfide occurrences. This feature is difficult to explain using the hydrothermal model for sulfarsenide formation, since the interaction of fluids, and sulfide/host rock reactions would not be limited to one side of the vein. However, the magmatic model of sulfarsenide crystallization would suggest that these concentrations formed via gravitational settling of magmatic crystals, or as in Figure 22, along vein margins where sulfide flow dynamics concentrated magmatic sulfarsenide and arsenide phenocrysts.

Another potential trap for sulfarsenides found in the Totten ore bodies is the surfaces of xenoliths which are common in contact sublayer rocks. Occurrences of large volumes of these inclusions in sulfides and sublayer rocks are referred to a “boulder beds” by Sudbury geologists. In principle, magmatic sulfarsenides could accumulate along the contacts of these inclusions; however, there is no real evidence in the geochemical or petrographic data of this study that supports this idea.

Geochemical and mineralogical variations can occur not only between different offset dykes, but between deposits hosted within the same offset (Pattison, 1979; Farrow and Lightfoot, 2002). Figure 23 is a comparison of the major and trace metal distribution between base metal sulfides (e.g., pyrrhotite, pentlandite, and chalcopyrite), arsenides,

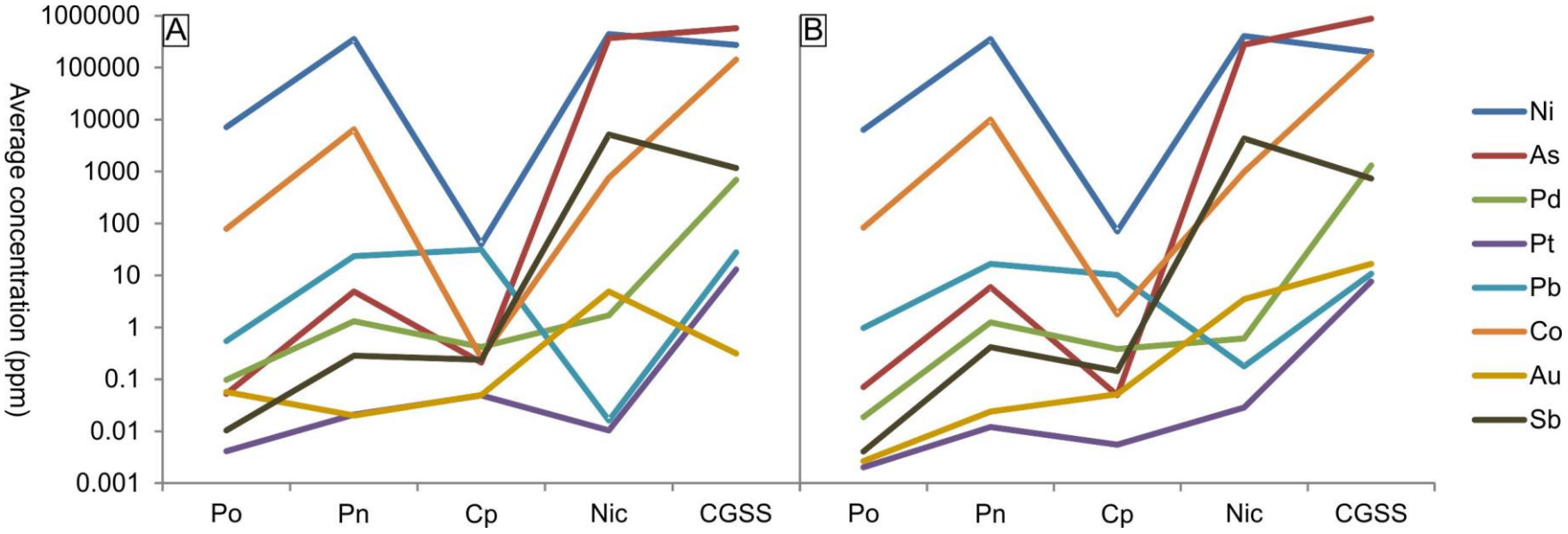

Figure 23. Comparison of mineral chemistry in the Main (A) and 238 (B) ore body assemblages. Average concentrations for each metal were calculated using the LA-ICP-MS data from this study. Abbreviations: pyrrhotite (Po), pentlandite (Pn), chalcopyrite (Cp), nickeline (Nic), and the sulfarsenide solid solution (CGSS).

and sulfarsenides in the Main and 238 ore bodies. The diagram shows that the distribution is almost the same in both deposits. This suggests that any processes which may have created or modified the occurrence of ore metals, had the same level of influence in both ore bodies and that the ore bodies were derived from the same parent sulfide liquid, which is in agreement with the similarities observed in thin sections from both the 238 and Main ore bodies (see sections 4.2, and 4.3).

The previous points on metal distribution suggest a level of uncertainty with regards to the representivity of the quantification of an ore composite sample by the Mineral Liberation Analyser (MLA), a device which uses SEM and EDS to quantify the mineralogy of a sample, much like what was done in this study. However unlike "manual" SEM-EDS, the SEM-MLA method is completely automated and can be used to analyse thousands of grains within a single sample. Reports of two MLA analyses of Totten ore composites were obtained for comparison to the results of this study from the equivalent samples. Both MLA analyses ran for approximately 13 hours and analyzed thousands of particles. In both samples no deleterious minerals were detected, which fails to explain the concentrations of As found in the mill concentrates for these samples by bulk rock analysis. Furthermore, no precious metal phases (e.g., electrum, PGM) were detected by MLA. The resolution of the MLA scan is proportional to the run time of the analysis (which is also directly related to the cost of the scan). It is possible that the MLA did not detect these precious and deleterious phases because the resolution was not high enough to detect the tiny (μm and nm scale, Appendix A10) inclusions of PGM and sulfarsenides common to the Totten ores. Furthermore, the samples analyzed by MLA were multi-kg ore composite samples representing a blend of different ore samples from a

stope or zone as a means to quantify the overall mineralogical character of a stope or zone in terms of process mineralogy. While this approach is common place in industry, it does not allow for a robust evaluation of localized sample heterogeneity. More frequent sampling within a planned ore volume using test drilling combined with assays, thin section petrography on single, small samples from different areas of the ore volume rather than larger composites serves to better characterize stope scale variations in deleterious and precious metals at Totten. While this would appear to be more labour intensive, the time to scan single thin sections by SEM is less and the resolution at which this can be carried out would be greater. Ideally, visual indicators for deleterious and precious metal abundance would allow specific areas of an ore volume to be potentially avoided or mined, or at least acknowledged as being potentially problematic before being blended and sent for processing. Manual SEM-EDS analysis of uncrushed ore samples also provides additional textural characterization (paragenetic constraints allow for detailed classification of mineralization domains at Totten) that is lost with MLA.

6.0 Conclusions

The results of the Totten metallurgical study have revealed key characteristics of the deposit which give new insights into the genesis of the ores, as well as findings which are relevant to mineral processing. These characteristics are as follows:

(i) The base metal sulfides are consistently poor in the deleterious metals (e.g., As and Pb). These concentrations were determined by LA-ICP-MS analysis of pyrrhotite (As_{main}= 0.05 ppm, n=30 analyses; As_{238}=0.07 ppm, n=60 analyses; Pb_{main}= 0.52 ppm, n=30 analyses; Pb_{238}= 0.88 ppm, n=60 analyses), pentlandite (As_{main}= 4.87 ppm, n=30

analyses; As_{238}= 5.93 ppm, n=62 analyses; Pb_{main}= 2.33 ppm, n=30 analyses; Pb_{238}=16.7 ppm, n=62 analyses), and chalcopyrite (As_{main}= 0.21 ppm, n=26 analyses; As_{238}= 0.05 ppm, n=59 analyses; Pb_{main}= 29.33 ppm, n=26 analyses; Pb_{238}= 9.3 ppm, n=59 analyses). Pentlandite also demonstrates elevated concentrations of Co (Co_{main}= 0.65 wt%, n=30 analyses; Co_{238}= 1.0 wt%, n=62 analyses).

(ii) The arsenide [nickeline (Nic), NiAs; Table 7] and sulfarsenide [cobaltite-gersdorffite-glaucodot solid solution (CGSS), (Co, Fe, Ni)AsS; Appendix A9] minerals, though volumetrically minor, account for the bulk of the As in the Totten ores (Appendix A10). In massive and semi-massive sulfides, pyrrhotite is the dominant host of CGSS (Tables 4 and 5; average grain size 809 μm^2, n=472 grains) and nickeline (Tables 4 and 5; average grain size 469 μm^2, n=80 grains). In disseminated sulfides (samples with less than 50% sulfides by volume, usually in the form of sulfide blebs and stringers, which are located in the margins of massive and semi massive sulfide zones) these deleterious phases are more abundant (total number of grains observed: n_{CGSS}=2885, n_{Nic}=638; Table 6), have greater volume (42305 μm^2 $average_{CGSS}$; 58256μm^2 $average_{Nic}$), and are primarily hosted in silicate minerals dispersed within sulfide samples, or along the boundary of silicates/sulfides. Whereas variations in abundance and mineralogy of As do not appear to correlate to variations in host lithology along the offset-dyke hosted deposits at Totten, the local association of As phases with host rock contacts may reflect locally low temperature near these contacts, nucleation sites and sites for settling of magmatic sulfarsenide and arsenide phenocrysts at these contacts, and wall rock influence on sulfide flow dynamics as magmatic sulfarsenides and arsenides were transported

into/moved around within the offset environment. Localized contamination by country rocks at Totten (isolated from the sulfides by QD) is unlikely.

(iii) In massive and semi-massive sulfide samples, the smaller sulfarsenide grains may contain cores of irarsite-hollingworthite [(Ir,Ru,Rh,Pt)AsS-(Rh,Pt,Pd)AsS, Table 7; Figure 7B, C, and F] and sperrylite [$PtAs_2$, Figure 7E]. The euhedral nature of the sulfarsenide inclusions (Figure 7A, B, C, D, E, and F) encased completely in *PGE+As depleted* base metal sulfides, and the occurrence of high temperature minerals at the cores of these grains agrees with previous studies that the *sulfarsenide minerals* are magmatic in origin (whereas many authors suggest that they formed from hydrothermal or metamorphic fluids). The genetic model in this study indicates that magmatic sulfarsenides may have nucleated on earlier PGM (irarsite-hollingworthite, and sperrylite) before becoming enclosed in crystallizing base metal sulfides. In some cases grains which achieved sufficient size sank towards the lower margins of the sulfide ore bodies. This is supported by the increased grain size, and sulfarsenide cumulates observed in disseminated samples (Figure 7D and G). Oxidation products of Ni-arsenides (annabergite, $Ni_3(AsO_4)_2.8H_2O$, “nickel bloom") are concentrated along the margins of sulfide veins underground and in drill core (Figure 22). In cases where the vein is horizontal, annabergite is observed *only* on the lower (with respect to gravity) side of the vein, providing a visual indication of As distribution. In principle, the abundant xenoliths found in association with the sulfide ores may have also served as a site for magmatic sulfarsenides to settle, however, no evidence was found that supports this hypothesis. An additional problem with the idea that sulfarsenides formed via secondary (e.g.,

hydrothermal, or metamorphic) fluids is that this model might be thought to require an association between sulfarsenides and the late galena-sphalerite-quartz-calcite-chlorite veins which are common in the South Range, cross cutting the ores at Totten. Since no correlation could be found between As (sulfarsenide controlled) and Zn+Pb concentrations (sphalerite and galena controlled) in the bulk rock database, it seems unlikely that this domain of As-enrichment exists, or is significant (Figure 17). A complete study of the structural domains related to As and PGE is suggested to captin or refute this argument.

(iv) The sulfarsenides demonstrate a wide range in composition [$(Ni_{0.76}Co_{0.14}Fe_{0.11})_{\Sigma 1.00}As_{0.99}S_{1.01}$-$(Ni_{0.17}Co_{0.68}Fe_{0.15})_{\Sigma 1.00}As_{0.88}S_{1.12}$; Figure 12], which may be explained as a function of the temperatures at which the individual crystals reached final equilibration (ranging from 300°C-600°C, Figure 12). This compositional variation may prove problematic for the removal of sulfarsenides during ore processing if the flotation circuits utilize an ideal composition of the sulfarsenides and Co/Ni ratios impact floatation efficiency/yield. Mass balance calculations have shown that even small concentrations of sulfarsenides (for example, 0.02 volume %) can significantly increase the bulk concentration of As to problematic levels.

(v) In plots of the ratio of Co/Ni *versus* As (Figure 14), four major trends are observed in the assay data from Totten and Garson ores: (i) samples in which Co/Ni ratios are greater than 0.06 and As concentration below 0.1wt% occur when Nic and CGSS grains are rare-absent (less than 0.3% by volume) and pentlandite controls the distribution of Ni-Co; (ii)

samples where the Co/Ni ratio is greater than 0.06, and the concentration of As is greater than 0.1wt%, in which the distribution of As, Co, and Ni is mainly controlled by CGSS; (iii) samples with Co/Ni ratios below 0.06, and elevated As concentrations, nickeline is the dominant controlling As phase; and (iv) for samples with Co/Ni ratios below 0.06 and low As concentrations (<0.01 wt%), in which sperrylite and irarsite-hollingworthite will be the dominant controls on As abundance.

(vi) The concentrations of Pt and Pd are low in pyrrhotite [Pt_{main}=0.004 ppm (n=30 analyses); Pt_{238}= 0.002 ppm (n=60 analyses); Pd_{main}= 0.097 ppm (n=30 analyses); Pd_{238}= 0.019 ppm (n=60 analyses)] and chalcopyrite [Pt_{main}= 0.05 ppm (n=26 analyses); Pt_{238}= 0.006 ppm (n=59 analyses); Pd_{main}= 0.42 ppm (n=26 analyses); Pd_{238}= 0.38 ppm (n=26 analyses)], whereas pentlandite is poor in Pt [Pt_{main}= 0.021 ppm (n=30 analyses), Pt_{238}= 0.011 ppm (n=62 analyses)], but contains elevated Pd [Pd_{main}= 1.31 ppm (n=30 analyses), Pd_{238}= 1.24 ppm (n=62 analyses)]. Mass balance calculations indicate that PGM are responsible for the distribution of the majority of bulk rock Pd and Pt. In individual sulfide ore samples where estimated and bulk rock assay concentrations are in agreement, sulfarsenides may contribute as much as 0.8% and 93% of the bulk concentrations of Pt and Pd respectively, whereas nickeline may contribute as much as 0.00003 % and 0.1% of the bulk concentrations of Pt and Pd respectively.

(vii) Sperrylite ($PtAs_2$, Table 7) is the only discrete Pt-mineral found within the Totten ore assemblage and accounts for the majority of bulk rock Pt found within the ores. In massive and semi-massive ores, pyrrhotite is the dominant host for sperrylite (Tables 4

and 5; average grain size 2183μm^2, n=41 grains), whereas sperrylite is usually hosted in silicates dispersed within sulfide samples, or along the boundary of sulfide/silicate minerals in disseminated sulfide samples (Table 6; average grain size 150μm^2, n=4 grains). The euhedral-subhedral nature of the sperrylite inclusions in the massive and semi-massive sulfides (Figure 8A), as well as the occurrence of sperrylite cores in sulfarsenides (Figure 7E) suggesting that sperrylite formed as an early magmatic phase. The formation of sperrylite sequestered Pt from the sulfide melt, resulting in base metal sulfides that are depleted in Pt.

(viii) Discrete Pd-phase observed in the Totten ores consist of palladian michenerite (PdBiTe, Table 7), froodite ($PdBi_2$, Table 7), and ungavaite (Pd_4Sb_3, Table 7). The dominant host phase for michenerite in massive sulfides is pyrrhotite (Table 4; average grain size 482μm^2, n=12 grains), pentlandite in semi-massive sulfides (Table 5; average grain size 67μm^2, n=6 grains), and in silicate minerals dispersed within disseminated sulfide samples (Table 6; average grain size 607μm^2, n=33 grains). Dominant hosts of froodite are chalcopyrite in massive sulfides (Table 4; average grain size 69μm^2, n=10 grains), pentlandite in semi-massive sulfides (Table 5; average grain size 58μm^2, n=23 grains), and silicate minerals dispersed within disseminated sulfides (Table 6; average grain size 40μm^2, n=53 grains). Ungavaite is associated with pyrrhotite in massive sulfides (Table 4; average grain size 54μm^2, n=1 grains), CGSS in disseminated sulfides (Table 6; average grain size 205μm^2, n=65 grains), and was not observed in semi-massive sulfides. The Pd minerals usually infill fractures and vugs (Figure 8B, C, D, and F), but also occur along the boundaries of sulfides and silicates (Figure 8H). It is unclear whether

these phases formed from a late semi-metal rich melt, or were formed by secondary processes (e.g., hydrothermal, metamorphic).

(ix) When the bulk rock concentrations of Pd and Pt are shown on a binary diagram (Figure 16), samples which are skewed towards elevated Pt with no corresponding increase in Pd, represent increases in the abundance of sperrylite (Pt carrier) without any increase in the abundance of Pd carriers. When samples skew towards high Pd without simultaneous increase in Pt, the abundances of Pd-carriers (michenerite, froodite, and ungavaite) and sulfarsenides (as previously mentioned, sulfarsenides can be a major host for Pd-carriers) increases without a corresponding increase in sperrylite. However, a positive correlation in the increase of both Pt and Pd purely indicates a spatial association of main host phases for Pt and Pd carriers (since it has been established that these respective metals have different discrete carriers).

(x) Galena (PbS) is the dominant Pb-carrier, with minor occurrences of altaite (PbTe, Table 7). The dominant hosts of galena are pyrrhotite in massive sulfides (Table 4; average grain size 240μm^2, n=535 grains), and silicates dispersed within semi-massive (Table 5; average grain size 117μm^2, n=405 grains) and disseminated sulfides (Table 6; average grain size 401μm^2, n=625 grains). Altaite is associated with pyrrhotite in massive and semi-massive sulfides (Tables 4 and 5; average grain size 711μm^2, n=29 grains), and the boundary between chalcopyrite and silicate minerals in disseminated sulfides (Table 6; average grain size 52μm^2, n=16 grains). Galena and altaite occur as inclusions infilling vugs and fractures (Figure 9B and D), but also form composite grains (single

conglomerated grains with multiple minerals present) with hessite (Ag_2Te, Table 7), tsumoite (BiTe, Table 7), and tellurobismuthite (Bi_2Te_3, Table 7).

(xi) The relative proportion of discrete metal carriers varies between thin sections, which leads to the under (and over) estimation of bulk rock concentrations of metals (Figure 11). This heterogeneity is present at all scales (hand sample, drill core, and stope; see Figures 18-21); therefore the analysis of multiple samples, taken at regular intervals, is required in order to be representative of the Totten ore assemblage. The mineral liberation analyzer (provided by Vale) measurements of a single composite ore sample would not have been representative of mineral assemblage variations on a stope scale. Furthermore, this analysis failed to detect any deleterious minerals (e.g., nickeline, sulfarsenides) in composite samples related to high As concentrations. Discrete PGM (michenerite, froodite, ungavaite) were also not observed in the composite sample by means of MLA analysis. This is likely the result of a scanning threshold which cannot distinguish tiny inclusions of discrete phases in massive sulfides. The analysis of multiple thin sections by SEM-EDS (as done in this study), appears to be more representative of the ore mineral assemblage. If done at the same level of resolution, MLA appears to be less cost/time effective than the analysis of multiple thin sections by SEM-EDS. Additionally, MLA provides less *in-situ* textural detail about the occurrence of accessory phases.

7.0 References

Ames, D.E., and Farrow, C.E.G., 2007, Metallogeny of the Sudbury mining camp, Ontario: Mineral Deposits Division, Geological Association of Canada Special Publication 5, p. 329-350.

Ames, D. E., Davidson, A. & Wodicka, N., 2008. Geology of the Giant Sudbury polymetallic mining camp, Ontario, Canada. Economic Geology, v. 103, pp. 1057-1077.

Bennett, S. L. & Heyding, R. D., 1966. Arsenides of the transition metals. VIII. Some binary and ternary group VIII diarsenides and their magnetic and electrical properties. Canadian Journal of Chemistry, v. 44, pp. 3017–3030.

Cabri , L. J., 1965. Phase relations in the Au-Ag-Te system and their mineralogical significance. Economic geology, v. 60, pp. 1569-1606.

Cabri, L. J. & Laflamme, J. H. G., 1976. The mineralogy of the platinum-group elements from some copper-nickel deposits of the Sudbury area, Ontario. Economic Geology, v. 71, p. 1159−1195.

Card, K. D., Gupta, V. K., McGrath, P. H. & Grant, F. S., 1984. The Sudbury Structure: its regional geological and geophysical setting *in* Pye, E.G., Naldrett, A.J., and Giblin, P.E., eds., The Geology and Ore Deposits of the Sudbury Structure. Ontario Geological Survey, Special Publication v.1, p. 25-43.

Carter, W. M., 2000. Sulphide, Sulpharsenide, and Platinum-Group Minerals from the 740 Deposit, Kelly Lake Orebody of the Copper Cliff Offset, Sudbury, Canada. B.Sc. thesis, Carleton University, Ottawa, 95 p.

Carter, W. M., Watkinson, D. H. & Jones, P. C., 2001. Post-magmatic Remobilization of Platinum-Group Elements in the Kelly Lake Ni-Cu Sulfide Deposit, Copper Cliff Offset, Sudbury. Exploration Mining Geology, v. 10, p. 95–110.

Cochrane, L. B., 1984. Ore Deposits of the Copper Cliff Offset *in* Pye, E.G., Naldrett, A.J., and Giblin, P.E., eds., The Geology and Ore Deposits of the Sudbury Structure. Ontario Geological Survey, Special Publication v.1, pp. 347-360.

Dare, S. A., Barnes, S. J., Prichard, H. M. & Fisher, P. C., 2010. The Timing and Formation of Platinum-Group Minerals from the Creighton Ni-Cu-Platinum-Group Element Sulfide Deposit, Sudbury, Canada: Early Crystallization of PGE-Rich Sulfarsenides. Economic geology, v.105, pp. 1071-1096.

Dare, S. A., Barnes, S. J., Prichard, H. M. & Fisher, P. C., 2011. Chalcophile and platinum-group element (PGE) concentrations in the sulfide minerals from the McCreedy East deposit, Sudbury, Canada, and the origin of PGE in pyrite. Mineralium Deposita, v. 46, pp. 381-407.

Dietz, R., 1964. Sudbury Structure as an astrobleme. The Journal of Geology, v. 72, pp. 412-434.

Dressler, B. O., 1984. Footwall of the Sudbury Igneous Complex, District of Sudbury. Ontario Geological Survey Miscellaneous Paper, v. 106, pp. 73-75.

Dressler, B. O., Peredery, W. V. & Muir, T. L., 1992. Geology and mineral deposits of the Sudbury structure; *in* Ontario Geological Survey Guidebook, v.8, p38.

Durazzo, A., and Taylor, L.A., 1982. Exsolution of the Mss-pentlandite system: textural and genetic implications for Ni-sulfide ores. Mineralium Deposita, v. 17, 313-332.

Elliot, R. P., 1965. Constitution of binary alloys, 1st supplement: Materials Science and Engineering Series. New York: McGraw-Hill. 877 p.

Farrow, C.E.G., and Watkinson, D.H., 1992. Alteration and the role of fluids in Ni, Cu and platinum-group element deposition, Sudbury Igneous Complex contact, Onaping-Levack area, Ontario. Mineralogy and Petrology, v. 46, pp. 67-83.

Farrow, C.E.G., and Watkinson, D.H., 1997. Diversity of precious-metal mineralization in footwall Cu-Ni-PGE deposits, Sudbury, Ontario: Implications for hydrothermal models of formation. Canadian Mineralogist, v. 35, pp. 817-839.

Farrow, C.E.G., and Watkinson, D.H., 1999. An evaluation of the role of fluids in Ni-Cu-PGE bearing, mafic-ultramafic systems: dynamic processes in magmatic ore deposits and their application in mineral exploration. Geological Association of Canada Short Course Notes 13, pp. 31-67.

Farrow, C. E. G. and Lightfoot, P. C., 2002. Sudbury PGE revisited: Toward an integrated model *in* Cabri, L.J, eds., The Geology, Geochemistry, Mineralogy and Mineral Beneficiation of Platinum-Group Elements. Canadian Institute of Mining, Metallurgy and Petroleum, Special Volume 54, pp. 13-130.

Farrow, C.E.G., Everest, J.O., King, D.M., and Jolette, C., 2005, Sudbury Cu (-Ni)-PGE systems: refining the classification using McCreedy West Mine and Podolsky Project case studies: Mineralogical Association of Canada, Short Course 35, p. 163-180.

Fleet, M. E., Chryssoulis, S. L., Stone, W. E. & Weisener, G., 1993. Partitioning of platinum-group elements and Au in the Fe-Ni-Cu-S system: Experiments on the fractional crystallization of sulfide melt. Contributions to Mineralogy and Petrology, v. 115, pp. 36-44.

French, B. M., 1967. Sudbury Structure, Ontario; Some Petrographic Evidence for Origin by Meteorite Impact. Science, v. 156, pp. 1094-1098.

Gervilla, F., Makovicky, M., Makovicky, E. & Rose-Hansen, J., 1994. The system Pd-Ni-As at 790° and 450°C. Economic Geology, v.89, pp. 1630-1639.

Giblin, P. E., 1984. History of Exploration and Development, of Geological Studies and Development of Geological Concepts *in* Pye, E.G., Naldrett, A.J., and Giblin, P.E., eds., The Geology and Ore Deposits of the Sudbury Structure. Ontario Geological Survey, Special Publication v.1, pp. 3-24.

Gilbert S., Danyushevsky L.V., Robinson P., Wohlgemuth-Ueberwasser C.C., Pearson P., Savard D., Norman M., Hanley J., 2012. A comparative study of five reference materials and the Lombard Meteorite for the determination of the platinum-group elements and gold by LA-ICP-MS. Geostandards and Geophysical Research, v. 57, pp. 51-64.

Golightly, J.P., 1994. The Sudbury Igneous Complex as an impact melt: Evolution and ore genesis *in* Lightfoot, P.C., Naldrett, A.J. (eds). Proceedings of the Sudbury-Noril'sk Symposium, Ontario Geological Survey, special volume 5, pp. 105-118.

Grant, R. W. & Bite, A., 1984. Sudbury Quartz Diorite Offset Dykes *in* Pye, E.G., Naldrett, A.J., and Giblin, P.E., eds., The Geology and Ore Deposits of the Sudbury Structure. Ontario Geological Survey, Special Publication v.1, pp. 275-300.

Hanley, J. J., 2007. The role of arsenic-rich melts and mineral phases in the development of high-grade Pt-Pd mineralization within komatiite-associated magmatic Ni-Cu sulphide horizons at Dundonald Beach South, Abitibi Subprovance, Ontario, Canada. Economic Geology, v. 102, pp. 305-317.

Hanley, J.J., Mungall, J.E., Bray, C.J., and Gorton, M.P., 2004. The origin of bulk rock and water-soluble Cl and Br enrichments in footwall Ni-Cu-PGE ore-hosting Sudbury Breccia in the Fraser copper zone, Strathcona embayment, Sudbury, Ontario, Canada. Canadian Mineralogist, v. 42, pp. 1777-1798.

Hanley, J.J., Mungall, J.E., Pettke, T., and Spooner, E.T.C., 2005. Ore metal redistribution by hydrocarbon-brine and hydrocarbon-halide melt phases, North Range footwall of the Sudbury Igneous Complex, Ontario, Canada. Mineralium Deposita, v. 40, pp. 237-256.

Hanley, J.J., Ames, D., Barnes, J., Sharp, Z., Guillong, M., 2011. Interaction of magmatic fluids and silicate melt residues with groundwater in the footwall of the Sudbury Igneous Complex, Ontario, Canada: New evidence from bulk rock geochemistry, fluid inclusions and stable isotopes. Chemical Geology, v. 281, pp. 1-25.

Hansen, M. & Anderko, K., 1958. Constitution of binary alloys. McGraw-Hill, New York. General Electric Co., Business Growth Services, 1305 p.

Hawley, J. E. & Stanton, R. L., 1962. The Facts: The Ores, Their Minerals, Metals and Distribution. *in* The Sudbury Ores: Their Mineralogy and Their Origin, Canadian Mineralogist, v. 7, pp. 30-145.

Hem, S. R. & Mackovicky, E., 2004. The system Fe-Co-Ni-As-S. II. Phase relations in the (Fe,Co,Ni)As1.5S0.5 section at 650°C and 500°C. The Canadian Mineralogist, v. 42, pp. 63-86.

Hoffman, E. L. & MacLean, W. H., 1976. Phase relations of michenerite and merenskyite in the Pd-Bi-Te system. Economic Geology, v. 71, pp. 1461-1468.

Houlé, M. G., Lesher, M. C. & Davis, P. C., 2012. Thermomechanical erosion at the Alexo Mine, Abitibi greenstone belt, Ontario: implications for the genesis of komatiite-associated Ni–Cu–(PGE) mineralization. Mineralium Deposita, v. 47, pp. 105-128.

Huminicki, M. A. E., Sylvester, P.J., Cabri, L.J., Lesher, C.M., and Tubrett, M., 2005. Quantitative mass balance of platinum group elements in the Kelly Lake Ni-Cu-PGE deposit, Copper Cliff offset, Sudbury. Economic Geology, Volume v. 100, pp. 1631–1646.

Keays, R.R. and Crocket, J.H., 1970. A study of precious metals in the Sudbury nickel irruptive ores. Economic Geology, v. 65, pp. 438-450.

Klemm, D. D., 1965. Synthesen und analysen in den Dreieckdiagrammen FeAsS-CoAsS-NiAsS un FeS2−CoS2−NiS2. Neus Jahrbuch fuer Mineralogie Abhandlungen, v. 103, pp. 205−255.

Krogh, T. E., McNutt, R. H. & Davis, G. L., 1982. Two High Precision U-Pb Zircon Ages for the Sudbury Nickel Irruptive. Canadian Journal of Eath Sciences, v. 19, pp. 723-728.

Lausen, C., 1930. Graphic intergrowth of niccolite and chalcopyrite, Worthington mine, Sudbury. Economic Geology, v. 25, pp. 356-364.

LeFort, D. T., 2012. A Mineralogical and Fluid Inclusion Study of Modified, Contact-Style Ni-Cu-PGE Ores in the #1 and #4 Shear Zones, Garson Mine, Sudbury, Ontario, Canada. M.Sc. thesis, Saint Mary's University, Halifax.

Lesher, C. M. & Arndt, N. T., 1995. REE and Nd isotope geochemistry, petrogenesis and volcanic evolution of contaminated komatiites at Kambalda, Western Australia. Lithos, v. 34, pp. 127-157.

Li, C., Naldrett, A.J., 1993, Platinum-group minerals from the Deep copper zone of the Strathcona deposits, Sudbury, Ontario. Canadian Mineralogist, v. 31, pp. 31-44.

Li, C., Naldrett, A.J., Coats, C.J.A., and Johannssen, P., 1992. Platinum, palladium, gold and copper-rich stringers at the Strahcona Mine, Sudbury: Their enrichment by fractionation of a sulfide liquid. Economic Geology, v. 87, pp. 1584-1598.

Lightfoot, P. C. & Farrow, C. E. G., 2002. Geology, geochemistry, and mineralogy of the Worthington Offset dyke: a genetic model for offset dyke mineralization in the Sudbury Igneous Complex. Economic Geology, v. 97, pp. 1419-1446.

Lightfoot, P. C. Hawkesworth, C.J., Hergt, J., Naldrett, A.J., Gorbachev, N.S., Fedorenko, V.A., and Doherty, W., 1993. Remobilisation of the continental lithosphere by a mantle plume: major-, trace-element, and Sr-, Nd-, and Pb-isotope evidence from picritic and tholeiitic lavas of the Noril'sk district, Siberian Trap, Russia. Contributions to Mineralogy and Petrology, Volume v. 114, pp. 171-188.

Lightfoot, P.C., and Keays, R.R., 2002. An integrated model for the origin of the Sudbury Igneous Complex and the associated Ni-Cu-PGE sulphide ores. Proceedings, 21st Century Pt-Pd Deposit: Current and Future Potential. Abstracts volume, 25th AGM, Mineral Deposits Study Group, pp. 47-48.

Lightfoot, P. C., Keays, R.R., Morrison, G.G., Bite, A., and Farrell, K.P., 1997. Geochemical relationships in the Sudbury Igneous Complex: Origin of the main mass and offset dykes. Economic Geology, Volume v. 97, pp. 289-307.

Lightfoot, P.C., Keays, R.R., and Doherty, W., 2001. Chemical evolution and origin of nickel sulfide mineralization in the Sudbury Igneous Complex, Ontario, Canada. Economic Geology, v. 96, pp. 1855-1875.

Lloyd, T. R., 2001. Totten Cu-Ni-PGE-Au Project Drury Township, Sudbury District. Inco Technical Services, internal report, 44p.

Alard, A.O., and Lorand, J.P., 2001. Volatile-rich metasomatism in Montferrier xenoliths (southern France): implications for the abundances of chalcophile and highly siderophile elements in the subcontinental mantle. Journal of Petrology, v. 52, pp. 2009-2045.

Magyarosi, Z., Watkinson, D. H. & Jones, P. C., 2002. Mineralogy of Ni-Cu-Platinum-Group Element Sulfide Ore in the 800 and 810 Orebodies, Copper Cliff South Mine, and P-T-X Conditions during the Formation of Platinum-Group Minerals. Economic Geology, v. 97, p. 1471–1486.

Makovicky, E., 2002. Ternary and quaternary phase systems in PGE. Canadian Institute of Mining, Metallurgy and Petroleum. Special Volume 54, pp. 131−175.

Makovicky, E., Karup-Moller, S., Mackovicky, M. & Rose-Hansen, J., 1990. Experimental studies on the phase systems Fe-Ni-Pd-S and Fe-Pt-Pd-As-S applied to PGE deposits. Mineralogy and Petrology, v.42, pp. 307-319.

Marshall, D., Watkinson, D., Farrow, C., Molnár, F., and Fouillac, A.M., 1999. Multiple fluid generations in the Sudbury igneous complex: fluid inclusion, Ar, O, H, Rb and Sr evidence. Chemical Geology, v. 154, pp. 1-19.

Melgarejo, J. C. & Martin, R. F., 2011. Atlas of Non-Silicate Minerals in Thin Section. Mineralogical Association of Canada. Québec, 522 p.

Michener, C. E. & Yates, A. B., 1944. Oxidation of Primary Nickel Sulphides. Economic Geology, v. 39, pp. 506-514.

Molnár, F., Watkinson, D.H., Jones, P.C., and Gatter, I., 1997. Fluid inclusion evidence for hydrothermal enrichment of magmatic or at the contact zone of the Ni-Cu-platinum-group element 4b deposit, Lindsley mine, Sudbury, Canada. Economic Geology, v. 92, pp. 674-685.

Molnár, F., Watkinson, D.H., Everest, J.O., 1999. Fluid-inclusion characteristics of hydrothermal Cu-Ni-PGE veins in granitic and metavolcanic rocks at the contact of Little Stobie deposit, Sudbury, Canada. Chemical Geology, v. 154, pp. 279-301.

Morimoto, N. & Kullerud, G., 1962. The Mo-S system. Carnegie Institution, Washington. Year B., v. 61, pp. 143-144.

Morrison, G.G., 1984. Morphilogical features of the Sudbury Structure in relation to an impact origin *in* Pye, E.G., Naldrett, A.J., and Giblin, P.E., eds., The Geology and Ore Deposits of the Sudbury Structure. Ontario Geological Survey, Special Publication v.1, pp. 57-64.

Morrison, G.G., Jago, B.C., and White, T.L., 1994. Footwall mineralization of the Sudbury Igneous complex *in* Lightfoot, P.C., and Naldrett, A.J. (eds.), Proceedings of the Sudbury-Noril'sk Symposium. Ontario Geological Survey, special volume 5, pp. 119-132.

Muir, T. L. & Peredery, W. V., 1984. The Onaping Formation *in* Pye, E.G., Naldrett, A.J., and Giblin, P.E., eds., The Geology and Ore Deposits of the Sudbury Structure. Ontario Geological Survey, Special Publication v.1, pp. 139-210.

Mukasa, S. B., Wilson, A. H. & Carlson, R. W., 1998. A multielement geochronologic study of the Great Dyke, Zimbabwe: significance of the robust and reset ages. Earth and Planetary Science Letters, v. 164, pp. 353-369.

Mungall, J.E., 2005. Magmatic Geochemistry of The Platinum-Group Elements. Mineralogical Association of Canada Short course 35, Oulu, Finland, p. 1-34.

Murphy, A. J. & Spray, J. G., 2002. Geology, Mineralization, and Emplacement of the Whistle-Parkin Offset Dyke, Sudbury. Economic Geology, v. 97, p. 1399–1418.

McDonald, A.M., Cabri, L.J., Stanley, C.J., Rudashevsky, N.S., Poirier, G., Mungall, J.E., Ross, K.C., Durham, B.R., Rudashevsky, V.N., 2005. Ungavaite, Pd_4Sb_3, a new intermetallic mineral species from the Mesamax Northwest deposit, Ungava egion, Québec, Canada: description and genetic implications. The Canadian Mineralogist, v. 43, pp. 1735-1744.

Naldrett, A. J., 1984a. Ni-Cu ores of the Sudbury Igneous Complex-Introduction *in* Pye, E.G., Naldrett, A.J., and Giblin, P.E., eds., The Geology and Ore Deposits of the Sudbury Structure. Ontario Geological Survey, Special Publication v.1, pp. 302-307.

Naldrett, A. J., 1984b. Mineralogy and Composition of the Sudbury Ores. *in* Pye, E.G., Naldrett, A.J., and Giblin, P.E., eds., The Geology and Ore Deposits of the Sudbury Structure. Ontario Geological Survey, Special Publication v.1, pp. 309-325.

Naldrett, A.J., and Kullerud, G., 1967. A Study of the Strathcona Mine and its bearing on the Origin of the Nickel-Copper Ores of the Sudbury District,, Ontario. Journal of Petrology, v. 8, pp. 453-531.

Naldrett, A. J. & Hewins, R. H., 1984. The main mass of the Sudbury igneous complex *in* Pye, E.G., Naldrett, A.J., and Giblin, P.E., eds., The Geology and Ore Deposits of the Sudbury Structure. Ontario Geological Survey, Special Publication v.1, pp. 233-251.

Naldrett, A. J., Hewins, R. H., Dressler, B. O. & Rao, B. V., 1984. The Contact Sublayer of the Sudbury igneous complex *in* Pye, E.G., Naldrett, A.J., and Giblin, P.E., eds., The Geology and Ore Deposits of the Sudbury Structure. Ontario Geological Survey, Special Publication v.1, pp. 254-273.

Naldrett, A.J., Asif, M., Schandl, E., Searcy, T., Morrison, G.G., Binney, W.P., and Moore, C., 1999. Platinum-group elements in the Sudbury ores: Significance with respect to the origin of different ore zones and to the exploration for footwall ores, Economic Geology, v. 94, pp. 185-210.

Pattison, E. F., 1979. The Sudbury sublayer. Canadian Mineralogist, v. 17, pp. 257-274.

Peredery, W. V., 1972. Chemistry of Fluidal Glasses and Melt Bodies in the Onaping Formation. *in* J. V. Guy-Bray, ed. New Developments in Sudbury Geology. Geological Association of Canada Special paper 10, pp. 49-59.

Pentek, A., Molnar, F., Watkinson, D.H., and Jones, P.C., 2008. Footwall-type Cu-Ni-PGE mineralization in the Broken Hammer area, Wisner Township, North Range, Sudbury Structure. Economic Geology and the Bulletin of the Society of Economic Geologists, v. 103(5), pp. 1005-1028.

Peregoedova, A., Barnes, S. J. & Baker , D. R., 2004. The formation of Pt-Ir alloys and Cu-Pd rich sulfide melts by partial desulfurization of Fe-Ni-Cu sulfides: Results of experiments and implications for natural systems. Chemical Geology, v. 208, pp. 247-264.

Rickard, J.H., 2000. Petrological and Mineralogical Study of Cu-Ni-PGE-bearing Ores within the 100 Orebody, Copper Cliff North Mine, Sudbury, Ontario. M.Sc. thesis Carleton University, Ottawa, 113 p.

Rollinson, H. R., 1993. Using Geochemical Data: Evaluation, Presentation, Interpretation. Longman Scientific & Technical, Harlow.

Rousell, D. H., 1984. The Onwatin and Chemsford Formations. *in* Pye, E.G., Naldrett, A.J., and Giblin, P.E., eds., The Geology and Ore Deposits of the Sudbury Structure. Ontario Geological Survey, Special Publication v.1, pp. 211-218.

Rousell, D. H., Fedorowich, J. S. & Dressler, B. O., 2003. Sudbury Breccia (Canada): a product of the 1850 Ma Sudbury Event and host to footwall Cu–Ni–PGE deposits. Earth-Science Reviews, v. 60, p. 147–174.

Scribbins, B. R. & Naldrett, A. J., 1984. Mafic and Ultramafic Inclusions in the Sublayer of the Sudbury Igneous Complex. Canadian Mineralogist, v. 22, pp. 67-75.

Seabrook, L., Prichard, H. M. & Fisher, P. C., 2004. Platinum-group minerals in the Raglan Ni-Cu-(PGE) sulfide deposit, Cape Smith, Québec, Canada. The Canadian Mineralogist, v. 42, pp. 485-497.

Sinyakova, E. F. & Kosyakov, V. I., 2012. The behavior of noble-metal admixtures during fractional crystallization of As- and Co-containing Cu–Fe–Ni sulfide melts. Russian Geology and Geophysics, v. 53, p. 1055–1076.

Skinner, B. J. et al., 1976. Phase relations in ternary portions of the system Pt-Pd-Fe-As-S. Economic Geology, v. 71, pp. 1469-1475.

Smith, A.Y., 1961. Experimental investigation of some textures of massive sulphide ores. M.Sc. thesis, Queen's University.

Souch, B. E., Podolsky, T. & Geological Staff, 1969. The sulfide ore of Sudbury: Their particular relationship to a distinctive inclusion-bearing species of the Nickel Irruptive *in* Wilson, H.D.B., eds., Magmatic Ore Deposits. Economic Geology Monograph 4.

Stevenson, J. S., 1972. The Onaping Ash-Flow Sheet, Sudbury, Ontario *in* Guy-Bray J. V., ed. New Developments in Sudbury Geology, Geological Association of Canada, Special Paper Number 10, 124p.

Stewart, M.C., 1999. Petrology of the Sulphides within the Copper Cliff Offset South of Kelly Lake. B.Sc. thesis, Carleton University, Ottawa.

Stewart, M. C., 2002. Petrology and mineralogy of Cu-Ni-PGE ore, Totten area, Worthington offset, Sudbury Igneous Complex M.Sc. thesis, Carleton University, Ottawa.

Szentpéteri, K., Watkinson, D. H., Molnar, F. & Jones, P. C., 2002. Platinum-group elements-Co-Ni-Fe sulfarsenides and mineral paragenesis in Cu-Ni-platinum-group element deposits, Copper Cliff north area, Sudbury, Canada. Economic Geology, v. 97, p. 1459−1470.

Takeno, S. & Moh, G. H., 1977. Liquidus reactions of the Mo-S system. Neues Jahrbuch für Mineralogie, v. 131, pp. 43-48.

Therriault, A. M., Fowler, A. D. & Grieve, R. A. F., 2002. The Sudbury Igneous Complex: A differentiated impact melt sheet. Economic Geology, v. 97, pp. 1521-1540.

Thomson, J. E., 1957. Geology of the Sudbury Basin. Ontario Department of Mines, Annual Report for 1956, v. 65, pp. 1-56..

Tuchscherer, M. G. & Spray, J. G., 2002. Geology, Mineralization, and Emplacement of the Foy Offset Dyke, Sudbury Impact Structure. Economic Geology, v. 97, p. 1377–1397.

Tomkins, A.G., Mavrogenes, J.A., Frost, B.R., and Pattison, D.R.M., 2006. Formation and fractionation of metamorphic sulfide melts. Geochimica et Cosmochimica Acta, v. 70, pp. A653.

Williams, H., 1957. Glowing Avalanche Deposits of the Sudbury Basin. Ontario Department of Mines, Annual Report for 1956, v. 65, pp.57-89.

Wilson S.A., Ridley W.I., Koenig A.E., 2002. Development of sulfide calibration standards for the laser ablation inductively-coupled plasma mass spectrometry. Journal of Analytical Atomic Spectrometry, v. 17, pp.406-409.

Wood, S.A., 2002. The aqueous geochemistry of the platinum-group elements with applications to ore deposits *in* Cabri, L.J. (ed.) The Geology, Geochemistry, Mineralogy and Mineral Benefication of Platinum-Group Elements. Canadian Institute of Mining Metallurgy and Petroleum, Special volume 54, pp. 211-249.

Wood, M., 2003. Arsenic in igneous systems: An experimental investigation. B.Sc. thesis, University of Toronto, 32 p.

Yund, R. A., 1961. Phase relations in the system Ni-As. Economic geology, v. 56, pp. 1273-1296.

Zurbrigg, H. F., 1957. The Frood-Stobie Mine. *in* Structural Geology of Canadian Ore Deposits. Canadian Institute of Mining and Metallurgy, v. 2, pp. 341-363.

8.0 Appendix

A1: Locations of Totten samples from diamond drill core

Project ID	Core ID	Depth (ft)	Project ID	Core ID	Depth (ft)	Project ID	Core ID	Depth (ft)	Project ID	Core ID	Depth (ft)	Project ID	Core ID	Depth (ft)	Project ID	Core ID	Depth (ft)
T1	1265390	529'	T25	1265770	436'	T49	1265980	219'9"-220'	T73	1265980	424'6"-424'10"	T97	1265980	998'9"-999'0.5"			
T2	1265390	564.5'	T26	1265770	436.5'	T50	1265980	199'9"-200'	T74	1265980	612'4"-612'8.5"	T98	1265980	877'10"-878'1.5"			
T3	1265540	494'	T27	1265750	432.5'	T51	1265980	179'9"-180'	T75	1265980	662'4"-662'8"	T99	1265980	864'8"-864'10"			
T4	1265710	356'	T28	1265500	704.5'	T52	1265980	359'10"-360'	T76	1265980	1024'-1024'4"	T100	1265980	802'10"-803'1"			
T5	1265710	418'	T29	1265900	567'	T53	1265980	229'7"-230'	T77	1265980	958'2"-958'6"	T101	1265980	1064'2.5"-6.5"			
T6	1265710	425'	T30	1265900	648'	T54	1265980	262'10"-263'2"	T78	1265980	571'1"-571'8"	T102	1265980	1129'3.5"-6.5"			
T7	1265750	452'	T31	1265800	450'	T55	1265980	1394"-240'	T79	1265980	553'3"-553'6"	T103	1265980	964'-964'2.5"			
T8	1265720	437.5'	T32	1265050	301'	T56	1265980	283'9"-11"	T80	1265980	465'8"-11.4"	T104	1265980	968'5.5"-969'11.5"			
T9	1265720	453'	T33	1265900	669'	T57	1265980	267'8"-268'	T81	1265980	474'10"-475'2"	T105	1265980	829'0.5"-3.5"			
T10	1265340	683.5'	T34	1265340	698'	T58	1265980	276'5"-276'8"	T82	1265980	575'5"-9"	T106	1265980	1157'11"-1158'2"			
T11	1265870	462'	T35	1265710	344'	T59	1265980	286'5"-11"	T83	1265980	490'4"-8"	T107	1265980	1077'9"-1078'6"			
T12	1265720	442'	T36	1265500	652'	T60	1265980	303'4"-7"	T84	1265980	507'4"-8"	T108	1265980	520'9"-521'1"			
T13	1265170	"#MU594576"	T37	1265900	649'	T61	1265980	314'-314'4"	T85	1265980	492'4"-8"	T109	1265980	535'1"-6"			
T14	1265720	442.5'	T38	1265770	402'	T62	1265980	299'-299'4"	T86	1265980	618'2.5"-618'6.5"	T110	1265980	1056'5"-8.5"			
T15	1265420	664.5'	T39	1265770	458'	T63	1265980	321'7"	T87	1265980	627'2"-627'6"	T111	1265980	753'6"-9.5"			
T16	1265420	665'	T40	1265720	396'	T64	1265980	326'6"	T88	1265980	640'5"-640'8"	T112	1265980	758'11.5"-759'3"			
T17	1265900	601'	T41	1265720	410'	T65	1265980	331'1"-5"	T89	1265980	848'-848'5.5"	T113	1265980	701'4"-7.5"			
T18	1265520	494.3'	T42	1265720	475'	T66	1265980	344'8"-345'	T90	1265980	906'5.5"-9.5"	T114	1265980	675'4"-6"			
T19	1265710	334'	T43	1265850	356'	T67	1265980	369'1"-2.5"	T91	1265980	778'2"-778'7"	T115	1265980	988'5"-988'9"			
T20	1265800	412'	T44	1265900	551'	T68	1265980	374'2"-5"	T92	1265980	749'9"-750'0.5"	T116	1265980	1145'11"-1146'4.5"			
T21	1265770	411'	T45	1265800	392'	T69	1265980	382'3"-7"	T93	1265980	450'7"-451'	T117	1265980	911'3"-8.5"			
T22	1265770	435.5'	T46	1265770	440'	T70	1265980	391'9"-12"	T94	1265980	433'3"-10"	T118	1265980	940'-940'4"			
T23	1265800	415'	T47	1265980	134'7"-9"	T71	1265980	406'9"-12"	T95	1265980	1002'7.5"-10"	T119	1265980	1015'8.5"-1016'0.5"			
T24	1265710	428'	T48	1265980	159'-159'2"	T72	1265980	416'-416'6"	T96	1265980	1005'5"-8.5"	T120	1265980	1122'8"-1123'			

A1 (continued): Locations of Totten samples from diamond drill core

Project ID	Core ID	Depth (ft)	Project ID	Core ID	Depth (ft)	Project ID	Core ID	Depth (ft)	Project ID	Core ID	Depth (ft)	Project ID	Core ID	Depth (ft)
T121	1265980	710'9"-711'0.5"	T145	971512	3284'4.5"-3285'1"	T169	971512	3280'5"-3281'10"	T193	1270880	758'3"-758'6"	T217	1270490	232'1"-232'5"
T122	1265980	686'-686'5.5"	T146	971512	3315'7"-3315'11.5"	T170	1270880	743'5"-743'7"	T194	1270880	779'2"-779'4"	T218	1270490	231'7"-232'1"
T123	1265980	591'9.5"-592'1"	T147	971512	3274'2.5"-3275'1"	T171	1270880	774'3"-774'6"	T195	1270500	344'9"345'	T219	1270490	232'6"-233'2.5"
T124	1265980	608'10"-609'2"	T148	971512	3279'3"-3279'7.5"	T172	1270880	770'6"770'9"	T196	1270500	363'7.5"-364'1"	T220	1270490	304'6"-305'4"
T125	1265980	573'11.5"-574'3.5"	T149	971512	3296'3"-3296'11.5"	T173	1270880	776'4"-776'6"	T197	1270500	381'9"-382'7.5"	T221	1270490	314'1.5"-314'9"
T126	1265980	768'1"-768'4.5"	T150	971512	3279'3"-3279'7.5"	T174	1270880	745'6"-746'	T198	1270500	405'5"-406'3.5"	T222	1270490	314'9"-315'1"
T127	1265980	733'10"-734'0.5"	T151	971512	3352'6"-3352'10.5"	T175	1270880	611'9"-612'1.5"	T199	1270500	415'10"-416'7"	T223	1270490	325'3.5"-325'10"
T128	1265980	457'8"-458'	T152	971512	3270'7.5"-3271'5"	T176	1270880	629'5"-629'11"	T200	1270500	492'5"-492'10"	T224	1270490	327'2"-327'8.5"
T129	1265980	464'3"-5"	T153	971512	3344'11"-3345'3"	T177	1270880	760'6"-760'8"	T201	1270500	342'-342'5"	T225	1270490	399'7"-400'
T130	1265980	786'8"-786'11.5"	T154	971512	3275'3"-3276'0.5"	T178	1270880	604'6"-604'9"	T202	1270500	698'7"699'5"	T226	1270490	364'7.5"-364'10"
T131	1265980	1185'4"-7.5"	T155	971512	3304'5"-3305'3"	T179	1270880	738'6"-739'9.5"	T203	1270500	477'2-477'9"	T227	1270490	324'4"-324'9"
T132	1265980	827'5.5"-827'8.5"	T156	971512	1008'-1008'1"	T180	1270880	772'6"-772'8"	T204	1270500	488'8.5"-489'0.5"	T228	1270490	341'2"-342'1"
T133	1265980	886'5"-886'7"	T157	971512	3300'5"-3301'8"	T181	1270880	707'1"-707'5"	T205	1270490	394'7"-394'11.5"	T229	1270490	342'4.5"-342'9.5"
T134	1265980	1100'6.5"-1101'3.5"	T158	971512	3282'6.5"-3283'4.5"	T182	1270880	764'8"-765'2"	T206	1270500	427'7"-428'3"	T230	1270480	330'7"-330'9"
T135	1265996	687'	T159	971512	3311'7"-3311'10"	T183	1270880	768'9"-769'2"	T207	1270390	371'4"-371'10.5"	T231	1270480	355'5"-355'7"
T136	1265500	1093'9.5"-1094'2"	T160	971512	3342'4"-3343'1.5"	T184	1270880	671'-671'4"	T208	1270490	412'2.5"-413'2.5"	T232	1270480	327'5"-327'9.5"
T137	1265980	1077'9"-1078'6"	T161	971512	3297'6.5"-3297'8.5"	T185	1270880	607'3.5"-607'9.5"	T209	1270500	506'5"506'8"	T233	971512	3317'3"-3320'2"
T138	1265980	1024'-1024'4"	T162	971512	3298'2.5"-3299'6.5"	T186	1270880	600'7"-601'	T210	1270500	57'3"-57'9"	T234	971512	3302'5"-3303'1"
T139	1265980	943'5"-944'	T163	971512	3348'6"-3348'9"	T187	1270880	740'7"-741'	T211	1270500	473'4"-474'	T235	1270500	358'10.5"-359'5.5"
T140	1265980	833'7"-833'11"	T164	971512	3297'3"-3298'5"	T188	1270880	545'10"-546'4"	T212	1270490	384'8"-385'0.5"	T236	1270480	672'2"-672'5.5"
T141	1265980	1217'11"-1218'1"	T165	971512	3331'9.5"-3334'11"	T189	1270880	550'5.5"-550'10.5"	T213	1270490	454'2"-454'9"	T237	1270500	357'8"-358'10.5"
T142	1265980	1222'4"-6"	T166	971512	3276'8.5"-3277'4.5"	T190	1270880	763'5"-763'8"	T214	1270490	363'6"-364'2"	T238	1270480	248'8'-248'10.5"
T143	1265980	1203'7.5"-9.5"	T167	971512	3321'0.5"-3321'4"	T191	1270880	775'6"-775'7"	T215	1270490	375'2"-375'6"			
T144	1265720	442'5"	T168	971512	3307'11"-3310'8"	T192	1270880	774'5"-774'7"	T216	1270490	317'3"-317'9.5"			

A2: Underground and surface sample locations

		Local system 73-Worthington		
Sample No.	Level	X(Easting)	Y(Northing)	Z(Elevation)
TU1	1250	24005	-969	11602
TU2	1250	24042	-963	11602
TU3	1250	24021	968	11602
TU4A	1250	24088	-1010	11602
TU4B	1250	24098	-997	11602
TU5	1250	24110	-1004	11602
TU6	1250	24150	-1001	11602
TU7	1250	24169	-1010	11602
TU8	1250	24198	-1001	11602
TU9	1250	24136	-989	11602
TU11	1250	24013	-978	11602
TU12	1250	24000	-942	11602
TU13	1250	23967	-958	11602
TU14	1250	23907	-975	11602
TU15	1250	23870	-997	11602
TU16A	1850	22152	-862	10998
TU16B	1850	22087	-891	11098
TU18A	1850	22014	-862	10998
TU18B	1850	21996	-878	10998
TU20	1250	-979	23898	11596
TU21	1250	-966	23933	11598
TU22	1250	-968	24000	11603
TU23	1250	-975	24250	11605
TU24	1250	-995	24255	11605
TU25	1850	-788	21771	10999
TU26	1850	-862	22006	10994
TU27	1850	-913	22291	10995
TU28	1850	-911	22312	10997
TU29	3850	-1223	21963	8998
TU30	3850	-1199	21799	9010
TU31	Surface	-1261	21502	13075
TU32	1850	-911	22312	10997

A3: Bulk rock analysis of samples from the Totten #2 Mine (ppm)

Sample	Ag	Al (wt%)	As	Au	Ba	Be	Bi	Ca (wt%)	Cd	Co	Cr	Cu	Fe (wt%)	Ga	K (wt%)	La	Mg (wt%)	Mn	Mo	Na (wt%)	Ni	P	Pb	Pd	Pt	S (wt%)	Sb	Sc	Sr	Th	Ti (wt%)	Tl	U	V	W	Zn
T1	175	3.43	BDL	0.541	200	0.6	5	0.51	51	41	48	218000	22.5	BDL	0.74	10	0.63	571	BDL	0.42	3020	110	71	0.299	6.31	23.8	BDL	11	62	BDL	0.13	BDL	BDL	67	BDL	864
T2	96.6	0.08	92	0.017	10	BDL	BDL	0.03	25.5	1905	289	150500	33.8	BDL	0.01	BDL	0.01	13	4	0.03	101000	BDL	87	1.83	1.175	33.2	BDL	3	4	BDL	0.01	BDL	BDL	49	BDL	475
T3	63.2	0.33	103	1.075	20	BDL	324	0.03	21.4	683	6	105500	39.3	BDL	0.06	BDL	0.08	45	1	0.02	55800	10	138	2.94	40.3	35.1	BDL	2	3	BDL	0.01	BDL	BDL	15	BDL	369
T4	4.8	1.74	37	0.025	130	0.5	8	0.5	BDL	578	21	2810	42.7	BDL	0.35	10	0.31	114	3	0.45	67900	120	31	0.548	0.998	31	BDL	4	66	BDL	0.12	BDL	BDL	178	BDL	26
T5	3.2	0.54	1020	0.081	50	BDL	21	0.25	BDL	1465	159	2810	ADL	BDL	0.11	BDL	0.12	86	4	0.14	48400	70	26	4.92	2.49	35.4	BDL	2	23	BDL	0.06	BDL	BDL	30	10	14
T6	2.2	0.06	17	0.013	10	BDL	22	0.07	BDL	1100	34	1580	ADL	BDL	0.01	BDL	0.02	9	3	0.01	44700	BDL	25	0.429	0.42	36.9	BDL	BDL	3	BDL	0.03	10	BDL	33	BDL	BDL
T7	3.1	0.02	25	0.158	10	BDL	20	0.05	BDL	1575	75	4290	ADL	BDL	BDL	BDL	0.02	BDL	4	0.01	47200	BDL	29	0.425	0.295	38.3	BDL	BDL	2	BDL	0.02	BDL	BDL	47	BDL	2
T8	5.8	0.01	17	0.017	10	BDL	11	0.01	BDL	2130	293	9570	ADL	BDL	BDL	BDL	0.01	BDL	5	BDL	56400	BDL	31	0.249	1.725	36.3	BDL	BDL	2	BDL	0.02	BDL	BDL	63	BDL	14
T9	9.7	0.1	27	0.024	10	BDL	BDL	0.15	BDL	2770	156	9550	ADL	BDL	0.01	BDL	0.04	115	6	0.01	72200	BDL	311	0.694	0.298	39.3	BDL	1	3	BDL	0.01	BDL	BDL	30	BDL	33
T10	7	0.04	61	0.014	10	BDL	127	0.06	BDL	549	3	574	ADL	BDL	BDL	BDL	BDL	BDL	3	BDL	32600	BDL	33	0.246	8.51	36.8	BDL	BDL	4	BDL	BDL	10	BDL	5	10	BDL
T11	3	1	28	0.028	90	BDL	8	0.07	BDL	1795	164	2210	48.7	BDL	0.22	10	0.17	576	4	0.04	50400	40	218	1.895	1.02	32.7	BDL	3	8	BDL	0.07	10	BDL	167	BDL	187
T12	4.2	0.02	15	0.008	BDL	BDL	2	0.02	BDL	1310	165	6360	ADL	BDL	BDL	BDL	BDL	BDL	5	BDL	44500	BDL	6	0.073	0.563	36	BDL	BDL	1	BDL	0.01	BDL	BDL	21	BDL	7
T13	194	0.2	BDL	0.245	BDL	BDL	57	0.08	67.2	617	8	202000	35.7	BDL	BDL	BDL	0.06	64	1	0.08	29300	10	57	0.262	9.81	33.6	BDL	3	8	BDL	0.01	BDL	BDL	6	10	1690
T15	51	1.97	23	0.04	100	BDL	6	0.9	4.6	1625	30	33800	36	BDL	0.3	BDL	0.53	237	2	0.61	84700	220	14	0.397	0.367	26.7	BDL	6	96	BDL	0.2	BDL	BDL	72	BDL	126
T16	68	2.83	34	0.193	120	0.5	6	1.4	12.4	1035	40	82200	26.6	BDL	0.33	20	0.7	289	2	0.94	56500	300	31	0.492	1.675	22.7	BDL	8	158	BDL	0.19	BDL	BDL	69	BDL	281
T17	14.4	4.59	36	3.38	290	0.9	154	1.15	1.5	1420	62	20500	27.6	BDL	0.96	10	0.7	314	1	1.64	73300	180	131	5.06	9.02	20.2	BDL	10	170	BDL	0.26	BDL	BDL	84	BDL	123
T18	13.2	7.02	7	0.13	230	1	7	3.58	4.1	61	137	15800	11.25	10	0.85	20	2.52	1120	1	0.65	1990	640	20	0.209	0.153	2.25	BDL	18	151	BDL	0.42	BDL	BDL	140	BDL	145
T19	7	8.06	1735	0.222	560	1.4	BDL	3.72	5.9	88	121	8420	7.26	20	1.78	30	2.66	892	1	2.29	2780	750	24	0.396	0.346	1.42	10	24	348	BDL	0.56	BDL	BDL	170	BDL	146
T20	3.2	6.67	20	0.269	450	1.1	6	3.63	2.4	117	142	5130	13.65	10	1.25	20	2.26	1025	1	1.66	7460	610	19	1.09	1.005	4.81	BDL	17	267	BDL	0.39	BDL	BDL	144	BDL	135
T21	2.7	7.53	3680	0.185	460	1.2	2	4.27	0.7	273	173	4780	10	10	1.15	20	2.47	936	2	2.3	6150	660	23	2.07	0.608	3.27	9	19	386	BDL	0.45	BDL	10	161	BDL	72
T22	5.8	3.77	18	0.024	250	0.5	BDL	1.92	BDL	666	142	7840	31.8	BDL	0.55	10	1.31	467	1	0.96	31700	300	12	0.201	1.445	20.2	BDL	10	174	BDL	0.22	BDL	BDL	91	BDL	52
T23	7.6	6.63	19	0.249	430	0.9	2	3.72	5	113	138	13050	13.95	10	1.15	20	2.25	1070	1	1.6	7620	620	17	0.652	0.947	6.34	BDL	17	255	BDL	0.4	BDL	BDL	144	BDL	188
T24	46.2	5.97	7	0.24	340	0.7	7	3.48	19	130	142	63200	15.85	10	0.94	10	2.19	897	1	1.15	2830	410	39	1.035	1.255	8.55	BDL	16	230	BDL	0.28	BDL	BDL	127	BDL	519
T25	8.9	5.36	12	0.051	380	0.8	2	2.56	1.9	460	170	20800	20.3	BDL	0.95	20	1.86	602	1	1.38	19750	450	17	0.186	2.96	11.75	BDL	14	249	BDL	0.26	BDL	BDL	107	BDL	129
T26	7.7	4.14	11	0.042	330	0.6	5	1.92	1.2	750	140	15050	28.2	BDL	0.7	10	1.45	468	1	1.01	33700	320	13	0.235	1.76	17.9	BDL	11	182	BDL	0.22	BDL	BDL	89	BDL	94
T27	20.6	4.24	8	0.067	190	1.3	8	1.35	4.7	757	14	35000	23.8	BDL	0.68	30	0.44	272	2	1.39	22000	830	33	0.22	3.22	16.6	BDL	10	186	BDL	0.29	BDL	BDL	51	BDL	260
T28	37.2	5.66	15	0.144	350	1.1	13	1.34	10.1	346	156	50800	14.65	BDL	1.53	20	1.7	340	2	1.67	13250	640	59	0.405	0.751	9.49	BDL	15	284	BDL	0.43	BDL	BDL	120	BDL	227
T29	7.6	7.62	6	0.164	150	1.3	2	4.65	1	107	106	10500	7.54	10	0.47	30	2.22	747	2	2.59	3030	800	58	0.622	0.373	2.26	BDL	20	346	BDL	0.56	BDL	10	165	BDL	106
T30	8.4	6.92	40	0.492	560	1.4	8	3.46	2.5	144	94	11850	10.6	10	1.44	30	1.81	924	1	1.55	5130	680	27	1.36	1.13	2.92	5	17	276	BDL	0.47	BDL	BDL	137	BDL	155
T32	1.4	7.61	20	0.055	480	1.5	BDL	4.01	BDL	68	115	1620	7.65	20	1.25	30	2.17	950	1	2.03	1470	750	27	0.233	0.15	0.99	BDL	19	297	BDL	0.52	BDL	10	156	BDL	99
T33	11.1	7.4	9	0.972	450	1.2	20	4.22	4.6	110	120	13000	9.49	10	1.28	30	2.23	964	1	1.78	4120	670	55	4.11	2.93	2.57	6	19	298	BDL	0.47	BDL	BDL	156	BDL	143
T34	14.6	6.97	3920	0.265	250	1.3	10	3.41	3.7	398	108	17300	9.22	10	0.99	30	2.14	619	1	2.26	7890	690	64	3.49	0.635	3.67	23	18	375	BDL	0.47	BDL	10	136	BDL	126
T35	7	6.47	217	0.05	500	0.7	BDL	4.13	4.5	69	159	9650	8.1	10	1.23	500	2.79	818	1	1.32	983	440	15	0.118	0.056	1.37	BDL	12	147	20	0.41	BDL	BDL	123	10	134
T36	7.6	5.16	28	0.283	300	1.3	7	1.67	0.6	356	50	4930	21.4	BDL	0.84	30	0.99	269	3	1.91	21900	630	51	0.79	6.2	8.79	5	11	335	BDL	0.41	BDL	BDL	77	BDL	16
T42	BDL	9.47	9	0.007	1010	2.1	BDL	0.48	BDL	22	130	328	3.96	30	3.33	40	1.22	378	BDL	0.76	98	310	32	0.01	0.011	0.1	BDL	16	178	BDL	0.31	BDL	BDL	132	BDL	83
T43	8.9	3.14	126	0.076	20	BDL	7	7.05	2.8	71	1200	10400	10.35	BDL	0.12	BDL	9.75	1500	BDL	0.22	1650	130	70	0.116	0.151	1.67	BDL	34	25	BDL	0.22	BDL	BDL	209	BDL	139
T44	25	5.59	19	0.084	520	1.1	5	1.32	2.4	425	75	27400	15.95	BDL	1.86	20	1.74	424	1	1.43	20900	560	32	0.536	0.66	7.54	BDL	16	219	BDL	0.44	BDL	BDL	151	BDL	147
T46	BDL	7.47	210	0.026	690	1.1	BDL	2.82	BDL	49	241	805	5.89	20	1.98	40	3.1	708	1	1.75	434	670	30	0.086	0.053	0.14	BDL	19	374	BDL	0.44	BDL	BDL	145	BDL	85
T69	3.2	12.6	2480	0.058	880	1.4	BDL	2.15	1.8	192	764	4050	5.91	20	2.88	40	4.11	437	23	2.81	2670	220	73	0.035	0.027	0.79	19	15	406	BDL	0.28	BDL	10	199	BDL	82
T72	0.6	7.81	5	0.018	610	1.3	BDL	6.09	BDL	50	20	406	9.43	20	0.78	20	2.39	1440	BDL	2.4	59	1200	63	0.003	0.005	1.02	8	35	397	BDL	0.9	BDL	10	308	BDL	120
T101	12	6.41	16	3.15	850	1.4	51	4.83	3.3	52	72	18350	8.35	10	1.44	20	1.82	757	1	1.46	1640	630	114	2.86	3.79	2.34	BDL	16	229	BDL	0.46	BDL	BDL	135	10	143
T103	1.9	5.83	BDL	0.015	570	BDL	BDL	1.5	1.1	55	101	2340	9.86	20	3.57	20	4.03	832	1	0.15	134	2050	6	0.006	0.006	0.29	BDL	8	23	BDL	0.73	BDL	BDL	108	BDL	143
T107	BDL	5.7	BDL	0.037	370	0.8	BDL	4.98	BDL	41	748	344	10	10	1.88	10	5.67	1625	BDL	0.87	783	320	18	0.07	0.045	0.06	BDL	34	77	BDL	0.32	BDL	BDL	230	BDL	126
T110	1.1	7.36	BDL	0.027	570	1.6	BDL	3.37	BDL	29	94	1250	6.89	20	1.76	40	1.82	839	1	1.94	480	740	50	0.076	0.04	0.18	BDL	17	285	BDL	0.55	BDL	10	147	BDL	96

Notes: Abbreviation BDL stands for below detection limit, ADL stands for above detection limit

A3 (continued): Bulk rock analysis of samples from the Totten #2 Mine (ppm)

Sample	Ag	Al (wt%)	As	Au	Ba	Be	Bi	Ca (wt%)	Cd	Co	Cr	Cu	Fe (wt%)	Ga	K (wt%)	La	Mg (wt%)	Mn	Mo	Na (wt%)	Ni	P	Pb	Pd	Pt	S (wt%)	Sb	Sc	Sr	Th	Ti (wt%)	Tl	U	V	W	Zn
T112	BDL	7.92	6	0.015	220	0.7	BDL	6.45	BDL	41	73	148	8.37	20	0.89	10	3.35	1335	BDL	1.56	103	390	12	0.035	0.023	0.07	BDL	32	206	BDL	0.56	BDL	10	208	BDL	100
T122	BDL	8.85	BDL	0.007	190	0.8	BDL	5.3	BDL	70	127	464	8.94	20	0.78	10	2.92	1280	3	1.27	210	160	10	0.009	0.011	0.7	7	30	248	BDL	1.04	BDL	BDL	258	10	106
T131	11.8	3.82	2310	1.05	660	BDL	63	6.56	0.5	109	1240	6590	8.17	10	1.28	BDL	9.19	1580	BDL	0.49	2860	120	11	0.294	0.213	0.69	20	34	52	BDL	0.22	BDL	BDL	199	BDL	104
T134	11.8	6.85	17	0.385	520	1.2	12	2.66	4.3	161	148	22900	12.15	10	1.81	30	2.33	508	3	2.07	9940	630	69	3.34	4.38	5.03	5	20	306	BDL	0.5	BDL	10	156	BDL	158
T135	20.7	0.92	20	0.028	90	BDL	BDL	0.33	BDL	1085	29	27600	44.5	BDL	0.15	BDL	0.22	47	5	0.33	63300	130	11	0.143	0.436	31.3	BDL	3	43	BDL	0.12	BDL	BDL	55	BDL	10
T136	8.5	7.22	5	2.35	490	1.4	64	3.99	1.6	60	83	6680	7.86	20	1.33	40	1.91	1020	1	1.84	1765	790	664	3.42	4.45	1.39	BDL	21	257	BDL	0.63	BDL	BDL	189	BDL	102
T139	3	7.21	471	0.093	400	0.8	BDL	3.36	1.4	55	59	2950	7.32	20	1.78	20	2.29	827	9	1.13	823	410	19	0.93	0.027	0.61	BDL	24	180	BDL	0.51	BDL	BDL	155	BDL	126
T141	11.9	0.38	85	0.458	20	BDL	116	0.18	BDL	2100	10	4390	45.2	BDL	0.05	BDL	0.14	30	1	0.11	125500	40	2	1.16	28.8	33.4	BDL	1	13	BDL	0.03	BDL	BDL	12	BDL	BDL
T142	20.3	1.3	77	7.14	80	BDL	349	0.6	0.9	803	19	16200	44.9	BDL	0.2	BDL	0.33	56	1	0.42	53200	120	45	3.6	28.3	28.4	BDL	4	56	BDL	0.09	BDL	BDL	25	BDL	45
T143	23	7.66	11	0.362	620	2.3	26	1.63	9.6	101	97	29400	10.65	10	2.24	30	2.08	462	1	2.53	4270	710	113	0.289	0.996	5.22	BDL	17	409	BDL	0.58	BDL	10	118	BDL	255
T144	4	0.03	12	0.044	BDL	BDL	3	0.03	BDL	1555	191	6440	ADL	BDL	BDL	BDL	0.01	BDL	5	0.01	49300	BDL	6	0.149	1.095	35.1	BDL	BDL	1	BDL	0.01	BDL	BDL	26	BDL	7
T145	13.6	0.38	10	0.097	30	BDL	68	0.15	BDL	1085	10	5310	ADL	BDL	0.08	BDL	0.11	57	BDL	0.08	52200	30	20	0.599	2.081	36.1	BDL	1	12	BDL	0.03	BDL	10	12	BDL	13
T146	47.7	5.21	6	1.801	150	0.9	22	2.72	10	251	174	72960	17.1	20	0.41	20	1.91	574	BDL	2	7360	490	545	1.935	1.033	12.25	BDL	17	276	BDL	0.35	BDL	BDL	134	BDL	248
T147	6.5	1.02	30	0.09	80	BDL	14	0.48	BDL	2110	11	4620	44.4	BDL	0.18	BDL	0.21	93	BDL	0.24	97500	80	14	0.487	1.16	31.2	BDL	2	34	BDL	0.08	BDL	10	21	BDL	50
T148	28.5	4.98	BDL	0.068	60	1.1	BDL	2.32	7.4	719	61	48710	20.6	10	1.2	20	1.08	623	BDL	1.04	32800	490	45	0.449	0.591	12.45	BDL	13	193	BDL	0.37	BDL	BDL	105	BDL	229
T149	45.9	3.85	BDL	0.774	60	0.7	59	1.86	14.2	459	67	85090	23	10	0.69	10	1.4	533	BDL	0.9	17950	380	746	1.051	3.188	16.4	BDL	12	166	BDL	0.27	10	BDL	90	BDL	306
T150	2.9	2.47	42	0.082	70	0.5	10	1.33	BDL	453	29	868	42.3	10	0.53	BDL	0.61	337	BDL	0.46	30100	210	17	0.269	1.017	25.4	BDL	8	68	BDL	0.19	BDL	BDL	63	BDL	18
T151	20.8	2.92	BDL	14.836	160	BDL	115	4.22	8.6	153	964	12950	16.05	10	0.51	10	6.08	1190	BDL	0.17	6680	290	1860	4.805	13.157	5.7	BDL	23	16	BDL	0.19	10	BDL	149	BDL	249
T152A	58.6	3.94	9	1.16	70	0.9	32	1.73	14.8	472	45	74380	25.4	10	0.75	10	0.85	359	BDL	0.86	17550	370	48	1.107	0.718	18.4	BDL	11	133	BDL	0.29	BDL	BDL	80	BDL	392
T152B	12.5	1.75	8	0.133	70	BDL	19	0.87	BDL	615	19	8690	46.9	BDL	0.21	BDL	0.35	155	BDL	0.42	28700	160	19	0.168	0.849	29.4	BDL	4	59	BDL	0.13	BDL	10	36	BDL	74
T153	39.1	4.64	BDL	6.221	230	0.6	35	3.55	15.6	216	520	55450	14.7	10	0.89	10	4.56	873	BDL	1.2	7860	220	322	0.24	0.355	8.64	BDL	23	220	BDL	0.23	BDL	BDL	167	BDL	360
T154	56.7	5.13	BDL	1.126	80	1	7	2.31	16.9	185	53	64230	16.75	20	0.9	20	1.17	561	BDL	1.08	5890	520	54	0.958	0.771	10.85	BDL	15	150	BDL	0.41	BDL	BDL	120	BDL	350
T155	54.5	3.76	BDL	0.198	120	0.7	36	1.11	17	776	63	66840	26.1	BDL	0.4	10	0.85	280	BDL	1.47	30800	360	104	0.512	1.425	20	BDL	10	174	BDL	0.25	BDL	BDL	68	BDL	479
T157	16.1	2.92	6	0.082	70	0.5	69	0.75	0.5	1160	276	12070	37.6	BDL	0.6	BDL	0.9	164	BDL	0.86	51800	110	40	1.154	0.852	25.7	BDL	7	125	BDL	0.13	10	10	84	BDL	96
T158	19.4	2.3	16	0.086	100	0.5	30	1.01	1.4	2360	23	28410	30.9	BDL	0.42	10	0.46	285	BDL	0.61	108000	220	48	1.72	0.893	24.7	BDL	6	82	BDL	0.2	BDL	BDL	53	BDL	121
T159	31.4	5	8	0.401	130	0.7	BDL	2.24	11.3	341	103	51440	20.9	10	0.49	20	1.54	474	BDL	1.92	15500	490	123	0.796	1.515	14.65	BDL	15	285	BDL	0.36	BDL	BDL	112	BDL	393
T161	4.7	8.11	BDL	0.015	1630	BDL	9	0.24	2	128	148	7790	16	20	4.75	20	7	788	BDL	0.03	4130	910	12	0.025	0.04	1.64	BDL	23	7	BDL	0.55	BDL	BDL	211	BDL	141
T162	2.7	1.42	30	0.061	100	BDL	24	0.62	BDL	906	18	1005	45.1	BDL	0.2	BDL	0.28	111	BDL	0.45	51600	130	22	0.407	0.075	29.8	BDL	3	53	BDL	0.1	10	10	35	BDL	8
T163	213	0.04	BDL	0.116	10	BDL	148	0.03	65.9	214	5	292100	32	10	0.02	40	0.02	BDL	BDL	0.01	4510	BDL	180	0.028	12.068	34.2	BDL	4	3	BDL	BDL	BDL	BDL	1	BDL	1190
T164	10.9	2.33	14	0.127	60	BDL	12	0.86	BDL	1485	184	6950	37.9	BDL	0.7	BDL	1.18	234	BDL	0.55	73600	140	30	0.74	1.306	25.7	BDL	6	73	BDL	0.12	BDL	10	55	BDL	43
T165	132	0.74	BDL	0.603	10	BDL	138	0.5	23.6	1065	43	110350	40.7	BDL	0.04	BDL	0.39	112	BDL	0.18	43300	50	989	0.918	17.356	32.9	BDL	4	29	BDL	0.05	BDL	10	20	BDL	597
T166	10.5	5.06	12	0.068	80	1.1	14	2.32	1	632	65	16470	19.5	10	1.15	20	1.18	589	BDL	1.07	31200	510	43	0.383	1.132	11.3	BDL	13	191	BDL	0.39	BDL	BDL	108	BDL	84
T167	21.4	4.46	BDL	2.949	140	0.5	48	4.32	5.7	153	629	53170	16.8	10	0.96	10	5.12	1075	BDL	0.94	14700	320	278	2.467	3.732	8.68	BDL	25	112	BDL	0.29	BDL	BDL	168	BDL	166
T168	17.7	2.31	22	0.221	90	BDL	45	1.09	1.2	789	88	15200	40.7	BDL	0.2	BDL	0.58	171	BDL	0.78	40600	190	270	0.728	3.935	27.6	BDL	6	86	BDL	0.18	10	10	64	BDL	87
T169	22.8	3.13	19	0.179	60	0.7	37	1.38	5.9	1050	28	47320	26.9	BDL	0.58	10	0.58	356	BDL	0.79	52800	300	72	0.83	0.557	19.45	BDL	7	139	BDL	0.21	BDL	10	53	BDL	191
T170	35.3	5.36	5	0.137	120	1	BDL	1.71	14.2	145	107	65850	15.2	10	0.79	20	0.85	373	2	1.81	4870	660	17	0.126	0.128	7.97	BDL	9	352	BDL	0.34	BDL	BDL	77	BDL	363
T171	4.3	3.59	12	0.053	160	0.6	7	1.48	BDL	379	427	2570	33.8	10	0.75	10	1.14	468	1	0.72	20600	320	16	0.153	0.361	21.4	BDL	9	109	BDL	0.22	BDL	BDL	117	BDL	28
T172	2.3	5.6	BDL	0.01	140	0.8	2	2.73	BDL	172	505	3080	23.5	10	0.99	20	1.67	723	2	1.23	8960	520	17	0.01	0.37	8.31	BDL	14	204	BDL	0.33	BDL	BDL	128	BDL	66
T173	5.9	1.26	17	0.013	100	BDL	3	0.44	BDL	647	276	1980	48.8	BDL	0.29	10	0.52	168	1	0.2	32500	100	19	0.027	0.575	30.6	BDL	3	31	BDL	0.1	BDL	BDL	175	BDL	BDL
T174	44	5.45	30	1.076	550	0.8	BDL	1.82	10.4	160	211	83330	17.4	10	1.36	20	1.58	511	2	1.14	4540	510	15	0.837	0.1	8.13	BDL	15	236	BDL	0.35	BDL	BDL	135	BDL	259
T175	2.5	7.15	1015	0.026	570	1.6	BDL	3.1	1.6	92	100	6250	8.67	20	1.49	40	1.52	800	2	1.95	2380	740	17	0.281	0.168	2.08	6	16	274	BDL	0.5	BDL	BDL	130	BDL	126
T176	1.7	8.68	BDL	0.004	190	2	BDL	5.77	0.7	108	98	2220	12.35	20	0.57	40	2.21	1055	1	2.66	1140	1010	29	0.015	0.028	3.93	BDL	21	410	20	0.65	BDL	BDL	173	BDL	106
T177	2.3	2.01	12	0.044	80	BDL	13	0.35	BDL	609	109	1570	44.8	BDL	0.51	BDL	0.36	188	1	0.65	32300	50	25	0.104	1.107	29.5	BDL	4	53	BDL	0.11	BDL	BDL	137	BDL	10
T178	0.6	7.88	74	0.009	600	1.6	BDL	3.95	BDL	43	119	491	6.97	20	1.59	30	2.05	956	2	1.95	553	780	16	0.103	0.053	0.47	5	19	345	BDL	0.52	BDL	BDL	153	BDL	108

Notes: Abbreviation BDL stands for below detection limit, ADL stands for above detection limit

A3 (continued): Bulk rock analysis of samples from the Totten #2 Mine (ppm)

Sample	Ag	Al (wt%)	As	Au	Ba	Be	Bi	Ca (wt%)	Cd	Co	Cr	Cu	Fe (wt%)	Ga	K (wt%)	La	Mg (wt%)	Mn	Mo	Na (wt%)	Ni	P	Pb	Pd	Pt	S (wt%)	Sb	Sc	Sr	Th	Ti (wt%)	Tl	U	V	W	Zn
T179	12.3	7.78	BDL	0.051	300	1.4	BDL	3.59	3.8	175	41	13310	17.1	10	0.68	40	1.95	751	1	2.43	6160	950	25	0.013	BDL	7.11	5	21	458	BDL	0.68	BDL	BDL	152	BDL	128
T180	3.3	0.01	66	0.011	10	BDL	10	0.02	BDL	836	594	1230	ADL	BDL	BDL	BDL	BDL	13	1	BDL	37600	BDL	27	0.055	0.18	36.4	BDL	BDL	BDL	BDL	0.01	BDL	BDL	45	BDL	BDL
T181	BDL	7.14	20	0.012	640	1.5	BDL	3.57	BDL	39	230	324	7.31	20	1.86	30	2.33	1065	2	1.64	360	720	15	0.065	0.037	0.23	BDL	18	252	BDL	0.51	BDL	BDL	145	BDL	124
T182	2.2	6.91	BDL	0.113	440	1.1	3	3.57	0.6	155	221	2910	14.75	20	1.01	30	1.98	809	2	1.68	6650	670	13	0.4	0.215	4.66	BDL	18	273	BDL	0.42	BDL	BDL	149	BDL	77
T183	4.5	7.12	BDL	0.03	500	1.1	BDL	3.75	0.8	76	340	15800	11.2	20	1.03	30	2.05	881	2	1.86	2760	680	13	0.105	0.065	3.4	BDL	18	290	BDL	0.42	BDL	BDL	145	BDL	100
T184	1.5	7.61	343	0.074	670	1.3	BDL	2.7	BDL	101	169	4020	8.04	20	2.49	30	2.3	765	3	1.79	2260	850	14	1.005	0.249	1.22	BDL	19	281	BDL	0.55	BDL	BDL	161	BDL	90
T185	0.6	5.49	BDL	0.006	90	1.1	3	3.98	BDL	150	88	455	13.2	10	0.23	20	1.55	742	1	1.77	1710	630	16	0.051	0.05	4.63	BDL	15	272	BDL	0.35	BDL	BDL	113	BDL	50
T186	0.5	7.49	10	0.02	570	1.5	BDL	3.77	BDL	41	105	639	6.93	20	1.45	30	1.89	947	2	1.95	533	760	17	0.123	0.065	0.7	5	19	304	BDL	0.52	BDL	BDL	150	20	103
T187	60.7	2.6	41	0.053	80	0.5	BDL	1.33	12.1	347	76	58810	34.2	BDL	0.22	10	0.63	285	2	0.73	11450	280	18	0.084	0.345	24.5	BDL	8	110	BDL	0.2	BDL	BDL	70	10	325
T188	BDL	4.05	17	0.001	140	BDL	BDL	7.18	BDL	61	1415	102	7.52	10	0.83	BDL	10.05	1720	BDL	0.52	341	60	4	0.007	0.016	0.03	BDL	40	71	BDL	0.19	BDL	BDL	276	BDL	119
T189	BDL	8.08	BDL	0.001	400	1.1	BDL	4.59	BDL	20	132	135	5.17	20	0.83	30	2.38	816	3	2.18	73	750	16	0.001	0.006	0.17	BDL	19	363	BDL	0.44	BDL	BDL	149	BDL	88
T190	1.9	6.77	BDL	0.127	390	1.1	7	3.52	BDL	145	169	2520	14.4	10	1.01	20	1.93	831	1	1.63	6340	640	11	0.468	0.283	5.12	6	17	254	BDL	0.41	BDL	BDL	149	BDL	63
T192	12	3.81	BDL	0.198	180	BDL	14	4.89	3.5	127	834	28870	17.15	10	0.91	10	5.94	1620	1	0.4	5130	240	8	1.039	0.706	6.18	BDL	28	31	BDL	0.12	BDL	BDL	116	BDL	181
T193	2.1	3.07	15	0.027	110	0.7	11	0.67	BDL	341	99	1740	39.2	BDL	0.76	10	0.44	240	1	0.94	21400	140	18	0.081	1.739	26.1	BDL	6	73	BDL	0.16	BDL	BDL	199	BDL	6
T194	19.4	1.34	14	0.019	110	BDL	BDL	0.92	4.1	14	39	53460	7.32	BDL	0.24	10	0.47	272	1	0.39	362	1120	6	0.01	BDL	4.72	BDL	2	39	BDL	0.05	BDL	BDL	18	BDL	201
T195	4.7	7.83	1090	0.053	530	1.7	2	2.89	2	42	85	5140	6.58	20	1.98	40	1.83	659	2	2.04	1740	770	23	0.333	0.019	0.92	BDL	19	302	20	0.59	BDL	BDL	151	20	112
T196	8.2	7.31	139	0.84	570	1.6	18	3.46	3.4	97	91	13110	8.76	20	1.48	30	1.68	826	3	1.86	5440	740	56	1.919	2.258	2.58	BDL	18	267	BDL	0.54	BDL	BDL	155	BDL	147
T197	2.2	7.9	136	0.049	490	1.8	BDL	3.78	1.1	36	101	2750	6.91	20	1.63	40	2.05	947	2	2.32	730	750	29	0.097	0.062	0.36	BDL	19	316	20	0.59	BDL	BDL	165	BDL	95
T198	0.9	7.77	225	0.051	590	1.8	2	3.53	BDL	63	95	1570	7.6	20	1.76	40	1.81	942	2	2.1	1630	760	35	0.226	0.149	0.83	5	19	293	20	0.56	BDL	BDL	157	BDL	107
T199	2.7	7.32	375	0.124	610	1.7	3	3.36	0.8	146	88	4350	10.25	20	1.71	30	1.66	948	2	1.88	4910	730	28	0.561	0.398	2.41	BDL	19	263	BDL	0.56	BDL	BDL	166	BDL	127
T200	9.1	6.64	24	0.021	530	1	BDL	3.16	6.9	22	124	8820	6.27	20	1.21	30	1.96	661	2	1.52	920	650	16	0.016	0.006	1.41	BDL	15	255	BDL	0.41	BDL	BDL	115	20	162
T201	8.7	7.04	4090	1.347	350	1.3	4	3.87	1.2	39	107	5880	6.44	20	1.2	30	1.98	827	2	1.68	3720	730	23	1.932	0.009	0.73	31	19	259	BDL	0.53	BDL	BDL	157	340	92
T203	6	7.92	1485	0.153	500	1.3	5	4.31	4.1	133	151	6890	7.61	20	1.31	30	2.4	939	3	1.89	1890	710	22	1.897	0.37	1.41	BDL	20	306	BDL	0.47	BDL	BDL	153	BDL	134
T204	10.9	7.9	83	0.115	560	1.2	BDL	3.99	7	36	138	11130	7.26	20	1.36	30	2.21	801	2	1.84	871	730	19	0.091	0.081	1.67	BDL	19	309	BDL	0.48	BDL	BDL	147	30	171
T205	8.8	7.55	16	0.18	710	1.4	3	1.77	2.1	118	123	10660	8.6	20	2.49	30	2.07	503	2	1.93	4200	760	62	0.543	0.594	2.58	BDL	20	314	BDL	0.54	BDL	BDL	167	BDL	105
T206	5.4	7.94	1670	0.106	490	2	2	4.22	2.3	90	85	6700	8.37	20	1.4	40	1.59	920	2	2.23	4160	830	57	0.653	0.249	2.01	11	18	309	20	0.59	BDL	BDL	153	130	139
T207	0.9	9.6	12	0.011	140	0.5	BDL	6.76	0.5	89	183	1100	8.46	20	0.46	10	3.74	1080	1	1.86	695	140	13	0.034	0.012	1.15	6	21	277	BDL	0.28	BDL	BDL	185	BDL	83
T208	2.9	7.11	BDL	0.112	630	1.7	BDL	3.18	0.7	125	90	3650	9.38	20	1.71	30	1.59	921	2	1.8	4100	800	35	0.519	0.339	1.86	BDL	17	281	BDL	0.52	BDL	BDL	146	BDL	122
T209	BDL	8.33	7	0.007	530	1.5	BDL	4.48	BDL	38	139	447	7.21	20	1.54	30	2.66	1000	4	1.99	191	790	31	0.02	0.016	0.3	BDL	24	302	BDL	0.56	BDL	BDL	181	BDL	140
T210	1.1	7.89	39	0.018	120	0.6	2	6.83	BDL	124	232	2410	10	20	0.48	10	4.2	1220	1	1.27	926	320	10	0.115	0.025	1.57	BDL	33	183	BDL	0.45	BDL	BDL	253	BDL	96
T211	10.1	6.77	BDL	0.089	450	1.1	BDL	3.49	12.8	21	119	13460	7.39	20	1.03	30	1.93	749	6	1.74	1570	640	20	0.11	0.003	2.12	BDL	17	276	BDL	0.41	BDL	BDL	130	110	268
T212	5.3	7.76	9	0.087	330	1.3	10	4.03	0.6	102	193	4910	7.32	20	1.11	30	2.74	744	2	2.49	2770	770	398	0.345	0.283	1.54	BDL	21	385	20	0.51	BDL	BDL	159	BDL	78
T213	2.3	6.74	11	0.016	440	1.1	BDL	3.53	BDL	25	119	3360	5.76	20	1.21	30	1.96	784	1	1.71	684	670	20	0.037	0.006	0.81	BDL	17	271	BDL	0.42	BDL	BDL	135	20	78
T214	27.2	6.76	23800	1.048	270	1.3	BDL	3.12	12.6	226	116	35150	9.06	10	0.85	30	1.84	619	2	2.37	22800	760	83	6.967	0.622	4.79	77	18	382	BDL	0.45	BDL	BDL	123	BDL	219
T215	2.9	6.02	165	0.049	300	1	BDL	4.52	1.2	52	659	3080	5.75	10	0.96	30	4.49	883	2	1.94	864	550	71	0.083	0.078	0.42	BDL	23	305	BDL	0.34	BDL	BDL	138	BDL	66
T216	16.6	7.39	335	0.404	660	1.3	7	2.35	4.2	97	139	22810	8.72	20	2.19	30	2.12	514	2	2.07	3860	670	90	0.552	0.771	3.32	6	18	358	BDL	0.44	BDL	BDL	130	BDL	117
T217	14.4	7.67	12	0.081	370	1.3	BDL	2.53	3.4	144	246	18830	13.75	10	2.26	20	3.25	645	1	2.2	7760	570	50	0.106	0.215	5.03	BDL	21	412	BDL	0.6	BDL	BDL	277	BDL	111
T218	23.7	4.95	6	0.348	230	0.8	13	3.17	9.4	205	547	35500	14.9	10	1.51	20	4.07	839	2	1.14	9280	480	40	0.261	0.619	6.37	BDL	21	196	BDL	0.37	BDL	BDL	163	BDL	249
T219	22.3	4.47	11	0.095	340	BDL	BDL	3.84	6.7	96	1390	28300	11.85	10	1.54	20	6.23	1115	1	0.37	4370	260	36	0.154	0.918	3.2	BDL	32	32	BDL	0.27	BDL	BDL	160	BDL	195
T220	54	5.27	62	0.114	110	1.2	BDL	1.83	13.6	263	67	71450	15.3	10	0.97	30	1.2	359	3	1.85	16750	540	37	0.245	0.824	8.27	7	13	255	BDL	0.35	BDL	BDL	94	BDL	365
T222	4.4	4.91	7	0.074	200	0.9	7	2.09	BDL	478	76	5380	18.8	BDL	0.95	10	1.72	522	3	1.78	34300	510	36	0.227	0.351	9.21	BDL	16	243	BDL	0.33	BDL	BDL	130	BDL	44
T223	26.1	5.71	12	1.16	80	1.1	27	2.51	5.3	739	122	34890	15.55	10	0.8	20	1.8	552	1	2.09	40400	610	160	2.308	4.183	9.03	BDL	17	269	BDL	0.38	BDL	BDL	156	BDL	218
T224	28.6	7.28	BDL	0.793	310	1.4	BDL	3.74	8.1	73	124	32150	9.19	20	1	30	2.24	777	3	2.54	2480	660	143	0.687	0.74	4.19	BDL	20	322	BDL	0.47	10	BDL	175	BDL	230
T225	BDL	3.84	82	0.011	170	BDL	BDL	7.51	BDL	57	1275	48	8.04	10	0.99	10	9.77	1670	BDL	0.51	535	130	7	0.04	0.031	0.02	BDL	39	44	BDL	0.24	BDL	BDL	246	BDL	93

Notes: Abbreviation BDL stands for below detection limit, ADL stands for above detection limit

A3 (continued): Bulk rock analysis of samples from the Totten #2 Mine (ppm)

Sample	Ag	Al (wt%)	As	Au	Ba	Be	Bi	Ca (wt%)	Cd	Co	Cr	Cu	Fe (wt%)	Ga	K (wt%)	La	Mg (wt%)	Mn	Mo	Na (wt%)	Ni	P	Pb	Pd	Pt	S (wt%)	Sb	Sc	Sr	Th	Ti (wt%)	Tl	U	V	W	Zn
T226	32.7	3.55	77700	3.25	280	0.5	BDL	2.48	6.1	138	336	30760	7.48	BDL	1.01	10	2.5	533	1	0.82	71300	300	41	16.64	0.227	3.22	196	16	117	BDL	0.23	BDL	BDL	108	BDL	158
T227	1.9	7.23	82	0.037	350	1.2	3	2.15	BDL	210	144	1310	12.35	10	2.18	20	2.48	466	2	1.9	11800	610	97	0.119	0.212	4.33	BDL	19	328	BDL	0.46	BDL	BDL	174	BDL	53
T228	27.3	7.25	96	0.793	240	1.4	3	3.77	9.8	41	114	39460	8.29	20	0.7	30	2.12	674	3	2.69	1200	700	219	0.552	0.426	3.87	BDL	20	386	BDL	0.5	BDL	BDL	163	BDL	195
T229	21.1	6.97	22	0.439	230	1.4	7	3.57	7.5	61	120	27690	7.61	20	0.58	30	1.9	648	2	2.58	2070	710	154	0.132	0.305	3.26	7	18	376	BDL	0.46	BDL	BDL	147	10	151
T230	1.8	7.98	134	0.063	580	1.5	BDL	4.08	BDL	73	129	2010	8.22	20	1.64	30	2.41	1095	1	2	1810	860	35	0.268	0.171	0.87	8	19	301	BDL	0.52	BDL	BDL	152	BDL	124
T231	1.3	4.81	1200	0.133	140	1.2	13	2.1	BDL	340	53	2530	23.8	10	0.78	20	0.86	511	3	1.43	20700	490	18	0.706	1.851	9.51	6	10	191	BDL	0.31	BDL	BDL	91	BDL	25
T232	5.1	7.57	294	0.082	540	1.7	BDL	3.47	2.7	91	101	6610	8.8	20	1.37	30	1.71	856	2	1.96	3630	920	25	0.412	0.302	1.87	6	18	298	BDL	0.57	BDL	BDL	147	BDL	129
T233	4.2	0.2	45	0.016	20	BDL	38	0.07	BDL	1235	5	1030	ADL	BDL	0.05	BDL	0.04	BDL	BDL	0.05	59000	BDL	163	0.83	1.711	37.2	BDL	1	6	BDL	0.01	BDL	10	8	BDL	4
T234	15.5	5.73	BDL	0.544	290	0.8	12	2.85	2.6	590	314	21660	16.1	10	1.46	20	3.52	737	BDL	1.35	27100	540	182	1.12	0.569	8.78	BDL	19	195	BDL	0.39	BDL	BDL	160	BDL	135
T235	7.7	7.88	5580	0.607	530	1.7	17	3.26	1.3	55	78	5100	5.84	20	1.78	30	1.99	651	2	2.17	5560	740	37	3.157	1.841	0.83	81	23	292	20	0.59	BDL	BDL	184	BDL	97
T237	8.1	7.2	4940	0.301	840	1.1	4	2.06	2.7	72	488	8350	8.4	20	3.08	30	3.06	796	1	1.27	6450	730	27	3.561	0.69	1.36	78	17	180	BDL	0.56	BDL	BDL	193	BDL	145
T238	BDL	7.97	BDL	0.002	480	1.3	BDL	4.41	BDL	28	129	143	6.25	20	1.41	30	2.28	1015	1	1.81	133	760	17	0.003	BDL	0.06	BDL	19	311	BDL	0.48	BDL	BDL	154	BDL	95
TU1	58.2	0.13	6	0.068	10	BDL	4	0.06	20.3	894	367	102500	43.3	BDL	BDL	BDL	0.05	35	4	0.01	51500	10	18	2.18	0.938	33.8	BDL	2	5	BDL	0.01	BDL	BDL	43	BDL	434
TU2	72.6	4.57	121	1.41	330	0.7	8	1.82	27.9	124	100	108000	19.5	10	1.11	20	0.89	577	2	0.69	3110	490	164	0.731	0.529	14.3	5	15	174	BDL	0.37	BDL	BDL	126	BDL	1480
TU3	96.3	2.24	114	0.322	20	BDL	24	0.47	29.4	514	88	141500	23.9	BDL	0.08	10	0.56	316	6	0.57	30500	180	288	0.955	0.296	21.7	BDL	6	69	BDL	0.12	BDL	BDL	38	BDL	830
TU4A	32.4	6.4	16	0.523	330	0.8	12	3.46	9.4	175	139	43500	16.85	10	0.73	20	2.08	1040	1	0.4	2800	520	11	3.75	2.04	5.64	BDL	17	132	BDL	0.35	BDL	BDL	130	BDL	420
TU4B	99.9	0.76	13500	10.75	10	BDL	50	1.3	21.4	5700	28	107500	20.4	BDL	BDL	BDL	0.41	172	1	0.01	8760	50	57	39.7	0.014	16.6	26	2	5	BDL	0.02	BDL	BDL	11	90	1030
TU5	6.6	4.99	29	0.173	280	0.7	2	3.06	BDL	578	144	3580	25.9	BDL	0.74	10	1.67	766	1	1.06	18150	370	21	1.085	1.695	9.49	BDL	13	189	BDL	0.24	BDL	BDL	118	BDL	43
TU6	8.6	0.03	90	0.126	BDL	BDL	BDL	0.07	BDL	1730	416	3050	ADL	BDL	BDL	BDL	0.03	BDL	7	BDL	50500	BDL	9	2.53	0.906	34.8	BDL	BDL	2	BDL	0.01	BDL	BDL	29	BDL	BDL
TU7	4	0.03	17	0.014	BDL	BDL	BDL	0.04	BDL	1400	258	3530	ADL	BDL	BDL	BDL	0.03	BDL	6	BDL	44500	BDL	6	0.278	1.01	35.8	BDL	BDL	2	BDL	0.01	BDL	BDL	26	BDL	BDL
TU8	27	0.09	43	0.04	10	BDL	13	0.03	BDL	1285	369	45700	ADL	BDL	BDL	BDL	0.04	58	5	0.01	40100	BDL	20	0.479	0.315	36.3	BDL	1	3	BDL	0.02	BDL	BDL	64	BDL	159
TU9	3.5	0.04	16	0.026	BDL	BDL	BDL	0.01	BDL	1230	177	668	49.2	BDL	0.01	BDL	0.02	BDL	3	0.01	41400	BDL	15	1.795	1.485	35.9	BDL	BDL	1	BDL	0.01	10	10	34	BDL	BDL
TU11	66.9	7.97	37300	18.15	1090	1.1	BDL	1.85	2.6	301	155	15650	9.82	BDL	2.94	20	2.44	799	1	1.61	36800	660	89	11.75	0.399	2.26	344	11	291	BDL	0.51	BDL	BDL	192	BDL	90
TU12	126	1.14	124	0.424	70	BDL	33	0.05	22	1810	14	98600	35.7	BDL	0.26	BDL	0.18	618	1	0.1	97200	30	74	2.86	0.832	30.5	BDL	3	18	BDL	0.04	BDL	BDL	15	BDL	607
TU13	91.2	0.8	125	0.568	70	BDL	68	0.08	36.3	716	9	146500	38.6	BDL	0.19	BDL	0.14	40	1	0.26	36700	20	36	2.11	24.1	32	BDL	3	17	BDL	0.03	BDL	BDL	12	10	565
TU14	3.5	7.72	BDL	0.178	760	0.9	BDL	1.97	2.2	60	146	5200	7.26	20	2.89	30	2.45	590	1	1	1200	730	41	0.11	0.057	0.84	BDL	19	186	BDL	0.47	BDL	BDL	151	BDL	176
TU15	17.3	5.47	17400	0.854	320	0.9	6	3.66	1.8	1645	104	9250	14.9	BDL	1.22	30	2.35	1135	2	0.69	28000	580	12	6.28	0.115	5.26	228	20	59	BDL	0.37	BDL	BDL	147	BDL	86
TU16A	23.4	5.91	51	0.099	300	1.1	7	2.42	8.9	132	85	42100	13.6	10	0.92	20	1.68	786	1	1.95	5630	560	26	0.471	1.07	5.36	BDL	17	182	BDL	0.43	BDL	10	134	BDL	417
TU16B	23.8	4.96	1340	0.133	390	0.9	10	2.33	2.7	708	94	33300	18.65	BDL	1.23	20	1.51	672	1	1.14	21500	270	59	3.03	3.11	7.8	6	12	174	BDL	0.27	BDL	BDL	106	10	188
TU18A	186	0.44	5	0.183	30	BDL	55	0.74	50.3	46	7	303000	29.4	BDL	0.05	BDL	0.14	158	4	0.09	3400	50	16	0.533	5	31.4	BDL	5	16	BDL	0.04	BDL	BDL	13	10	1285
TU18B	19	0.97	53	3.35	50	BDL	373	0.59	BDL	644	11	5630	48.2	BDL	0.13	BDL	0.26	147	1	0.27	46800	90	1715	3.22	22.5	33.1	BDL	2	25	BDL	0.07	BDL	BDL	20	BDL	9
TU20	4.6	8.45	BDL	0.056	410	1.3	BDL	4.29	1.2	54	153	5490	7.57	20	1.58	30	2.53	1080	1	1.38	1010	780	52	0.094	0.037	0.9	BDL	20	239	BDL	0.5	BDL	10	159	BDL	102
TU21	44.4	9.89	8700	4.417	610	2.4	BDL	2.21	15.3	103	154	42250	10.9	20	2.15	20	1.49	494	4	3.41	12450	290	673	4.619	4.666	5.34	104	15	346	BDL	0.38	BDL	BDL	135	BDL	1315
TU22	106	0.02	19	0.016	BDL	BDL	BDL	0.03	49.5	262	296	221800	40.3	BDL	BDL	BDL	0.01	11	5	0.01	12300	BDL	41	0.239	1.288	36	16	3	3	BDL	0.01	BDL	10	17	BDL	933
TU23	50.7	3.17	12700	0.65	130	BDL	BDL	0.41	8	4930	569	116800	20.3	10	0.6	BDL	2.53	472	3	0.02	11750	190	29	30.45	0.927	14.4	20	11	7	BDL	0.23	BDL	BDL	111	BDL	433
TU24	32.1	5.84	7	0.116	270	1	BDL	4.23	6.7	88	44	64840	12.1	20	0.43	30	1.32	811	2	0.8	2070	720	17	1.599	0.124	5.68	5	20	265	BDL	0.54	BDL	BDL	193	BDL	297
TU27	12	3.87	21	0.099	150	0.8	BDL	1.75	1.5	932	66	15350	34	BDL	0.46	10	0.94	468	1	1.37	39300	390	42	0.369	1.344	19.8	BDL	9	163	BDL	0.24	BDL	BDL	95	BDL	160
TU28	4.9	4.13	15	0.072	90	0.9	14	2.19	BDL	795	58	4250	33.6	BDL	0.28	10	1.06	527	3	1.6	35400	420	40	1.005	0.435	19.25	BDL	11	207	BDL	0.34	BDL	BDL	100	BDL	38
TU29	0.7	8.48	255	0.016	530	1.4	BDL	4.46	BDL	72	151	884	7.62	20	1.38	40	2.5	981	2	2.15	839	770	19	0.169	0.068	0.74	BDL	21	332	20	0.5	BDL	BDL	164	BDL	85
TU30	3.6	8.12	11	0.198	460	1.4	3	3.67	1.1	172	139	7840	10.8	20	1.55	30	2.44	770	2	2.33	5540	800	29	0.557	0.557	2.83	BDL	21	398	20	0.57	BDL	BDL	174	BDL	120
TU31	16.8	5.77	6580	7.403	110	1.3	225	2.5	10.2	1830	65	19720	15.8	10	1.35	20	1.57	436	1	1.96	28100	630	111	13.561	39.968	10.65	41	15	254	BDL	0.47	BDL	BDL	111	BDL	314
TU32	4.5	2.76	9100	1.62	120	BDL	143	0.58	BDL	5890	486	10720	18.85	BDL	0.52	10	1.82	315	45	0.18	9530	310	16	2.068	0.715	10.55	7	14	26	BDL	0.1	BDL	BDL	126	BDL	89

Notes: Abbreviation BDL stands for below detection limit, ADL stands for above detection limit

A4: LA-ICPMS analyses of pyrrhotite (ppm)

Sample	Ore body	^{34}S	^{57}Fe	^{59}Co	^{60}Ni	^{61}Ni	^{65}Cu	^{66}Zn	^{75}As	^{77}Se	^{99}Ru	^{101}Ru	^{102}Ru	^{103}Rh	^{105}Pd	^{106}Pd	^{107}Ag	^{108}Pd	^{109}Ag	^{111}Cd	^{118}Sn	^{121}Sb	^{125}Te	^{189}Os	^{193}Ir	^{195}Pt	^{197}Au	^{202}Hg	^{205}Tl	^{206}Pb	^{208}Pb	^{209}Bi
T9	238 OB	398109	591926	129.58	4581.98	4551.1	0.1303	BDL	0.0753	124.52	0.247	0.242	0.242	BDL	BDL	0.00107	0.321	BDL	0.365	0.053	0.078	0.00309	0.281	0.0049	0.00208	0.00109	BDL	BDL	BDL	0.535	0.66	1.004
T9	238 OB	379810	591926	128.67	4440.56	4467.97	0.1031	BDL	0.0295	115.66	0.214	0.203	0.21	BDL	0.00144	0.00106	0.597	0.00443	0.594	BDL	0.0715	0.00077	0.239	BDL	0.00086	BDL	0.00422	0.1095	0.00069	0.508	0.606	1.125
T9	238 OB	376309	591926	117.5	3643.51	3654.84	0.0678	BDL	0.0187	118.73	0.247	0.239	0.229	BDL	0.00124	0.00081	0.489	0.00039	0.477	BDL	0.0728	0.00076	0.159	0.00549	BDL	BDL	0.00108	0.1086	0.01056	0.926	1.036	0.749
T9	238 OB	358285	591926	132.85	3380.09	3389.81	0.1465	BDL	0.0222	111.13	0.209	0.193	0.186	BDL	0.00103	0.00324	1.501	0.00413	1.58	0.0144	0.0564	BDL	0.0969	0.0005	0.00037	BDL	0.00084	0.0565	BDL	0.831	0.995	1.115
T9	238 OB	392383	591926	127.87	4733.39	4767.27	0.0764	BDL	0.0229	118.61	0.282	0.259	0.25	0.00039	BDL	BDL	0.341	BDL	0.359	BDL	0.056	0.00433	0.308	0.00806	0.00027	0.00157	0.00095	0.0485	BDL	0.391	0.475	0.759
T9	238 OB	368578	591926	125.39	5409.89	5350.11	0.0604	BDL	0.0193	110.63	0.221	0.212	0.215	0.00029	0.00059	BDL	0.622	0.00583	0.623	0.0285	0.0544	BDL	0.312	0.00106	BDL	0.00133	0.00643	0.0879	BDL	0.416	0.481	0.487
T12	238 OB	369145	591926	103.7	5427.88	5455.86	0.12	BDL	BDL	111.56	0.574	0.557	0.558	BDL	BDL	0.00054	0.262	0.00087	0.268	0.0118	0.0831	0.00223	0.247	0.0301	0.00278	0.00247	0.00068	0.0762	0.00076	0.261	0.301	0.383
T12	238 OB	372927	591926	115.58	5437.3	5462.02	0.133	BDL	0.0228	112.25	0.551	0.558	0.551	0.00043	0.00044	0.009	0.346	0.00091	0.352	0.029	0.0957	BDL	0.153	0.0269	BDL	0.00057	BDL	0.0321	BDL	0.739	0.856	0.73
T12	238 OB	358791	591926	112.84	5043.31	4971.36	0.123	BDL	0.0152	110.37	0.573	0.568	0.524	0.00054	BDL	0.00049	0.516	0.00108	0.541	BDL	0.0703	0.00259	0.276	0.0323	0.00042	BDL	BDL	0.0739	BDL	0.278	0.344	0.276
T12	238 OB	367771	591926	99.27	4480.98	4516.3	0.105	BDL	0.0354	112.41	0.599	0.581	0.575	BDL	0.00036	BDL	0.25	0.00162	0.239	BDL	0.0616	BDL	0.176	0.0263	BDL	BDL	BDL	0.0336	0.00124	0.492	0.56	0.63
T12	238 OB	382071	591926	104.9	5105.34	5078.1	0.0778	BDL	0.0409	116.18	0.557	0.554	0.538	0.00027	0.0072	BDL	0.246	0.00356	0.252	0.016	0.0739	BDL	0.212	0.027	BDL	0.00265	BDL	0.0162	0.00112	0.648	0.77	0.409
TU1	238 OB	368891	591928	35.79	9052.06	11257.5	0.0437	BDL	0.19	104.82	0.0097	0.0223	0.049	0.00025	BDL	0.00017	0.3	BDL	0.26	0.043	0.0846	0.00044	0.0153	0.00277	0.00015	0.0025	0.00157	0.103	0.00194	0.286	0.325	0.371
TU1	238 OB	379692	591928	38.2	8764.43	9199.7	0.106	0.19	0.0336	115.39	0.7	0.61	0.65	BDL	BDL	0.0033	0.357	BDL	0.382	0.013	0.0968	BDL	0.068	0.0078	0.00097	BDL	0.00093	0.06	0.0111	1.64	1.69	0.521
TU1	238 OB	387054	591928	38.23	7357.17	7476.49	0.191	BDL	0.0052	138.91	0.0137	0.0221	0.044	0.00047	0.0032	0.0164	0.72	0.0097	0.65	0.029	0.124	0.00542	0.49	0.0045	BDL	BDL	0.00222	0.0358	0.00048	1.22	1.28	1.14
TU1	238 OB	375050	591928	46.22	8547.3	8661.94	0.369	0.45	0.0315	115.15	0.067	0.09	0.098	0.00113	BDL	BDL	0.513	0.00169	0.552	0.0035	0.103	BDL	0.084	0.00178	BDL	0.00057	0.00077	0.086	BDL	0.85	0.77	0.66
T7	238 OB	360024	591931	133.64	4976.02	5017.45	0.076	BDL	BDL	123	0.129	0.117	0.13	0.0003	0.0034	0.00149	0.219	0.0022	0.2	BDL	0.0519	BDL	0.274	0.0039	BDL	0.0017	0.0018	0.077	BDL	0.292	0.333	0.296
T7	238 OB	364149	591931	111.4	4347.88	4294.33	0.045	0.13	0.0417	120.92	0.144	0.112	0.113	BDL	0.002	0.00093	0.206	BDL	0.225	0.048	0.0422	0.00248	0.4	0.00217	BDL	0.0019	BDL	0.055	0.00013	0.6	0.67	0.44
T7	238 OB	361926	591931	98.93	3609.78	3593.53	0.151	0.192	0.003	118.55	0.119	0.104	0.119	0.032	BDL	BDL	0.212	BDL	0.224	BDL	0.0623	0.00223	0.4	0.0042	BDL	BDL	0.0018	BDL	0.00332	1.13	1.23	0.83
T7	238 OB	390871	591931	124.43	5009.98	4948.74	0.041	0.51	0.0239	117.84	0.144	0.11	0.122	0.00129	BDL	BDL	0.193	0.00164	0.192	BDL	0.0552	BDL	0.33	0.00229	0.00067	0.0016	BDL	BDL	0.00052	0.378	0.48	0.366
T10	MOB	360498	591923	59.82	8573.75	8680.27	1.333	BDL	0.063	198.75	0.02	0.0386	0.0611	BDL	BDL	BDL	0.234	BDL	0.241	BDL	0.0966	BDL	0.276	BDL	BDL	BDL	BDL	0.102	BDL	0.275	0.3	0.833
T10	MOB	364667	591923	62.63	8700.9	8931.39	1.848	BDL	BDL	205.04	0.0614	0.0421	0.0805	BDL	BDL	0.0022	0.141	BDL	0.143	BDL	0.0631	BDL	0.134	BDL	BDL	BDL	BDL	0.071	BDL	0.0902	0.1124	0.142
T10	MOB	375847	591923	60.4	7437.1	7692.16	0.893	BDL	0.059	204.91	0.0199	0.044	0.0705	BDL	BDL	BDL	0.204	BDL	0.232	BDL	0.151	BDL	0.229	BDL	BDL	BDL	BDL	0.098	BDL	0.396	0.408	0.527
T10	MOB	366496	591923	63.27	8649.68	8777.22	1.147	BDL	BDL	200.24	0.0254	0.0559	0.0624	BDL	BDL	BDL	0.239	BDL	0.212	BDL	0.0783	BDL	0.277	0.0085	BDL	BDL	BDL	0.064	0.0018	0.0725	0.0881	0.157
T8	238 OB	375824	591923	106.24	5634.91	5622.31	0.144	BDL	0.026	116.34	0.448	0.443	0.442	BDL	BDL	BDL	0.302	BDL	0.324	BDL	0.0713	BDL	0.583	0.0399	BDL	BDL	BDL	BDL	BDL	0.341	0.395	0.145
T8	238 OB	377488	591923	106.84	5534.73	5537.77	0.099	BDL	0.034	114.22	0.458	0.41	0.417	BDL	BDL	BDL	0.158	BDL	0.162	0.03	0.0709	BDL	0.367	0.0315	BDL	BDL	BDL	0.062	0.00127	0.218	0.239	0.277
T8	238 OB	373542	591923	104.97	4193.02	4202.56	0.111	BDL	BDL	113.7	0.436	0.429	0.415	BDL	BDL	BDL	0.248	0.0085	0.261	BDL	0.0599	BDL	0.275	0.0205	BDL	0.0033	BDL	BDL	0.00519	0.441	0.488	0.261
T8	238 OB	387301	591923	105.35	5546.8	5507.96	0.052	BDL	0.04	116.74	0.435	0.435	0.418	BDL	BDL	BDL	0.229	0.0028	0.223	BDL	0.0541	BDL	0.418	0.0193	BDL	BDL	BDL	BDL	0.00183	0.226	0.269	0.212
T17	MOB	404012	591922	93.58	4348.86	4100.99	0.235	BDL	BDL	149.27	0.018	0.0142	0.0386	BDL	0.137	BDL	0.447	BDL	0.396	BDL	0.674	BDL	0.52	BDL	BDL	BDL	BDL	BDL	BDL	0.595	0.56	3.28
T17	MOB	414640	591922	79.7	2674.74	2761.38	0.228	BDL	BDL	165.05	0.023	BDL	0.0147	BDL	BDL	BDL	0.344	BDL	0.369	BDL	0.168	BDL	0.33	BDL	BDL	BDL	BDL	BDL	BDL	0.559	0.632	2.69
T17	MOB	473820	591922	79.86	3788.22	3646.03	BDL	BDL	BDL	169.21	0.025	BDL	0.0252	BDL	BDL	BDL	0.142	BDL	0.139	BDL	0.09	0.0152	0.2	BDL	BDL	BDL	BDL	BDL	BDL	0.169	0.175	1.004
T17	MOB	444029	591922	82.43	3316.27	3208.96	0.58	BDL	BDL	166.07	0.063	BDL	0.0245	0.0016	BDL	BDL	0.192	BDL	0.205	BDL	0.133	0.023	BDL	BDL	BDL	BDL	0.099	0.29	BDL	0.468	0.495	2.38
T26	238 OB	395390	591922	90.65	8569.68	8539.48	0.153	BDL	BDL	100.63	0.321	0.353	0.301	BDL	BDL	BDL	1.02	BDL	1.02	BDL	0.0387	0.0116	0.57	BDL	BDL	BDL	BDL	BDL	0.0086	4.63	5.27	3.77
T26	238 OB	389998	591922	73.67	7232.8	7156.61	0.07	BDL	BDL	107.25	0.075	0.0986	0.135	BDL	0.00068	BDL	0.292	BDL	0.261	BDL	0.0568	BDL	0.41	BDL	BDL	BDL	BDL	0.074	BDL	0.281	0.328	0.552
T26	238 OB	377671	591922	93.18	6465.93	6366.46	0.123	BDL	BDL	100.82	0.303	0.354	0.321	BDL	BDL	BDL	0.363	0.0027	0.327	BDL	0.0431	BDL	0.211	BDL	BDL	BDL	BDL	0.094	BDL	0.364	0.387	0.676
T26	238 OB	382434	591922	66.45	7480.72	7061.01	0.087	BDL	0.072	107.91	0.195	0.183	0.188	BDL	BDL	BDL	0.445	BDL	0.435	BDL	0.0411	BDL	1.01	BDL	BDL	BDL	BDL	BDL	BDL	0.735	0.82	0.633
T26	238 OB	368726	591922	84.37	7230.9	7212.49	0.073	BDL	BDL	96.78	0.112	0.127	0.138	BDL	BDL	BDL	0.528	BDL	0.528	0.059	0.0679	0.0045	0.528	BDL	BDL	BDL	BDL	BDL	BDL	1.333	1.582	2.12
TU18B	MOB	390716	591923	65.82	8458.89	8435.01	BDL	BDL	BDL	206	0.022	0.0295	0.0477	BDL	BDL	BDL	0.28	BDL	0.286	BDL	0.032	BDL	0.182	BDL	BDL	BDL	BDL	BDL	BDL	0.255	0.317	1.468
TU18B	MOB	403175	591923	67.91	7806.2	7868.63	BDL	BDL	BDL	209.57	0.013	0.0279	0.0464	BDL	BDL	BDL	0.179	BDL	0.195	BDL	0.0527	BDL	0.099	BDL	0.00161	BDL	BDL	BDL	0.00153	0.158	0.183	1.131
TU18B	MOB	405373	591923	93.24	8231.83	8343.53	0.124	BDL	0.06	217.53	0.0365	0.0444	0.0504	BDL	BDL	BDL	0.158	BDL	0.165	BDL	0.041	0.0059	0.232	BDL	BDL	BDL	BDL	BDL	BDL	2.21	2.65	0.774
TU18B	MOB	416420	591923	76.51	8702.46	8653.44	0.151	BDL	0.087	218.57	0.0159	0.0344	0.0506	BDL	BDL	BDL	0.278	BDL	0.251	BDL	0.0466	BDL	0.136	BDL	BDL	BDL	BDL	BDL	BDL	0.284	0.288	1.247
TU18B	MOB	386011	591923	80.87	8496.29	8634.11	0.68	BDL	0.028	182.06	0.031	0.042	0.0429	BDL	0.0025	BDL	0.233	BDL	0.266	0.049	0.048	0.0054	0.182	BDL	BDL	BDL	BDL	0.078	BDL	0.141	0.145	0.637
TU18B	MOB	579819	591922	68.12	6686.01	6947.36	0.14	BDL	0.0286	251.68	0.0128	0.0264	0.0426	BDL	0.0081	0.00204	0.279	BDL	0.262	BDL	0.0459	BDL	0.098	BDL	BDL	BDL	BDL	BDL	0.00133	0.148	0.193	0.727
TU18B	MOB	397169	591923	68.17	8473.88	8617.56	0.227	BDL	0.024	211.17	0.0299	0.0331	0.0556	BDL	BDL	0.0029	0.497	BDL	0.495	0.047	0.0402	0.004	0.135	BDL	BDL	BDL	BDL	0.073	BDL	0.382	0.489	2.244

Notes: Abbreviation BDL stands for below detection limits

A4 (continued): LA-ICPMS analyses of pyrrhotite (ppm)

Sample	Ore body	^{34}S	^{57}Fe	^{59}Co	^{60}Ni	^{61}Ni	^{65}Cu	^{66}Zn	^{75}As	^{77}Se	^{99}Ru	^{101}Ru	^{102}Ru	^{103}Rh	^{105}Pd	^{106}Pd	^{107}Ag	^{108}Pd	^{109}Ag	^{111}Cd	^{118}Sn	^{121}Sb	^{125}Te	^{189}Os	^{193}Ir	^{195}Pt	^{197}Au	^{202}Hg	^{205}Tl	^{206}Pb	^{208}Pb	^{209}Bi
TU16B	MOB	423414	591923	92.93	8558.58	8400.13	BDL	BDL	BDL	154.12	0.0181	0.026	0.0452	BDL	BDL	BDL	0.0488	BDL	0.0554	BDL	0.0615	BDL	0.255	BDL	BDL	BDL	0.066	BDL	BDL	0.088	0.1028	0.38
TU16B	MOB	422050	591923	86.59	9936.56	9944.88	0.176	BDL	0.048	150.61	0.0247	0.0346	0.0572	BDL	BDL	BDL	1.185	0.0076	1.18	BDL	0.0493	0.006	0.114	BDL	BDL	0.0057	BDL	BDL	0.0098	0.539	0.61	1.306
TU16B	MOB	403892	591923	90.92	9266.56	9102.42	BDL	BDL	BDL	155.74	0.014	0.0253	0.0524	0.0434	BDL	BDL	0.15	0.0072	0.158	0.038	0.0504	BDL	0.296	BDL	BDL	0.004	BDL	0.137	BDL	0.195	0.243	0.895
TU16B	MOB	400300	591923	104.49	9405.94	9431.38	0.296	BDL	BDL	157.18	0.0189	0.0289	0.0469	BDL	BDL	BDL	0.282	BDL	0.282	BDL	0.0518	BDL	0.611	BDL	BDL	BDL	BDL	BDL	BDL	0.3	0.341	1.305
TU16B	MOB	428825	591923	86.65	8593.65	8590.54	BDL	0.72	BDL	162.84	0.0117	0.0258	0.0344	BDL	BDL	BDL	0.184	BDL	0.206	BDL	0.053	BDL	0.231	BDL	BDL	BDL	BDL	BDL	BDL	0.192	0.207	0.684
TU16B	MOB	432583	591923	90.64	9642.6	9546.21	BDL	BDL	BDL	157.58	0.011	0.031	0.0597	BDL	0.0069	BDL	0.182	0.0072	0.168	0.111	0.0435	BDL	0.168	BDL	BDL	BDL	BDL	0.159	BDL	0.223	0.247	0.922
TU13	238 OB	399814	591923	57.22	9083.81	9084.25	BDL	BDL	BDL	276.02	BDL	0.0396	0.0565	BDL	BDL	0.0046	3.59	BDL	3.69	0.063	0.0369	BDL	2.93	0.0075	0.0045	BDL	BDL	BDL	BDL	5.12	5.92	2.81
TU13	238 OB	372532	591923	45.38	8189.47	8056.49	2.47	0.64	BDL	252.49	BDL	0.039	0.0423	BDL	0.05	0.0134	0.496	BDL	0.515	BDL	0.049	0.0063	BDL	BDL	BDL	BDL	0.0108	BDL	0.0335	1.61	1.95	1.406
TU13	238 OB	382791	591923	50.03	7725.12	7600	0.076	0.38	BDL	245.95	BDL	0.0259	0.0375	BDL	0.0024	0.0067	0.288	BDL	0.317	0.068	0.064	0.0036	0.304	BDL	BDL	BDL	BDL	0.061	BDL	1.026	1.149	1.209
TU13	238 OB	398566	591923	55.22	7422.59	7245.85	BDL	0.61	0.062	273.04	BDL	0.0171	0.0349	BDL	BDL	0.0077	0.409	BDL	0.404	0.104	0.0817	BDL	0.158	BDL	BDL	BDL	0.0018	0.1	0.0036	3.93	4.71	1.129
TU7	238 OB	557530	591922	109.95	4938.91	5145.72	BDL	0.478	0.65	135.73	0.513	0.523	0.514	0.00239	BDL	BDL	0.1048	BDL	0.111	BDL	0.0721	BDL	0.167	BDL	BDL	BDL	BDL	0.113	BDL	0.202	0.231	0.155
TU7	238 OB	561967	591922	96.77	4894.4	5202.35	0.328	0.366	BDL	132.55	0.59	0.566	0.568	BDL	BDL	BDL	0.1831	0.0073	0.1741	BDL	0.1107	BDL	0.314	0.0285	BDL	BDL	BDL	0.062	BDL	0.392	0.459	0.464
TU7	238 OB	590750	591922	96.18	5348.18	5464.28	0.094	BDL	0.335	128.34	0.548	0.561	0.537	0.0068	BDL	BDL	0.14	BDL	0.145	BDL	0.0747	0.0043	0.307	0.0113	BDL	BDL	BDL	BDL	BDL	0.256	0.292	0.155
TU7	238 OB	550408	591922	98.97	5348.01	5371.73	BDL	0.22	0.199	129.61	0.502	0.552	0.526	0.0049	BDL	BDL	0.128	BDL	0.131	BDL	0.106	BDL	0.262	0.0191	BDL	BDL	BDL	BDL	BDL	0.235	0.254	0.191
T34	MOB	416720	591922	63.31	6337.3	6440.31	0.225	BDL	BDL	142.79	0.039	0.033	0.0457	BDL	BDL	BDL	0.1179	BDL	0.1209	BDL	0.054	BDL	BDL	BDL	0.00083	BDL	BDL	BDL	BDL	0.447	0.527	0.285
T34	MOB	414901	591922	64.49	5661.45	6381.28	0.48	BDL	BDL	179.22	BDL	BDL	BDL	BDL	0.51	BDL	0.218	BDL	0.165	BDL	BDL	BDL	0.36	BDL	BDL	BDL	BDL	0.59	0.0123	0.539	0.489	0.314
T34	MOB	405907	591922	72.56	5829.26	5855.5	0.439	BDL	BDL	115.82	0.0217	0.0243	0.032	BDL	0.0121	0.0392	0.17	0.0077	0.165	BDL	0.072	BDL	0.113	BDL	BDL	BDL	BDL	BDL	0.002	0.905	1.093	1.253
T34	MOB	436782	591922	75.9	6846.85	6547.84	0.169	BDL	0.08	142.57	0.104	0.12	0.132	BDL	BDL	BDL	0.369	BDL	0.349	0.091	0.077	0.0203	0.24	BDL	BDL	BDL	0.0073	BDL	BDL	3.38	2.73	2.67
T34	MOB	428560	591922	64.13	5538.16	5517.58	0.572	BDL	0.075	148.82	0.0317	0.0256	0.033	BDL	BDL	BDL	0.153	0.0036	0.159	BDL	0.048	BDL	BDL	BDL	BDL	BDL	BDL	BDL	BDL	0.323	0.318	0.353
T44	MOB	378816	591922	97.43	5258.48	5289.66	0.133	BDL	BDL	136.97	0.0935	0.0936	0.0889	0.091	BDL	BDL	0.116	BDL	0.1238	BDL	0.0491	BDL	BDL	BDL	BDL	BDL	BDL	0.053	BDL	0.742	0.76	0.794
T44	MOB	368317	591922	102.71	4781.66	4759.37	0.239	BDL	BDL	108.99	0.1166	0.1139	0.1127	BDL	0.0022	0.0035	0.1245	0.0028	0.1327	BDL	0.0374	0.0033	0.066	BDL	BDL	0.0027	BDL	0.075	BDL	0.694	0.789	0.579
T44	MOB	360287	591922	90.86	6472.3	6504.53	0.788	BDL	0.026	135.94	0.1455	0.1285	0.135	BDL	BDL	0.0153	0.1449	0.0029	0.1415	0.032	0.0382	BDL	0.106	0.0164	BDL	BDL	BDL	BDL	BDL	0.407	0.445	0.633
T44	MOB	370959	591922	79.17	6071.09	6119.5	0.411	BDL	BDL	129.76	0.073	0.083	0.0924	BDL	BDL	BDL	0.134	0.00198	0.1206	BDL	0.0254	BDL	0.116	0.013	BDL	BDL	BDL	0.075	0.00137	0.363	0.397	0.639
T3	238 OB	382336	591927	41.35	4451.42	4516.22	0.756	BDL	BDL	359.46	BDL	0.0163	0.0193	BDL	BDL	BDL	0.632	BDL	0.577	0.075	0.0729	0.0086	0.221	BDL	BDL	BDL	0.0049	BDL	0.0044	2.32	2.69	5.09
T3	238 OB	373017	591927	48.45	5057.14	5198.75	0.101	BDL	0.0504	342.34	0.008	0.0162	0.0216	BDL	BDL	0.002	1.05	BDL	0.99	BDL	0.0472	0.00161	0.295	BDL	BDL	BDL	BDL	0.107	BDL	0.891	0.986	3.57
T3	238 OB	371514	591927	54.81	5761.03	6155.74	0.119	BDL	0.045	431.58	0.008	0.0099	0.0252	BDL	BDL	BDL	0.819	BDL	0.804	BDL	0.0508	BDL	0.155	BDL	BDL	BDL	BDL	BDL	BDL	0.441	0.496	2.43
T3	238 OB	376299	591927	53.76	6714.84	6925.19	0.207	0.83	0.0582	364.59	0.0108	0.0159	0.0317	BDL	BDL	BDL	0.85	0.00176	0.862	BDL	0.0568	BDL	0.204	BDL	BDL	BDL	0.00145	0.176	BDL	0.305	0.342	1.88
T3	238 OB	346373	591927	45.38	4902.91	4864.37	0.18	0.168	0.079	333.3	0.0112	0.0149	0.0214	0.00061	0.0024	BDL	0.718	BDL	0.787	0.0158	0.081	BDL	0.266	BDL	BDL	BDL	BDL	0.111	0.424	1.93	2.36	3
T3	238 OB	380193	591927	46.79	5329.54	5313.74	0.554	BDL	0.093	345.21	0.0123	0.0117	0.0242	BDL	BDL	0.002	0.569	BDL	0.575	BDL	0.0521	BDL	0.411	BDL	BDL	BDL	BDL	0.121	0.00127	0.352	0.496	2.5
T2	238 OB	366443	591930	28.06	12031.2	12308.2	0.147	BDL	0.033	137.08	0.524	0.566	0.528	BDL	0.008	BDL	0.501	0.0164	0.551	BDL	0.0487	BDL	0.095	0.052	BDL	BDL	BDL	0.086	BDL	3.19	2	4.23
T2	238 OB	395160	591930	25.33	8818.98	8752.08	0.051	0.29	0.042	137.38	0.424	0.444	0.426	BDL	BDL	0.0099	0.457	0.0036	0.462	BDL	0.0295	0.011	0.097	0.0109	BDL	BDL	0.0019	0.095	0.0086	0.93	1.01	1.23
T2	238 OB	394496	591930	27.94	10927.2	11395.2	0.079	BDL	BDL	151.57	0.516	0.574	0.55	BDL	BDL	0.0047	0.276	BDL	0.292	BDL	0.0519	BDL	BDL	0.0296	BDL	BDL	BDL	0.108	BDL	0.261	0.247	0.318
T2	238 OB	373831	591931	31.3	11275.8	11418.9	0.065	BDL	0.044	134.16	0.375	0.403	0.406	BDL	0.0056	0.0043	0.181	BDL	0.182	0.037	0.0534	0.0026	0.106	0.0185	BDL	BDL	BDL	0.112	BDL	0.442	0.493	0.615
T2	238 OB	371724	591931	28.2	10778.1	10572.6	0.067	BDL	0.165	134.6	0.401	0.464	0.461	BDL	0.093	0.0047	0.279	BDL	0.239	BDL	0.046	BDL	0.048	0.0352	BDL	BDL	BDL	0.058	BDL	0.261	0.295	0.342
T2	238 OB	380205	591931	28.63	11837.7	11808.9	BDL	BDL	0.051	128.21	0.0124	0.036	0.0617	BDL	BDL	BDL	0.193	BDL	0.186	0.04	0.0641	BDL	0.096	BDL	BDL	BDL	0.0017	0.058	0.00121	1.63	1.92	1.56
TU8	238 OB	389177	591938	130.59	5582.32	5514.29	0.062	BDL	0.0202	126.84	0.216	0.229	0.244	BDL	BDL	BDL	0.303	BDL	0.294	BDL	0.0248	BDL	0.284	0.0056	BDL	0.0049	BDL	BDL	BDL	0.12	0.145	0.219
TU8	238 OB	389347	591938	96.21	3245.87	3230.89	0.057	BDL	BDL	122.92	0.232	0.21	0.192	0.00127	0.0036	BDL	0.63	BDL	0.57	BDL	0.0423	BDL	0.164	BDL	BDL	BDL	BDL	0.085	0.00298	0.57	0.64	0.76
TU8	238 OB	395297	591939	116.07	3993.31	3756.69	0.063	0.42	BDL	133.91	0.221	0.178	0.222	BDL	BDL	BDL	0.243	BDL	0.259	BDL	0.0622	0.0051	0.258	BDL	BDL	BDL	BDL	0.103	BDL	0.406	0.419	0.84
TU8	238 OB	381014	591939	118.39	4387.86	4273.69	0.104	0.194	0.035	121.78	0.238	0.248	0.236	0.00114	BDL	BDL	0.59	BDL	0.56	0.021	0.0534	BDL	0.297	BDL	BDL	BDL	0.0037	0.056	BDL	0.59	0.66	0.92
TU8	238 OB	389828	591940	120.51	4936.72	4904.69	0.062	0.27	0.064	121.23	0.287	0.252	0.267	BDL	0.143	0.0109	0.79	BDL	0.69	0.028	0.073	0.0027	0.127	0.0111	BDL	BDL	0.0049	BDL	0.00187	1.03	1.13	0.56
TU8	238 OB	376430	591940	124.69	4851.33	4865.53	BDL	BDL	0.02	119.07	0.259	0.232	0.253	0.00056	BDL	BDL	0.218	BDL	0.211	BDL	0.0459	BDL	0.127	BDL	BDL	BDL	BDL	BDL	BDL	0.231	0.267	0.328
T6	238 OB	389105	591950	70.33	5205.87	5143.56	BDL	BDL	0.057	125.89	0.293	0.269	0.244	BDL	BDL	BDL	0.36	BDL	0.34	BDL	0.0446	0.0033	0.153	0.007	BDL	BDL	BDL	BDL	BDL	0.193	0.231	0.222
T6	238 OB	398564	591951	75.41	5201.54	5038.36	0.058	BDL	BDL	129.13	0.237	0.229	0.219	BDL	BDL	BDL	0.27	BDL	0.27	0.028	0.054	0.0046	0.34	BDL	0.00129	BDL	BDL	0.074	0.0038	1.35	1.49	0.63
T6	238 OB	354727	591951	60.2	4629.45	4254.95	0.066	0.33	0.03	115.88	0.267	0.225	0.201	BDL	BDL	BDL	0.163	BDL	0.152	0.039	0.0353	BDL	0.162	BDL	0.003	BDL	0.0012	0.109	0.0023	0.217	0.247	0.151
T6	238 OB	390000	591952	73.24	6665.03	6545.12	0.18	1.59	0.057	131.25	0.238	0.257	0.241	BDL	0.0453	BDL	0.172	BDL	0.163	0.049	0.054	BDL	0.58	BDL	BDL	BDL	BDL	BDL	0.00055	0.218	0.25	0.195
T6	238 OB	413899	591953	54.16	8807.68	8782.48	0.67	5.51	0.032	129.25	0.23	0.276	0.266	BDL	BDL	0.0021	0.16	BDL	0.187	BDL	0.069	BDL	0.26	0.0099	BDL	BDL	BDL	BDL	0.078	BDL	0.244	0.272	0.24
T6	238 OB	417489	591954	68.01	5597.81	5537.24	0.14	BDL	BDL	133.89	0.263	0.268	0.262	BDL	BDL	0.00132	0.2	BDL	0.24	BDL	0.0368	BDL	0.34	BDL	BDL	BDL	BDL	BDL	BDL	0.72	0.86	0.186

Notes: Abbreviation BDL stands for below detection limits

A5: LA-ICPMS analyses of pentlandite (ppm)

Sample	Ore body	^{34}S	^{57}Fe	^{59}Co	^{60}Ni	^{61}Ni	^{65}Cu	^{66}Zn	^{75}As	^{77}Se	^{99}Ru	^{101}Ru	^{102}Ru	^{103}Rh	^{105}Pd	^{106}Pd	^{107}Ag	^{108}Pd	^{109}Ag	^{111}Cd	^{118}Sn	^{121}Sb	^{125}Te	^{189}Os	^{193}Ir	^{195}Pt	^{197}Au	^{202}Hg	^{205}Tl	^{206}Pb	^{208}Pb	^{209}Bi
T9	238 OB	325807	325540	11872.4	330280	324869	5.44	BDL	0.15	121.4	3.49	1.334	2.03	0.00032	1.27	1.28	9.55	1.24	9.31	0.0418	0.0623	0.113	5.03	0.0019	0.00015	0.00187	0.0094	0.0637	0.152	4.91	5.1	1.77
T9	238 OB	357172	325540	13307.5	345382	340183	1.78	2.98	0.0615	105.15	3.76	1.297	2.06	0.00059	1.45	1.49	4.35	1.47	4.38	0.0115	0.0713	0.17	1.072	0.00402	BDL	0.0027	0.00172	0.0158	0.393	2.62	2.88	0.375
T9	238 OB	334232	325540	12896.3	337516	329925	9.3	BDL	0.0566	108.25	3.86	1.35	2.15	0.00145	1.29	1.32	6.65	1.3	7	BDL	0.0459	0.0899	0.563	0.0158	0.00037	0.00566	0.0093	BDL	0.00557	3.21	3.68	1.166
T9	238 OB	331698	325540	12871.5	325423	318302	6.89	BDL	0.696	108.71	3.8	1.21	1.95	0.00138	1.77	1.82	11.66	1.79	11.85	0.0276	0.0561	0.461	27.35	BDL	0.00045	0.0016	0.0083	0.1173	0.71	4.1	4.68	0.841
T9	238 OB	352077	325540	13199.8	341576	340624	10.82	BDL	0.134	100.93	3.92	1.31	2.1	0.00128	1.66	1.71	10.29	1.68	10.33	BDL	0.0708	0.244	7.56	BDL	BDL	0.00249	0.00254	BDL	0.0265	0.1573	0.201	0.0583
T9	238 OB	341248	325540	13098.8	330591	327562	4.97	BDL	0.0134	102.66	3.64	1.09	1.87	BDL	1.36	1.35	8.81	1.3	9.13	BDL	0.062	0.1485	0.592	BDL	BDL	0.00107	0.00422	0.0417	0.0194	0.248	0.299	0.0653
T12	238 OB	337319	325540	12224.1	343075	341496	0.716	BDL	0.046	96.06	3.43	1.3	1.99	BDL	0.3	0.297	0.641	0.279	0.65	BDL	0.0594	0.0698	1.14	0.0139	BDL	BDL	BDL	0.0351	0.079	0.657	0.738	0.11
T12	238 OB	332969	325540	13775.8	341501	341417	1.31	0.321	0.0031	103.22	3.99	1.37	2.07	0.00067	0.362	0.339	0.726	0.352	0.681	0.031	0.0792	0.0107	0.319	0.0136	BDL	0.00183	BDL	0.0471	BDL	0.0793	0.125	0.093
T12	238 OB	325936	325540	15175.3	351044	345105	0.322	BDL	0.0608	103	4.61	1.58	2.3	0.00027	0.69	0.7	0.359	0.69	0.353	0.0132	0.0752	0.0254	0.203	0.0459	BDL	0.0027	0.00055	0.0358	0.00241	0.563	0.618	0.094
T12	238 OB	410433	325540	10386.5	347585	343848	1.71	BDL	BDL	129.44	2.88	1.34	2.21	BDL	BDL	0.016	5.42	BDL	5.48	0.095	0.285	BDL	0.87	0.0191	BDL	BDL	BDL	BDL	0.74	30.94	32.84	8.12
T12	238 OB	330726	325540	13647.5	348226	345761	0.289	BDL	0.0092	99.49	4.05	1.56	2.21	0.00077	0.221	0.217	0.348	0.208	0.329	0.02	0.0693	0.0284	0.328	0.0171	BDL	0.00048	BDL	0.0573	0.00052	1.42	1.6	0.756
TU1	238 OB	333574	325541	5175.79	323902	322235	7.25	BDL	11	100.23	1.76	1.32	2.17	5.01	3.05	3.1	17.07	2.97	16.99	0.21	0.263	1.03	34.05	0.12	0.126	0.178	0.03	0.073	5.97	40.59	43.03	3.26
TU1	238 OB	333738	325541	5278.88	345093	343426	2.46	1.15	33.47	102.57	1.44	1.15	1.94	0.088	2.82	2.81	7.84	2.82	7.74	0.037	0.143	0.91	25.7	0.0079	0.0032	0.00108	0.0117	0.0317	2.84	16.59	17.59	6.63
TU1	238 OB	343579	325541	5104.37	342579	341650	7.07	2.07	7.12	126.85	2.13	1.98	2.65	0.168	2.67	2.69	17.45	2.77	18.06	0.103	0.133	1.23	27.34	0.026	0.0127	0.00113	0.035	0.082	1.64	13.9	14.84	2.14
TU1	238 OB	328981	325541	4588.63	341688	338321	2.58	0.35	7.22	111.57	1.62	1.36	2.2	0.153	3.23	3.08	18.6	3.23	19.53	0.13	0.0859	1.12	46.6	0.0331	0.006	0.0031	0.0162	0.068	2.35	17.42	18.01	6.02
TU1	238 OB	360296	325541	5437.4	345633	345036	6.08	BDL	8.12	111.14	1.45	1.08	1.75	0.0254	3.7	3.8	19.55	3.64	18.48	0.2	0.401	1.49	58.82	BDL	0.0046	BDL	0.007	0.128	6.89	47.25	52.18	15.14
TU1	238 OB	312679	325541	5493.4	309199	304897	4.03	2.37	4.01	117.29	2.11	1.61	2.28	0.147	2.2	2.18	22.54	2.24	22.77	0.17	0.193	1.29	17.65	0.0245	0.0109	0.00091	0.031	0.068	3.69	31.05	32.59	1.19
T7	238 OB	336964	325543	13755.4	353817	358733	0.247	BDL	0.318	104.22	3.72	1.13	1.84	0.0008	1.09	1.07	0.325	1.07	0.308	BDL	0.0324	0.085	9.98	0.0068	BDL	0.00044	BDL	0.048	0.281	1.69	1.87	0.338
T7	238 OB	326893	325543	13060.2	355366	353112	0.0089	BDL	0.0194	103.77	3.27	0.98	1.71	0.00031	0.28	0.26	0.238	0.29	0.128	BDL	0.0491	0.0181	4.22	0.0078	0.00128	0.0073	BDL	0.072	0.141	0.57	0.438	0.0368
T7	238 OB	329985	325543	13082.2	362303	363013	0.37	BDL	4.04	142.92	3.5	1.22	1.94	0.00169	0.42	0.43	1.16	0.42	1.06	0.04	0.0602	0.231	72.83	0.00182	BDL	0.0019	0.0077	0.0089	0.271	3.6	3.95	1.23
T7	238 OB	331601	325543	13261.7	354603	357343	0.155	0.131	0.43	113.53	4.01	1.51	2.27	0.0038	0.31	0.28	0.301	0.31	0.29	BDL	0.0481	0.076	11.15	0.0202	0.00052	BDL	0.001	0.0217	0.0145	0.374	0.303	0.095
T10	MOB	331539	325538	7326.07	335497	333911	0.351	BDL	BDL	180.64	1.918	1.122	1.889	BDL	0.253	0.282	0.742	0.279	0.713	BDL	0.0622	0.0105	0.131	BDL	BDL	BDL	0.0029	BDL	0.0032	0.227	0.301	0.0206
T10	MOB	341712	325538	6927.38	337423	336628	0.371	BDL	0.081	179.99	1.839	1.107	1.875	BDL	0.1299	0.1097	1.384	0.1098	1.344	BDL	0.0588	0.0093	0.563	BDL	BDL	BDL	BDL	BDL	0.0033	2.16	2.42	0.856
T10	MOB	341181	325538	7294.28	327562	335884	0.362	BDL	0.075	191.66	1.906	1.103	1.859	BDL	0.192	0.189	0.773	0.187	0.739	BDL	0.081	0.0876	0.19	BDL	0.0102	BDL	0.0027	0.081	0.0077	4.84	5.05	0.995
T10	MOB	338351	325538	6910.35	331466	334740	0.315	BDL	0.04	178.38	1.859	1.122	1.857	BDL	0.296	0.269	1.391	0.275	1.327	BDL	0.174	0.0429	0.567	BDL	BDL	BDL	BDL	BDL	0.1629	8.02	9.17	2.61
T8	238 OB	327394	325538	14621.5	336880	333141	0.384	BDL	BDL	98.89	4.08	1.38	2.14	BDL	0.936	0.996	0.374	0.954	0.407	BDL	0.0518	0.0137	0.506	0.0513	BDL	BDL	BDL	0.072	0.00184	0.0443	0.0683	0.0277
T8	238 OB	346363	325538	10629.9	343027	344582	0.129	BDL	0.062	105.49	3.15	1.437	2.14	BDL	0.0392	0.0371	0.424	0.0303	0.431	BDL	0.056	0.0215	0.142	0.0235	BDL	BDL	BDL	BDL	0.0039	0.607	0.636	0.383
T8	238 OB	344719	325538	14271.4	349012	344445	0.222	BDL	0.066	105.63	4.13	1.422	2.25	BDL	0.875	0.865	0.31	0.877	0.293	BDL	0.1058	0.39	2.07	0.0287	BDL	BDL	BDL	BDL	1.355	8.24	8.66	0.926
T8	238 OB	347373	325538	13861.3	340071	343543	0.177	BDL	BDL	104.35	3.89	1.428	2.18	0.00175	0.632	0.595	0.226	0.602	0.213	BDL	0.09	0.227	0.316	0.0295	BDL	BDL	BDL	0.093	0.0301	0.0145	0.0152	0.0035
T17	MOB	356579	325538	7553.92	351971	344203	0.152	BDL	1.2	158.27	1.93	1.094	1.86	BDL	1.371	1.44	0.708	1.387	0.636	BDL	0.032	0.271	13.75	0.0129	BDL	BDL	BDL	BDL	BDL	0.377	0.456	0.619
T17	MOB	399235	325538	7384.4	371127	367176	BDL	BDL	BDL	156.45	2.1	1.062	1.87	BDL	1.4	1.3	1.38	1.295	1.24	0.119	0.1	0.331	2.56	BDL	BDL	BDL	0.03	BDL	BDL	0.777	1.058	1.54
T17	MOB	413708	325538	7558.95	356057	343775	BDL	BDL	1.34	146.27	1.81	1.09	1.85	0.0065	1.77	1.81	1.51	1.74	1.48	BDL	0.15	0.287	39.89	BDL	BDL	BDL	0.018	BDL	0.0094	0.341	0.451	0.787
T17	MOB	390798	325538	7838.81	373368	386088	BDL	BDL	6.44	229.13	1.61	1.11	1.84	0.01	0.988	1.2	1.1	1.29	1.11	BDL	BDL	0.432	45.43	BDL	BDL	BDL	0.036	BDL	BDL	0.488	0.337	0.776
T17	MOB	379966	325538	7303.98	365001	361702	0.27	BDL	3.92	215.21	1.6	1.02	2.03	0.0141	1.25	1.4	0.734	1.3	0.719	BDL	0.081	0.354	39.52	BDL	BDL	BDL	0.059	BDL	BDL	0.707	1.233	0.933
T26	238 OB	339967	325538	9493.96	369687	365253	0.164	BDL	BDL	94.83	2.39	1.189	1.89	0.00113	0.118	0.096	0.406	0.09	0.399	BDL	0.074	0.06	0.397	BDL	BDL	BDL	0.003	BDL	0.0704	1.65	1.71	0.297
T26	238 OB	353477	325538	9815.38	374545	376979	0.17	BDL	BDL	100.76	2.52	1.181	1.98	BDL	0.217	0.237	0.259	0.253	0.249	BDL	0.06	0.117	0.64	BDL	BDL	BDL	BDL	BDL	0.113	0.214	0.282	0.404
T26	238 OB	345203	325538	9403.13	378079	368787	0.126	BDL	BDL	94.09	2.36	1.185	1.95	BDL	0.152	0.159	0.239	0.143	0.227	BDL	0.062	0.0356	0.385	BDL	0.0025	BDL	BDL	BDL	0.0434	0.0193	0.0145	0.0028
T26	238 OB	346176	325538	9615.16	370559	366580	0.235	BDL	BDL	89.99	2.78	1.465	2.14	BDL	0.295	0.356	0.448	0.346	0.464	BDL	0.054	0.1031	2.66	BDL	BDL	BDL	BDL	BDL	0.381	0.115	0.1374	0.302
TU18B	MOB	389636	325538	5830.88	370392	370360	0.78	BDL	0.094	189.97	1.74	1.16	1.76	BDL	0.093	0.061	1.92	0.11	1.56	BDL	0.118	0.035	0.83	BDL	BDL	BDL	BDL	BDL	3.78	11.54	13.71	5.13
TU18B	MOB	396145	325538	5925.94	386826	379840	1.23	BDL	0.23	160.47	1.45	1.019	1.97	0.0138	0.05	0.079	20.79	0.0365	20.45	0.096	0.291	0.324	48.17	BDL	BDL	BDL	0.0148	0.097	3.55	624.7	830.55	46.15
TU18B	MOB	391920	325538	5613.48	315844	306230	6.1	BDL	BDL	151.03	1.46	0.81	1.51	BDL	0.278	0.23	35.49	0.199	36.6	BDL	0.044	0.114	7.11	BDL	BDL	BDL	0.0295	BDL	0.019	2.37	2.1	0.343
TU18B	MOB	369403	325538	5277.51	337116	352505	BDL	BDL	BDL	156.61	1.25	0.88	1.9	BDL	0.049	0.056	1.18	0.08	1.22	BDL	0.098	0.128	BDL	BDL	BDL	BDL	BDL	BDL	2	8.65	8.95	10.47
TU18B	MOB	492173	325538	6496.47	383885	359131	5.75	BDL	0.32	205.94	1.72	1.07	1.59	BDL	0.055	0.171	19.54	0.112	17.17	0.65	0.142	0.116	0.52	BDL	BDL	BDL	BDL	BDL	0.15	8.07	8.5	3.3
TU18B	MOB	416768	325538	5368.48	322609	328519	5.62	BDL	0.522	203.9	1.27	0.918	1.65	0.0046	0.595	0.229	38.36	0.283	36.93	BDL	0.074	0.189	9.07	0.03	BDL	BDL	BDL	BDL	0.433	13.16	15.76	8.11

Notes: Abbreviation BDL stands for below detection limits

A5 (continued): LA-ICPMS analyses of pentlandite (ppm)

Sample	Ore body	^{34}S	^{57}Fe	^{59}Co	^{60}Ni	^{61}Ni	^{65}Cu	^{66}Zn	^{75}As	^{77}Se	^{99}Ru	^{101}Ru	^{102}Ru	^{103}Rh	^{105}Pd	^{106}Pd	^{107}Ag	^{108}Pd	^{109}Ag	^{111}Cd	^{118}Sn	^{121}Sb	^{125}Te	^{189}Os	^{193}Ir	^{195}Pt	^{197}Au	^{202}Hg	^{205}Tl	^{206}Pb	^{208}Pb	^{209}Bi
TU16B	MOB	370162	325538	6098.83	370996	373905	0.579	BDL	0.234	160.66	1.46	1.108	2.04	0.002	1.65	1.73	0.928	1.78	0.953	BDL	0.05	0.039	1.79	BDL	BDL	BDL	0.0107	BDL	0.0057	0.245	0.284	0.311
TU16B	MOB	426325	325538	6251.15	343084	369640	BDL	BDL	0.22	143.27	1.64	1.05	1.66	BDL	1.63	1.69	0.65	1.49	0.76	BDL	0.057	0.018	0.2	BDL	BDL	0.025	BDL	0.43	0.02	0.8	1.109	0.215
TU16B	MOB	358499	325538	6218.37	380258	375884	0.97	BDL	BDL	127.57	1.67	1.2	1.9	BDL	1.84	1.67	0.954	1.6	1.031	BDL	BDL	0.07	1.26	BDL	BDL	BDL	0.0087	0.17	0.0276	0.498	0.575	0.225
TU16B	MOB	368989	325538	6679.45	385301	376157	BDL	BDL	0.352	148.71	1.64	1.081	1.95	BDL	1.73	1.78	0.808	1.61	0.669	BDL	0.074	0.081	5.34	BDL	BDL	BDL	0.0262	0.131	0.0087	0.414	0.392	0.589
TU16B	MOB	498942	325538	5948.58	350839	355966	1.61	BDL	0.216	175.24	1.47	1.163	1.922	BDL	1.36	1.49	12.29	1.45	12.71	BDL	BDL	0.157	9.5	BDL	BDL	BDL	0.0124	BDL	0.178	8.54	9.42	2.82
TU16B	MOB	532941	325538	6880.63	351701	357350	0.32	BDL	0.161	182.93	1.53	1.043	1.808	0.0053	1.55	1.61	1.313	1.6	1.352	BDL	BDL	BDL	0.25	BDL	BDL	BDL	BDL	BDL	0.0561	0.206	0.213	0.0536
TU16B	MOB	362411	325538	6770.88	377754	378461	0.156	BDL	BDL	143.65	1.49	1.11	2.01	BDL	1.55	1.48	2.11	1.52	2.24	BDL	0.037	0.11	0.51	BDL	BDL	BDL	0.027	BDL	0.006	0.452	0.578	0.847
TU13	238 OB	369612	325538	6234.72	296911	295364	116.66	BDL	1.98	190.14	1.66	0.95	1.38	BDL	0.605	0.447	20.76	0.483	29.7	0.38	0.202	0.459	28.47	BDL	BDL	BDL	0.027	0.73	0.91	24.04	30.84	5.81
TU13	238 OB	518172	325538	7011.71	337823	337861	92.7	4.94	5.39	394.77	1.65	0.85	1.77	BDL	1.5	1.29	150.62	BDL	131.46	0.45	0.56	1.23	131.52	BDL	BDL	BDL	BDL	1.21	2.26	36.17	41.29	23.24
TU13	238 OB	530385	325538	6591.73	322631	332089	3.37	BDL	0.49	298.6	1.59	1.1	1.81	BDL	1.02	1.07	14.45	BDL	14.02	BDL	0.271	0.18	4.05	BDL	BDL	BDL	0.046	BDL	3.22	20.9	22.16	10.19
TU13	238 OB	368525	325538	5799.79	366173	343604	2.11	4.85	4.2	248.53	1.68	0.88	1.61	BDL	2.43	2.28	3.83	2.3	5.04	0.4	3.78	1.41	57.66	0.021	0.012	BDL	0.038	0.36	4.75	48.45	50.5	14.86
TU7	238 OB	489514	325538	15351.6	314760	317927	4.55	BDL	0.063	117.83	4.15	1.458	2.146	BDL	1.52	1.42	1.178	1.51	1.159	BDL	0.0745	0.0617	0.394	0.0352	0.00233	BDL	BDL	0.052	0.0251	0.83	0.888	0.0425
TU7	238 OB	473286	325538	12298.6	324223	317723	0.109	0.36	4.87	121.96	3.11	1.214	1.82	0.278	0.055	0.072	0.179	0.067	0.141	BDL	0.088	0.096	0.41	BDL	BDL	BDL	BDL	BDL	BDL	0.69	0.915	1.49
TU7	238 OB	490909	325538	15002.3	308581	320059	3.49	0.36	0.553	118.93	3.94	1.369	2.108	0.0141	1.09	1.13	1.633	1.11	1.705	BDL	0.066	0.0394	0.219	0.0197	0.0027	BDL	0.111	0.112	0.00357	0.0737	0.0785	0.0281
TU7	238 OB	477121	325538	14177.3	310021	317888	12.78	BDL	27.68	118.7	4.13	1.721	2.395	1.04	0.6	0.59	2.59	0.6	2.63	BDL	0.1002	0.0504	1.94	0.127	0.0478	0.008	BDL	0.079	0.325	5.33	5.69	1.019
TU7	238 OB	469104	325538	14320.6	329148	331073	3.18	5.5	1.08	124.58	3.7	1.546	2.086	0.0449	0.69	0.66	2.32	0.66	2.35	BDL	0.047	0.0253	0.53	0.037	0.0025	BDL	0.008	BDL	0.0016	0.153	0.248	0.0932
TU7	238 OB	462265	325538	15150.7	323166	332248	1.53	11.04	BDL	126.33	4.03	1.495	2.098	BDL	1.09	1.04	1.809	1.07	1.75	BDL	0.083	0.0738	1.06	BDL	BDL	0.01	BDL	BDL	0.0282	0.793	0.906	0.237
T34	MOB	414190	325538	5211.33	333784	377843	BDL	BDL	2.69	144.8	1.28	1.14	1.75	0.0074	1.71	1.92	3.33	1.71	2.08	BDL	BDL	0.389	28.71	BDL	BDL	BDL	BDL	BDL	0.0173	0.059	0.047	0.083
T34	MOB	394290	325538	5088.7	366327	365889	BDL	10.92	16.41	119.25	1.149	1.114	1.922	BDL	1.09	0.99	1.388	0.99	1.511	BDL	0.095	0.434	23.34	BDL	0.0077	BDL	BDL	BDL	0.0609	0.908	1.007	1.229
T34	MOB	353366	325538	4860.06	357669	364125	2.27	BDL	20.21	129.26	1.065	1.169	1.889	BDL	1.07	1.03	1.479	1	1.464	BDL	0.107	0.331	56.62	BDL	BDL	0.017	BDL	BDL	0.0148	0.23	0.258	0.192
T34	MOB	390894	325538	4673.08	368626	363797	0.41	BDL	34.89	115.61	1.25	0.946	1.866	BDL	1.12	1.21	1.95	1.2	1.8	0.257	0.103	0.445	43.78	0.043	BDL	BDL	0.0147	BDL	0.439	1.425	1.41	0.169
T44	MOB	316414	325538	7839.65	347011	351838	0.395	BDL	6.3	133.61	1.948	1.132	1.882	0.013	2.99	2.94	0.765	2.95	0.77	BDL	0.0221	0.74	40.29	BDL	BDL	BDL	BDL	BDL	0.0183	0.186	0.203	0.366
T44	MOB	317327	325538	6988.19	354465	355611	0.242	BDL	1.53	114.46	1.696	1.097	1.864	0.0208	4.26	4.32	1.239	4.29	1.257	BDL	0.0517	0.731	4.19	0.0102	BDL	BDL	BDL	BDL	0.0089	0.337	0.186	0.221
T44	MOB	315860	325538	7393.65	350683	346714	0.313	BDL	11.44	116.56	1.937	1.194	1.934	0.0608	3.06	2.99	1.677	3.08	1.318	BDL	0.0443	1.058	26.22	0.025	BDL	BDL	BDL	BDL	0.096	0.4	0.291	0.0646
T44	MOB	326774	325538	7986.58	351729	353805	0.322	BDL	8.08	128.37	1.949	1.075	1.841	0.0086	3.82	3.67	1.148	3.8	1.092	0.054	0.087	0.983	40.25	BDL	BDL	BDL	0.0083	BDL	0.0146	0.221	0.247	0.476
T3	238 OB	335979	325540	4218.54	326713	340702	4.84	BDL	3.1	307.84	0.9	0.961	1.632	0.0017	2.18	2.19	23.48	2.23	22.93	0.032	0.233	0.941	10.56	BDL	BDL	BDL	0.04	0.081	8	61.18	63.62	42.84
T3	238 OB	319136	325541	3693.22	312716	309531	6.23	BDL	13.14	385.43	0.818	0.846	1.566	0.0022	2.31	2.34	36.1	2.3	33.97	0.052	0.347	1.166	21.91	BDL	BDL	BDL	0.0321	0.1	18.16	108.01	104.26	71.89
T3	238 OB	321353	325541	4066.84	319246	330355	6.67	BDL	5.18	303.41	0.964	0.861	1.501	0.00211	1.01	0.96	44.05	0.921	45.31	0.049	0.367	0.87	16.76	BDL	BDL	BDL	0.056	0.11	13.61	89.25	91.75	55.43
T3	238 OB	333719	325541	4175.35	319861	328313	7.77	BDL	2.08	294.47	0.955	0.902	1.525	0.00323	1.28	1.3	47.41	1.24	46.84	0.055	0.652	0.793	10.12	BDL	BDL	BDL	0.054	0.143	16.97	108.88	112.58	67.56
T3	238 OB	343795	325541	3921.25	360678	384505	2.41	BDL	27.04	427.61	0.899	0.962	1.665	BDL	1.7	1.75	14.38	1.77	14.45	0.023	0.436	2.94	49.05	BDL	BDL	BDL	0.12	0.057	16.66	60.83	65.97	29.05
T3	238 OB	352627	325541	4136.4	344874	364298	6.76	BDL	5.19	357.23	0.954	0.993	1.75	BDL	1.57	1.56	32.28	1.52	33.95	0.03	0.525	0.826	11.81	BDL	BDL	BDL	0.048	BDL	12.48	87.78	94.32	62.52
T2	238 OB	358941	325543	5667.93	373936	400294	57.82	0.53	17.32	131.36	1.74	1.4	2.08	BDL	2.41	2.44	34.13	2.32	35.09	0.192	0.095	0.35	36.16	0.036	0.0047	BDL	0.0145	0.11	3.27	9.48	9.75	1.88
T2	238 OB	369581	325543	6207.22	351463	389133	41.67	BDL	23.3	165.24	1.5	1.25	2.13	BDL	1.96	2.04	18.28	2.03	18.63	BDL	BDL	0.35	38.74	0.057	BDL	BDL	0.018	0.25	3.53	20.38	19.85	16.93
T2	238 OB	407632	325543	6315.07	406835	387083	4.25	BDL	7.81	168.35	1.77	1.41	2.31	BDL	2.78	2.87	29.75	2.64	31.66	BDL	BDL	0.407	39.88	0.079	BDL	BDL	BDL	0.65	3.77	32.63	37.18	22.76
T2	238 OB	346609	325543	5338.47	345220	373213	5.03	1.46	9.62	114.5	1.16	0.99	1.52	0.0119	1.59	1.45	26.76	1.69	26.94	0.049	0.055	0.363	25.95	BDL	BDL	0.016	0.0089	BDL	0.416	11.29	8.28	16.23
T2	238 OB	376124	325544	5592.27	380300	385813	2.19	BDL	50.75	182.18	1.6	1.9	2.23	BDL	2.97	3.06	25.94	2.99	26.25	BDL	0.092	0.295	37.62	0.116	BDL	BDL	BDL	BDL	2.45	13.35	14.64	3.88
T2	238 OB	327264	325544	5971.77	339710	352221	3.43	BDL	2.34	81.67	1.75	1.5	1.97	BDL	1.38	1.22	25.18	1.22	26.41	0.19	0.059	0.662	3.38	BDL	BDL	BDL	BDL	BDL	5.3	46.42	51.3	17.85
TU8	238 OB	323842	325548	12363.2	363513	367896	1.26	BDL	BDL	96.73	2.87	0.986	1.64	BDL	0.408	0.404	5.98	0.422	6.14	BDL	0.0477	0.114	0.75	BDL	0.00107	BDL	0.0019	BDL	0.041	0.73	0.74	0.43
TU8	238 OB	315636	325548	13051.7	371693	364301	3.02	1.57	0.257	112.07	3.25	1.31	1.92	BDL	2.38	2.28	8.8	2.28	8.94	BDL	0.06	0.46	18.12	BDL	BDL	BDL	BDL	BDL	0.132	1.03	1.03	0.181
TU8	238 OB	376691	325549	12916.5	398238	402725	1.28	BDL	0.15	124.39	3.08	1.23	2.07	BDL	1.38	1.41	4.92	1.42	4.9	BDL	0.053	0.54	1.09	BDL	0.005	BDL	BDL	0.176	0.007	0.063	0.198	0.202
TU8	238 OB	331425	325549	12814.4	353509	348576	4.57	0.35	0.087	108.76	2.95	1.087	1.78	BDL	0.584	0.537	14.7	0.59	13.29	0.025	0.062	0.228	2.73	0.0126	BDL	BDL	0.0082	0.157	0.071	0.68	0.88	0.165
TU8	238 OB	334423	325549	12813.4	372718	385329	3.71	BDL	0.041	103.09	3.38	1.27	1.73	BDL	0.8	0.8	17.03	0.72	17.73	0.05	0.081	0.222	20.92	BDL	BDL	BDL	0.0054	0.098	0.052	0.52	0.66	0.58
T6	238 OB	368893	325555	10779.2	368638	363808	0.25	BDL	0.045	120.65	2.56	1.23	1.85	BDL	0.516	0.519	0.38	0.515	0.38	BDL	0.068	0.0134	0.43	BDL	BDL	BDL	BDL	0.076	BDL	0.098	0.114	0.039
T6	238 OB	376293	325556	9771.74	359849	361191	0.173	BDL	0.059	117.2	2.28	1.132	1.9	0.00091	BDL	0.0057	0.42	0.0039	0.45	0.017	0.048	0.0051	0.31	BDL	0.00253	BDL	BDL	0.071	0.0184	0.88	1.04	0.132
T6	238 OB	386194	325556	11162.3	368249	367981	0.16	BDL	BDL	125.7	2.97	1.24	1.95	BDL	0.74	0.67	0.37	0.66	0.38	0.026	0.075	0.141	11.77	BDL	BDL	BDL	BDL	BDL	0.042	0.046	0.047	0.009
T6	238 OB	361409	325557	11412.2	375739	366633	0.22	BDL	BDL	151.91	2.54	1.143	1.94	0.0122	0.331	0.288	0.28	0.324	0.3	0.05	0.063	0.0274	7.21	BDL	0.00163	BDL	BDL	BDL	0.0018	0.99	1.21	0.2
T6	238 OB	380497	325557	10720.5	386688	406072	0.34	BDL	BDL	128.16	2.75	1.29	1.95	BDL	0.165	0.195	0.74	0.194	0.74	0.044	0.075	0.065	1.28	BDL	0.0325	0.0037	BDL	BDL	0.29	6.76	8.1	0.95
T6	238 OB	360037	325557	10240.1	345772	343042	0.29	BDL	BDL	111.76	2.42	1.05	1.6	BDL	0.129	0.148	0.74	0.122	0.72	BDL	0.058	0.0179	0.41	BDL	BDL	BDL	0.0022	0.079	0.0068	1.49	1.67	0.39

Notes: Abbreviation BDL stands for below detection limits

A6: LA-ICPMS analyses of chalcopyrite (ppm)

Sample	Ore body	^{34}S	^{57}Fe	^{59}Co	^{60}Ni	^{61}Ni	^{65}Cu	^{66}Zn	^{75}As	^{77}Se	^{99}Ru	^{101}Ru	^{102}Ru	^{103}Rh	^{105}Pd	^{106}Pd	^{107}Ag	^{108}Pd	^{109}Ag	^{111}Cd	^{118}Sn	^{121}Sb	^{125}Te	^{189}Os	^{193}Ir	^{195}Pt	^{197}Au	^{202}Hg	^{205}Tl	^{206}Pb	^{208}Pb	^{209}Bi
T9	238 OB	453904	304319	10.49	271.03	277.87	353583	227.98	0.179	83.25	0.288	0.0969	0.00861	9.74	17.65	0.11	3.67	0.088	3.66	4.18	2.81	0.72	0.882	BDL	0.175	0.0202	0.0103	BDL	0.241	25.89	26.89	3.14
T9	238 OB	350273	304319	0.294	22.57	22.65	346040	286.15	0.0028	105.16	0.224	0.1076	0.00234	9.4	17.18	0.121	4.99	0.092	5.02	5.2	17.05	0.425	1.32	BDL	0.0001	0.00044	0.0125	BDL	0.0235	22.21	23.36	2.97
T9	238 OB	365806	304319	61.98	24.74	25.72	353244	340.05	0.0067	93.06	0.207	0.1057	0.00096	9.76	17.44	0.147	5.37	0.114	5.49	6.38	2.6	0.941	2.06	BDL	BDL	0.00344	0.0301	BDL	0.0563	46.46	49.41	8.89
T9	238 OB	613659	304319	0.467	35.98	41.3	417414	340.88	0.054	170.13	0.26	0.156	0.0046	11.35	19.43	0.134	5.44	0.086	5.64	7.4	8.98	0.53	4.56	BDL	BDL	0.0231	0.055	0.468	0.0396	40.82	45.74	9.2
T9	238 OB	437611	304319	0.171	28.31	25.15	366146	366.16	0.0963	137.98	0.178	0.104	BDL	9.91	17.62	0.137	3.02	0.112	2.87	7.07	10.63	0.298	3.5	BDL	0.00051	BDL	0.0157	0.0401	0.023	13.8	14.22	2.82
T9	238 OB	528866	304319	0.235	35.62	37.85	393349	485.5	0.204	160.76	0.254	0.132	0.0047	10.61	18.88	0.289	4.22	0.216	4.28	10.68	7.19	0.59	2.76	0.0091	BDL	BDL	0.0206	BDL	0.0138	25.72	28.18	5.66
T12	238 OB	313591	304319	0.397	46.86	43.04	321014	250.44	0.0089	99.28	0.178	0.089	0.00147	8.59	15.52	0.142	1.25	0.097	1.31	6.67	8.93	0.0541	2.66	0.00105	0.00012	0.00046	0.133	0.0441	0.00469	4.56	5	0.99
T12	238 OB	337909	304319	1.57	183.3	54.91	350651	300.2	BDL	112.86	0.193	0.094	0.00082	9.34	16.66	0.147	0.86	0.109	0.86	7.82	6.36	0.073	2.09	BDL	BDL	BDL	0.0226	0.0349	0.00014	5	5.36	0.97
T12	238 OB	368333	304320	0.434	52.94	50.51	354929	256.15	BDL	99.76	0.182	0.114	0.00227	9.34	16.34	0.145	1.63	0.096	1.7	7.5	2.85	0.118	2.16	BDL	0.00084	BDL	0.036	0.0312	0.0247	13.15	14.14	2.23
T12	238 OB	394422	304320	0.147	31.41	29.28	343864	264.51	0.0656	128.56	0.187	0.131	0.00139	9.12	16.86	0.178	1.16	0.103	1.15	8.85	8.99	0.0336	4.48	BDL	BDL	BDL	0.052	0.0306	BDL	5.63	6.11	1.1
T12	238 OB	353415	304320	0.321	43.28	45.06	342707	265.39	0.0097	109.09	0.2	0.089	BDL	9.25	16.39	0.161	1.24	0.111	1.3	8.71	13.43	0.079	3.42	BDL	BDL	BDL	0.0094	0.0368	0.00039	8.58	9.42	1.42
TU1	238 OB	339282	304321	0.247	63.11	62.95	345093	379.77	0.0189	103.43	0.199	0.09	0.00143	9.24	17.08	0.62	3.9	0.47	3.86	31.21	54.19	0.0219	2.33	0.00122	BDL	BDL	0.054	0.057	0.00083	3.61	3.93	1.99
TU1	238 OB	379460	304321	0.126	64.33	49.99	362454	400.89	BDL	96.92	0.18	0.081	BDL	9.75	18.04	0.75	13.43	0.56	13.88	40.81	56.5	0.0189	5.07	0.00286	BDL	BDL	0.066	0.081	0.0045	6.9	7.49	1.5
TU1	238 OB	346353	304321	0.209	51.09	51.17	351404	347.54	BDL	99.47	0.198	0.092	0.00291	9.58	17.19	0.66	10.4	0.48	10.52	35.88	32.97	0.0215	7.17	BDL	BDL	0.0018	0.0145	0.05	0.00039	2.56	2.86	0.97
TU1	238 OB	343208	304321	0.229	58.83	56.59	354297	682.39	0.026	101.95	0.195	0.091	0.00162	9.3	17.13	0.91	5.09	0.69	5.11	50.97	29.65	0.0181	3.51	0.00157	0.00042	0.0031	0.0131	0.082	BDL	1.79	1.96	0.75
TU1	238 OB	337223	304321	0.22	52.76	52.1	354852	398.78	0.0173	90.11	0.201	0.088	0.00284	9.31	17.24	0.72	11.7	0.55	11.71	36.78	42.31	0.0075	6.03	0.00283	0.00025	0.00157	0.025	0.041	0.00058	1.41	1.62	0.97
T7	238 OB	345273	304323	1.12	72.27	72.95	341679	254.16	BDL	111.48	0.198	0.087	0.00119	9.37	17.27	0.092	2	0.056	1.99	4.2	1.28	0.087	3.84	0.004	BDL	0.00053	0.0088	0.0291	BDL	8.05	8.88	1.22
T7	238 OB	379912	304323	1.3	42.43	35.77	351175	254.34	0.056	111.81	0.231	0.111	0.0148	9.76	17.67	0.09	2.7	0.053	2.88	4.28	1.23	0.076	6.31	0.009	BDL	BDL	0.0113	BDL	0.00041	2.98	3.18	0.74
T7	238 OB	350725	304323	0.226	29.36	30.28	340808	299.24	BDL	146.86	0.203	0.094	0.00055	9.53	17.78	0.098	2.38	0.069	2.31	4.36	1.19	0.101	6.34	BDL	BDL	BDL	0.004	0.049	0.00132	7.52	8	1.36
T7	238 OB	343849	304323	0.343	41.5	39.71	346619	325.46	BDL	110.97	0.223	0.111	0.00029	9.47	17.02	0.108	1.89	0.073	1.88	4.46	1.38	0.167	2.98	0.0035	0.00029	0.00042	0.082	BDL	0.00075	9.68	10.53	1.73
T10	MOB	345258	304317	0.0862	19.16	20.27	338945	339.61	BDL	184.56	0.216	0.1074	BDL	9.69	17.47	0.547	1.109	0.394	1.109	29.95	6.75	0.1423	0.18	BDL	BDL	BDL	0.0054	BDL	BDL	4.85	5.49	0.678
T10	MOB	374094	304317	0.0577	24.57	25.94	338037	276.75	BDL	94.88	0.225	0.119	BDL	9.65	17.62	0.392	0.941	0.325	1.09	25.06	17.05	0.0235	0.35	BDL	BDL	BDL	BDL	BDL	0.006	0.884	0.845	0.106
T10	MOB	411364	304317	0.08	21.65	22.42	361369	266.6	0.176	180.2	0.278	0.069	0.0079	9.35	17.67	0.407	1.82	0.295	1.83	23.87	13	0.245	3.35	BDL	BDL	BDL	BDL	BDL	BDL	5.28	5.8	0.788
T10	MOB	479626	304317	0.061	19.48	20.77	381932	302.75	0.44	238.25	0.232	0.063	BDL	10.23	18.98	0.548	2.25	0.44	2.23	36.15	22.06	0.442	5.04	BDL	BDL	BDL	0.026	BDL	BDL	7.74	9.23	1.497
T8	238 OB	360680	304317	0.1775	29.09	29.72	355502	397.15	BDL	113.31	0.209	0.1002	BDL	9.56	17.57	0.212	1.83	0.163	1.88	11.81	7.13	0.0371	4.15	BDL	BDL	BDL	0.0101	0.092	0.0021	4.73	5.2	0.744
T8	238 OB	344657	304317	0.422	40.59	41.63	340680	224.08	0.034	105.77	0.205	0.103	0.00103	9.46	17.49	0.1025	0.917	0.0921	0.91	6.1	5.1	0.136	2	BDL	BDL	BDL	0.0311	0.081	0.0112	8.14	8.91	1.545
T8	238 OB	370427	304317	0.778	55	52.95	348749	470.64	BDL	117.04	0.203	0.11	BDL	9.59	17.31	0.266	2.39	0.196	2.48	12.9	10.46	0.1103	2.95	BDL	BDL	BDL	0.0629	BDL	BDL	8.6	9.33	1.458
T8	238 OB	388977	304317	3.77	210.97	212.64	350457	244.78	BDL	129.51	0.229	0.12	BDL	9.46	17.59	0.113	1.158	0.102	1.188	7.25	4.43	0.182	2.23	BDL	BDL	BDL	0.05	BDL	0.155	14.46	15.47	2.72
T8	238 OB	378420	304317	0.442	43.44	38.65	341044	237.09	BDL	116.48	0.236	0.079	0.0044	9.59	17.39	0.146	1.074	0.112	1.15	7.48	6.68	0.163	1.56	BDL	BDL	BDL	0.0094	0.099	0.0313	7.41	7.88	1.272
T17	MOB	438795	304317	0.073	32.93	40.02	353388	282.43	BDL	184.38	0.235	0.125	BDL	10.28	17.71	0.562	1.64	0.365	1.67	23.68	61.81	0.251	0.98	BDL	BDL	BDL	0.055	BDL	0.0098	8.06	9.04	5.37
T17	MOB	398077	304317	0.106	25.91	24.21	344390	303.01	BDL	150.18	0.249	0.103	BDL	9.21	17.73	0.515	1.56	0.337	1.46	20.75	48.52	0.276	1.48	0.024	BDL	BDL	0.029	BDL	0.016	8.92	10.08	3.56
T17	MOB	439297	304317	0.099	27.71	31.55	358948	326.99	0.2	102.27	0.293	0.05	BDL	9.38	18.15	0.445	2.34	0.327	2.11	18.76	65.82	1.16	3.09	BDL	BDL	BDL	BDL	BDL	0.041	30.82	35.44	14.1
T17	MOB	431009	304317	0.068	29.24	30.27	338550	368.68	BDL	131.1	0.159	0.066	0.013	9.08	16.39	0.612	1.91	0.326	1.93	25.31	33.26	1.1	0.8	BDL	BDL	0.049	0.015	BDL	0.0167	19.38	21.05	8.23
T26	MOB	357599	304317	0.78	32.04	29.91	351676	390.78	BDL	99.57	0.212	0.093	BDL	9.27	17.16	0.387	14.39	0.268	14.35	21.49	11.31	0.0183	7.32	BDL	BDL	BDL	0.0293	BDL	0.00143	1.022	1.279	0.765
T26	238 OB	360501	304317	0.224	22.15	13.81	361407	395.11	0.048	98.63	0.205	0.095	BDL	9.02	17.05	0.242	17.25	0.161	17.58	12.52	19.36	0.0626	10.01	BDL	BDL	BDL	0.0466	BDL	BDL	2.31	2.55	1.286
T26	238 OB	359925	304317	0.0908	9.64	8.42	346160	258.85	BDL	96.33	0.226	0.097	BDL	9.06	17.1	0.17	12.34	0.131	13.04	9.97	5.53	0.365	0.378	0.0138	BDL	BDL	0.0293	BDL	0.0416	12.06	12.88	3.68
T26	238 OB	353973	304317	0.603	29.16	27.66	350925	362.13	BDL	99.82	0.176	0.0878	0.0019	8.97	16.68	0.439	10.89	0.314	10.74	23.4	12.17	0.0439	3.86	BDL	BDL	BDL	0.0344	0.085	BDL	1.64	1.83	0.949
T26	238 OB	338739	304317	0.521	22.47	21.01	338100	327.42	BDL	88.35	0.172	0.0852	BDL	8.9	16.41	0.249	15.58	0.172	15.79	12.75	13.4	0.0175	6.89	0.004	BDL	BDL	0.0219	0.048	0.00126	1.197	1.297	0.556
TU18B	MOB	476636	304317	0.078	24.06	24.64	364699	232.28	BDL	156.33	0.237	0.078	BDL	9.64	18.33	0.178	1.33	0.145	1.24	15.32	1.131	0.255	BDL	BDL	BDL	BDL	0.412	BDL	BDL	9.54	11.14	5.84
TU18B	MOB	430291	304317	2.008	176.03	195.4	369895	417.23	BDL	235.46	0.102	0.133	0.0068	9.69	18.37	0.464	1.46	0.383	1.193	32.52	0.771	0.174	0.66	BDL	BDL	BDL	0.04	BDL	0.0256	9.41	10.99	6.3
TU18B	MOB	825213	304317	0.166	15.66	26.77	390188	27.89	BDL	507.18	0.35	BDL	BDL	9.72	17.27	0.51	2.75	0.45	2.5	59.95	BDL	BDL	2.22	BDL	0.086	BDL	BDL	2.42	BDL	585.17	617.01	18.67

Notes: Abbreviation BDL stands for below detection limits

A6 (continued): LA-ICPMS analyses of chalcopyrite (ppm)

Sample	Ore body	^{34}S	^{57}Fe	^{59}Co	^{60}Ni	^{61}Ni	^{65}Cu	^{66}Zn	^{75}As	^{77}Se	^{99}Ru	^{101}Ru	^{102}Ru	^{103}Rh	^{105}Pd	^{106}Pd	^{107}Ag	^{108}Pd	^{109}Ag	^{111}Cd	^{118}Sn	^{121}Sb	^{125}Te	^{189}Os	^{193}Ir	^{195}Pt	^{197}Au	^{202}Hg	^{205}Tl	^{206}Pb	^{208}Pb	^{209}Bi
TU16B	MOB	444212	304317	0.03	22.47	27	340357	221.39	BDL	156.37	0.232	0.069	BDL	9.42	16.77	0.196	0.696	0.077	0.768	13.26	1.69	0.182	1.53	BDL	BDL	BDL	0.016	0.33	0.042	7.57	8.71	3.46
TU16B	MOB	361619	304317	0.0994	38.99	36.37	358487	323.25	BDL	143.98	0.228	0.094	BDL	9.61	17.86	0.26	0.499	0.195	0.485	15.27	1.951	0.116	0.316	0.0059	BDL	BDL	0.0169	BDL	0.0028	3.84	4.3	1.761
TU16B	MOB	368332	304317	0.1499	30.97	29.57	353000	386.98	BDL	138.74	0.215	0.108	0.00152	9.23	16.98	0.285	0.489	0.212	0.487	17.62	0.79	0.0903	0.259	BDL	BDL	BDL	0.0082	BDL	0.00204	3.56	3.94	1.259
TU16B	MOB	367926	304317	0.26	36.54	32.72	335662	380.13	BDL	145.55	0.193	0.121	BDL	9.14	17.09	0.214	0.75	0.204	0.668	15.41	1.681	0.213	1.16	BDL	0.0015	BDL	0.0214	BDL	0.0064	4.02	4.72	2.65
TU16B	MOB	365496	304317	0.538	43.96	47.52	343412	449.3	BDL	138.59	0.181	0.101	BDL	9.13	16.6	0.285	0.904	0.228	0.89	17.43	0.55	0.484	0.76	BDL	BDL	BDL	0.0246	0.051	0.0076	7.22	8.41	3.69
TU16B	MOB	375265	304317	0.428	42.66	44.53	351191	421.12	BDL	144.88	0.187	0.068	0.0016	9.14	16.74	0.293	0.863	0.209	0.856	16.05	0.573	0.514	1.26	BDL	BDL	BDL	0.0157	BDL	0.0059	9.25	10.52	5.86
TU13	238 OB	364071	304317	0.416	56.62	56.6	356303	567.73	0.0209	233.47	0.202	0.098	0.0041	9.01	16.57	1.219	17.4	0.943	17.8	75.37	26.74	0.0333	16.98	0.005	BDL	BDL	0.024	0.045	BDL	2.91	3.36	2.022
TU13	238 OB	356137	304317	0.1446	42.98	43.82	350541	324.48	0.0136	222.21	0.206	0.089	0.0021	8.86	16.07	0.654	11.83	0.511	12.19	42.9	21.59	0.0118	8.02	BDL	0.00094	BDL	0.0251	BDL	BDL	1.01	1.163	1.178
TU13	238 OB	356047	304317	0.364	162.79	158.67	346625	325.84	BDL	231.37	0.117	0.118	BDL	9.01	16.64	0.914	13.95	0.738	14.33	56.53	22.06	0.0302	12.06	BDL	BDL	BDL	0.053	BDL	0.0022	3.47	3.92	2.88
TU13	238 OB	344396	304317	0.169	46.79	46.45	341664	693.49	BDL	219.34	0.166	0.084	0.0054	8.84	16.11	1.23	9.38	0.897	9.55	72.35	20.87	0.0182	4.35	BDL	BDL	BDL	0.067	0.067	0.00204	1.81	2.02	1.838
TU7	238 OB	496292	304317	0.656	59.51	65	319719	444.21	0.0205	125.31	0.207	0.1021	0.00203	8.38	15.62	0.251	1.261	0.198	1.24	15.86	17.73	0.0859	1.53	BDL	BDL	BDL	0.131	BDL	BDL	9.58	10.51	1.631
TU7	238 OB	489110	304317	0.293	32.44	48.78	316566	361.25	BDL	122.11	0.162	0.0884	BDL	8.44	15.61	0.215	1.294	0.166	1.319	14.69	16.63	0.0444	3.09	BDL	BDL	BDL	0.0229	BDL	BDL	5.9	6.93	1.237
TU7	238 OB	519524	304317	0.1304	23.8	14.68	321424	319.93	BDL	147.39	0.202	0.093	BDL	8.51	15.57	0.201	0.776	0.141	0.746	12.3	5.07	0.09	1.28	BDL	BDL	BDL	BDL	0.07	0.0023	12.79	13.57	1.305
TU7	238 OB	660592	304317	0.124	29.95	31.3	320630	270.51	BDL	163.58	0.212	0.095	BDL	8.66	15.88	0.172	0.949	0.134	0.943	12.43	8.23	0.157	4.5	BDL	BDL	BDL	0.022	BDL	BDL	4.05	4.37	0.9
T34	MOB	339251	304317	0.318	38.68	38.67	339818	359.57	BDL	104.08	0.203	0.105	0.0013	9.07	16.45	0.56	8.34	0.396	8.44	34.42	21.86	0.0227	10.92	BDL	BDL	BDL	0.0122	BDL	0.00124	1.769	2	0.479
T34	MOB	355749	304317	0.397	42.86	42.88	349216	380.08	BDL	105.28	0.208	0.1053	0.00281	9.25	16.79	0.6	7.1	0.433	7.34	34.34	21.33	0.0223	8.84	BDL	BDL	BDL	0.092	0.068	BDL	1.83	2.08	0.544
T34	MOB	352801	304317	0.092	31.22	30.84	352561	481.78	BDL	95.75	0.208	0.098	BDL	9.17	16.75	0.69	3.47	0.49	3.48	38.63	23.37	0.0643	5.59	BDL	BDL	BDL	0.135	BDL	0.00266	3.77	4.12	1.508
T34	MOB	349935	304317	0.1884	37.5	36.95	338742	355.4	BDL	105.98	0.212	0.0929	0.00176	8.93	15.85	0.57	10.3	0.403	10.25	32.55	19.1	0.0139	13.71	BDL	BDL	BDL	0.0088	BDL	0.00104	1.197	1.323	0.266
T44	MOB	350158	304317	0.1304	50.61	51.97	352024	436.86	BDL	113.19	0.205	0.0892	BDL	8.93	16.21	0.389	4.97	0.279	4.98	20.33	5.16	0.0206	6.16	BDL	BDL	BDL	0.0252	BDL	0.00155	14.7	15.9	0.941
T44	MOB	349223	304317	0.1407	28.01	29.66	346912	361.58	0.0287	101.71	0.194	0.1031	BDL	8.87	16.19	0.3	3.2	0.224	3.07	17.77	5.07	0.0209	4.21	BDL	0.178	BDL	0.0092	0.06	0.0016	3.69	3.84	0.773
T44	MOB	335575	304317	0.1459	37.11	51.43	332971	336.54	BDL	104.98	0.173	0.093	0.00193	8.85	16.11	0.315	5.72	0.231	6.04	15.67	7.17	0.0254	7.97	BDL	BDL	BDL	0.03	BDL	0.00163	2.07	2.29	0.809
T44	MOB	329706	304317	0.1651	34.15	34.7	344595	409.45	BDL	102.86	0.199	0.0834	0.00118	8.89	15.88	0.35	1.98	0.246	1.88	18.91	6.61	0.0542	3.08	BDL	BDL	BDL	0.067	BDL	0.00334	6.94	7.43	1.181
T3	238 OB	355086	304320	0.457	69.83	71.97	356785	394.93	BDL	339.97	0.197	0.0929	0.0048	8.62	15.64	0.578	10.29	0.492	10.59	32.92	84.4	0.0872	4.42	BDL	BDL	BDL	0.253	BDL	0.00355	15.85	16.74	10.43
T3	238 OB	376909	304320	0.159	53.58	54.18	344000	589.92	BDL	334.24	0.212	0.0999	0.0032	8.34	14.78	0.95	8.65	0.681	8.62	60.33	83.29	0.183	10.04	BDL	0.00169	BDL	0.192	0.068	0.0082	12.36	14.2	16.28
T3	238 OB	357178	304320	0.202	39.48	41.64	345398	378.07	0.236	319.51	0.181	0.0877	0.00324	8.34	15.25	0.609	5.48	0.49	5.57	35.94	80.46	0.128	1.07	BDL	BDL	BDL	0.167	0.06	0.0011	7.04	8.14	6.51
T3	238 OB	339685	304320	4.47	814.39	1231.11	334907	243.65	0.0135	323.21	0.179	0.088	0.0112	7.62	14.14	0.34	6.47	0.271	6.5	15.94	40.12	0.196	0.526	BDL	BDL	BDL	0.134	0.164	0.0252	12.46	13.17	6.38
T3	238 OB	360000	304320	0.168	45.24	45.55	358089	328.64	0.048	334.5	0.221	0.0895	0.0059	8.54	15.66	0.544	5.12	0.435	5.26	29.95	119.37	0.171	1	BDL	BDL	BDL	0.229	0.039	0.00123	7.5	8.36	7.24
T3	238 OB	360910	304321	0.0984	50.49	48.88	356218	423.46	0.0238	332.36	0.194	0.085	0.0018	8.64	15.69	1.09	9.41	0.846	9.95	68.82	79.97	0.211	8.92	BDL	BDL	BDL	0.113	0.058	0.00088	11.08	12.82	16.79
T2	238 OB	342140	304323	0.193	60.15	61.23	348101	466.9	BDL	97.37	0.183	0.0972	BDL	8.22	15.09	0.686	5.65	0.55	5.58	41.61	2.51	0.0079	5.02	BDL	BDL	BDL	0.0033	0.052	BDL	3.16	3.5	1.51
T2	238 OB	351929	304323	0.157	51.6	48.94	350627	310.33	BDL	111.6	0.178	0.0871	0.0039	8.42	15.25	0.481	3.61	0.349	3.53	25.72	2.73	0.0084	1.78	BDL	BDL	BDL	BDL	BDL	BDL	2.36	2.71	3.27
T2	238 OB	352192	304323	0.153	57.65	59.15	337793	324.5	0.029	129.19	0.201	0.096	BDL	8.91	15.85	0.593	2.85	0.492	2.91	34.86	2.75	BDL	1.76	BDL	BDL	BDL	0.0016	0.179	BDL	2.6	3.02	1.65
T2	238 OB	358518	304324	0.132	58.92	63.07	360734	378.26	0.0178	98.23	0.2	0.098	0.0048	8.81	15.42	0.645	6.9	0.536	7.04	33.74	2.82	0.0029	7.43	BDL	BDL	BDL	0.0026	0.119	BDL	2.02	2.24	2.17
T2	238 OB	345961	304324	0.24	40.03	41.32	344361	280.26	0.017	137.73	0.174	0.0848	0.0041	8.11	14.22	0.444	4.64	0.318	4.4	23.16	2.87	0.0045	1.48	BDL	BDL	BDL	0.0076	0.136	BDL	2.39	2.63	1.27
T2	238 OB	369829	304324	0.178	53.16	54.15	338931	329.13	BDL	114.61	0.183	0.1032	0.00396	8.71	16.06	0.71	3.12	0.569	3.16	37.29	2.93	0.00218	1.69	BDL	BDL	BDL	BDL	0.044	BDL	2.18	2.46	1.99
TU8	238 OB	363746	304328	1.01	52.38	53.79	342486	284.37	0.0184	117.13	0.218	0.0903	BDL	8.17	14.7	0.141	4.01	0.09	3.88	8.2	5.24	0.144	5.13	BDL	BDL	BDL	0.018	BDL	0.026	5.9	6.34	0.86
TU8	238 OB	390249	304329	0.238	63.52	66.12	357617	413.95	0.051	125.44	0.163	0.091	BDL	9.01	15.9	0.199	12.18	0.164	11.38	12.67	9.53	0.275	7.26	BDL	BDL	BDL	0.034	BDL	0.0093	10.25	10.87	1.61
TU8	238 OB	348671	304329	0.233	27.91	55.67	351782	277.6	0.025	110.3	0.201	0.088	BDL	8.5	15.63	0.116	2.68	0.083	2.77	6.91	4.17	0.283	1.23	BDL	0.0011	BDL	0.074	BDL	0.0043	11.5	12.56	1.36
TU8	238 OB	372838	304330	0.63	39.03	43.95	350307	336.45	0.027	118.57	0.183	0.0918	BDL	8.68	15.23	0.16	2.13	0.118	2.04	9.66	7.07	0.186	3.14	BDL	BDL	BDL	0.073	0.093	0.0064	11.76	12.46	1.36
T6	238 OB	398341	304336	5.4	11.81	10.39	360066	400.09	0.09	114	0.185	0.086	BDL	8.65	14.82	0.205	5.34	0.167	5.17	16.56	0.72	0.045	2.76	BDL	BDL	BDL	BDL	0.089	BDL	10.53	11.24	1.48
T6	238 OB	399877	304337	0.137	23.54	23.81	362471	273.03	BDL	127.9	0.199	0.094	BDL	8.6	15.38	0.18	5.38	0.123	5.3	14.15	0.66	0.094	2.1	BDL	BDL	BDL	0.034	BDL	0.0211	16.73	18.99	2.41
T6	238 OB	423580	304317	0.166	20.59	22.6	366299	498.32	BDL	159.55	0.264	0.114	BDL	11.17	19.08	0.389	5.98	0.275	6.24	22.9	1.011	0.106	1.36	BDL	BDL	BDL	BDL	BDL	BDL	15.15	16.58	2.3
T6	238 OB	433897	304317	0.117	12.57	13.24	366857	515.52	BDL	155.62	0.232	0.142	BDL	10.51	18.38	0.361	5.97	0.269	5.94	21.51	1.171	0.04	1.53	BDL	BDL	BDL	BDL	0.72	BDL	8.71	9.7	0.818
T6	238 OB	425170	304317	0.125	9.74	13.73	369256	337.35	BDL	218.82	0.314	0.107	BDL	10.7	19.26	0.37	9.97	0.312	10.2	17.75	1.2	0.098	15.43	BDL	BDL	BDL	BDL	BDL	0.0093	12.39	14.33	1.835
T6	238 OB	427918	304317	0.144	15.87	18.92	366194	474.52	BDL	157.19	0.251	0.127	0.0236	9.99	17.7	0.298	7.03	0.238	7.08	21.64	1.095	0.081	4.38	BDL	BDL	BDL	0.026	BDL	BDL	6.1	6.7	0.56

Notes: Abbreviation BDL stands for below detection limits

A7: LA-ICPMS analyses of the cobaltite-gersdorffite-glaucodot solid solution (ppm)

Sample	Ore body	^{34}S	^{57}Fe	^{59}Co	^{60}Ni	^{61}Ni	^{65}Cu	^{66}Zn	^{75}As	^{77}Se	^{99}Ru	^{101}Ru	^{102}Ru	^{103}Rh	^{105}Pd	^{106}Pd	^{107}Ag	^{108}Pd	^{109}Ag	^{111}Cd	^{118}Sn	^{121}Sb	^{125}Te	^{189}Os	^{193}Ir	^{195}Pt	^{197}Au	^{202}Hg	^{205}Tl	^{206}Pb	^{208}Pb	^{209}Bi
T10	MOB	403462	79985.3	197834	223629	236050	0.742	BDL	523926	503.13	51.48	0.874	23.74	2.54	765.11	754.7	0.43	779.18	0.177	0.069	0.073	1261.63	46.57	BDL	BDL	2.284	4	0.181	0.00208	0.105	0.24	30.74
T10	MOB	442331	79985.3	176505	308606	307392	0.47	BDL	587710	687.23	43.84	1.066	37.86	2.36	1206.71	1226.51	0.136	1275.75	0.091	BDL	0.059	2819.34	73.63	BDL	BDL	1.605	0.235	BDL	BDL	0.518	0.421	18.44
T10	MOB	318594	79985.3	78083.7	318318	335339	0.41	0.32	406734	625.89	18.94	2.19	28.18	8.58	815.44	854.38	0.269	935.85	0.3	0.052	0.151	2859.73	78.04	0.9	11.32	27.83	0.119	BDL	0.0021	1.97	2.34	52.08
T10	MOB	380278	79985.3	246751	188057	161108	0.625	0.3	538274	282.91	61.24	0.855	13.71	0.112	429.75	415.64	0.073	404.04	0.0314	BDL	0.102	492.49	19.31	BDL	BDL	24.04	BDL	BDL	BDL	0.199	0.201	2.93
T131	N/A	629865	79985.3	394089	326608	347405	89.9	0.58	1664941	578.53	90.99	0.9	4.6	0.169	115.8	118.27	245.29	114.75	234.26	0.23	0.083	1129.7	725.54	BDL	BDL	0.88	325.46	BDL	0.031	55.83	59.59	2322.33
T131	N/A	731049	79985.3	423462	364317	377493	124.01	BDL	2080176	805.98	82.95	0.85	2.68	0.035	39.09	39.35	145.7	40.07	134.49	0.68	0.34	1424.32	189.81	0.127	BDL	0.177	31.2	BDL	BDL	26.6	34.76	231.76
T131	N/A	646556	79985.3	397899	281496	289192	3403.71	22.36	1723531	854.33	88.11	0.83	2.45	0.28	43.27	41.24	1215.23	41.51	1325.81	1.21	0.398	866.73	3070.61	BDL	0.022	0.83	2.53	0.72	0.354	3094.98	3622.13	2381.29
T34	MOB	360332	79985.3	124494	299512	349530	1.51	BDL	812037	492.33	31.48	4.75	36.71	7.65	978.01	1029.31	5.99	1097.44	6.26	0.124	0.231	1609.81	132.46	0.293	0.12	0.332	0.32	BDL	0.123	375.26	391.86	170.77
T34	MOB	304895	79985.3	93436.3	290063	284932	BDL	0.34	706467	399.54	32.18	7.48	30.52	63.09	826.84	843.81	0.08	838.7	0.082	0.203	0.019	1055.55	42.94	0.39	0.67	3.18	0.018	0.167	BDL	0.306	0.116	8.61
T34	MOB	312724	79985.3	163990	219932	222912	0.267	BDL	638439	242.41	41.34	3.36	19.97	10.67	583.92	596.28	BDL	613.33	BDL	0.055	0.067	439.18	15.87	0.24	0.101	8.62	BDL	BDL	BDL	0.0102	0.0138	2.04
T34	MOB	275571	79985.3	132308	242156	246468	10.78	0.25	675903	312.01	33.45	1.67	19.56	3.15	612.27	594.2	0.657	603.78	0.553	0.068	0.066	805.6	47.31	0.083	0.055	0.195	0.05	BDL	0.0107	9.99	12.06	26.4
T34	MOB	403923	79985.3	122116	251928	251280	0.77	0.3	979867	445.08	30.22	2.82	18.53	4.41	528.37	523.38	0.296	531.71	0.22	0.07	0.088	1078.26	32.03	0.173	0.59	0.47	0.015	0.32	0.0177	0.806	0.874	6.26
T34	MOB	432405	79985.3	128108	281763	293783	2.26	0.35	631092	504.73	47.52	11.6	32.18	18.1	710.4	689.05	0.303	708.29	0.054	0.126	0.124	1099.68	45.58	2.63	0.666	33.59	BDL	BDL	BDL	0.133	0.172	10.42
T34	MOB	397252	79985.3	188654	273377	272036	0.138	0.221	503199	445.58	56.43	9.35	27.28	18.98	602.6	604.97	0.0703	626.67	0.18	0.055	0.1127	690.41	46.16	1.111	0.255	11.49	0.0058	0.145	BDL	0.0366	0.0377	8.14
T34	MOB	333308	79985.3	145048	265451	264806	915.94	3.29	385666	373.97	39.02	2.84	25.5	4.84	697.94	753.02	3.02	814.26	2.99	0.157	0.105	817.35	71.16	0.472	0.12	27.91	0.0482	0.141	0.0229	69	74.57	94.72
T34	MOB	319249	79985.3	144051	226410	261463	BDL	0.15	375408	342.29	36.72	3.59	20.16	2.84	571.24	587.06	0.033	580.6	0.035	BDL	0.128	684.27	21.82	0.714	0.405	22.45	0.037	0.16	BDL	0.063	0.0221	5.01
T34	MOB	424750	79985.3	95804.6	342999	326792	0.29	BDL	542839	584.44	27.66	2.08	25.26	0.378	832.22	851.39	0.137	845.94	0.0141	0.106	0.134	1698.88	81.22	1.53	3.44	0.604	0.027	0.34	0.0054	0.118	0.146	26.79
T34	MOB	327906	79985.3	133715	216690	228773	9.16	BDL	816078	363.23	31.43	0.82	7.81	0.0171	245.8	243.74	0.246	240.86	0.15	BDL	0.118	811.11	31.7	0.07	0.178	0.308	0.024	BDL	BDL	0.434	0.497	7.1
T34	MOB	432405	79985.3	128108	281763	293783	2.26	0.35	631092	504.73	47.52	11.6	32.18	18.1	710.4	689.05	0.303	708.29	0.054	0.126	0.124	1099.68	45.58	2.63	0.666	33.59	BDL	BDL	BDL	0.133	0.172	10.42
T34	MOB	397252	79985.3	188654	273377	272036	0.138	0.221	503199	445.58	56.43	9.35	27.28	18.98	602.6	604.97	0.0703	626.67	0.18	0.055	0.1127	690.41	46.16	1.111	0.255	11.49	0.0058	0.145	BDL	0.0366	0.0377	8.14
T34	MOB	333308	79985.3	145048	265451	264806	915.94	3.29	385666	373.97	39.02	2.84	25.5	4.84	697.94	753.02	3.02	814.26	2.99	0.157	0.105	817.35	71.16	0.472	0.12	27.91	0.0482	0.141	0.0229	69	74.57	94.72
T34	MOB	319249	79985.3	144051	226410	261463	BDL	0.15	375408	342.29	36.72	3.59	20.16	2.84	571.24	587.06	0.033	580.6	0.035	BDL	0.128	684.27	21.82	0.714	0.405	22.45	0.037	0.16	BDL	0.063	0.0221	5.01
T34	MOB	424750	79985.3	95804.6	342999	326792	0.29	BDL	542839	584.44	27.66	2.08	25.26	0.378	832.22	851.39	0.137	845.94	0.0141	0.106	0.134	1698.88	81.22	1.53	3.44	0.604	0.027	0.34	0.0054	0.118	0.146	26.79
TU4B	238 OB	291114	79985.3	116189	248536	244738	0.264	BDL	876260	293.47	27.77	0.716	58.97	0.0054	1880.1	1959.69	450.1	2023.57	546.51	BDL	0.061	896.87	1029.68	BDL	BDL	4.38	8.09	0.122	0.0214	21.38	22.28	414.53
TU4B	238 OB	296701	79985.3	246017	148502	158905	130.16	2.37	825401	222.19	63.55	0.476	28.35	0.0159	891.36	911.74	4.87	1007.54	4.99	0.138	0.089	538.12	1000.39	BDL	BDL	6.18	61.58	BDL	BDL	16.09	17.53	2870.84
TU4B	238 OB	377659	79985.3	244484	172137	164441	0.473	BDL	987450	302.26	60.17	0.421	22.16	0.0508	736.11	732.79	7.25	733.28	7.39	0.468	0.041	748.84	105.31	BDL	BDL	17.67	0.154	0.147	0.0114	6.79	7.49	84.41
TU4B	238 OB	280210	79985.3	134390	206388	219005	0.115	0.448	754633	231.37	32.54	0.662	42.6	0.0125	1324.42	1381.27	21.92	1494.49	29.07	0.122	0.113	566.1	75.99	BDL	BDL	9.09	0.082	BDL	0.0237	7.41	8.3	9.15
TU4B	238 OB	419887	79985.3	208991	207677	183663	915.73	1.08	1038091	320.69	53.39	0.542	42.95	0.048	1392.16	1410.16	0.448	1506.95	0.966	0.154	0.118	923.06	43.82	BDL	BDL	0.84	1.36	BDL	0.0573	7.24	7.08	22.59
TU4B	238 OB	245162	79985.3	107596	218352	219480	11.06	0.5	716694	234.96	24.99	0.68	49.01	0.0023	1574.04	1727.4	2.64	1858.22	2.53	0.064	0.05	723.22	104.86	BDL	BDL	BDL	27.69	0.066	0.0016	0.97	1.48	208.31

Notes: Abbreviation BDL stands for below detection limits

A8: LA-ICPMS analyses of nickeline (ppm)

Sample	Ore body	^{34}S	^{57}Fe	^{59}Co	^{60}Ni	^{61}Ni	^{65}Cu	^{66}Zn	^{75}As	^{77}Se	^{99}Ru	^{101}Ru	^{102}Ru	^{103}Rh	^{105}Pd	^{106}Pd	^{107}Ag	^{108}Pd	^{109}Ag	^{111}Cd	^{118}Sn	^{121}Sb	^{125}Te	^{189}Os	^{193}Ir	^{195}Pt	^{197}Au	^{202}Hg	^{205}Tl	^{206}Pb	^{208}Pb	^{209}Bi
T131	N/A	2630.06	BLD	569.14	439287	530524	BLD	BLD	374312	193.18	0.45	1.72	3.12	BLD	8.78	10.19	0.27	9.06	0.045	BLD	BLD	5098.96	533.61	0.088	0.86	BLD	9.95	BLD	BLD	0.323	0.275	3.21
T131	N/A	2186.36	BLD	715.5	439287	424040	BLD	BLD	315966	105.22	1.43	2.66	3.69	0.039	6.34	6.12	0.135	6.26	0.131	0.15	BLD	4568.88	378.62	0.71	0.319	0.073	8.16	BLD	BLD	0.093	0.064	5.13
T131	N/A	5497.55	BLD	888.19	439287	444032	BLD	BLD	508359	225.96	1.28	2.31	3.68	0.114	5.54	5.25	BLD	5.55	0.146	BLD	BLD	6428.86	792.98	0.59	0.074	BLD	7.74	BLD	0.026	0.163	BLD	11.12
T131	N/A	2959.4	BLD	783.31	439287	492311	BLD	BLD	429420	143.78	1.56	3.52	3.49	0.165	4.13	4.66	0.176	4.2	0.075	0.52	0.24	6211.58	453.89	0.41	0.074	BLD	5.59	BLD	BLD	BLD	0.057	8.14
T131	N/A	2696.37	38.86	926.26	439287	442405	BLD	BLD	338127	124.56	3.01	4.2	5.05	0.492	6	6.11	0.097	6.03	0.074	0.137	0.165	5187.05	368.96	0.443	0.176	0.034	6.34	BLD	BLD	BLD	0.0158	6.46
T131	N/A	3020.78	159.58	809.4	439287	431390	2.2	BLD	346150	129.94	3.17	4.25	5.33	0.522	7.45	7.43	0.098	7.31	0.114	0.061	0.129	4923.94	415.54	0.47	0.205	BLD	8.61	BLD	BLD	0.087	0.0907	7.67
T131	N/A	2584.68	145.43	671.37	439287	438883	0.237	0.169	322082	103.84	3.51	4.72	5.64	0.522	7.65	7.07	0.104	6.81	0.09	0.04	0.133	4638.56	321.99	0.518	0.291	0.009	7.52	BLD	BLD	0.0329	0.0312	6.19
T131	N/A	1782.23	35.07	670.61	439287	429550	BLD	BLD	314587	87.14	2.48	3.36	4.31	0.59	5.92	6.15	0.093	5.87	0.061	0.118	0.171	4228	252.5	0.379	0.131	0.028	5.46	0.19	BLD	0.1	0.079	7.95
T131	N/A	2516.86	40.8	666.61	439287	429473	0.228	BLD	319662	100.38	3.27	4.42	5.42	0.529	5.71	5.82	0.091	7.02	0.093	BLD	0.106	4332.03	295.9	0.544	0.263	0.018	6.93	BLD	BLD	BLD	0.0129	6.34
T131	N/A	2120.1	BLD	606.47	439287	457998	BLD	BLD	362096	131.57	0.867	2.1	3.48	0.0693	15.86	18.31	0.136	15.19	0.169	BLD	0.133	4656.25	295.38	0.396	0.0396	BLD	4.5	BLD	BLD	0.039	0.0325	15.33
T131	N/A	1678.11	30.44	803.27	439287	424328	0.33	BLD	339499	109.96	0.96	1.99	3.43	0.09	17.4	17.34	0.076	17.38	0.183	0.155	0.187	4403.5	302.28	0.73	0.094	BLD	5.91	BLD	BLD	0.032	0.079	2.58
T34	MOB	985.62	106.5	726.95	439287	438108	0.164	BLD	322319	32.29	0.762	1.9	2.86	0.0681	1.319	1.278	0.0683	1.329	0.0777	0.045	0.0834	4697.94	303.68	0.088	0.0864	BLD	4.67	0.088	BLD	0.0081	0.006	7.97
T34	MOB	1009.63	99.26	662.43	439287	422014	BLD	BLD	329072	33.43	0.892	2.124	3.05	0.0841	1.408	1.415	0.104	1.353	0.091	BLD	0.0821	4783.53	299.54	0.096	0.097	0.0079	5.04	0.077	BLD	0.0377	0.0354	6.68
T34	MOB	2160.72	126.97	835.82	439287	450099	0.077	3.85	363737	33.76	1.063	2.116	3.11	0.303	1.547	1.524	0.0735	1.514	0.088	0.053	0.0738	4827.24	313.91	0.106	0.09	BLD	4.79	0.069	BLD	0.0143	0.0127	7.24
T34	MOB	1056.52	113.59	895.71	439287	453716	1.77	6.61	376958	34.93	1.03	2.209	3.19	0.416	1.51	1.443	0.108	1.401	0.123	0.036	0.082	5146.22	335.43	0.083	0.0913	BLD	4.71	0.121	BLD	0.0248	0.0276	9.6
T34	MOB	1253.21	95.98	759.8	439287	462983	BLD	BLD	377003	46.91	0.99	2.19	3.08	0.009	1.337	2.121	0.134	1.139	0.114	BLD	0.098	6595	554.2	0.172	0.373	BLD	6.52	BLD	BLD	0.0262	0.011	7.87
T34	MOB	1316.06	109.09	677.02	439287	442930	0.067	2.21	361041	44.12	0.499	1.684	2.57	0.0059	2.46	2.55	0.0641	2.51	0.079	BLD	0.0903	4605.32	574.96	0.371	0.187	BLD	6.75	BLD	BLD	0.0216	0.008	4.48
T34	MOB	11925.2	73.24	643.32	439287	440566	0.235	BLD	366965	39.94	0.812	2.14	2.95	0.0056	3.14	1.817	0.091	1.84	0.103	BLD	0.106	4673.41	383.89	1	1.15	BLD	4.6	0.105	BLD	0.0119	0.0073	9.96
T34	MOB	628.79	103.05	708.77	439287	436836	1.03	BLD	423057	36.51	0.686	1.7	2.91	0.024	1.374	1.504	0.114	1.41	0.113	0.049	0.145	5904.01	306.58	0.056	0.062	0.013	4.44	BLD	0.0038	BLD	BLD	21.15
T34	MOB	969.14	127.22	825.57	439287	455261	BLD	BLD	412724	31.25	0.961	2.15	3.26	0.27	1.343	1.442	0.115	1.355	0.124	BLD	0.13	5461.16	315.93	0.087	0.079	BLD	4.15	0.214	BLD	BLD	0.0281	13.55
T34	MOB	850.37	77.59	867.32	439287	447816	1.13	BLD	360331	32.63	1.18	2.34	3.23	0.304	1.48	1.505	0.102	1.36	0.128	0.039	0.086	4573.32	268.77	0.132	0.098	BLD	3.65	0.096	0.0064	BLD	0.0092	16.35
TU11	238 OB	1560.92	125.49	1139.36	439287	401470	0.69	0.74	274979	38.41	0.231	1.19	1.82	0.0105	0.61	0.719	0.306	0.702	0.344	0.098	0.051	4287.39	283.98	BLD	BLD	BLD	3.47	0.18	BLD	0.195	0.176	8.66

Notes: Abbreviation BDL stands for below detection limits

A9: EDS analyses of sulfarsenides (wt%)

Sample	Ore Body	Ore type	As	Ni	Co	Fe	S	Total	Atomic formula
T7	238	MASU	47.7	8.3	16.0	6.7	21.3	100.0	$(Ni_{0.27}Co_{0.51}Fe_{0.23})_{\Sigma 1.00}As_{0.98}S_{1.02}$
T7	238	MASU	48.4	11.3	13.6	5.8	20.9	100.0	$(Ni_{0.37}Co_{0.44}Fe_{0.20})_{\Sigma 1.00}As_{1.00}S_{1.00}$
T7	238	MASU	47.2	8.9	16.0	6.7	21.1	100.0	$(Ni_{0.28}Co_{0.50}Fe_{0.22})_{\Sigma 1.00}As_{0.98}S_{1.02}$
T7	238	MASU	48.2	12.3	12.7	6.2	20.6	100.0	$(Ni_{0.39}Co_{0.40}Fe_{0.21})_{\Sigma 1.00}As_{1.00}S_{1.00}$
T8	238	MASU	47.5	8.3	16.6	6.0	21.6	100.0	$(Ni_{0.27}Co_{0.53}Fe_{0.20})_{\Sigma 1.00}As_{0.97}S_{1.03}$
T8	238	MASU	47.4	8.1	18.2	5.0	21.4	100.0	$(Ni_{0.26}Co_{0.58}Fe_{0.17})_{\Sigma 1.00}As_{0.97}S_{1.03}$
T8	238	MASU	40.8	11.7	15.8	7.8	24.0	100.0	$(Ni_{0.33}Co_{0.44}Fe_{0.23})_{\Sigma 1.00}As_{0.84}S_{1.16}$
T8	238	MASU	47.4	8.5	16.7	5.9	21.6	100.0	$(Ni_{0.27}Co_{0.53}Fe_{0.20})_{\Sigma 1.00}As_{0.97}S_{1.03}$
T6	238	MASU	47.8	8.9	15.4	6.3	21.6	100.0	$(Ni_{0.29}Co_{0.50}Fe_{0.21})_{\Sigma 1.00}As_{0.97}S_{1.03}$
T6	238	MASU	48.1	10.0	14.6	6.6	20.7	100.0	$(Ni_{0.32}Co_{0.46}Fe_{0.22})_{\Sigma 1.00}As_{1.00}S_{1.00}$
T6	238	MASU	47.9	10.5	13.0	6.8	21.8	100.0	$(Ni_{0.34}Co_{0.42}Fe_{0.23})_{\Sigma 1.00}As_{0.97}S_{1.03}$
T6	238	MASU	48.7	10.9	12.7	7.7	20.0	100.0	$(Ni_{0.35}Co_{0.40}Fe_{0.25})_{\Sigma 1.00}As_{1.02}S_{0.98}$
T6	238	MASU	46.7	10.8	15.5	5.9	21.2	100.0	$(Ni_{0.33}Co_{0.48}Fe_{0.19})_{\Sigma 1.00}As_{0.97}S_{1.03}$
T2	238	MASU	46.2	11.1	15.3	6.1	21.4	100.0	$(Ni_{0.34}Co_{0.47}Fe_{0.20})_{\Sigma 1.00}As_{0.96}S_{1.04}$
T2	238	MASU	46.3	11.3	16.0	4.9	21.5	100.0	$(Ni_{0.35}Co_{0.49}Fe_{0.16})_{\Sigma 1.00}As_{0.96}S_{1.04}$
T2	238	MASU	46.8	13.1	14.2	4.2	21.8	100.0	$(Ni_{0.41}Co_{0.45}Fe_{0.14})_{\Sigma 1.00}As_{0.96}S_{1.04}$
T2	238	MASU	45.4	11.7	14.8	5.8	22.4	100.0	$(Ni_{0.36}Co_{0.45}Fe_{0.19})_{\Sigma 1.00}As_{0.93}S_{1.07}$
T2	238	MASU	46.8	12.7	13.9	4.7	21.9	100.0	$(Ni_{0.40}Co_{0.44}Fe_{0.16})_{\Sigma 1.00}As_{0.95}S_{1.05}$
TU3	238	MASU	47.5	11.5	15.6	4.5	21.0	100.0	$(Ni_{0.36}Co_{0.49}Fe_{0.15})_{\Sigma 1.00}As_{0.98}S_{1.02}$
TU3	238	MASU	46.4	12.9	13.9	5.2	21.6	100.0	$(Ni_{0.40}Co_{0.43}Fe_{0.17})_{\Sigma 1.00}As_{0.96}S_{1.04}$
TU3	238	MASU	47.4	11.6	14.6	4.9	21.5	100.0	$(Ni_{0.37}Co_{0.46}Fe_{0.16})_{\Sigma 1.00}As_{0.97}S_{1.03}$
TU6	238	MASU	46.8	10.9	15.8	6.6	20.1	100.0	$(Ni_{0.32}Co_{0.47}Fe_{0.21})_{\Sigma 1.00}As_{1.00}S_{1.00}$
TU6	238	MASU	46.8	12.3	12.8	7.1	21.0	100.0	$(Ni_{0.38}Co_{0.39}Fe_{0.23})_{\Sigma 1.00}As_{0.98}S_{1.02}$
TU6	238	MASU	45.8	7.5	21.6	4.4	20.7	100.0	$(Ni_{0.22}Co_{0.64}Fe_{0.14})_{\Sigma 1.00}As_{0.97}S_{1.03}$
TU6	238	MASU	45.8	7.8	20.2	5.4	20.8	100.0	$(Ni_{0.23}Co_{0.60}Fe_{0.17})_{\Sigma 1.00}As_{0.97}S_{1.03}$
TU13	238	MASU	46.3	18.6	9.3	4.8	21.0	100.0	$(Ni_{0.57}Co_{0.28}Fe_{0.15})_{\Sigma 1.00}As_{0.97}S_{1.03}$
TU13	238	MASU	46.5	12.8	14.5	5.2	21.0	100.0	$(Ni_{0.39}Co_{0.44}Fe_{0.17})_{\Sigma 1.00}As_{0.97}S_{1.03}$
TU13	238	MASU	46.5	14.2	12.3	5.5	21.5	100.0	$(Ni_{0.44}Co_{0.38}Fe_{0.18})_{\Sigma 1.00}As_{0.96}S_{1.04}$
TU13	238	MASU	46.0	14.8	11.8	6.7	20.6	100.0	$(Ni_{0.44}Co_{0.35}Fe_{0.21})_{\Sigma 1.00}As_{0.98}S_{1.02}$
T3	238	MASU	43.8	16.9	11.6	4.9	22.9	100.0	$(Ni_{0.50}Co_{0.34}Fe_{0.15})_{\Sigma 1.00}As_{0.90}S_{1.10}$
TU16B	238	DISS	46.7	11.9	14.8	5.1	21.6	100.0	$(Ni_{0.37}Co_{0.46}Fe_{0.17})_{\Sigma 1.00}As_{0.96}S_{1.04}$
TU16B	238	DISS	46.9	15.0	11.5	5.5	21.2	100.0	$(Ni_{0.47}Co_{0.35}Fe_{0.18})_{\Sigma 1.00}As_{0.97}S_{1.03}$
TU16B	238	DISS	46.8	11.5	13.3	7.6	20.8	100.0	$(Ni_{0.35}Co_{0.40}Fe_{0.24})_{\Sigma 1.00}As_{0.98}S_{1.02}$
TU16B	238	DISS	45.2	10.1	14.6	8.5	21.6	100.0	$(Ni_{0.30}Co_{0.43}Fe_{0.27})_{\Sigma 1.00}As_{0.94}S_{1.06}$
TU16B	238	DISS	47.2	12.5	13.5	5.2	21.6	100.0	$(Ni_{0.40}Co_{0.43}Fe_{0.17})_{\Sigma 1.00}As_{0.97}S_{1.03}$
T21	238	DISS	48.2	16.9	8.5	6.1	20.4	100.0	$(Ni_{0.53}Co_{0.27}Fe_{0.20})_{\Sigma 1.00}As_{1.01}S_{0.99}$
T21	238	DISS	50.0	16.6	7.8	5.7	20.0	100.0	$(Ni_{0.55}Co_{0.26}Fe_{0.20})_{\Sigma 1.00}As_{1.03}S_{0.97}$
T21	238	DISS	46.1	19.5	6.0	6.7	21.8	100.0	$(Ni_{0.60}Co_{0.18}Fe_{0.22})_{\Sigma 1.00}As_{0.95}S_{1.05}$
T21	238	DISS	47.9	20.3	5.0	6.2	20.6	100.0	$(Ni_{0.64}Co_{0.16}Fe_{0.21})_{\Sigma 1.00}As_{1.00}S_{1.00}$
T21	238	DISS	47.3	13.5	10.5	7.1	21.7	100.0	$(Ni_{0.43}Co_{0.33}Fe_{0.24})_{\Sigma 1.00}As_{0.97}S_{1.03}$
TU4B	238	DISS	42.7	21.7	12.9	7.4	15.3	100.0	$(Ni_{0.51}Co_{0.30}Fe_{0.18})_{\Sigma 1.00}As_{1.09}S_{0.91}$
TU4B	238	DISS	44.5	8.7	18.1	4.5	24.2	100.0	$(Ni_{0.28}Co_{0.57}Fe_{0.15})_{\Sigma 1.00}As_{0.88}S_{1.12}$
TU4B	238	DISS	46.5	12.5	13.4	5.6	22.2	100.0	$(Ni_{0.39}Co_{0.42}Fe_{0.18})_{\Sigma 1.00}As_{0.95}S_{1.05}$
TU21	238	DISS	43.3	18.6	9.8	5.6	22.7	100.0	$(Ni_{0.54}Co_{0.28}Fe_{0.17})_{\Sigma 1.00}As_{0.90}S_{1.10}$
TU21	238	DISS	42.6	20.2	8.1	6.0	23.0	100.0	$(Ni_{0.58}Co_{0.23}Fe_{0.18})_{\Sigma 1.00}As_{0.88}S_{1.12}$
TU21	238	DISS	41.5	17.3	12.3	5.7	23.2	100.0	$(Ni_{0.49}Co_{0.35}Fe_{0.17})_{\Sigma 1.00}As_{0.87}S_{1.13}$
TU21	238	DISS	43.6	20.4	8.7	4.7	22.7	100.0	$(Ni_{0.60}Co_{0.26}Fe_{0.14})_{\Sigma 1.00}As_{0.90}S_{1.10}$
T10	Main	MASU	44.8	11.2	12.6	8.9	22.6	100.0	$(Ni_{0.34}Co_{0.38}Fe_{0.28})_{\Sigma 1.00}As_{0.92}S_{1.08}$
T10	Main	MASU	47.5	12.8	14.0	5.0	20.8	100.0	$(Ni_{0.40}Co_{0.44}Fe_{0.16})_{\Sigma 1.00}As_{0.99}S_{1.01}$
T10	Main	MASU	46.8	11.5	14.9	5.4	21.4	100.0	$(Ni_{0.36}Co_{0.46}Fe_{0.18})_{\Sigma 1.00}As_{0.97}S_{1.03}$
T10	Main	MASU	47.3	14.1	13.1	4.3	21.1	100.0	$(Ni_{0.45}Co_{0.41}Fe_{0.14})_{\Sigma 1.00}As_{0.98}S_{1.02}$

Notes: Atomic formula calculated on the basis of 3 atoms

A9 (continued): EDS analyses of sulfarsenides (wt%)

Sample	Ore Body	Ore type	As	Ni	Co	Fe	S	Total	Atomic formula
T17	Main	MASU	47.2	10.2	15.1	6.6	20.9	100.0	$(Ni_{0.32}Co_{0.47}Fe_{0.22})_{\Sigma 1.00}As_{0.98}S_{1.02}$
T17	Main	MASU	48.1	11.8	13.9	4.7	21.5	100.0	$(Ni_{0.39}Co_{0.45}Fe_{0.16})_{\Sigma 1.00}As_{0.98}S_{1.02}$
T17	Main	MASU	46.5	10.4	14.9	6.6	21.5	100.0	$(Ni_{0.32}Co_{0.46}Fe_{0.22})_{\Sigma 1.00}As_{0.96}S_{1.04}$
T17	Main	MASU	45.5	14.7	9.9	7.6	22.3	100.0	$(Ni_{0.45}Co_{0.30}Fe_{0.25})_{\Sigma 1.00}As_{0.93}S_{1.07}$
T233C	Main	MASU	47.7	10.7	16.2	4.3	21.1	100.0	$(Ni_{0.34}Co_{0.51}Fe_{0.15})_{\Sigma 1.00}As_{0.98}S_{1.02}$
T144	Main	MASU	41.3	10.4	18.2	6.0	24.1	100.0	$(Ni_{0.30}Co_{0.52}Fe_{0.18})_{\Sigma 1.00}As_{0.85}S_{1.15}$
T152B	Main	MASU	48.3	10.8	14.9	5.5	20.6	100.0	$(Ni_{0.34}Co_{0.47}Fe_{0.18})_{\Sigma 1.00}As_{1.00}S_{1.00}$
T15	Main	INMS	47.2	11.7	14.3	5.3	21.5	100.0	$(Ni_{0.37}Co_{0.45}Fe_{0.18})_{\Sigma 1.00}As_{0.97}S_{1.03}$
T15	Main	INMS	46.9	13.6	12.9	5.3	21.4	100.0	$(Ni_{0.43}Co_{0.40}Fe_{0.17})_{\Sigma 1.00}As_{0.97}S_{1.03}$
T15	Main	INMS	48.5	11.7	13.1	6.1	20.7	100.0	$(Ni_{0.37}Co_{0.42}Fe_{0.21})_{\Sigma 1.00}As_{1.00}S_{1.00}$
T15	Main	INMS	47.7	8.9	15.5	5.7	22.3	100.0	$(Ni_{0.29}Co_{0.51}Fe_{0.20})_{\Sigma 1.00}As_{0.96}S_{1.04}$
T145	Main	INMS	47.7	11.3	14.4	5.7	21.0	100.0	$(Ni_{0.36}Co_{0.45}Fe_{0.19})_{\Sigma 1.00}As_{0.98}S_{1.02}$
T157	Main	INMS	33.6	15.2	13.7	10.3	27.1	100.0	$(Ni_{0.38}Co_{0.34}Fe_{0.27})_{\Sigma 1.00}As_{0.69}S_{1.31}$
T164	Main	INMS	41.4	13.3	15.1	6.8	23.4	100.0	$(Ni_{0.38}Co_{0.42}Fe_{0.20})_{\Sigma 1.00}As_{0.86}S_{1.14}$
T164	Main	INMS	38.7	11.7	16.5	8.4	24.7	100.0	$(Ni_{0.32}Co_{0.44}Fe_{0.24})_{\Sigma 1.00}As_{0.80}S_{1.20}$
T164	Main	INMS	41.5	11.2	16.4	7.4	23.5	100.0	$(Ni_{0.32}Co_{0.46}Fe_{0.22})_{\Sigma 1.00}As_{0.86}S_{1.14}$
T191	Main	INMS	39.9	11.0	16.2	8.0	25.0	100.0	$(Ni_{0.31}Co_{0.46}Fe_{0.24})_{\Sigma 1.00}As_{0.81}S_{1.19}$
T193	Main	INMS	46.5	18.5	8.1	6.9	20.0	100.0	$(Ni_{0.55}Co_{0.24}Fe_{0.22})_{\Sigma 1.00}As_{1.00}S_{1.00}$
T193	Main	INMS	43.0	15.1	11.1	9.2	21.7	100.0	$(Ni_{0.42}Co_{0.31}Fe_{0.27})_{\Sigma 1.00}As_{0.92}S_{1.08}$
TU31B	Main	INMS	42.2	17.8	11.2	5.8	23.0	100.0	$(Ni_{0.51}Co_{0.32}Fe_{0.17})_{\Sigma 1.00}As_{0.88}S_{1.12}$
TU31B	Main	INMS	42.9	20.2	8.9	6.1	22.0	100.0	$(Ni_{0.57}Co_{0.25}Fe_{0.18})_{\Sigma 1.00}As_{0.91}S_{1.09}$
TU31B	Main	INMS	42.3	18.6	10.2	5.2	23.7	100.0	$(Ni_{0.54}Co_{0.30}Fe_{0.16})_{\Sigma 1.00}As_{0.87}S_{1.13}$
TU31B	Main	INMS	42.8	18.9	10.2	4.5	23.6	100.0	$(Ni_{0.56}Co_{0.30}Fe_{0.14})_{\Sigma 1.00}As_{0.87}S_{1.13}$
TU31B	Main	INMS	38.2	18.4	12.7	5.0	25.8	100.0	$(Ni_{0.51}Co_{0.35}Fe_{0.15})_{\Sigma 1.00}As_{0.78}S_{1.22}$
T142	Main	INMS	42.77	14.56	14.04	4.59	24.05	100.0	$(Ni_{0.44}Co_{0.42}Fe_{0.14})_{\Sigma 1.00}As_{0.86}S_{1.14}$
T142	Main	INMS	41.5	23.8	5.6	6.1	23.0	100.0	$(Ni_{0.67}Co_{0.16}Fe_{0.18})_{\Sigma 1.00}As_{0.87}S_{1.13}$
T142	Main	INMS	38.3	16.1	12.4	6.9	26.2	100.0	$(Ni_{0.45}Co_{0.35}Fe_{0.20})_{\Sigma 1.00}As_{0.77}S_{1.23}$
T34	Main	DISS	47.1	15.8	10.6	5.6	21.0	100.0	$(Ni_{0.49}Co_{0.33}Fe_{0.18})_{\Sigma 1.00}As_{0.98}S_{1.02}$
T34	Main	DISS	47.3	17.1	9.6	4.5	21.5	100.0	$(Ni_{0.54}Co_{0.31}Fe_{0.15})_{\Sigma 1.00}As_{0.97}S_{1.03}$
T34	Main	DISS	47.5	18.6	7.4	5.2	21.2	100.0	$(Ni_{0.59}Co_{0.23}Fe_{0.17})_{\Sigma 1.00}As_{0.98}S_{1.02}$
T34	Main	DISS	47.9	23.9	4.3	3.2	20.7	100.0	$(Ni_{0.76}Co_{0.14}Fe_{0.11})_{\Sigma 1.00}As_{0.99}S_{1.01}$
T34	Main	DISS	47.7	17.6	8.6	5.0	21.1	100.0	$(Ni_{0.56}Co_{0.27}Fe_{0.17})_{\Sigma 1.00}As_{0.98}S_{1.02}$
T44	Main	DISS	47.2	11.3	15.4	5.4	20.8	100.0	$(Ni_{0.35}Co_{0.47}Fe_{0.17})_{\Sigma 1.00}As_{0.98}S_{1.02}$
T44	Main	DISS	46.6	11.5	14.9	5.6	21.3	100.0	$(Ni_{0.36}Co_{0.46}Fe_{0.18})_{\Sigma 1.00}As_{0.97}S_{1.03}$
T44	Main	DISS	45.9	13.9	13.1	5.3	21.8	100.0	$(Ni_{0.43}Co_{0.40}Fe_{0.17})_{\Sigma 1.00}As_{0.95}S_{1.05}$
T44	Main	DISS	46.8	9.6	15.8	6.6	21.3	100.0	$(Ni_{0.30}Co_{0.49}Fe_{0.21})_{\Sigma 1.00}As_{0.97}S_{1.03}$
T44	Main	DISS	46.8	10.4	15.3	6.4	21.1	100.0	$(Ni_{0.32}Co_{0.47}Fe_{0.21})_{\Sigma 1.00}As_{0.97}S_{1.03}$
T29	Main	DISS	47.8	12.2	13.8	4.9	21.3	100.0	$(Ni_{0.39}Co_{0.44}Fe_{0.17})_{\Sigma 1.00}As_{0.98}S_{1.02}$
T29	Main	DISS	47.7	10.1	13.4	5.6	23.2	100.0	$(Ni_{0.35}Co_{0.46}Fe_{0.20})_{\Sigma 1.00}As_{0.94}S_{1.06}$
T29	Main	DISS	46.9	9.2	16.1	6.1	21.7	100.0	$(Ni_{0.29}Co_{0.51}Fe_{0.20})_{\Sigma 1.00}As_{0.96}S_{1.04}$
T29	Main	DISS	46.1	10.1	14.0	7.6	22.2	100.0	$(Ni_{0.32}Co_{0.44}Fe_{0.25})_{\Sigma 1.00}As_{0.94}S_{1.06}$
T29	Main	DISS	45.6	10.6	16.2	5.5	22.0	100.0	$(Ni_{0.33}Co_{0.50}Fe_{0.18})_{\Sigma 1.00}As_{0.94}S_{1.06}$
T226	Main	DISS	45.9	16.3	11.6	5.5	20.7	100.0	$(Ni_{0.48}Co_{0.34}Fe_{0.17})_{\Sigma 1.00}As_{0.97}S_{1.03}$
TU32	Main	DISS	42.6	6.1	22.6	5.0	23.7	100.0	$(Ni_{0.18}Co_{0.67}Fe_{0.15})_{\Sigma 1.00}As_{0.87}S_{1.13}$
TU32	Main	DISS	42.3	6.0	23.7	5.0	23.1	100.0	$(Ni_{0.17}Co_{0.68}Fe_{0.15})_{\Sigma 1.00}As_{0.88}S_{1.12}$
TU32	Main	DISS	42.0	7.8	22.1	4.5	23.8	100.0	$(Ni_{0.23}Co_{0.64}Fe_{0.14})_{\Sigma 1.00}As_{0.86}S_{1.14}$
TU32	Main	DISS	41.8	7.2	23.5	4.3	23.2	100.0	$(Ni_{0.20}Co_{0.67}Fe_{0.13})_{\Sigma 1.00}As_{0.87}S_{1.13}$
TU32	Main	DISS	44.9	21.3	5.3	5.8	22.7	100.0	$(Ni_{0.65}Co_{0.16}Fe_{0.19})_{\Sigma 1.00}As_{0.92}S_{1.08}$
T134	N/A	DISS	46.9	12.4	13.8	5.1	21.8	100.0	$(Ni_{0.39}Co_{0.44}Fe_{0.17})_{\Sigma 1.00}As_{0.96}S_{1.04}$
T134	N/A	DISS	47.7	17.0	10.8	3.8	20.6	100.0	$(Ni_{0.53}Co_{0.34}Fe_{0.13})_{\Sigma 1.00}As_{0.99}S_{1.01}$
T134	N/A	DISS	31.7	7.5	11.4	18.4	31.0	100.0	$(Ni_{0.20}Co_{0.30}Fe_{0.51})_{\Sigma 1.00}As_{0.61}S_{1.39}$
T143	N/A	DISS	42.8	14.6	14.0	4.6	24.1	100.0	$(Ni_{0.44}Co_{0.42}Fe_{0.14})_{\Sigma 1.00}As_{0.86}S_{1.14}$

Notes: Atomic formula calculated on the basis of 3 atoms

A10: Quantitative mass balance of samples from the Totten #2 Mine

Sample	Location	Ore Body	Ore Type	Distribution of metals between major and trace pahses	Discrete phase description
T10	DH: 1265340 683.5'	MOB	MASU	Ni: Po (17%), Pn (81%), CGSS (2%) As: Cp (1.7%), Nic (0.1%), CGSS (96.9%), Spr (1.3%) Pt: CGSS (0.2%), Spr (99.8%) Pd: Po (0.1%), Pn (0.9%), CGSS (99%) Pb: Po (7.2%), Cp (0.1%), Pn (15.8 %), CGSS (0.1%), Gn (76.8%) Co: Po (4%), Pn (55.5%), CGSS (40.5%)	CGSS: Typically forms subhedral-euhedral crystals in BMS and, more rarely, in Sg. May contain inclusions of Nic and Tsu, Cp sometimes occurs as fracture infillings (30μm^2-1mm^2, 3185μm^2 average). Gn: Anhedral inclusions in BMS, less commonly rims CGSS in contact with silicates (8-625μm^2, 57μm^2 average). Hes: Anhedral grains hosted within Po and Pn (3-200μm^2, 29μm^2 average). Nic: A single anhedral inclusion (sieve infill) in CGSS (1500μm^2). Spr: Anhedral-subhedral grains in Po, may be rimmed by Pb-Bi-Te phases (8800-14400μm^2, 11257μm^2). Tsu: Anhedral inclusions in BMS or Sg, appears to infill fractures and vugs in host. May rim CGSS and Spr (4-70000μm^2, 617μm^2 average).
T34	DH: 1265340 698'	MOB	DISS	Ni: Po (4.5%), Cp (0.1%), Pn (13.9%), Nic (47.3%), CGSS (34.2%) As: Nic (34.5%), CGSS (65.5%) Pt: Po (0.1%), Cp (0.8%), Nic (0.1%), CGSS (99%) Pd: Po (0.2%), Cp (1%), Pn (0.1%), Nic (0.2%), CGSS (98.5%) Pb: Po (0.7%), Cp (2.3%), CGSS (0.2%), Gn (96.8%) Co: Po (0.3%), Pn (1.1%), Nic (0.5%), CGSS (98.1%)	CGSS: Euhedral-subhedral grains in BMS, Nic, and Sg, grains typically found in the margins of BMS/Nic veins and blebs, fractures and sieves are infilled by these same minerals (117-478686μm^2, 49541μm^2 average). Gn: Anhedral inclusion which infill fracure in BMS, Nic, CGSS, Sg, and may rim CGSS grains (9-256μm^2, 41μm^2 average). Hes: Anhedral inclusion which infill fracure in BMS, Nic, CGSS, Sg (4-120μm^2, 20μm^2 average). Nic: Anhedral grains confined to a quartz-sulfide vein or sulfide blebs adjcent to this vein. may contain inclusions of BMS, CGSS, and Sg (144-542400μm^2, 13435μm^2 average). Pil: Anhedral inclusions which infill fractures and vugs in BMS, Nic, and Sg (13.5-28μm^2, 19μm^2 average). Tel: An anhedral inclusion in Nic (12.25μm^2, 1 grain). Tsu: Anhedral inclusions in Nic and CGSS (4-25μm^2, 9μm^2 average). Ung: Anhedral inclusions in Nic and CGSS (49-264μm^2, 108μm^2 average).
T44	DH: 1265900 551'	MOB	DISS	Ni: Po (2%), Pn (98%) As: Pn (2.9%), CGSS (97.1%) Pt: Po (2.3%), Cp (6.3%), Pn (9.7%), CGSS (2.5%), Spr (79.2) Pd: Po (0.1), Cp (7.1%), Pn (85%), CGSS (5.6%), Frd (0.3%), Mch (1.9%) Pb: Po (2.4%), Cp (20%), Pn (1%), CGSS (0.2%), Gn (76.4%) Co: Po (1.5%), Pn (97.8%), CGSS (0.7%)	Alt: An anhedral inclusion in Cp (0.3μm^2, 1 grain). CGSS: Euhedral-subhedral inclusions in the BMS and Sg, may contain Ir-Hol cores (20-3248μm^2, 292μm^2 average). Frd: Anhedral inclusions in Po, Cp, and Sg (5-36μm^2, 18μm^2 average). Gn: Anhedral inclusions in BMS and Sg, may rim CGSS grains (0.09-84μm^2, 11μm^2 average). Hed: An anhedral inclusion in Sg (2.25μm^2, 1 grain). Hes: An anhedral inclusion in Pn (12μm^2, 1 grain). Ir-Hol: A small inclusion in CGSS (0.45μm^2, 1 grain). Mch: Anhedral inclusions in the BMS (0.09-72μm^2, 8μm^2 average). Spr: Anhedral inclusions in Sg and Po (48-121μm^2, 85μm^2 average). Ung: Anhedral inclusion in Po which infills a fracture (4.2μm^2, 1 grain).
TU18B	Level: 1850 -878(X), 21996(Y), 10998(Z)	MOB	MASU	Ni: Po (12.7%), Pn (87.3%) As: Po (49%), Cp (1%), Pn (50%) Pt: Po (52.4%), Cp (3.5%), Pn (44.1%) Pd: Po (15.8%), Cp (19.5%), Pn (64.7%) Pb: Cp (0.1%), Pn (0.7%), Gn (99.2%) Co: Po (7.5%), Pn (92.5%)	Gn: Anhedral inclusions in BMS, which may infill fractures and vugs (0.04-10500μm^2, 972μm^2 average). Tsu: Anhedral inclusions in BMS, most commonly in Po (0.01-20000μm^2, 234μm^2).
T15	DH: 1265420 664.5'	MOB	INMS	Ni: Po (2.8%), Pn (97.2%) As: Po (0.2%), Pn (5.5%), CGSS (94.3%) Pt: Po (17.5%), Cp (15.7%), Pn (60.5%), CGSS (6.3%) Pd: Po (3.7%), Cp (8.5%), Pn (78.3%), CGSS (5.9%), Mch (3.6%) Pb: Po (2.6%), Cp (12%), Pn (41.9%), Gn (43.4%), Alt (0.1%) Co: Po (1.4%), Pn (98.4%), CGSS (0.2%)	Alt: Anhedral inclusion in Sg immediately adjacent to sulfides (11μm^2, 1 grain) CGSS: Subhedral-euhedral inclusions in BMS, may shares fractures with its host (4-1548μm^2, 420μm^2 average). Gn: Anhedral inclusions within BMS or along BMS-Sg boundary, infills fractures (2-1294μm^2, 153μm^2 average). Hes: Anhedral inclusions in Pn, Cp (3-6μm^2, 4μm^2 average) Tel: Anhedral inclusions in BMS and Sg immediately adjacent to sulfides (4-2220μm2, 250μm^2). Ir-Hol: Anhedral inclusions found at the center of CGSS (0.8-24μm^2, 8μm^2 average). Mch: Anhedral inclusion along the boundary of Po/Sg (120μm^2, 1 grain).

Notes: Percentages represent the proportion of the total metal content of each sample that is associated with each mineral phase. Abbreviations: massive sulfide (MASU), semi-massive sulfide (INMS), disseminated sulfide (DISS), pyrrhotite (Po), pentlandite (Pn), chalcopyrite (Cp), altaite (Alt), galena (Gn), tellurobismuthite (Tel), tsumoite (Tsu),hessite (Hes), electrum (El), sperrylite (Spr), michenerite (Mch), froodite (Frd), ungavaite (Ung), molybdenite (Mo), sulfarsenide solid solution (CGSS), silicate gangue (Sg), base metal sulfides (BMS), nickeline (Nic), platinum-group minerals (PGM), pilsenite (Pil), and hedleyite (Hed).

A10 (continued): Quantitative mass balance of samples from the Totten #2 Mine

Sample	Location	Ore Body	Ore Type	Distribution of metals between major and trace pahses	Discrete phase description
T29	DH: 1265900 567'	MOB	DISS	Ni: Po (9.7%), Cp (0.1%), Pn (90.1%), CGSS (0.1%) As: Pn (0.7%), CGSS (0.5%), Spr (7.4%), CGSS (91.4%) Pt: Spr (100%) Pd: Po (0.2%), Cp (1.5%), Pn (1.4%), CGSS (0.8%), Frd (18.8%), Mch (77.3%) Pb: Po (0.5%), Cp (5.5%), Pn (2%), Gn (91.8%), Alt (0.2%) Co: Po (4.9%), Pn (93.2%), CGSS (1.9%)	Alt: An anhedral inclusion along Cp/Sg boundary (5μm^2, 1 grain). El: Anhedral inclusions in Sg (24-99μm^2, 43μm^2 average). CGSS: Subhedral-euhedral inclusions in BMS which may demonstrate sieve texture, or may be rimed by Gn (1-95μm^2, 20μm^2 average). Frd: Anhedral inclusions in Sg, adjacent to sulfide blebs (10-36μm^2, 24μm^2 average). Gn: Anhedral inclusions, which may infill fractures in BMS and CGSS; rims CGSS (1-95μm^2, 20μm^2 average). Ir-Hol: Subhedral inclusions in Cp, or more commonly as anhedral inclusions at the center of CGSS (2-5μm^2, 3μm^2 average). Mch: Anhedral inclusions in Sg, adjacent to sulfide blebs (3-256μm^2, 122μm^2 average). Spr: A subhedral inclusion in Sg, adjacent to sulfide blebs (230μm^2, 1 grain). Tel: Anhedral inclusions in BMS and Sg; infills fractures within BMS and rims CGSS (3-119μm^2, 25μm^2 average). Tsu: Anhedral inclusions in Sg or Cp (6-18μm^2, 17μm^2 average).
T33	DH: 1265900 669'	MOB	DISS	Ni: Po (3.5%), Pn (96.5%) As: Po (0.9%), Cp (1.6%), Pn (38.5%), Spr (59%) Pt: Cp (0.3%), Pn (0.1%), Spr (99.6%) Pd: Po (0.1%), Cp (1.7%), Pn (1.6%), Frd (87%), Mch (9.6%) Pb: Po (0.3%), Cp (8.1%), Pn (2.8%), Gn (88.8%) Co: Po (1.7%), Cp (0.1%), Pn (98.2%)	El: Anhedral inclusions in Pn and Sg (3-6μm^2, 4μm^2 average). Frd: Anhedral inclusions within BMS or adjacent to sulfide blebs (16-188μm^2, 87μm^2 average). Gn: Anhedral inclusions in BMS and Sg; infills fractures BMS (2-283μm^2, 29μm^2 average). Mch: Anhedral inclusions in Sg, adjacent to sulfide blebs (2-28μm^2, 11μm^2 average). Spr: An anhedral inclusion along Cp/Sg boundary (71μm^2, 1 grain). Tel: Anhedral inclusions in Cp and Sg; Sg occurences are immediately adjacent to sulfides (2-203μm^2, 58μm^2 average). Tsu: Anhedral inclusions in Cp and Sg adjacent to sulfides (85-384μm^2, 189μm^2 average).
T141	DH: 1265980 1217'11"-1218'1"	MOB	INMS	Ni: Po (2.9%), Pn (97.1%) As: Po (0.1%), Pn (7%), Nic (6.9%), Spr (85.8%), CGSS (0.2%) Pt: Spr (100%) Pd: Po (4.7%), Cp (0.8%), Pn (94.5%) Pb: Po (5.5%), Cp (1.7%), Pn (84.2%), Gn (8.7%) Co: Po (1.5%), Pn (98.5%)	CGSS: Subhedral inclusion in Pn (13μm^2, 1 grain). Gn: Anhedral inclusions which infill fractures in BMS (6-56μm^2, 20μm^2 average). Hed: Anhedral inclusions in Po (12-64μm^2, 38μm^2 average). Hes: Anhedral inclusions in Po (12-84μm^2, 41μm^2 average). Mo: Subhedral lathes in Po (83-1852μm^2, 767μm^2 average). Nic: Anhedral inclusions in Po (34-313μm^2, 133μm^2 average). Pil: Anhedral inclusions which infill fractures and vugs in BMS and Sg (11-3117μm^2, 428μm^2). Spr: Anhedral inclusions in Po (837-16103μm^2, 5956μm^2 average). Tel: Anhedral inclusions in Po (7-36μm^2, 22μm^2 average). Tsu: Anhedral inclusions in BMS and Sg (89-434μm^2, 257μm^2 average).
T142	DH: 1265980 1222'4"-6"	MOB	INMS	Ni: Po (7.7%), Pn (92.3%) As: Po (0.4%), Pn (8.1%), Nic (22.1%), Spr (28%), CGSS (41.4%) Pt: Pn (0.1%), Spr (99.9%) Pd: Po (4.8%), Cp (2.9%), Pn (34.3%), CGSS (0.8%), Frd (57.2%) Pb: Po (7.7%), Cp (9.6%), Pn (42.9%), Gn (39.8%) Co: Po (4%), Pn (96%)	CGSS: Euhedral-anhedral inclusions in BMS and Sg immediately adjacent to sulfides; may demonstrate sieve texture with infill by BMS and other discrete phases (85-1414μm^2, 433μm^2 average). El: An anhedral inclusion in Sg (30μm^2, 1 grain). Gn: Anhedral inclusions in BMS and CGSS which may infill fractures and vugs; may form composite grains with Hes and Tel (2-150μm^2, 29μm^2 average). Hed: An anhedral inclusion in Sg (290μm^2, 1 grain). Hes: Anhedral inclusions in Pn, may infill fractures and vugs; forms composite grains with Gn (28-33μm^2, 31μm^2 average). Mo: Subhedral lathe along the boundary between Pn and Sg; fractures in Mo infilled by Tsu (90μm^2, 1 grain). Nic: Anhedral inclusions in Po (12-1020μm^2, 283μm^2 average). Pil: Anhedral inclusions in BMS and Sg, may infill fractures and vugs (29-369μm^2, 140μm^2 average). Spr: A subhedral inclusion in Sg adjacent to BMS (1462μm^2, 1 grain). Tel: Anhedral inclusions in BMS and Sg, may infill fractures and form composite grains with Gn (5-5534µm2, 1853µm2 average). Tsu: Anhedral inclusions in BMS and Sg, may infill fractures and vugs; can form composite grains with Gn (15-2310μm^2, 227μm^2).
T147	DH: 971512 3274'2.5"-3275'1"	MOB	INMS	Ni: Po (16.8%), Pn (83.2%) As: Po (0.6%), Pn (4.7%), CGSS (94.7%) Pt: Po (62.8%), Cp (2.5%), Pn (30.9%), CGSS (3.8%) Pd: Po (22.8%), Cp (2.3%), Pn (68.6%), CGSS (6.3%) Pb: Po (27.5%), Cp (5.7%), Pn (63.4%), Gn (3.4%) Co: Po (9%), Pn (90.8%), CGSS (0.3%)	CGSS: Subhedral-anhedral inclusions in BMS and Sg, which may be rimmed by Hes and contain Ir-Hol cores (0.5-2092μm^2, 479μm^2 average). Gn: An anhedral inclusion along the boundary of Po and Sg (38μm^2, 1 grain). Hes: Anhedral inclusions in BMS and Sg, which may infill fractures (2-1407μm^2, 744μm^2 average). Ir-Hol: Anhedral inclusions in BMS (761-3349μm^2, 1885μm^2 average). Tel: Anhedral inclusions infilling fractures in Po/Pn (1545-11453μm^2, 6499μm^2 average). Tsu: Anhedral inclusion infilling fractures in Pn/Po (1210-5357μm^2, 1741μm^2).

Notes: Percentages represent the proportion of the total metal content of each sample that is associated with each mineral phase. Abbreviations: massive sulfide (MASU), semi-massive sulfide (INMS), disseminated sulfide (DISS), pyrrhotite (Po), pentlandite (Pn), chalcopyrite (Cp), altaite (Alt), galena (Gn), tellurobismuthite (Tel), tsumoite (Tsu),hessite (Hes), electrum (El), sperrylite (Spr), michenerite (Mch), froodite (Frd), ungavaite (Ung), molybdenite (Mo), sulfarsenide solid solution (CGSS), silicate gangue (Sg), base metal sulfides (BMS), nickeline (Nic), platinum-group minerals (PGM), pilsenite (Pil), and hedleyite (Hed).

A10 (continued): Quantitative mass balance of samples from the Totten #2 Mine

Sample	Location	Ore Body	Ore Type	Distribution of metals between major and trace pahses	Discrete phase description
T143	DH: 1265980 1203'7.5"-9.5"	MOB	MASU	**Ni:** Po (4.9%), Cp (0.1%), Pn (94.7%), CGSS (0.3%) **As:** Pn (0.2%), Nic (5.2%), CGSS (88%), Spr (6.6%) **Pt:** CGSS (0.1%), Spr (99.9%) **Pd:** Po (0.5%), Cp (10.4%), Pn (5.4%), CGSS (9.2%), Frd (74.5%) **Pb:** Po (0.8%), Cp (36.4%), Pn (7.3%), CGSS (0.1%), Gn (55.4%) **Co:** Po (2.4%), Pn (92.4%), CGSS (5.2%)	CGSS: Euhedral-subhedral inclusions in the BMS and Sg; may contain Ir-Hol cores (96-1363μm^2, 480μm^2 average). El: An anhedral inclusion hosted in Sg (3-30μm^2, 16.5 grain). Frd: Anhedral inclusions in BMS and Sg (12-190μm^2, 125μm^2 average). Gn: Anhedral inclusions in BMS and Sg; inclusions may infill fractures and vugs in the BMS, or form composite grains with BiTe-minerals (8-170μm^2, 40μm^2 average). Hed: An anhedral inclusion in Sg (5-54μm^2, 28μm^2 average). Hes: Anhedral inclusions in Pn and Po, usually within fractures or intergrown with Gn (28-33μm^2, 31μm^2 average). Mo: A subhedral lathe along Po-Pn boundary (84μm^2, 1 grain). Nic: Anhedral inclusions in Po (40-976μm^2, 215μm^2 average). Pil: Anhedral inclusions in BMS, Sg, and CGSS which infill vugs and fractures (18-279μm^2, 163μm^2 average). Spr: An anhedral inclusion in Po (1350μm^2, 1 grain). Tel: Anhedral inclusions which may infill fractures and vugs in BMS and show intergrowth with Gn (10-1780μm^2, 238μm^2 average). Tsu: Anhedral inclusions in BMS and Sg, may infill fractures and vugs in BMS (4-2465μm^2, 268μm^2 average).
T160	DH: 971512 3342'4"-3343'1.5"	MOB	MASU	**Ni:** Po (32.2%), Cp (7.8%), Pn (60%) **As:** Po (3%), Cp (88%), Pn (8.9%) **Pt:** Po (0.9%), Cp (98.9%), Pn (0.2%) **Pd:** Po (0.4%), Cp (99.3%), Pn (0.3%) **Pb:** Cp (1.8%), Gn (98.2) **Co:** Po (19%), Cp (8.6%), Pn (72.4%)	Gn: Anhedral inclusions in BMS and Sg, may infill fractures and vugs in BMS (49-27474μm^2, 1724μm^2 average). Hes: Anhedral inclusions in Po, may infill fractures or vugs (104-1137μm^2, 725μm^2 average). Pil: A subhedral inclusion in Po (23313μm^2, 1 grain). Tel: Anhedral inclusions in Cp, which may infill fractures and vugs (784-2520μm^2, 1485μm^2 average). Tsu: An anhedral inclusion infilling a fracture in Po (8870μm^2, 1 grain).
T180	DH: 1270880 772'6"-772'8"	MOB	MASU	**Ni:** Po (13.9%), Pn (86.1%) **As:** Po (0.2%), Pn (1.5%), CGSS (98.3%) **Pt:** Po (53.5%), Cp (0.6%), Pn (32.9%), CGSS (13%) **Pd:** Po (17%), Cp (0.5%), Pn (64.1%), CGSS (18.3%) **Pb:** Po (22.2%), Cp (1.4%), Pn (64.1%), Gn (4%), Alt (8.3%) **Co:** Po (7.3%), Pn (91.9%), CGSS (0.8%)	Alt: Anhedral inclusions which may infill fractures in Po (12-35μm^2, 21μm^2 average). CGSS: Euhedral inclusions in Po and Pn (118-1641μm^2, 1761μm^2 average). Gn: Anhedral inclusions in Po which may infill vugs and fractures (4-15μm^2, 9μm^2 average). Hes: Anhedral inclusions in Po and CGSS which may infill vugs and fractures; can form composite grains with Tel (16-2986μm^2, 628μm^2 average). Tel: Anhedral inclusions in Po and Pn, which may infill fractures and vugs and forms composite grains with hessite (13-525μm^2, 113μm^2 average). Tsu: Anhedral inclusions in Po, may infill fractures and vugs (14-2516μm^2, 1265μm^2 average).
T152A	DH: 971512 3270'7.5"-3271'5"	MOB	INMS	**Ni:** Po (12.5%), Cp (0.1%), Pn (87.4%) **As:** Po (5.9%), Cp (4.9%), Pn (64.9%), CGSS (24.3%) **Pt:** Po (20.7%), Cp (64.9%), Pn (14.4%) **Pd:** Po (7.5%), Cp (60.7%), Pn (31.8%) **Pb:** Po (4.6%), Cp (74.9)%, Pn (15%), Gn (3.4%), Alt (2.1%) **Co:** Po (6.6%), Cp (0.1%), Pn (93.3%)	Alt: An anhedral grain infilling a fracture in Po (52μm^2, 1 grain). CGSS: Subhedral inclusions in BMS (11-19μm^2, 15μm^2 average). Gn: Anhedral fracture infillings in BMS (5-63μm^2 , 34μm^2 average). Hes: Anhedral inclusions in BMS and Sg, possibly within fractures or vugs; forms composite grains with Tsu (19-88μm^2, 41μm^2 average). Tel: Anhedral inclusions in Po (26-195μm^2 , 11μm^2 average). Tsu: Anhedral inclusions in the BMS and CGSS, may infill fractures and vugs in CGSS (3-1147μm^2, 187μm^2 average).
T145	DH: 971512 3284'4.5"-3285'1"	MOB	INMS	**Ni:** Po (10.7%), Pn (89.3%) **As:** Po (0.7%), Pn (9.8%), CGSS (88.4%), Spr (1.1%) **Pt:** Po (1.7%), Cp (0.1%), Pn (1.4%), CGSS (0.1%), Spr (96.7%) **Pd:** Po (15.6%), Cp (1.8%), Pn (79.4%), CGSS (3.2%) **Pb:** Po (15.4%), Cp (3.6%), Pn (59.8%), Gn (21.3%) **Co:** Po (5.5%), Pn (94.3%), CGSS (0.2%)	CGSS: Euhedral inclusions in BMS which may be rimmed by Tsu (106-558μm^2 , 272μm^2 average). Gn: Anhedral inclusions in Sg adjacent to sulfides or less commonly in BMS (12-235μm^2 , 76μm^2 average). Hes: Anhedral inclusions in BMS which infill vugs and fractures (10-127μm^2, 68μm^2 average). Mo: A subhedral lath along the boundary between Po and Sg (308μm^2, 1 grain). Pil: An anhedral inclusion along the boundary between Po and Sg (22μm^2, 1 grain). Spr: An anhedral inclusion in Po (52μm^2, 1 grain). Tel: Anhedral inclusions in BMS which may infill fractures and vugs (16-663μm^2, 223μm^2 average). Tsu: Anhedral inclusions in BMS and Sg, may infill fractures and vugs in BMS, and rim CGSS (14-3606μm^2, 378μm^2 average).

Notes: Percentages represent the proportion of the total metal content of each sample that is associated with each mineral phase. Abbreviations: massive sulfide (MASU), semi-massive sulfide (INMS), disseminated sulfide (DISS), pyrrhotite (Po), pentlandite (Pn), chalcopyrite (Cp), altaite (Alt), galena (Gn), tellurobismuthite (Tel), tsumoite (Tsu),hessite (Hes), electrum (El), sperrylite (Spr), michenerite (Mch), froodite (Frd), ungavaite (Ung), molybdenite (Mo), sulfarsenide solid solution (CGSS), silicate gangue (Sg), base metal sulfides (BMS), nickeline (Nic), platinum-group minerals (PGM), pilsenite (Pil), and hedleyite (Hed).

A10 (continued): Quantitative mass balance of samples from the Totten #2 Mine

Sample	Location	Ore Body	Ore Type	Distribution of metals between major and trace pahses	Discrete phase description
T150	DH: 971512 3279'3"-3279'7.5"	MOB	INMS	**Ni:** Po (18%), Pn (82%) **As:** Po (0.5%), Pn (3.7%), CGSS (95.8%) **Pt:** Po (65.3%), Cp (0.5%), Pn (29.4%), CGSS (4.8%) **Pd:** Po (24.4%), Cp (0.5%), Pn (67.3%), CGSS (7.8%) **Pb:** Po (31.4%), Cp (1.4%), Pn (66.5%), Gn (0.7%) **Co:** Po (9.7%), Pn (90%), CGSS (0.3%)	CGSS: Euhedral inclusions in BMS, may contain Ir-Hol cores (1-514μm^2, 117μm^2). Gn: An anhedral fracture infill in CGSS (6μm^2, 1 grain). Hes: Anhedral inclusions in BMS, may infill fractures (8-296μm^2, 111μm^2 average). Ir-Hol: May occur as anhedral inclusions at the center of CGSS, or as subhedral inclusions in BMS (1-2850μm^2, 384μm^2 average). Tel: Anhedral inclusions in BMS and Sg, may infill fractures and vugs in BMS (23-773μm^2, 169μm^2 average). Tsu: Anhedral inclusions in BMS and CGSS, may infill fractures and vugs (11-215μm^2, 77μm^2 average).
T169	DH: 971512 3280'5"-3281'10"	MOB	INMS	**Ni:** Po (6.9%), Pn (93.1%) **As:** Po (0.2%), Pn (4.3%), Spr (4.3%), CGSS (91.2%) **Pt:** Po (0.1%), Cp (0.1%), Pn (0.2%), Spr (99.6%) **Pd:** Po (6.5%), Cp (12.5%), Pn (53%), CGSS (5%), Frd (11.7%), Mch (11.3%) **Pb:** Po (7.3%), Cp (28.4%), Pn (45.7%), Gn (18.7%) **Co:** Po (3.5%), Pn (96.2%), CGSS (0.3%)	CGSS: Euhedral inclusions in BMS that may show Ir-Hol cores; can be rimed by BiTe minerals and Spr (61-1032μm^2, 308μm^2 average). Frd: Anhedral fracture infill in Pn (55μm^2, 1 grain). Gn: Anhedral inclusions in Sg immediately adjcent to BMS (32-99μm^2, 68μm^2 average). Hes: Anhedral inclusions in Pn (22-25μm^2, 24μm^2 average). Ir-Hol: Anhedral inclusions at the center of CGSS grains (8-15μm^2, 12μm^2 average). Mch: An anhedral inclusion within a fracture in Pn (64μm^2, 1 grain). Mo: Subhedral lathes in Po; fractures may be infilled by Bi-Te phases (150μm^2, 2 grains). Pil: An anhedral inclusion which infills a vug in Po (99μm^2, 1 grain). Spr: An anhedral inclusion in Po that is interstitial to several CGSS grains (614μm^2, 1 grain). Tel: Anhedral-subhedral inclusions in Po and Sg (5-1118μm^2, 413μm^2 average). Tsu: Anhedral inclusions in BMS, which may infill fractures and vugs, or rim CGSS (23-371μm^2, 116μm^2 average).
T233C	DH: 971512 3317'3"-3320'2"	MOB	MASU	**Ni:** Po (9%), Pn (91%) **As:** Po (0.2%), Pn (3.9%), Spr (42%), CGSS (53.9%) **Pt:** Spr (100%) **Pd:** Po (13.3%), Cp (0.4%), Pn (81.3%), CGSS (5%) **Pb:** Po (0.7%), Pn (3.1%), Gn (96.2%) **Co:** Po (4.6%), Pn (95.2%), CGSS (0.2%)	CGSS: Subhedral-euhedral inclusions in Po and Pn (110-1862μm^2, 478μm^2 average). Gn: Anhedral inclusions in Po and Pn, may infill fractures and vugs (24-2760μm^2, 271μm^2 average). Hes: Anhedral inclusions in Po, may infill fractures and vugs (173-2647μm^2, 1150μm^2 average). Pil: Anhedral inclusion along Pn/Po boundary (2945μm^2, 1 grain). Spr: Anhedral inclusion in Po (3719μm^2, 1 grain). Tel: Anhedral inclusions in Po which may infill fractures and vugs (102-769μm^2, 435μm^2 average). Tsu: Anhedral inclusions in Po and Pn, may infill fractures and vugs (291-4186μm^2, 1514μm^2 average).
T226	DH: 1270490 364'7.5"-364'10"	MOB	DISS	**Ni:** Po (0.2%), Pn (0.6%), CGSS (99.2) **As:** Nic (100%) **Pt:** Po (1%), Cp (16.9%), Pn (0.3%), Nic (75.6%), CGSS (6.2%) **Pd:** Po (0.1%), Cp (4.6%), Pn (0.2%), CGSS (95.1%) **Pb:** Cp (3.6%), Nic (4.5%), Gn (90%), Alt (1.7%) **Co:** Po (1.2%), Cp (0.1%), Pn (6.8%), Nic (88.4%), CGSS (3.5%)	Alt: Anhedral inclusions in Nic and Cp which infill fractures and vugs (10-97μm^2, 44μm^2 average). CGSS: Anhedral inclusions in Nic; inclusions appear to be reminants of re-absorbed CGSS (50-404μm^2, 281μm^2 average). El: Anhedral inclusions in Nic, may infill fractures and vugs (5-43μm^2, 25μm^2 average). Gn: Anhedral inclusions in Nic and Po, inclusions may infill fractures and vugs (6-2328μm^2, 209μm^2 average). Hes: Anhedral inclusions in Nic and Po, inclusions may infill fractures and vugs (4-1725μm^2, 146μm^2 average). Nic: Anhedral grains within BMS blebs and veins; Nic grains are typically found on the margins of BMS blebs and veins; may contain inclusions of BMS and discrete phases (737-1777113μm^2, 125698μm^2 average). Tsu: An anhedral inclusion in Sg adjacent to a BMS bleb (371μm^2, 1 grain).
TU31B	Level: Surface Outcrop -1261(X), 21502(Y), 13075(Z)	MOB	INMS	**Ni:** Po (0.8%), Pn (84.6%), Nic (0.4%), CGSS (14.2%) **As:** Nic (0.8%), CGSS (99.1%), Spr (0.1%) **Pt:** CGSS (0.8%), Spr (99.2%) **Pd:** Cp (0.2%), Pn (0.7%), CGSS (93.4%), Frd (5.7%) **Pb:** Cp (1.6%), Pn (2.2%), CGSS (3.5%), Gn (92.7%) **Co:** Pn (18%), CGSS (82%)	CGSS: Subhedral-anhedral inclusions in BMS and Sg which may show sieve texture (639-1675860μm^2, 327338μm^2 average). Frd: Anhedral inclusions in Cp and Sg (17-343μm^2, 96μm^2 average). Gn: Anhedral inclusions in BMS, CGSS, and Sg; inclusions in CGSS infill sieves (13-2859μm^2, 885μm^2 average). Hed: An anhedral inclusion in Sg (6μm^2, 1 grain). Hes: Anhedral inclusions in BMS which infill vugs and fractures (41-54μm^2, 49μm^2 average). Mo: Subhedral lathes in Pn (534-790μm^2, 664μm^2). Nic: Anhedral grains which may infill sieves in CGSS; inclusions in CGSS mayshow graphic textures with Cp; in sulfide blebs Nic occurs along the margins, Nic blebs also occur in Sg adjacent to sulfides (96-288600μm^2, 1975μm^2). Pil: Anhedral inclusionsin BMS, Sg, and CGSS which infill vugs and fractures (7-2287μm^2, 179μm^2). Spr: Anhedral inclusions in Cp/Sg; inclusions in sulfide blebs occur near their margins; occurences in Sg are adjacent to sulfide blebs (59-124μm^2, 750μm^2 average). Tel: Anhedral inclusions in BMS, CGSS, and Sg, which infill fractures and vugs (19-965μm^2, 292μm^2 average). Tsu: Anhedral inclusions in BMS and Sg (17-216μm^2, 82μm^2 average).

Notes: Percentages represent the proportion of the total metal content of each sample that is associated with each mineral phase. Abbreviations: massive sulfide (MASU), semi-massive sulfide (INMS), disseminated sulfide (DISS), pyrrhotite (Po), pentlandite (Pn), chalcopyrite (Cp), altaite (Alt), galena (Gn), tellurobismuthite (Tel), tsumoite (Tsu),hessite (Hes), electrum (El), sperrylite (Spr), michenerite (Mch), froodite (Frd), ungavaite (Ung), molybdenite (Mo), sulfarsenide solid solution (CGSS), silicate gangue (Sg), base metal sulfides (BMS), nickeline (Nic), platinum-group minerals (PGM), pilsenite (Pil), and hedleyite (Hed).

A10 (continued): Quantitative mass balance of samples from the Totten #2 Mine

Sample	Location	Ore Body	Ore Type	Distribution of metals between major and trace pahses	Discrete phase description
TU32	Level: 1850 -911(X), 22312(Y), 10997(Z)	MOB	DISS	**Ni:** Po (4.6%), Pn (65%), Nic (0.4%), CGSS (30%) **As:** Nic (0.4%), CGSS (99.6%) **Pt:** Po (0.1%), Cp (0.2%), Pn (0.2%), CGSS (99.4%) **Pd:** Cp (0.2%), Pn (0.3%), CGSS (99.3%), Mch (0.2%) **Pb:** Po (5.9%), Cp (55.3%), Pn (38.6%), CGSS (0.2%) **Co:** Po (0.2%), Pn (7.4%), CGSS (92.4%)	CGSS: Subhedral inclusions in BMS and Sg which may demonstrate sieve texture (4-1000367μm^2, 18684μm^2 average). El: An anhedral inclusion along the boundary of Po/Sg (41μm^2, 1 grain). Mch: An anhedral inclusion infilling a fracture in CGSS (23μm^2, 1 grain). Nic: Anhedral inclusions along the margins of sulfide blebs (13892-15976μm^2, 14934μm^2 average). Pil: Anhedral inclusions in BMS and CGSS, inclusions infill fractures and vugs (8-132564μm^2, 9171μm^2 average). Tel: Anhedral inclusions in BMS and CGSS which infill fractures and vugs (102-284μm^2, 136μm^2 average). Tsu: Anhedral inclusions in BMS and Sg which infill fractures and vugs (7-305μm^2, 83μm^2 average).
T193	DH: 1270880 758'3"-758'6"	MOB	INMS	**Ni:** Po (19.1%), Pn (80.9%) **As:** Po (0.5%), Pn (3%), CGSS (96.5%) **Pt:** Po (65.6%), Cp (1.5%), Pn (27.6%), CGSS (5.3%) **Pd:** Po (25.1%), Cp (1.5%), Pn (64.4%), CGSS (9%) **Pb:** Po (32.4%), Cp (3.8%), Pn (63.8%) **Co:** Po (10.3%), Pn (89.3%), CGSS (0.4%)	CGSS: Euhedral-anhedral inclusions in BMS (22-6242μm^2, 1194μm^2 average). Hes: Anhedral inclusions in BMS which infill fractures and vugs (4-58μm^2, 12μm^2 average). Ir-Hol: Anhedral inclusion at the center of a CGSS grain (3μm^2, 1 grain). Pil: Anhedral inlusion in Po (30μm^2, 1 grain). Tel: Anhedral inclusions in BMS and Sg, infilling fractures and vugs (7-142μm^2, 48μm^2).
T191	DH: 1270880 775'6"-775'7"	MOB	INMS	**Ni:** Po (69.8%), Cp (0.2%), Pn (30%) **As:** Po (2.3%), Cp (0.7%), Pn (1.5%), CGSS (95.5%) **Pt:** Po (46.2%), Cp (51%), Pn (2%), CGSS (0.8%) **Pd:** Po (24%), Cp (68.1%), Pn (6.2%), CGSS (1.7%) **Pb:** Po (14.1%), Cp (80.6%), Pn (2.8%), Gn (2.5%) **Co:** Po (53%), Cp (0.2%), Pn (46.4%), CGSS (0.4%)	CGSS: Euhedral-subhedral inclusions in the BMS (91-825μm^2, 452μm^2 average). El: Anhedral inclusion in Po (9μm^2, 1 grain). Gn: Anhedral inclusions in Po which infill fractures and vugs (6-24μm^2, 16μm^2 average). Hes: Anhedral inclusions in the BMS which infill fractures and vugs, may also rim CGSS (11-115μm^2, 40μm^2 average). Ir-Hol: Anhedral inclusion at the center of a CGSS grain (0.85μm^2, 1 grain). Pil: Anhedral inclusions in Po (23-28μm^2, 25μm^2 average). Tel: Anhedral inclusions in BMS and Sg which infill fractures and vugs (13-290μm^2, 69μm^2 average). Tsu: Anhedral inclusions in Cp/Po (7-13μm^2, 14μm^2 average).
T164	DH: 971512 3297'3"-3298'5"	MOB	INMS	**Ni:** Po (2.9%), Pn (97.1%) **As:** Po (0.2%), Pn (11.5%), CGSS (62.8%), Spr (25.5%), **Pt:** Pn (0.1%), Spr (99.9%) **Pd:** Po (4.5%), Cp (1.7%), Pn (91.6%), CGSS (2.2%) **Pb:** Po (2.3%), Cp (1.7%), Pn (35.7%), Gn (60.3%) **Co:** Po (1.4%), Pn (98.5%), CGSS (0.1%)	CGSS: Euhedral-anhedral inclusions in BMS and Sg (79-615μm^2, 246μm^2). Gn: Anhedral inclusions in Sg (22-196μm^2, 93μm^2 average). Hes: Anhedral inclusions in BMS (8-48μm^2, 35μm^2 average). Mo: Subhedral lathes in Po/Pn (124-284μm^2, 291μm^2). Spr: Anhedral inclusions in BMS (13-556μm^2, 242μm^2). Tel: Anhedral inclusions in BMS and Sg; BMS inclusions may infill fractures (21-138μm^2, 74μm^2). Tsu: Anhedral inclusion in Cp (22μm^2, 1 grain).
T157	DH: 971512 3300'5"-3301'8"	MOB	INMS	**Ni:** Po (7.2%), Pn (92.8%) **As:** Po (0.9%), Cp (0.1%), Pn (18.5%), Spr (0.5%), CGSS (80%) **Pt:** Po (4.4%), Cp (1.2%), Pn (5.6%), Spr (88.7%), CGSS (0.1%) **Pd:** Po (7%), Cp (4.9%), Pn (54.4%), CGSS (1%), Frd (15.3%), Mch (17.4%) **Pb:** Po (8.5%), Cp (12.1%), Pn (50.7%), Gn (21.6%), Alt (7.1%) **Co:** Po (3.7%), Pn (96.3%)	Alt: Anhedral inclusion in Sg (125μm^2, 1 grain). CGSS: Euhedral-subhedral inclusion in BMS (35-485μm^2, 166μm^2 average). Frd: An anhedral inclusion in Pn (66μm^2, 1 grain). Gn: Anhedral inclusions in BMS and Sg, which may infill fractures (14-241μm^2, 67μm^2 average). Hes: Anhedral inclusions in Po/Pn which infill vugs and fractures (5-48μm^2, 17μm^2 average). Ir-Hol: Anhedral inclusions at the center of CGSS grains (2-58μm^2, 21μm^2 average). Mch: Anhedral inclusions in Pn/Sg which may infill fractures (4-60μm^2, 18μm^2 average). Mo: Anhedral inclusion along the boundary of Pn/Sg (1279μm^2, 1 grain). Spr: Anhedral inclusion in Pn (16μm^2, 1 grain). Tel: Anhedral inclusions in BMS and Sg, may infill fractures and vugs (13-343μm^2, 83μm^2 average). Tsu: Anhedral inclusions in BMS and Sg, which may infill fractures and vugs (19-158μm^2, 44μm^2 average).

Notes: Percentages represent the proportion of the total metal content of each sample that is associated with each mineral phase. Abbreviations: massive sulfide (MASU), semi-massive sulfide (INMS), disseminated sulfide (DISS), pyrrhotite (Po), pentlandite (Pn), chalcopyrite (Cp), altaite (Alt), galena (Gn), tellurobismuthite (Tel), tsumoite (Tsu),hessite (Hes), electrum (El), sperrylite (Spr), michenerite (Mch), froodite (Frd), ungavaite (Ung), molybdenite (Mo), sulfarsenide solid solution (CGSS), silicate gangue (Sg), base metal sulfides (BMS), nickeline (Nic), platinum-group minerals (PGM), pilsenite (Pil), and hedleyite (Hed).

A10 (continued): Quantitative mass balance of samples from the Totten #2 Mine

Sample	Location	Ore Body	Ore Type	Distribution of metals between major and trace pahses	Discrete phase description
T152B	DH: 971512 3270'7.5"-3271'5"	MOB	MASU	**Ni:** Po (15.7%), Pn (84.3%) **As:** Po (0.5%), Pn (4.1%), Nic (1%), CGSS (93.1%), Spr (1.3%) **Pt:** Po (1%), Cp (0.1%), Pn (0.5%), Spr (98.3%), CGSS (0.1%) **Pd:** Po (20.3%), Cp (6.8%), Pn (66.2%), CGSS (6.7%) **Pb:** Po (21.9%), Cp (14.7%), Pn (54.8%), Gn (8.5%) **Co:** Po (8.3%), Pn (91.4%), CGSS (0.3%)	CGSS: Euhedral-subhedral inclusions in BMS which may have cores of Ir-Hol (29-729μm^2, 243μm^2 average). Gn: Anhedral inclusions in Cp and Sg (25-98μm^2, 61μm^2 average). Hes: Anhedral inclusions in BMS and Sg, may infill fractures and vugs (7-117μm^2, 45μm^2 average). Ir-Hol: Anhedral inclusions at the center of CGSS grains (0.36-4μm^2, 2μm^2 average). Mo: Subhedral lathes in Pn, Po, and Sg (1037-6444μm^2, 3740μm^2 average). Nic: Anhedral inclusion along Pn/Sg boundary (132μm^2, 1 grain). Spr: Anhedral inclusions in BMS, also occurs at center of Rh-zoned CGSS (14-48μm^2, 35μm^2 average). Tel: Anhedral inclusions in BMS, may rim CGSS (21-29μm^2, 25μm^2 average). Tsu: Anhedral inclusion in BMS, may rim CGSS (4-456μm^2, 90μm^2 average).
T144	DH: 1265720 442'	MOB	MASU	**Ni:** Po (9.3%), Pn (90.7%) **As:** Po (0.6%), Pn (9.9%), Spr (3.7%), CGSS (85.8%) **Pt:** Po (0.5%), Pn (0.5%), Spr (99%) **Pd:** Po (13.6%), Cp (3.1%), Pn (80.2%), CGSS (3.1%) **Pb:** Po (12.9%), Cp (6%), Pn (58.6%), Gn (9.2%), Alt (13.4%) **Co:** Po (4.8%), Pn (95.1%), CGSS (0.1%)	Alt: Anhedral inclusions in BMS (144-310μm^2, 227μm^2 average). CGSS: Euhedral-subhedral inclusion in BMS, may contain Ir-Hol core (19-1104μm^2, 187μm^2 average). Gn: Anhedral inclusions in BMS, may infill fractures (8-156μm^2, 41μm^2 average). Ir-Hol: Anhedral inclusions in BMS, also occurs at the center of CGSS grains (3-22μm^2, 8μm^2 average). Spr: Anhedral inclusion in Po (238μm^2, 1 grain). Tel: Anhedral inclusions in Pn/Po, infills fractures and vugs (62-9310μm^2, 3339μm^2 average). Tsu: Anhedral inclusion in Po (29μm^2, 1 grain).
T7	DH: 1265750 452'	238	MASU	**Ni:** Po (8%), Pn (92%) **As:** Po (0.1%), Pn (0.5%), CGSS (92.6%), Spr (6.8%) **Pt:** Po (0.1%), Spr (99.9%) **Pd:** Po (2.4%), Cp (1.3%), Pn (67.9%), CGSS (28.4%) **Pb:** Po (24.7%), Cp (4.3%), Pn (9.3%), Gn (19.3%), Alt (42.4%) **Co:** Po (5.7%), Pn (93.9%), CGSS (0.4%)	Alt: Anhedral inclusions infilling fractures in BMS and Sg (1.5-182μm^2, 49μm^2 average). CGSS: Subhedral-euhedral inclusions in BMS, may contain inclusions of Spr, Tsu, and Ir-Hol (13.2-2457μm^2, 229μm^2 average). Gn: Anhedral inclusions in BMS and Sg (4-63μm^2, 18μm^2 average). Hes: Anhedral inclusions in Po and Sg (6.75-22.75μm^2, 15μm^2 average). Ir-Hol: Anhedral inclusions in BMS and at the center of CGSS grains (0.64-1665μm^2, 40μm^2 average). Spr: Anhedral inclusions in Cp and CGSS (8-420μm^2, 227μm^2 average). Tsu: Anhedral inclusions which may infill fractures in BMS and CGSS (0.5-1078μm^2, 46μm^2).
T8	DH: 1265750 437.5'	238	MASU	**Ni:** Po (9.5%), Pn (90.5%) **As:** Po (0.4%), Pn (4.3%), CGSS (95.3%) **Pt:** Po (45.6%), Cp (5.6%), Pn (43.1%), CGSS (5.8%) **Pd:** Po (13.1%), Cp (4.1%), Pn (75.4), CGSS(7.4%) **Pb:** Po (8.7%), Cp (7.7%), Pn (11.3%), Gn (40.9%), Alt (31.2%) **Co:** Po (4.3%), Pn (95.5%), CGSS (0.2%)	Alt: Anhedral inclusions in Po/Pn (2-169μm^2, 19μm^2 average). CGSS: Euhedral-subhedral inclusions hosted in Po/Pn, may be rimmed by Tel (12-1776μm^2, 412μm^2). Gn: Anhedral inclusions in BMS and infills fractures in CGSS (0.25-279μm^2, 17μm^2 average). Hes: Anhedral inclusions in Po (4-100μm^2, 52μm^2 average). Ir-Hol: Anhedral inclusions in the BMS and at the core of CGSS grains (1-22μm^2, 2μm^2 average). Tel: Anhedral inclusions in BMS, may rim CGSS (168-6448μm^2, 2927μm^2 average).
TU16B	Level: 1850 -891(X), 22087(Y), 11098(Z)	238	DISS	**Ni:** Po (3.5%), Pn (96.5%) **As:** Pn (0.2%), CGSS (99.8%) **Pt:** Po (12.6%), Cp (37.3%), Pn (45.1%), CGSS (5%) **Pd:** Po (0.4%), Cp (23.4%), Pn (67.8%), CGSS (8.4%) **Pb:** Po (0.4%), Cp (23.4%), Pn (67.8%), CGSS (8.4%) **Co:** Po (2%), Pn (97.3%), CGSS (0.7%)	CGSS: Euhedral-subhedral inclusions in the BMS and Sg (49-1000μm^2, 319μm^2 average). Gn: Anhedral inclusions in the BMS and Sg (8-200μm^2, 49μm^2 average). Tsu: Anhedral inclusions in BMS, and Sg, may rim CGSS (2-1600μm^2, 50μm^2 average).

Notes: Percentages represent the proportion of the total metal content of each sample that is associated with each mineral phase. Abbreviations: massive sulfide (MASU), semi-massive sulfide (INMS), disseminated sulfide (DISS), pyrrhotite (Po), pentlandite (Pn), chalcopyrite (Cp), altaite (Alt), galena (Gn), tellurobismuthite (Tel), tsumoite (Tsu),hessite (Hes), electrum (El), sperrylite (Spr), michenerite (Mch), froodite (Frd), ungavaite (Ung), molybdenite (Mo), sulfarsenide solid solution (CGSS), silicate gangue (Sg), base metal sulfides (BMS), nickeline (Nic), platinum-group minerals (PGM), pilsenite (Pil), and hedleyite (Hed).

A10 (continued): Quantitative mass balance of samples from the Totten #2 Mine

Sample	Location	Ore Body	Ore Type	Distribution of metals between major and trace pahses	Discrete phase description
T6	DH: 1265710 425'	238	MASU	**Ni:** Po (9.4%), Pn (90.6%) **As:** Po (0.2%), CGSS (99.8%) **Pt:** Po (70.7%), Cp (1.5%), Pn (17.1%), CGSS (10.7%) **Pd:** Po (1.9%), Cp (1.8%), Pn (66.9%), CGSS (29.4%) **Pb:** Po (9.2%), Cp (1%), Pn (4.5%), Gn (0.7%), Alt (84.5%) **Co:** Po (3.8%), Pn (95.9%), CGSS (0.3%)	Alt: Anhedral inclusions in Po, Pn, CGSS, and Sg; inclusions in BMS and CGSS typically appear to be fracture and vug infills (1-412μm^2, 41μm^2 average). CGSS: Euhedral inclusions in BMS (15-2040μm^2, 508μm^2 average). Gn: Anhedral inclusions which infill fractures in the BMS (0.4-10μm^2, 4μm^2 average).
T21	DH: 1265770 411'	238	DISS	**Ni:** Po (4.5%), Pn (12.6%), Nic (74%), CGSS (8.9%) **As:** Nic (69.4%), CGSS (30.6%) **Pt:** Po (0.4%), Cp (0.8%), Pn (0.1%), Nic (1.2%), CGSS (97.5%) **Pd:** Po (0.1%), Cp (0.4%), Pn (0.2%), Nic (3%), CGSS (92.7%), Mch (3.6%) **Pb:** Po (0.7%), Cp (6.5%), Pn (0.9%), Nic (2.8%), CGSS (0.1%), Gn (88%) **Co:** Po (0.8%), Pn (4.8%), Nic (2.4%), CGSS (92%)	CGSS: Euhedral-anhedral grains which may show sieve texture, typically found along the outer margin of, or adjacent to sulfide blebs; may be rimmed by Hes and Gn (127-254466μm^2, 28544μm^2 average). Gn: Anhedral inclusions which may infill fractures in BMS, and rims CGSS (1-144μm^2, 20μm^2). Hes: Anhedral inclusions in BMS and Nic, rims CGSS (0.5-17μm^2, 10μm^2 average). Ir-Hol: Anhedral inclusion in Rh-zoned CGSS (1μm^2, 1 grain) Mch: An anhedral inclusion in silicate gangue adjacent to a sulfide bleb (41μm^2, 1 grain). Nic: Anhedral grains along the outer margins of sulfide blebs, or as inclusions in Sg adjacent to sulfide blebs (47-591394μm^2, 32389μm^2 average).
T2	DH: 1265390 564.5'	238	MASU	**Ni:** Po (2%), Pn (98%) **As:** Pn (9.2%), CGSS (90.8%) **Pt:** Po (4.8%), Cp (39.6%), Pn (47.8%), CGSS (7.8%) **Pd:** Po (0.6%), Cp (22.5%), Pn (58.9%), CGSS (5%), Ung (13%) **Pb:** Po (2.3%), Cp (10.3%), Pn (67%), Gn (20.4%) **Co:** Po (0.3%), Pn (99%), CGSS (0.7%)	CGSS: Euhedral-subhedral inclusions in BMS and along the BMS-Sg contact, sometimes demonstrating sieve texture (16-3050μm^2, 497μm^2 average). Gn: Anhedral inclusions, infills fractures and vugs in BMS (2-224μm^2, 16μm^2 average). Hes: Forms anhedral inclusions in BMS and sulfarsenides, infills fractures, and rims CGSS (5-578μm^2, 92μm^2 average). Ir-Hol: Anhedral inclusions at the center of CGSS (3-48μm^2, 20μm^2 average). Nic: Anhedral inclusions in Po (9-12μm^2, 10μm^2 average). Tel: Anhedral inclusions in BMS which infill fractures and vugs, rims CGSS (15-645μm^2, 84μm^2 average).
TU1	Level: 1250 -969(X), 24005(Y), 11602(Z)	238	MASU	**Ni:** Po (7.5%), Pn (92.5%) **As:** Po (1.6%), Cp (0.3%), Pn (91.6%), **Pt:** Po (1.6%), Cp (1.3%), Pn (11.6%), Spr (85.5%) **Pd:** Po (0.1%), Cp (11.2%), Pn (23.3%), Frd (16.6%), Mch (48.8%) **Pb:** Po (8.6%), Cp (16.9%), Pn (68.3%), Gn (2.7%), Alt (3.5%) **Co:** Po (2.4%), Pn (97.6%)	Alt: Anhedral grains which infill fractures in Po and Cp (20-38μm^2, 30μm^2 average). CGSS: A subhedral inclusion in Po (63μm^2, 1 grain). Frd: Anhedral inclusions in Po and Cp, may infill vugs and fractures (1-241μm^2, 54μm^2 average). Gn: Anhedral inclusions in Po and Cp which may infill fractures (2-18μm^2, 10μm^2 average). Hes: Anhedral inclusions in BMS and Sg, may sometimes infill fractures or occur along grain boundaries (4-190μm^2, 29μm^2 average). Ir-Hol: Anhedral inclusions in BMS and at the center of CGSS (5-365μm^2, 31μm^2 average). Mch: Anhedral inclusions in Po and Pn (18-705μm^2, 166μm^2 average). Mo: Subhedral-anhedral inclusions in Po and Cp (30-821μm^2, 426μm^2 average). Spr: A single anhedral inclusion in Po (21μm^2, 1 grain). Trk: Hosted within what may be a healed Cp fracture with argentopentlandite (8μm^2, 1 grain). Tel: Anhedral inclusions which may infill fractures within BMS (6-21μm^2, 14μm^2 average).
TU3	Level: 1250 -968(X), 24021(Y), 11602(Z)	238	MASU	**Ni:** Po (5.2%), Pn (94.8%) **As:** Pn (1.3%), CGSS (98.7%) **Pt:** Po (10.6%), Cp (60.6%), Pn (19.5%), CGSS (9.3%) **Pd:** Po (0.7%), Cp (10.9%), Pn (8.3%), CGSS (2.8%), Frd (1%), Mch (76.3%) **Pb:** Po (0.1%), Cp (3.5%), Pn (1%), Gn (94.6%), Alt (0.8%) **Co:** Po (2.5%), Cp (0.1%), Pn (96.3%), CGSS (1.1%)	Alt: Anhedral inclusions along fractures in Pn (27-259μm^2, 121μm^2 average). CGSS: Euhedral-subhedral inclusions in BMS, may show Ir-Hol cores (28-2154μm^2, 302μm^2). Frd: An anhedral inclusion in Cp (8μm^2, 1 grain). Gn: Anhedral grains infilling fractures in BMS (3-5908μm^2, 607μm^2 average). Hes: Anhedral inclusions in Cp and Po which may infill fractures and vugs (6-46μm^2, 24μm^2 average). Ir-Hol: Anhedral inclusions at the center of CGSS grains (0.4-13μm^2, 5μm^2 average). Mch: Anhedral inclusion infilling a vug in Cp (732μm^2, 1 grain). Mo: Subhedral-anhedral inclusions in BMS, sometimes infilling vugs (121-18920μm^2, 6752μm^2 average). Tel: Anhedral inclusions which may infill fractures in BMS, CGSS, and Mo (4-84μm^2, 21μm^2 average).

Notes: Percentages represent the proportion of the total metal content of each sample that is associated with each mineral phase. Abbreviations: massive sulfide (MASU), semi-massive sulfide (INMS), disseminated sulfide (DISS), pyrrhotite (Po), pentlandite (Pn), chalcopyrite (Cp), altaite (Alt), galena (Gn), tellurobismuthite (Tel), tsumoite (Tsu),hessite (Hes), electrum (El), sperrylite (Spr), michenerite (Mch), froodite (Frd), ungavaite (Ung), molybdenite (Mo), sulfarsenide solid solution (CGSS), silicate gangue (Sg), base metal sulfides (BMS), nickeline (Nic), platinum-group minerals (PGM), pilsenite (Pil), and hedleyite (Hed).

A10 (continued): Quantitative mass balance of samples from the Totten #2 Mine

Sample	Location	Ore Body	Ore Type	Distribution of metals between major and trace pahses	Discrete phase description
TU6	Level: 1250 -1001(X), 24150(Y), 11602(Z)	238	MASU	**Ni:** Po (9%), Pn (91%) **As:** Po (0.2%), Pn (2.5%), CGSS (97.3%) **Pt:** Po (43.9%), Cp (1.8%), Pn (43.9%), CGSS (10.4%) **Pd:** Po (12.1%), Cp (1.2%), Pn (73.9%), CGSS (12.8%) **Pb:** Po (16.9%), Cp (3.4%), Pn (79.3%), Alt (0.4%) **Co:** Po (4.6%), Pn (94.8%), CGSS (0.6%)	Alt: Anhedral inclusions in Po (4-6μm^2, 5μm^2 average). CGSS: Euhedral-subhedral inclusions in BMS, may demonstrate irarsite-hollingworthite cores; sometimes shows sieve texture (16-1675μm^2, 267μm^2 average). Hes: Anhedral inclusions in BMS, CGSS, and Sg; may infill fractures or occur along grain boundaries (4-442μm^2, 82μm^2 average). Ir-Hol: Subhedral-anhedral inclusions in BMS, forms anhedral inclusions at the center of CGSS (1-30μm^2, 9μm^2 average). Mo: Subhedral-anhedral lathes in Pn and Po (11-1607μm^2, 273μm^2 average). Trk: Subhedral-anhedral inclusions in Cp and Po (19-44μm^2, 36μm^2 average). Tel: An anhedral inclusion in Po (10μm^2, 1 grain).
TU13	Level: 1250 -958(X), 23967(Y), 11602(Z)	238	MASU	**Ni:** Po (8.2%), Cp (0.1%), Pn (91.7%) **As:** Po (6.8%), Cp (2.1%), Pn (90.6%), CGSS (0.5%) **Pt:** Po (14.7%), Cp (63.9%), Pn (21.4%) **Pd:** Po (1.7%), Cp (73.2%), Pn (25.1%) **Pb:** Po (18.9%), Cp (16.5%), Pn (57.6%), Gn (7%) **Co:** Po (2.9%), Pn (97.1%)	Alt: Anhedral inclusions in Cp, may infill fractures (10-19μm^2, 14μm^2 average). CGSS: Subhedral-anhedral inclusions in Po (5-12μm^2, 6μm^2 average). Gn: Anhedral inclusions in BMS, CGSS and Sg; may form composite grains with Tel, and infill fractures and vugs in BMS and CGSS (4-2090μm^2, 109μm^2 average). Hes: Anhedral inclusions in BMS, which may infill fractures and vugs (5-1926μm^2, 110μm^2 average). Tel: Anhedral inclusions in BMS, which may infill fractures and vugs and form composite grains with Gn (1-500μm^2, 55μm^2 average).
T3	DH: 1265540 494'	238	MASU	**Ni:** Po (4.6%), Cp (0.1%), Pn (95.2%) **As:** Po (0.2%), Cp (0.2%), Pn (8.5%), CGSS (91.1%) **Pt:** Po (18.7%), Cp (44.7%), Pn (33%), CGSS (3.6%) **Pd:** Po (0.2%), Cp (38.3%), Pn (58%), CGSS (3.5%) **Pb:** Po (2.6%), Cp (16.9%), Pn (71.6%), Gn (8.9%) **Co:** Po (3.4%), Pn (96%), CGSS (0.6%)	CGSS: Subhedral inclusion in Cp with sieve texture (8519μm^2, 1 grain). Gn: Anhedral inclusions in BMS which may infill fractures (3-183μm^2, 33μm^2 average). Hes: Anhedral inclusion in Cp (9μm^2, 1 grain). Pil: Anhedral inclusions in Po infilling fractures (108-331μm^2, 220μm^2 average). Tel: Anhedral inclusions in BMS, may infill fractues (6-2010μm^2, 451μm^2 average). Tsu: Anhedral inclusions in BMS, may infill fractures and vugs (11-12356μm^2, 931μm^2 average).
TU4B	Level: 1250 -997(X), 24098(Y), 11602(Z)	238	DISS	**Ni:** Po (0.8%), Cp (0.1%), Pn (15%), CGSS (84.1%) **As:** CGSS (100%) **Pt:** Cp (0.4%), CGSS (99.6%) **Pd:** Cp (0.2%), CGSS (84.2%), Frd (2%), Ung (13.6%) **Pb:** Po (0.4%), Cp (80.7%), Pn (3.6%), CGSS (12.8%), Alt (2.4%) **Co:** Pn (0.6%), CGSS (99.4%)	Alt: Anhedral inclusions in CGSS (19-54μm^2, 36μm^2 average). CGSS: Anhedral-subhedral grains with sieve texture and infill by BMS, Bi-Te minerals, Nic, El, PGM, and Gn (1494-8457670μm^2, 342120μm^2 average). El: Anhedral inclusions in CGSS infilling sieves and fractures (14-373μm^2, 89μm^2 average). Frd: Anhedral inclusions in BMS, and may infill fractures and vugs in CGSS (4-155μm^2, 41μm^2 average). Gn: Anhedral inclusions in Po, Cp, and CGSS, may infill fractures and vugs (5-52μm^2, 28μm^2 average). Hed: Anhedral inclusions in CGSS (3-169μm^2, 40μm^2 average). Hes: Anhedral inclusions in CGSS, may infill fractures and vugs (10-872μm^2, 134μm^2 average). Mch: Anhedral inclusion in CGSS (70μm^2, 1 grain). Nic: Anhedral inclusions which infill sieves in CGSS (18-536μm^2, 201μm^2 average). Pil: Anhedral inclusions which infill sieves in CGSS (5-536μm^2, 122μm^2 average). Tel: Anhedral inclusions which infill sieves in CGSS (4-71μm^2, 27μm^2 average). Tsu: Anhedral inclusions which infill sieves in CGSS (4-433μm^2, 67μm^2 average). Ung: Anhedral inclusions which infill sieves in CGSS (43-1994μm^2, 581μm^2 average).
TU21	Level: 1250 -966(X), 23933(Y), 11598(Z)	238	DISS	**Ni:** Po (0.1%), Cp (0.1%), Pn (3.3%), Nic (80.8%), CGSS (15.7%) **As:** Nic (58.3%), CGSS (41.7%) **Pt:** Cp (1.4%), Nic (0.7%), CGSS (97.8%) **Pd:** Cp (0.2%), Nic (0.5%), CGSS (25.6%), Mch (14.9%), Ung (58.8%) **Pb:** Cp (0.2%), Gn (99.8%) **Co:** Pn (0.8%), Nic (1.5%), CGSS (97.7%)	CGSS: Euhedral-subhedral grains hosted in Cp and Nic, typically along the margins of sulfide blebs and veins (50-603454µm2, 1470µm2 average). El: Anhedral inclusions in BMS, Nic, and Sg, inclusions may infill fractures (36-4734µm2, 754µm2 average). Gn: Anhedral inclusions in Cp, Nic, CGSS, and Sg; inclusions infill fractures and vugs in Nic, Cp, and CGSS (8-476379µm2, 3835µm2 average). Hes: Anhedral inclusions in Nic, Sg, and Cp; infills fractures and vugss in Nic and Cp; rims CGSS grains (4-3974µm2, 261µm2 average). Mch: Anhedral inclusion in Sg adjacent to sulfides (4251µm2, 1 grain). Nic: Forms anhedral blebs in BMS and Sg; blebs may be rimmed by small euhedral CGSS grains (478-16727706µm2, 207944µm2 average). Tel: Anhedral inclusions in Nic, Sg, and Cp (34-805µm2, 294µm2 average). Ung: Anhedral inclusions in Nic and CGSS, which infill fractures and vugs (11-680µm2, 131µm2 average).

Notes: Percentages represent the proportion of the total metal content of each sample that is associated with each mineral phase. Abbreviations: massive sulfide (MASU), semi-massive sulfide (INMS), disseminated sulfide (DISS), pyrrhotite (Po), pentlandite (Pn), chalcopyrite (Cp), altaite (Alt), galena (Gn), tellurobismuthite (Tel), tsumoite (Tsu),hessite (Hes), electrum (El), sperrylite (Spr), michenerite (Mch), froodite (Frd), ungavaite (Ung), molybdenite (Mo), sulfarsenide solid solution (CGSS), silicate gangue (Sg), base metal sulfides (BMS), nickeline (Nic), platinum-group minerals (PGM), pilsenite (Pil), and hedleyite (Hed).

A10 (continued): Quantitative mass balance of samples from the Totten #2 Mine

Sample	Location	Ore Body	Ore Type	Distribution of metals between major and trace pahses	Discrete phase description
T19	DH: 1265710 334'	238	DISS	**Ni:** Po (1.4%), Pn (79.9%), Nic (18.6%) **As:** Nic (99.6%), CGSS (0.4%) **Pt:** Po (4.8%), Cp (51.5%), Pn (26.5%), Nic (10.3%), CGSS (6.9%) **Pd:** Po (1.1%), Cp (29.6%), Pn (36.1%), Nic (26.5%), CGSS (6.7%) **Pb:** Cp (1.4%), Pn (0.7%), Nic (0.1%), Gn (97.8%) **Co:** Po (0.8%), Pn (96.7%), Nic (1.9%), CGSS (0.6%)	El: Anhedral inclusions in Sg adjacent to sulfides (6-115419μm^2, 12374μm^2 average). CGSS: Subhedral-anhedral inclusions in Cp and in Sg immediately adjacent to sulfides, may demonstrate seive texture (2-620μm^2, 84μm^2 average). Gn: Anhedral inclusions in Cp, Pn, and Sg (6-6440μm^2, 84μm^2 average). Hes: Anhedral inclusions in Pn and Sg (6-3220μm^2, 1077μm^2 average). Nic: Anhedral inclusions in Sg and BMS; may infill sieves in CGSS (2-246168μm^2, 13192μm^2 average). Tel: An anhedral inclusion in Nic (36-1694μm^2, 781μm^2 average). Tsu: Anhedral inclusions in Nic and Sg (3-109699μm^2, 11319μm^2 average).
T134	DH: 1265980 1100'6.5"-1101'3.5	N/A	DISS	**Ni:** Po (2.6%), Pn (97.2%), Nic (0.2%) **As:** Pn (0.9%), Nic (53.2%), CGSS (41.6%), Spr (4.3%) **Pt:** Spr (100%) **Pd:** Cp (0.4%), Pn (0.7%), CGSS (0.1%), Frd (2.1%), Mch (96.7%) **Pb:** Po (0.2%), Cp (3%), Pn (2.1%), Gn (89%), Alt (5.7%) **Co:** Po (0.1%), Pn (98%), CGSS (0.7%)	Alt: Anhedral inclusions infilling fracturesin Cp, or along Cp/Sg grain boundaries (68-434μm^2, 177μm^2 average). CGSS: Anhedral-euhedral inclusions within BMS and Sg; inclusions in Sg are spatially associated with sulfide blebs (7-2376μm^2, 380μm^2 average). El: An anhedral grain infilling a vug in Cp (25μm^2, 1 grain). Frd: Anhedral inclusions in BMS and Sg, may infill fractures or vugs in sulfides (3-24μm^2, 14μm^2 average). Gn: Anhedral inclusions within BMS and Sg, in sulfides Gn can occur as fracture infill (1-945μm^2, 81μm^2 average). Hed: Anhedral inclusions in Sg (1-3μm^2, 2μm^2 average). Hes: Anhedral inclusions in BMS, may infill fractures and vugs (15-31μm^2, 23μm^2 average). Mch: Anhedral inclusions along the outer margins of sulfide veins and blebs (5-1037μm^2, 331μm^2 average). Nic: Anhedral-subhedral grains adjacent to, or along the outer margins of sulfide blebs and veins (148-416μm^2, 401μm^2 average). Spr: Anhedral inclusions in Pn and Sg (12-240μm^2, 216μm^2 average). Tel: Anhedral inclusions within BMS, or along BMS and Sg boundaries (2-127μm^2, 29μm^2 average). Tsu: An anhedral inclusion in Sg (2μm^2, 1 grain).
T13	DH: 1265170 "#MU594576"	N/A	MASU	**Ni:** Po (5.1%), Cp (0.1%), Pn (94.8%) **As:** Cp (0.1%), Pn (1.2%), Spr (98.7%) **Pt:** Spr **Pd:** Po (1%), Cp (20.6%), Pn (11.7%), Mch (66.6%) **Pb:** Po (0.4%), Cp (15.9%), Pn (3.5%), Gn (79.6%), Alt (0.6%) **Co:** Po (2.6%), Pn (97.4%)	Alt: Anhedral inclusions and infills fractures in Cp (5-79μm^2, 27μm^2 average). Gn: Anhedral inclusions, infills fractures and vugs in BMS and Sg; forms compsoite grains with Tel and Hes (4-5783μm^2, 109μm^2 average) . Hes: Anhedral inclusions that infill fractures and vugs in BMS; forms composite grains with Gn (6-1675μm^2, 68μm^2 average). Mch: Anhedral inclusion along the boundary between Cp/Po (549μm^2, 1 grain). Spr: Anhedral-subhedral inclusions in Po (140-16327μm^2, 5536 averageμm^2). Tel: Anhedral inclusions in BMS or Sg, appears to infill fractures and vugs in host (14-3573μm^2, 329μm^2 average).

Notes: Percentages represent the proportion of the total metal content of each sample that is associated with each mineral phase. Abbreviations: pyrrhotite (Po), pentlandite (Pn), chalcopyrite (Cp), altaite (Alt), galena (Gn), tellurobismuthite (Tel), tsumoite (Tsu),hessite (Hes), electrum (El), sperrylite (Spr), michenerite (Mch), froodite (Frd), ungavaite (Ung), molybdenite (Mo), sulfarsenide solid solution (CGSS), silicate gangue (Sg), base metal sulfides (BMS), nickeline (Nic), platinum-group minerals (PGM), pilsenite (Pil),
and hedleyite (Hed).

Chapter 3: The use of biotite chemistry as a pathfinder for magmatic Ni-Cu-PGE (platinum group element) mineralization associated with the Sudbury Igneous Complex

Michael R. Warren*[1], Jacob J. Hanley[1], Doreen E. Ames[2], and Simon E. Jackson[2]

[1]Department of Geology, Saint Mary's University, Halifax, Nova Scotia, Canada

[2]Geological Survey of Canada, Ottawa, Ontario, Canada

*corresponding author email address: michael.warren90@gmail.com

Number of Pages: 61

Number of Figures: 15

Number of Tables: 2

1.0 Abstract

It has been well established that micas and amphiboles are able to accommodate monovalent and divalent metal cations (e.g. Ag^{1+}, Cu^{1+},Co^{2+}, Cu^{2+}, Ni^{2+}), as well as halogens (e.g. Cl and F) through structural substitutions. Substitutions occur within the M-octahedral sites (divalent cations replacing Fe^{2+} and Mg^{2+}), the interlayer cation site (monovalent cations replacing K^{+}), and the replacement of hydroxide by Cl and F. Mechanisms which control these substitutions may include: (i) the unit cell dimensions, which may be controlled by the conditions of crystallization/equilibration, and permissibility-avoidance phenomena (e.g. Ni-Cl avoidance, Fe-Cl permissibility); and (ii) the local availability of sunstitutes (e.g. the activities of F and Cl in a hydrothermal fluid).

A great deal of research has been done on the halogen content of biotite, since it has been shown that these concentrations are partly a function of the activity of the halogens within the fluid or melt phase with which biotite equilibrated. Under certain conditions, halogens may represent important transport mechanisms for specific ore metals (Au, Cu, platinum-group elements), therefore the halogen content of biotite (and other minerals such as amphiboles and apatites) have been considered as an exploration pathfinder for ore deposits (such as porphyry, SEDEX, VMS, and magmatic Ni-Cu-PGE deposits). Recent discoveries have also shown elevated concentraions of ore metals in biotite associated with Ni-Cu-PGE (e.g. Sudbury Igneous Complex), and Ni-poor PGE-rich (Bushveld and Stillwater complexes) mafic to ultramafic sulfide deposits. Despite these findings, a robust evaluation of biotite trace metal chemistry as a pathfinder for ore deposits has not yet been done.

The Sudbury Igneous Complex (SIC) is a 1.85 Ga impact melt sheet, which contains significant resources of Ni-Cu-PGE sulfide ores, found within an array of ore-forming environments. The quartz diorite offset ores are of particular importance owing to their elevated base and precious metal tenors relative to other Sudbury ores. Biotite is ubiquitous throughout the SIC and the surrounding country rocks, furthermore biotite has grown in association with a variety of magmatic, metamorphic, and hydrothermal events. Therefore in this study we investigate the chemistry of biotite from the Totten #2 mine, Worthington offset, and surrounding country rocks in order to: (i) investigate the spatial variation of biotite (both chemical and textural); (ii) relate any variations to host rock chemistry, the occurrence and abundance of sulfides, and discrete biotite populations (i.e. magmatic vs. hydrothermal vs. metamorphic); and (iii) compare biotite chemistry from the Worthington offset to other ore-forming (and barren) Sudbury environments, as well as other mafic-ultramafic deposits worldwide.

Sampling was done using a diamond drill core running perpendicular to sulfide ore in the Worthington offset and intersecting a variety of country rocks found in the vicinity of the Totten #2 mine. Laser ablation-inductively coupled plasma-mass spectroscopy (LA-ICP-MS) was prefromed on biotite from the various lithologies sampled by the diamond drill core. Elevated concentrations of Ni (43.9-2684.1 ppm, 1644 ppm average) were measured in biotite hosted within sulfide- and inclusion-rich quartz dirorite (IQD) relative to the ore-proximal quartz diorite (QD), and surrounding country rocks, with the exception of elevated Ni measured in some country rocks (1031-1420 ppm, 1200 ppm average). This suggests that Ni in biotite can not be used on its own as a pathfinder for Ni-Cu-PGE sulfide ore.

No other systematic variations of ore metal concentrations (e.g. Cu, Co, As, PGE) were discovered with respect to sulfide ore. However, three distinct populations of biotite were distinguished based on textural and chemical criteria: (i) Ni- and Cr- poor (average concentration of 216.3 ppm and 196 ppm respectively) anhedral biotite intergrown with amphibole clusters (found within country rocks, QD and post-offset diabse dykes); (ii) coarse grained biotite with moderate Ni and elevated Cr concentrations (average concentration of 1200 ppm and 3900 ppm respectively; occurs within a select group of country rock samples associated with trace ammounts of base metal sulfides); and (iii) coarse grained euhedral-subhedral biotite lathes with elevated Ni and moderate Cr concentrations (average concentration of 1644 ppm and 862 ppm average respectively; occur exclusively in IQD).

Using a binary diagram of Ni+Cr concentrations in biotite *versus* X_{Mg} values of biotite, it is possible to distinguish two different controls on cation substitution in biotite: (i) Low Ni+Cr concentrations (< 1000 ppm) which show a positive correlation between Ni+Cr and X_{Mg}, indicating that at these concentrations, the Ni+Cr content of biotites is controlled by crystallography (i.e. avoidance and permissibility phenomena); (ii) High Ni+Cr concentrations (≥ 1000 ppm) where there is no correlation between Ni+Cr concentrations and X_{Mg}, suggesting that there is another control (e.g. host rock chemistry) that influences biotite chemistry. This is further supported by the narrow range in X_{Mg} between these two groups, since there is a significant increase in biotite Ni and Cr concentrations without concomitant changes in X_{Mg}.

Additionally, it was found that a binary diagram of the Ni/Cr ratio of biotite *versus* Ni can be used to differentiate between ore-associated biotite from biotite found in other

lithologies. On this diagram,ore-hosting IQD biotites which contain elevated Ni and moderate Cr can be discriminated from biotite from QD and the country rocks (which have low-moderate Ni and low-elevated Cr). Since this signature can only be detected in close proximity (meter scale) to sulfide ore, it would be irrelevant for drill core and underground exploration. However, this technique could potentially be applied to biotite and its weathering products in soils as a vector for surface exposures of ore-hosting IQD.

Despite the already established fact that the Ni content of biotite is not useful on its own as an exploration pathfinder for Ni-Cu-PGE sulfide deposits, comparing the measured Ni concentrations of biotite from this study to other other barren and ore-forming environments, has allowed us to make some important remarks: (i) Ni concentrations in biotite vary greatly between different environments (both barren and ore-forming), indicating the importance of establishing local "background" Ni concentrations in biotite in order to identify what is truly anamolous for that environment; and (ii) large ranges in data with average Ni concentrations in biotite skewed towards low values in some environments suggests the presence of outliers (i.e. contaminated analyses not representative of true dissolved concentrations). These contaminated analyses may have resulted from discrete sulfide inclusions in biotite, or from biotites in direct contact with sulfide grains that has experienced equilibration (diffusion of cations across the sulfide-biotite grain boundary) resulting in avoidance and permissibility phenomena (chemical zoning in biotite). In this study, the analytical method (LA-ICP-MS) allowed us to identify and remove the influence of sulfide inculsions during the analysis of biotite. Furthermore, compositional maps were created in order to confirm that elevated Ni in biotite from this study was not a consequence chemical zoning in biotite.

In conclusion, future work should focus on evaluating variations in biotite chemistry in other ore-forming environments, as well as the potential of using biotite chemistry in surface exploration techniques. In either case, this study highlights important considerations which must be made to ensure a robust investigation: (i) it is important to study biotites from different lithologies and at various distances to known occurences of ore in order to establish "background" concentrations; (ii) The concentration of a single element (e.g. Ni) may not represent an appropriate pathfinder on its own, (iii) the analytical technique must be chosen carefully, although more expensive, LA-ICP-MS provides methods of reducing the risk of contamination, which would result in unrepresentative analyses by other techniques (i.e. EMP).

2.0 Introduction

The incorporation of specific divalent (e.g., Co^{2+}, Cu^{2+}, Ni^{2+}) and monovalent (e.g., Ag^{1+}, Cu^{1+}) metal cations into the structure of micas and amphiboles is well documented in experimental studies (e.g., Klingsberg and Roy, 1957; Hazen and Wones, 1972; Klein and Ito, 1968; Della Ventura et al., 1993). In micas, the substitution of divalent cations occurs within the octahedral M(1-3) sites (that contain Fe^{2+}, Mg^{2+}, Co^{2+}, Cu^{2+}, Ni^{2+}, Zn^{2+}, and Pb^{2+}), whereas monovalent cations replace K in the interlayer sites (Klingsberg and Roy, 1957; Hazen and Wones, 1972; Hazen and Burnham, 1973; Takeda and Morosin, 1975). The capacity for trioctahedral micas to accommodate structural substitutions is strongly influenced by both the ionic radius of the substitute, and the structural parameters of the occupancy site within the mica unit cell (Hazen and Wones, 1972; Volfinger and Robert, 1980; Volfinger et al., 1985). Early experimental work has shown that these unit cell parameters are not significantly influenced by the temperature or

pressure at which the biotite *crystallizes*, and that variations in unit cell dimensions are due to the nature of the cations occupying the interlayer and octahedral sites (Klingsberg and Roy, 1957; Crowley and Roy, 1960; Hazen and Wones, 1972). However, more recently it has been shown that biotite crystals that experience *reequilibration* at T and f_{O2} different than those conditions of formation, show changes in unit cell dimensions due to exchange reactions with their surroundings involving common cations within the biotite structure (e.g., Takeda and Morosin, 1975; Russell and Guggenheim, 1999; Chon et al., 2003). Further complexity in substitution behavior occurs due to exclusionary and acceptance phenomena (e.g. Ni-Cl avoidance; Volfinger et al., 1985). Analytical techniques, such as LA-ICP-MS and EMP, allow quantification of these geochemical variations *in-situ* in samples where multiple generations of metal bearing micas might be present.

Geochemical studies have shown that the Cl and F contents of biotite that equilibrated with hydrothermal solutions are partly a function of the activity of these halogens within the fluid or melt phase from which they crystallized (Munoz, 1984; Munoz and Swenson, 1981; Finch et al., 1995; Coulson, 2001). Since ligands such as chloride may be important for the transportation of specific ore metals (e.g., Au, Cu, platinum-group elements) under certain conditions (e.g. Wood, 1987; Mountain and Wood, 1988; Sassani and Shock, 1990; Gammons, 1995, 1996; Gammons and Williams-Jones, 1995; Xiong and Wood, 2000; Frank et al., 2002; Hanley et al., 2005; Hack and Mavrogenes, 2006; Brugger et al., 2007; Zajacz et al., 2011; and others therein), or may occur in significant concentrations within ore-forming fluids and melts, it is not surprising that biotite halogen geochemistry has been studied in detail as a potential pathfinder mineral for ore

deposits. To date, studies of biotite halogen geochemistry have focused mainly on characterizing ore-forming fluids within porphyry deposits (e.g., Gunow et al., 1980; Sisson, 1987; Shelby and Nesbitt, 2000; Mohammad et al., 2010; Rasmussen and Mortensen, 2012; Siahcheshm et al., 2012), but have also been applied to other ore-forming environments including SEDEX (Jiang et al., 1994), VMS (Zaleski, 1989), and magmatic Ni-Cu-PGE deposits (e.g., Stillwater Complex: Boudreau and McCallum, 1985, Boudreau et al., 1986; Bushveld Complex : Boudreau et al., 1986; and the Sudbury Igneous Complex 'SIC': Farrow, 1994; Li and Naldrett, 1993; Magyarosi et al., 2002; Stewart, 2002; Hanley and Mungall, 2003; Stewart, 2011; and Tuba, 2012). However, independent of the presence of ore metals, halogens may be enriched in hydrothermal solutions that exsolve from magmas during the normal evolution of a magmatic system. Halogen abundance in the fluid phase will be related to the temperature and degree of crystallization, Cl and F content of the magma at the time of exsolution, and the partitioning behavior of these elements. Halogen abundance is perhaps coincidentally high in mineralized systems, owing in part to a lack of data for barren systems, as well as unrecognized factors that influence their abundance unrelated to mineralization.

The few published studies of trace element variability related to mineralization in mafic-ultramafic Ni-Cu-PGE settings, have been carried out at Sudbury, Ontario. Within a diversity of Sudbury ore styles and associated alteration assemblages, elevated concentrations of Ni have been reported in biotite, amphibole and chlorite in proximity to sulfides (Farrow, 1994; Li and Naldrett, 1993; Magyarosi et al., 2002; Hanley and Mungall, 2003; Stewart, 2011; Tuba, 2012; Ames and Kjarsgaard, 2013; and others therein). Biotite is an appropriate mineral for study as a pathfinder/indicator mineral,

because it is ubiquitous throughout both the SIC and all surrounding country rocks, having grown in association with specific and easily discernible magmatic, metamorphic, and hydrothermal events that are well documented in the literature (e.g. Coats and Snajdr, 1984; Thomson et al., 1985; Corfu and Andrews, 1986; Noble and Lightfoot, 1992; Li and Naldrett, 1993; Farrow, 1994; Magyarosi, 1998; Magyarosi et al., 2002; Farrow and Watkinson, 2002; Stewart, 2002; Hanley and Mungall 2003; Tuba, 2012; Ames and Kjarsgaard, 2013). However, there has been no robust evaluation of the factors controlling the Ni enrichment in biotite, and its reliability as a routine exploration tool for Ni-Cu-PGE sulfide ore deposits in the Sudbury environments. In this study we investigate the chemistry of biotite in the Totten offset deposit and surrounding country rocks. Totten is a magmatic Ni-Cu-PGE sulfide deposit hosted within a radial dyke of quartz diorite that is interpreted as part of the earliest crystallized phase of the SIC (Lightfoot et al., 2001). Despite evidence of complex interaction of with its metasedimentary and metavolcanic country rocks, and overprinting by syn- to post-emplacement hydrothermal and metamorphic events, the dyke remains a spatially distinct unit hosting isolated sulfide ore bodies with disseminated halos (Zurbrigg et al., 1957; Cochrane, 1984; Grant and Bite, 1984; Lightfoot et al., 1997; Lightfoot and Farrow, 2002; Murphy and Spray, 2002; Tuchscherer and Spray, 2002; Stewart, 2011). The objectives of this study are to: (i) investigate the spatial variation of biotite in and surrounding the Worthington offset dyke hosting the Totten deposit; (ii) relate any variations to host lithology trace element content, sulfide presence and abundance, and discrete biotite populations (i.e., magmatic vs. hydrothermal vs. metamorphic); and (iii)

compare the chemistry of biotite from the Worthington offset to biotite from other Sudbury environments, as well as other magmatic Ni-Cu-PGE deposits worldwide.

2.1 Regional geology of the Sudbury Igneous Complex

The elliptical (60 x 30 km; Ames et al., 2008) Sudbury structure in Ontario, Canada, occurs at the contact of the Archean Superior Province, and the Early Proterozoic Southern Province (Card et al., 1984; Ames et al., 2008; Figure 1). Contained within the Sudbury structure is the Sudbury basin comprised of the Whitewater group and the Sudbury Igneous Complex (SIC). The widely accepted theory that the Sudbury Structure was produced through a hypervelocity meteorite impact was established by the discovery of shatter cones in the surrounding country rocks (Dietz, 1964), and was further supported by subsequent observations of inferred impact-related features and their comparison to known impact sites (e.g., French, 1967, 1970; Dence, 1972; Peredery, 1972). The approximate age of this astrobleme was determined to be 1.85 Ga ±1 Ma (Krogh et al., 1982), making it one of the oldest preserved impact structures on Earth. The SIC itself represents an impact melt sheet, largely sourced from crustal material, with other constituents that differentiated during slow cooling (Dietz, 1964; Naldrett and Hewins, 1984; Grieve, 1991; Deutsch and Grieve, 1994; Therriault et al., 2002; Mungall et al., 2004). The SIC is an atypical layered intrusion in that (i) it has a crustal geochemical and isotopic signatures with no mantle constituents; (ii) its felsic unit (granophyric residue) is much thicker than what is usually seen in layered intrusions; (iii) it has an overall intermediate composition rather than mafic-ultramafic bulk composition; and (iv) fine scale igneous layering is absent (Naldrett and Hewins, 1984; Therriault et al., 2002). The SIC is also unique as an impact-related melt sheet since its thickness is

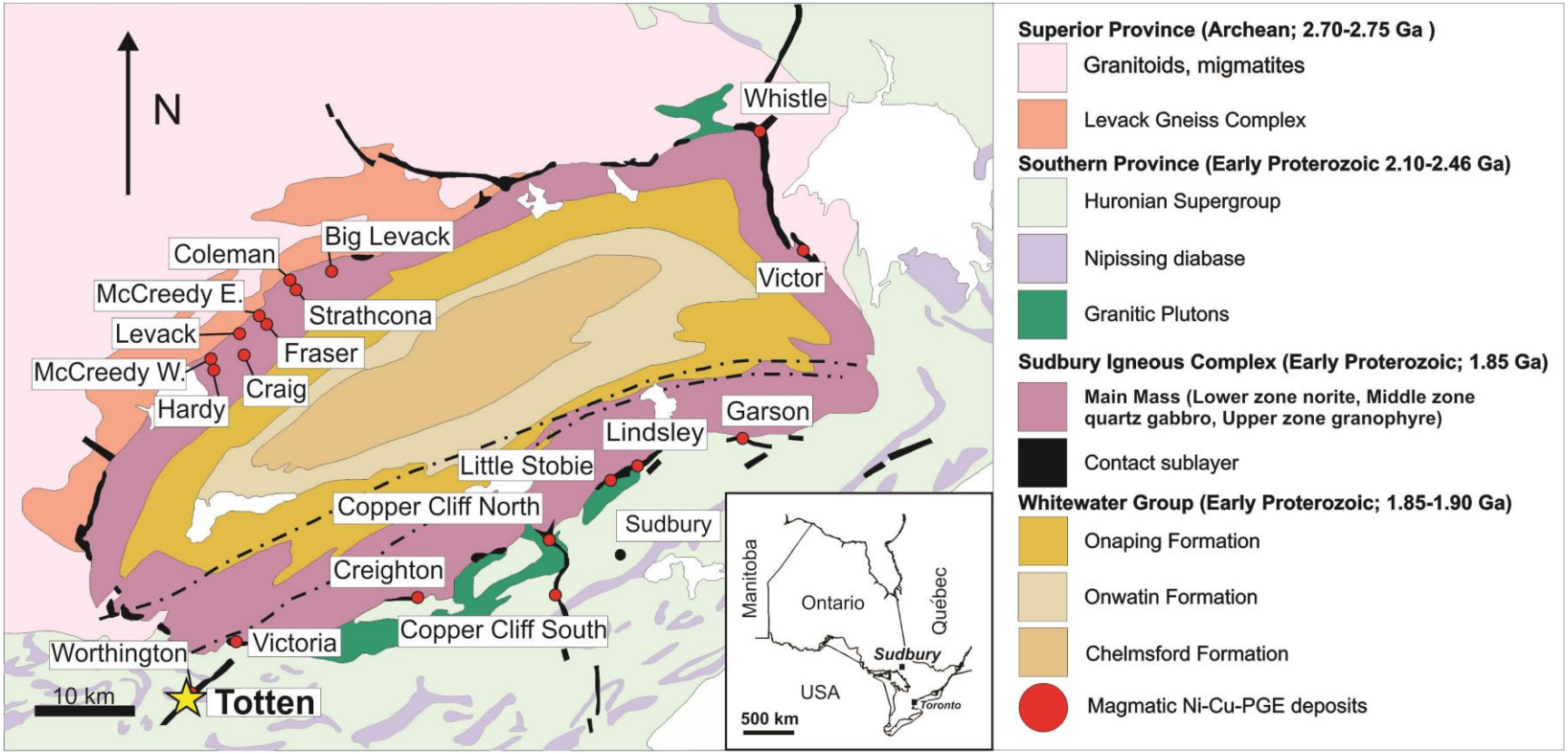

Figure 1. Geological map of the Sudbury Igneous complex, including the locations of major Ni-Cu-PGE deposits. Modified after Rousell et al., 2003; and Ames et al., 2008.

much greater than other impact melts, and it demonstrates layering resulting from differentiation (Lightfoot et al., 2001; Therriault et al., 2002).

The SIC is divided into the main mass and contact sublayer. The main mass of the SIC is divided into the North and South Ranges, and is composed from base to top of norite, 'transitional' quartz gabbro, and granophyre (Naldrett and Hewins, 1984; and references therein). The contact sublayer is a volumetrically minor component of the SIC, but hosts important Ni-Cu-PGE deposits. The contact sublayer can be subdivided into two groups: (i) an igneous texture rock of noritic, gabbroic, and dioritic composition, and (ii) metamorphic textured leucocratic breccia (Pattison, 1979). The sublayer occurs as discontinuous lenses along the margins of the SIC within structural traps known as "embayments", and as structurally controlled radial and concentric offset dykes occurring within country rocks (Pattison, 1979; Grant and Bite, 1984; Naldrett et al., 1984; Farrow and Lightfoot, 2002). Parts of the contact sublayer (called inclusion-rich quartz diorite) often contains inclusions of country rocks, quartz diorite (in the case of offset dykes, where there is evidence of multiple sublayer injection events), and mafic-ultramafic inclusions whose origin is unclear (Pattison, 1979; Scribbins et al., 1984).

2.2 Geology of the Worthington offset

Detailed descriptions of the geology of the Worthington offset are given by Lloyd (2001), Stewart (2002), and Lightfoot and Farrow (2002). The Worthington offset is located near the southwest margin of the SIC between the Denison and Drury townships (Figure 2). The Worthington offset is a radial-type dyke which extends more than 15 km away from the SIC. The dyke pinches and swells along its length, ranging in thickness from 30 to 100 meters and dips approximately 80 degrees to the southeast. The Creighton

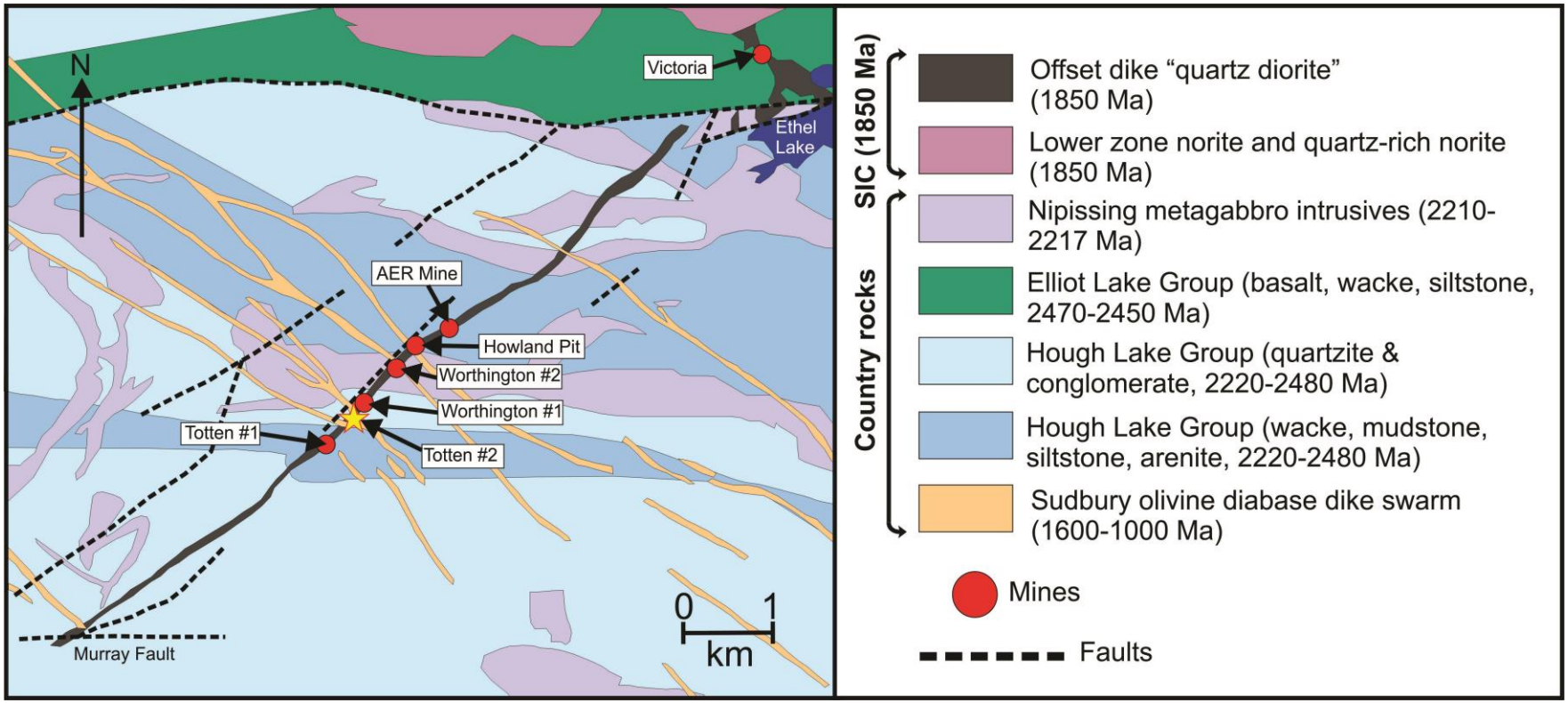

Figure 2. Local geology of the Worthington offset, and locations of Ni-Cu-PGE mines. Modified after Lightfoot and Farrow (2002); and Ames et al. (2008). The focus of this study is the Totten #2 mine, which is marked with a star.

fault in the northern portion of the offset environment, and the Murray fault in the south, has caused dextral displacement of the Worthington dyke. The dyke is comprised of inclusion-poor quartz diorite (QD), and a central zone of inclusion-rich quartz diorite (IQD). Although both varieties of QD contain sulfides, economic zones of sulfide mineralization are associated with IQD. Inclusions in the IQD are typically subrounded, consisting mainly of amphibolite, metagabbro, and lesser QD inclusions. Inclusions of metasedimentary country rocks are rare. Occurrences of IQD are usually localized to the center of swells in the width of the offset, enclosed by QD. However, in areas where the offset dyke is in contact with Nipissing amphibolite-metagabbro country rocks (otherwise known as Sudbury gabbro), the contact is defined by a megabreccia of amphibolite clasts (of similar texture and geochemistry to the gabbroic country rocks) supported by an IQD matrix. Locally, this megabreccia is present across the offset. The contact between the Worthington offset and other country rocks is generally sharp, whereas the contact between QD and IQD ranges from sharp to diffuse.

In the vicinity of the Totten Mine area, the Worthington offset cross cuts metasediments, and Sudbury gabbro. These Huronian metasediments consist of conglomerate, sandstone, phyllite and argillite of the Pecors formation, a member of the Hough Lake group (Stewart, 2002). Sudbury gabbro is a term used to describe the 2.2 Ga Nipissing diabase, which commonly intrudes the sequences of the Huronian Supergroup (Corfu and Andrews, 1986; Noble and Lightfoot, 1992). The composition and mineralogy of these intrusives is complex, owing to the assimilation of country rocks, variable rates of cooling, and syn- post emplacement modification by primary (magmatic) and secondary (metamorphism, hydrothermal alteration) processes. The SIC and its

surrounding country rocks, are cross cut by the 1.2 Ga Sudbury diabase dyke swarm (Krogh et al., 1987; Dudás et al., 1994). These units are typically fine to medium grained with sharp contacts with their country rocks. Biotite (primary or secondary origin is unclear) occurs as an accessory phase in these rocks (Lloyd, 2001).

3.0 Methods

3.1 Sampling strategy

In order to study the variations in the trace metal content of biotite as a function of distance from ore, host rock lithology, and to define the normal "background" levels of ore metals contained within biotite (both primary and secondary) from the Worthington area, samples were collected from a diamond drill core intersecting the Worthington offset dyke and associated sulfide mineralization within country rocks, QD, and IQD, with the intersection being sub-perpendicular to the dyke. A selection of 19 representative samples of the major barren and mineralized lithologies was chosen for detailed investigation, over a perpendicular-to-dyke traverse in drill core of approximately 370 meters. Additionally, selection was also based on biotite grains being of sufficient size (approximately $\geq$ 0.2 mm) and abundance (approximately 1% by volume) for multiple representative analyses by LA-ICP-MS. These parameters were necessary in order to ensure that: (i) biotite chemistry within samples was homogenous, (ii) biotite grain boundaries could be avoided in order to reduce contamination by adjacent minerals, (iii) reasonable detection limits were maintained which are a function of the mass sampled during ablation, and (iv) A maximum number of analyses could be obtained per sample. Major units intersected by the drill hole were identified using Vale drill logs and are described as metagabbro (a term Vale geologists use to describe the local metamorphic wackes, siltstones, mudstones, arenites, conglomerates, quartzites, and basalts of the

Huronian Supergroup, not to be confused with Nipissing gabbro), Sudbury diabase dykes, quartz diorite, inclusion-rich quartz diorite, and a conglomerate (Lloyd, 2001, describes the conglomerate as a metasedimentary matrix-supported unit with quartz, argillite, and granitic clasts that vary widely in modal abundance). Two additional samples were collected from the active underground mining to represent "ore-associated" biotite in close proximity to sulfide ore. Polished thick sections were produced for each sample for LA-ICP-MS analysis.

3.2 Trace metal content of biotite by LA-ICP-MS

The trace metal analysis and compositional mapping of biotite grains was performed by laser ablation-inductively coupled plasma-mass spectroscopy (LA-ICP-MS), at the Geological Survey of Canada, Ottawa. Details of the conditions for the analyses (including beam size, and standards used) are summarized in Table 1. Grain boundaries, cleavage planes, and grains which contained visible inclusions were avoided in order to reduce contamination. The isotopes Ca^{42} (whose count rate increases when amphibole and plagioclase are encountered) and K^{39} (whose count rate decreases when chlorite is encountered) were monitored in order to avoid contamination from other hydroxysilicates. Data reduction was done using the Glitter^{TM} software package, which can select portions of each signal that have consistent count rates, eliminating any sources of contamination in the signal. Furthermore quality control standards (BCR-2G, NISTSRM612) were were analyzed to ensure the accuracy of results (which are in agreement with accept values, section 4.1) The internal standard used was Al, an average for Al was calculated using biotite data determined from EMP for the Worthington area by Magyarosi (1998), which shows that the Al content of biotite is consistent throughout

Table 1: LA-ICP-MS operating conditions

LA	
Model	Photon Machines Analyte.193
Wavelength	193 nm
Pulse duration (FWHM)	4 ns
Repetition rate	10 Hz
Spot diameter	26-86 μm
Energy density	ca. 4 J/cm^2
Primary (calibration) standard	**GSD-1G:** Synthetic basaltic glass duped with over fifty different trace metals
Secondary quality control standards	**BCR-2G**: glass standard produced through the melting of the USGS standard BCR-2, a natural basalt **NISTSRM612:** Synthetic glass duped with a variety of trace elements
ICP-MS	
Model	Agilent 7700x with additional interface rotary pump which approximately doubles instrument sensitivity
Forward power	1550 kW
Shield torch	Used
Sampling depth	7 mm
Gas flows (He carrier mixed downstreamn from cell with Ar make up):	
Carrier (HE)	0.6 L/min
Make up (Ar)	1.08 L/min
ThO^+/Th^+	<0.3%
U^+/Th^+ (NIST 612)	ca. 1.05
Data acquisition parameters	
Data acquisition protocol	Time Resolved Analysis
Scanning mode	Peak hopping, 1 point per blank
Dwell time per isotope	10 ms for all masses (earlier analyses) or as indicated below
Detector mode	Pulse counting except analogue for isotopes in italics below
Isotopes determined (dwell time ms)	^{23}Na(5), ^{25}Mg(5), ^{27}Al(5),^{29}Si(5),^{34}S(5), ^{39}K(5), ^{42}Ca(5), ^{49}Ti (10), ^{55}Mn(10),^{57}Fe(5), ^{59}Co(10), ^{60}Ni(5), ^{61}Ni(10), ^{65}Cu(10), ^{66}Zn(10), ^{75}As(10), ^{77}Se(10), ^{88}Sr(5), ^{89}Y(5), ^{90}Zr(5), ^{99}Ru(15), ^{101}Ru(15), ^{102}Ru(15), ^{103}Rh(15), ^{105}Pd(15), ^{106}Pd(15), ^{107}Ag(15), ^{108}Pd(15), ^{109}Ag(15), ^{111}Cd(10), ^{118}Sn(15), ^{121}Sb(10), ^{125}Te(10), ^{181}Ta(5), ^{185}Re(15), ^{189}Os(15), ^{193}Ir(15), ^{195}Pt(15), ^{197}Au(15), ^{202}Hg(10), ^{205}Tl(10), ^{206}Pb(10), ^{208}Pb(10), ^{209}Bi(10)
Quadrupole settling time	1-5 ms depending upon mass jump
Analysis time	120 s: ~40 s gas blank, up to ~80 s of ablation
Internal standard:	Al_2O_3 (18.44 wt%; Magyarosi, 1998)

the Worthington area. This was later independently confirmed for biotite in the samples in this study by SEM-EDS analysis.

3.3 SEM analysis of Totten Biotite

Silicon drift detectors (SDD), such as the INCA X-max 80mm 2 EDS system used by the scanning electron microscope (SEM) at Saint Mary's University, may perform with comparable accuracy and precision to wavelength dispersive spectrometers (WDS; Ritchie et al., 2012; Owen, 2012). Therefore, biotite from this study were analyzed using EDS in order to monitor the changes in major element geochemistry as a function of distance from the Totten ores, and host lithology. The device used was a LEO 1450 VP SEM, with an accelerating voltage of 25 kV. The beam current ranged from 5-20 nA and a working distance between 19-22mm was used. Backscattered electron images (BSE), were used in order to locate grains of biotite during EDS analysis.

3.4 Bulk rock analysis

In order to compare the changes in the trace metal content of biotite, relative to bulk rock geochemistry, samples were analyzed by X-Ray fluorescence spectroscopy (XRF), at Saint Mary's University, Canada. 1 gram of crushed sample was mixed with a lithium borate flux in a platinum crucible. Using a Claisse Fluxy fusion device, each sample was heated to approximately 1050°C to produce a 30 mm disk. These disks were then analyzed using a Philip's PW2400 XRF, and sample location was managed using a Philip's PW2510 102 sample position changer. The X-rays used to induce fluorescence are produced using a 3kW Rh anode. The Philip's PW2400 is a wavelength-dispersive sequential spectrometer, which uses natural and synthetic crystals to disperse photons. In

addition to the major elements, trace elements such as Co, Ni, Cu, and Pb were also analyzed.

4.0 Results

4.1 Variations in the metal content of biotite

The results of the LA-ICP-MS and SEM-EDS analyses of biotite from the Totten mine area are given in Table 2. Biotite demonstrates a wide range in concentrations of Cr (12.9-5893.9 ppm, 832 ppm average; n=292), Ba (142.9-5234.1 ppm, 2367.7 ppm), Co (35.3-133.1 ppm, 89.2 ppm average), Zn (61.5-388.1 ppm, 220.6 ppm average), Ti (866-20667 ppm, 11244.3 ppm average), Rb (39.9-827.9 ppm, 503.4 ppm), Cs (3.8-161.1 ppm, 39.5 ppm average), and Mn (686.3-2274.9 ppm, 1259.2 ppm average). There is no systematic variation in the concentrations of these elements as a function of lithology, or distance to sulfide ore. Elevated concentrations of Ni (43.9-2684.1 ppm, 1644 ppm average; n=76; Figure 3) were discovered in biotite hosted in the sulfide- and inclusion-rich quartz diorite (IQD). This is much greater than the concentrations found in biotite from the QD and other lithologies (43.9-687.4 ppm, 216.3 ppm average; n=219), with the exception of some anomalous biotite measurements within the Huronian country rocks (Figure 3). Interestingly, these country rock samples contain trace ammounts of pyrrhotite, pentlandite, and chalcopyrite. The anomalous country rock analyses indicate that the Ni content of biotite alone cannot be used as an exploration tool for Ni-Cu-PGE deposits. Another diagram comparing the dissolved Ni in biotite to bulk rock Ni demonstrates no systematic variation in relation to sulfide ore (Figure 4). Although IQD hosted biotite contain elevated concentrations of Ni, the ratio of dissolved Ni in biotite to bulk rock Ni is suppressed by an even greater increase in the bulk rock concentration.

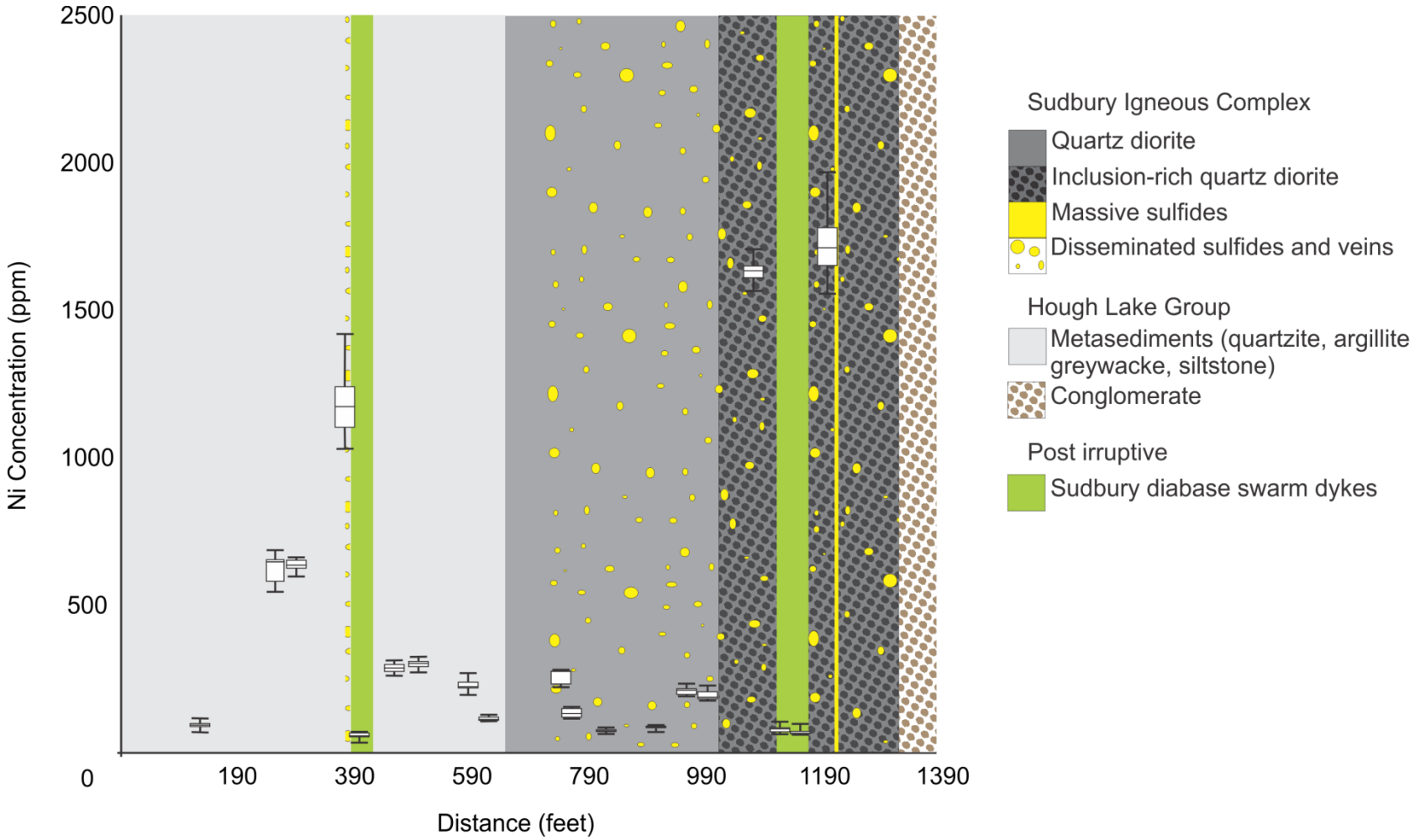
2500
2000
1500
1000
500
0
Ni Concentration (ppm)
190
390
590
790
990
1190
1390
Distance (feet)
Sudbury Igneous Complex
Quartz diorite
Inclusion-rich quartz diorite
Massive sulfides
Disseminated sulfides and veins
Hough Lake Group
Metasediments (quartzite, argillite greywacke, siltstone)
Conglomerate
Post irruptive
Sudbury diabase swarm dykes

Figure 3 (previous page). Box-plots of the Ni-concentration in biotite along Totten drill hole 1265980. For each sample the maximum, minimum, first quartile (upper box), third quartile (lower box), and mean (separation between boxes) values are given. Lithological units were added using data from Vale drill logs. Altough sulfides are shown in both QD and IQD, the relative proportions of sulfide mineralization are not distinguished, and it is important to note that sulfides are more abundant in the IQD samples than in QD.

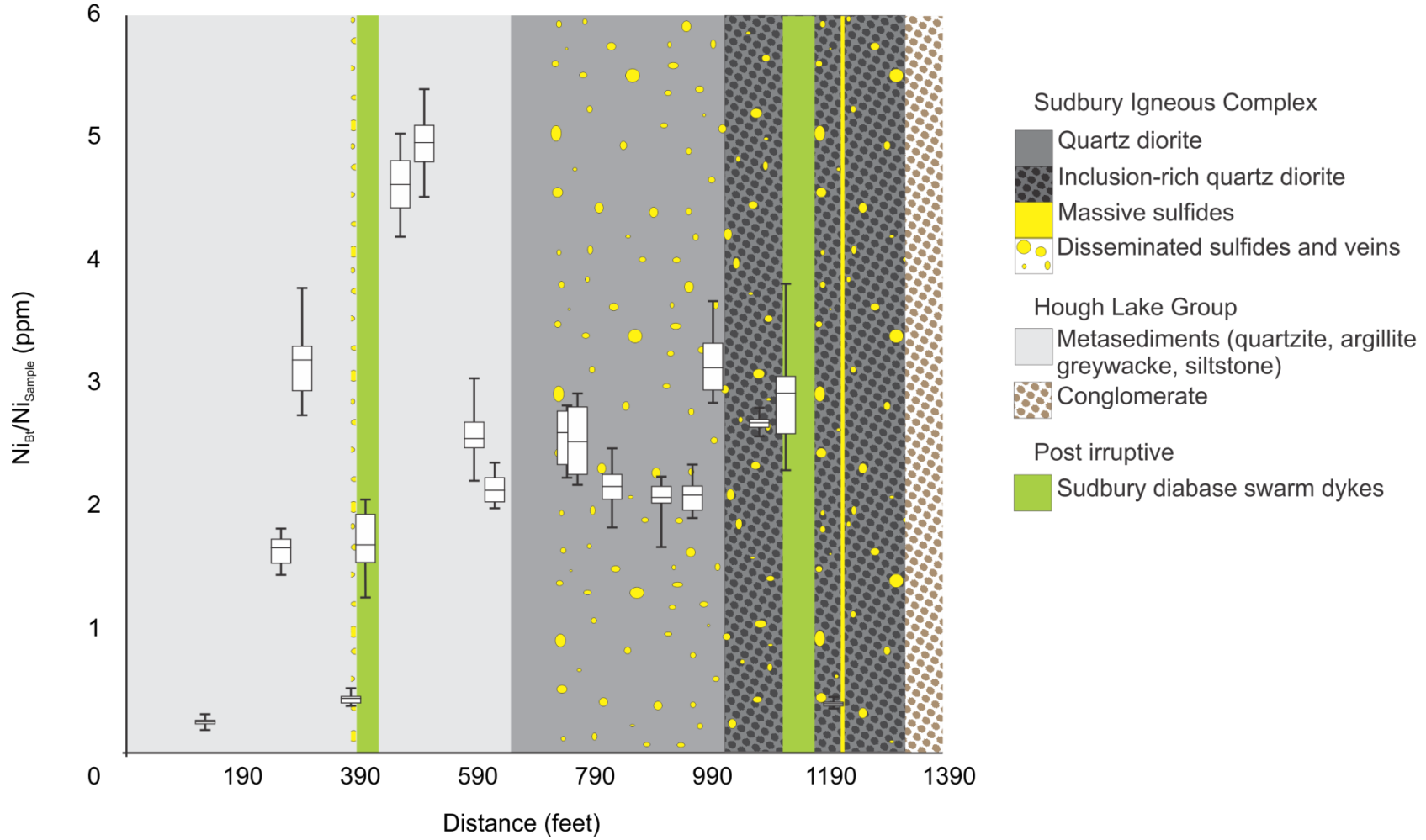
6
5
4
3
2
1
0
Ni_{Bt}/Ni_{Sample} (ppm)
190
390
590
790
990
1190
1390
Distance (feet)
Sudbury Igneous Complex
Quartz diorite
Inclusion-rich quartz diorite
Massive sulfides
Disseminated sulfides and veins
Hough Lake Group
Metasediments (quartzite, argillite greywacke, siltstone)
Conglomerate
Post irruptive
Sudbury diabase swarm dykes

Figure 4 (previous page). Box-plots of the ratio of Ni contained within biotite (Bt) and the bulk rock concentration of Ni along Totten drill hole 1265980. For each sample the maximum, minimum, first quartile (upper box), third quartile (lower box), and mean (separation between boxes) values are given. Lithological units were added using data from Vale drill logs. Altough sulfides are shown in both QD and IQD, the relative proportions of sulfide mineralization are not distinguished, and it is important to note that sulfides are more abundant in the IQD samples than in QD.

Table 2: Biotite compositions in the Totten area (SEM-EDS/ LA-ICPMS)

	Country Rocks																Sudbury diabase swarm dykes					
	T47		T54		T87		T69		T80		T84		T123		T62		T71		T106		T120	
	Range	Average (n)	Range	Average (n)	Range	Average (n)	Range	Average (n)	Range	Average (n)	Range	Average (n)	Range	Average (n)	Range	Average (n)	Range	Average (n)	Range	Average (n)	Range	Average (n)
MgO (wt%)	9.88-10.7	10.2 (16)	13.8-15.3	14.8 (10)	9.83-11.2	10.7 (8)	15.1-15.8	15.6 (9)	11.7-13.1	12.5 (9)	10.2-11.4	10.8 (9)	10.3-12.1	11.4 (9)	13.3-14.9	14.1 (11)	9.2-10.5	9.7 (8)	7.6-9.3	8.48 (9)	7.63-9.53	8.55 (9)
Al_2O_3 (wt%)	17.9-19.7	18.7 (16)	16-17.4	16.7 (10)	18-19.4	18.5 (8)	17.6-18.2	17.9 (9)	17.9-19.1	18.5 (9)	18.5-19.4	19.1 (9)	17.6-19.7	18.9 (9)	16-17.6	17 (11)	17.7-18.7	18.1 (8)	17.3-18.8	18.1 (9)	15.5-19.3	18.3 (9)
SiO_2 (wt%)	42-43.7	42.6 (16)	41.9-43.9	42.7 (10)	39.6-41.7	40.5 (8)	42.1-42.7	42.4 (9)	40.6-42.7	41.3 (9)	39.5-41.2	40.4 (9)	41.2-43.1	42 (9)	42-44.2	42.9 (11)	40.9-42.5	41.9 (8)	40.8-43.4	41.6 (9)	40.1-44.1	42 (9)
K_2O (wt%)	8.45-9.38	8.98 (16)	9.53-10.1	9.83 (10)	9.59-10.2	9.88 (8)	9.73-10.1	9.95 (9)	9.46-10.3	9.97 (9)	9.5-10.1	9.87 (9)	9.28-10	9.57 (9)	8.98-10.1	8.7 (11)	9.06-9.62	9.28 (8)	8.84-9.94	9.23 (9)	8.64-10.1	9.25 (9)
TiO_2 (wt%)	1.48-1.87	1.64 (16)	1.51-2.02	1.74 (10)	1.75-2.36	2 (8)	1.23-1.64	1.43 (9)	1.52-1.72	1.62 (9)	1.56-1.94	1.76 (9)	1.25-1.99	1.67 (9)	1.58-2.06	1.8 (11)	1.56-2	1.77 (8)	1.28-2.31	1.92 (9)	1.18-2.97	1.82 (9)
FeO (wt%)	16.5-18.8	17.8 (16)	13.6-15.3	14.3 (10)	16.4-19.1	18.3 (8)	12.5-12.9	12.7 (9)	15.5-16.4	16 (9)	17.5-18.8	18.2 (9)	15.5-17.5	16.4 (9)	14.1-15	14.6 (11)	18.2-20	19.2 (8)	19.6-22	20.7 (9)	18.2-23.7	20.1 (9)
Ca (ppm)	BDL-158	87.7 (10)	BDL-374	133 (3)	BDL-173	87.5 (6)	BDL-61	28.1 (4)	BDL-70.7	34.1 (9)	BDL-43.8	25.3 (4)	BDL-158	73.8 (5)	BDL-205	98.3 (6)	BDL-25.5	25.5 (1)	BDL-43.6	43.6 (1)	BDL-201	87.3 (3)
Cr (ppm)	547-1162	773	3793-5894	4642	143-190	165	1762-4822	3077	366-518	447	293-382	350	174-583	290	3105-4659	3982	16.1-40.1	23.8	6.29-52.3	20.5	4.44-12.9	8.97
Mn (ppm)	1084-1299	1166 (16)	686-847	770 (13)	918-1066	976 (12)	964-1202	1044 (15)	919-1061	971 (15)	688-771	725 (7)	829-1179	999 (13)	751-1807	908 (10)	1753-1959	1860 (11)	1866-2085	2013 (11)	1973-2275	2154 (6)
Co (ppm)	58.8-77.6	68.7 (16)	79.4-97.7	90.9 (13)	89.1-104	96.6 (12)	35.3-45.1	38.4 (15)	83.4-94.6	88.6 (15)	92.3-99.9	95.6 (7)	98.3-133	109 (13)	89-105	97.3 (10)	69.5-85.8	78.7 (11)	93.1-112	100 (11)	97-114	107 (6)
Ni (ppm)	69.6-117	93.9 (16)	546-687	628 (13)	107-127	115 (12)	1031-1420	1200 (15)	261-314	288 (15)	273-326	300 (7)	197-271	227 (13)	598-663	637 (10)	43.9-71.6	58.8 (11)	62-98.4	70.2 (11)	63.6-105	80.8 (6)
Cu (ppm)	BDL-0.148	0.130 (4)	BDL-0.260	0.138 (4)	BDL-4.22	1.04 (7)	BDL-0.750	0.195 (8)	BDL-0.287	0.127 (10)	BDL-0.257	0.163 (3)	BDL-25	8.04 (9)	BDL-0.230	0.205 (2)	BDL	-	BDL-0.124	0.116 (2)	BDL-4.02	4.02 (1)
Zn (ppm	171-224	203 (16)	113-149	130 (13)	253-302	283 (12)	93.1-127	116 (15)	124-144	134 (15)	201-231	212 (7)	205-274	245 (13)	123-166	136 (10)	316-381	338 (11)	300-359	325 (11)	336-388	357 (6)
As (ppm)	BDL-0.253	0.185 (5)	BDL-0.71	0.509 (6)	BDL-0.57	0.358 (10)	BDL-0.7	0.35 (13)	BDL-0.291	0.169 (5)	BDL-0.36	0.291 (5)	BDL-0.41	0.214 (5)	BDL-0.6	0.444 (7)	BDL-0.35	0.223 (2)	BDL-0.56	0.327 (6)	BDL-0.18	0.18 (1)
Rb (ppm)	491-610	539 (16)	434-642	542 (13)	442-529	504 (12)	371-490	441 (15)	443-631	544 (15)	578-828	678 (7)	474-676	577 (13)	473-622	556 (10)	322-418	386 (11)	319-407	359 (11)	331-409	369 (6)
Sr (ppm)	0.189-1.56	0.536 (16)	0.38-0.687	0.528 (13)	0.097-0.315	0.191 (12)	0.249-0.534	0.342 (15)	0.240-0.876	0.446 (15)	0.541-4.34	1.43 (7)	0.131-0.968	0.33 (13)	0.547-1.25	0.761 (10)	0.274-0.734	0.493 (11)	0.187-0.71	0.37 (11)	0.321-5.97	1.4 (6)
Y (ppm)	0.0278-0.273	0.0733 (16)	BDL-0.074	0.0274 (11)	0.0196-0.0641	0.0363 (12)	0.0123-0.109	0.041 (15)	0.0362-3.72	0.789 (15)	0.082-27.8	7.1 (7)	0.0248-0.0717	0.0391 (13)	BDL-1.03	0.156 (9)	0.0368-0.86	0.135 (11)	0.035-0.09	0.0598 (11)	0.0415-0.062	0.0574 (6)
Pd (ppm)	BDL-0.035	0.035 (1)	BDL	-	BDL	-	BDL	-	BDL	-	BDL-0.025	0.025 (1)	BDL-0.013	0.00995 (2)	BDL	-	BDL-0.022	0.022 (1)	BDL	-	BDL	-
Ag (ppm)	BDL-0.028	0.028 (1)	BDL-0.047	0.0289 (3)	BDL	-	BDL	-	BDL-0.0106	0.0106 (1)	BDL-0.0269	0.0184 (2)	BDL-0.0212	0.0161 (4)	BDL-0.035	0.035 (1)	BDL	-	BDL-0.036	0.0171 (5)	BDL	-
Cd (ppm)	BDL-0.095	0.0667 (3)	BDL-0.125	0.111 (2)	BDL-0.097	0.077 (2)	BDL-0.079	0.051 (5)	BDL-0.098	0.0698 (4)	BDL	-	BDL-0.071	0.0675 (2)	BDL	-	BDL-0.16	0.16 (1)	BDL	-	BDL-0.137	0.122 (3)
Sn (ppm)	0.146-0.527	0.3 (16)	0.450-0.667	0.549 (13)	0.304-0.809	0.433 (12)	0.29-14.4	1.33 (15)	1.22-2.19	1.85 (15)	1.28-2.05	1.61 (7)	0.228-0.461	0.335 (13)	0.329-0.644	0.508 (10)	0.2-1.43	0.565 (11)	0.178-0.276	0.221 (11)	0.097-0.289	0.191 (6)
Sb (ppm)	BDL-0.0188	0.0143 (6)	BDL-0.032	0.032 (1)	BDL-0.023	0.0205 (5)	BDL-0.036	0.0199 (12)	BDL-0.02	0.0145 (11)	BDL-0.019	0.014 (5)	BDL-0.0338	0.0231 (6)	BDL-0.048	0.034 (3)	BDL-0.03	0.0196 (5)	BDL-0.025	0.0215 (2)	BDL-0.023	0.023 (1)
Cs (ppm)	40.9-64.2	49.9 (16)	45.8-70.4	60.5 (13)	16.5-46.3	32.3 (12)	11.7-45.8	23.3 (15)	29.2-55	41.7 (15)	38.0-73.4	50.4 (7)	11.1-67.4	32.3 (13)	52.5-83.6	63.5 (10)	18.0-43.9	34.3 (11)	10.5-31	23.2 (11)	15.7-23.5	19.6 (6)
Ba (ppm)	2450-3032	2669 (16)	1325-1625	1439 (13)	2223-2486	2389 (12)	1147-2312	1618 (15)	1298-1585	1429 (15)	417-471	439 (7)	2037-3279	2578 (13)	1892-2313	2142 (10)	4195-5234	4821 (11)	4175-4695	4500 (11)	4350-4580	4457 (6)
Pb (ppm)	0.242-3.54	0.901 (16)	0.063-1.09	0.335 (13)	0.193-0.856	0.368 (12)	0.18-1.05	0.374 (15)	0.256-1.88	0.718 (15)	0.639-1.97	1.01 (7)	0.312-2.14	0.893 (13)	0.102-0.85	0.318 (10)	0.510-3.22	1.79 (11)	0.54-2.52	1.29 (11)	0.52-1.9	1.08 (6)
Bi (ppm)	BDL-0.0113	0.00596 (8)	BDL-0.0101	0.00685 (2)	BDL-0.086	0.0269 (5)	BDL-0.044	0.0118 (8)	BDL-0.0079	0.00513 (6)	BDL-0.108	0.0256 (6)	BDL-0.155	0.047 (6)	BDL-0.0284	0.0207 (3)	BDL-0.022	0.0117 (3)	BDL-0.0104	0.00615 (6)	BDL-0.006	0.006 (2)

Notes: Abbreviation BDL stands for below detection limit. Major elements analyzed by EDS, trace elements by LA-ICPMS. Major element concentrations are slightly elevated since analyses are anhydrous. Average values were calculated excluding analyses below detection limits (the number of analyses, "n", are given for each calculation).

Table 2 (continued): Biotite compositions in the Totten area (SEM-EDS/ LA-ICPMS)

	Quartz diorite												Inclusion-rich quartz diorite							
	T92		T97		T117		T126		T132		T103		T137		T143		TU11		TU14	
	Range	Average (n)	Range	Average (n)	Range	Average (n)	Range	Average (n)	Range	Average (n)	Range	Average (n)	Range	Average (n)	Range	Average (n)	Range	Average (n)	Range	Average (n)
MgO (wt%)	10.1-12	11.2 (9)	11-12.4	11.7 (9)	10.1-11	10.7 (9)	10-11.2	10.4 (8)	9.32-9.86	9.61 (22)	11.4-12	11.8 (9)	11-12.4	11.6 (9)	12.8-14	13.2 (8)	10-10.8	10.3 (9)	10.6-12.4	11.4 (8)
Al_2O_3 (wt%)	17.7-20.7	19 (9)	17.8-18.8	18.4 (9)	18.2-18.5	18.4 (9)	17.7-19.4	18.5 (8)	17-18.5	17.7 (22)	17.6-18.7	18 (9)	17.7-18.8	18.1 (9)	17.3-18.1	17.6 (8)	16.7-18.3	17.5 (9)	16.6-19.8	18.4 (8)
SiO_2 (wt%)	39.9-42.8	41.6 (9)	41.7-43.1	42.7 (9)	39.9-41.4	40.5 (9)	40.1-41.7	40.8 (8)	39.6-41.9	40.5 (22)	40.1-40.9	40.6 (9)	41.4-42.9	42.2 (9)	40.7-42.5	41.3 (8)	39-41.5	40.5 (9)	40.1-42.5	41.2 (8)
K_2O (wt%)	9.35-10.2	9.64 (9)	8.98-9.69	9.37 (9)	9.59-10.2	9.91 (9)	9.32-10.2	9.64 (8)	9.41-10.2	9.87 (22)	9.95-10.2	10.1 (9)	9.12-10.1	9.61 (9)	9.62-10.4	10 (8)	8.84-10.1	9.52 (9)	8.86-9.95	9.34 (8)
TiO_2 (wt%)	1.35-2.29	1.86 (9)	1.25-1.87	1.66 (9)	1.73-1.99	1.87 (9)	1.41-2.21	1.89 (8)	1.59-2.23	1.98 (22)	1.39-1.87	1.67 (9)	1.36-1.83	1.57 (9)	1.17-1.91	1.68 (8)	1.45-2.15	1.86 (9)	1.64-1.97	1.82 (8)
FeO (wt%)	15.7-18.4	16.7 (9)	15.1-17.2	16.2 (9)	17.7-19.4	18.6 (9)	18.1-19.1	18.8 (8)	19.4-21.1	20.3 (22)	17.6-18.1	17.8 (9)	16-17.3	16.9 (9)	14.7-17	16.2 (8)	19-22.9	20.3 (9)	17-19.1	17.8 (8)
Ca (ppm)	BDL- 61.8	42.5 (3)	BDL-284	89.5 (8)	BDL-55.8	34.1 (5)	BDL-240	92.3 (8)	BDL-177	66.8 (12)	BDL-212	61.5 (6)	BDL-94.4	94.4 (1)	BDL-64.1	26.3 (5)	BDL-196	50.7 (9)	BDL-170	60.5 (10)
Cr (ppm)	24.4-672	131	67.5-494	201	52.1-119	77.5	6.51-91	28.3	38.9-110	66.2	81.8-207	165	2006-2455	2241	325-553	426	220-568	400	51.7-637	382
Mn (ppm)	1107-1350	1264 (13)	1305-1507	1414 (18)	904-1177	1027 (20)	940-1129	1047 (18)	1178-1438	1286 (22)	1037-1227	1126 (14)	1434-1669	1602 (19)	991-1760	1124 (11)	1744-2100	1873 (18)	1183-1331	1258 (13)
Co (ppm)	107-131	122 (13)	78.5-90.2	84 (18)	92.3-107.2	100 (20)	90.3-106	100 (18)	82.4-101	94.5 (22)	91.1-105	99.1 (14)	84.8-93.6	89.2 (19)	49.3-69.9	60.8 (11)	49.4-102	85.2 (18)	62.3-93.8	79 (13)
Ni (ppm)	223-282	260 (13)	177-228	195 (18)	70.3-94.3	87.3 (20)	116-156	135 (18)	63.9-86.2	76 (22)	191-235	210 (14)	1567-1708	1634 (19)	1557-1969	1729 (11)	1996-2684	2431 (18)	1281-1652	1475 (13)
Cu (ppm)	BDL-3.51	0.644 (10)	BDL-1.22	0.266 (8)	BDL-0.361	0.233 (10)	BDL-0.62	0.215 (10)	BDL-6.01	0.816 (12)	BDL-7.21	1.47 (8)	BDL-0.207	0.173 (2)	BDL-0.413	0.187 (5)	BDL-0.822	0.286 (12)	BDL-7.05	1.58 (11)
Zn (ppm	229-279	257 (13)	244-304	268 (18)	248-297	274 (20)	261-311	281 (18)	232-314	278 (22)	201-247	229 (14)	252-284	267 (19)	112-141	126 (11)	61-87.2	80.1 (18)	109-139	122 (13)
As (ppm)	BDL-0.34	0.25 (3)	BDL-0.4	0.198 (10)	BDL-0.36	0.244 (9)	BDL-0.46	0.281 (14)	BDL-0.54	0.263 (16)	0.280-22.4	3.03 (14)	BDL-0.25	0.25 (1)	BDL-0.18	0.145 (2)	0.250-7.65	2.34 (18)	BDL-0.138	0.117 (2)
Rb (ppm)	544-667	614 (13)	430-576	491 (18)	438-541	483 (20)	486-596	557 (18)	464-554	512 (22)	435-525	492 (14)	492-598	566 (19)	39.9-394	343 (11)	355-556	494 (18)	391-492	441 (13)
Sr (ppm)	0.099-0.657	0.268 (13)	0.192-3.22	0.457 (18)	0.127-0.41	0.258 (20)	0.138-4.33	0.671 (18)	0.195-0.75	0.348 (22)	0.116-0.74	0.391 (14)	0.162-0.559	0.266 (19)	0.245-1.09	0.416 (11)	0.341-1.06	0.623 (18)	0.419-0.987	0.636 (13)
Y (ppm)	0.0176-0.0495	0.0335 (13)	0.0148-0.116	0.0487 (18)	0.0236-0.0505	0.0342 (20)	0.0174-0.0753	0.0431 (18)	0.0267-0.643	0.0992 (22)	0.0105-0.102	0.0244 (14)	BDL-0.0824	0.0275 (18)	0.0369-1.46	0.345 (11)	0.0333-0.278	0.129 (18)	0.0264-2.55	0.777 (13)
Pd (ppm)	BDL-0.044	0.044 (1)	BDL-0.028	0.028 (1)	BDL-0.019	0.019 (1)	BDL-0.0186	0.0186 (1)	BDL-0.061	0.061 (1)	BDL	-	BDL	-	BDL	-	BDL	-	BDL	-
Ag (ppm)	BDL-0.0256	0.0199 (2)	BDL-0.0246	0.0246 (1)	BDL-0.034	0.0257 (3)	BDL-0.0088	0.0088 (1)	BDL-0.023	0.0187 (2)	BDL-0.0186	0.0186 (1)	BDL-0.02	0.02 (1)	BDL-0.025	0.0165 (4)	BDL-0.022	0.022 (2)	BDL-0.032	0.0205 (4)
Cd (ppm)	BDL-0.12	0.12 (1)	BDL-0.095	0.095 (1)	BDL-0.082	0.062 (2)	BDL-0.059	0.041 (3)	BDL-0.081	0.081 (1)	BDL-0.145	0.104 (2)	BDL-0.08	0.075 (3)	BDL-0.073	0.073 (1)	BDL-0.147	0.093 (2)	BDL-0.079	0.07 (3)
Sn (ppm)	0.207-0.346	0.267 (13)	0.383-0.748	0.528 (18)	0.327-0.797	0.629 (20)	0.248-0.618	0.387 (18)	0.587-2.93	0.945 (22)	0.64-8.92	1.31 (14)	1.27-1.65	1.41 (19)	0.34-2.72	2.17 (11)	0.387-3.84	0.858 (18)	1.22-2.04	1.56 (13)
Sb (ppm)	BDL-0.037	0.0283 (8)	BDL-0.041	0.0163 (7)	BDL-0.029	0.0198 (7)	BDL-0.023	0.0175 (9)	BDL-0.103	0.0303 (7)	BDL-0.243	0.0681 (7)	BDL-0.0173	0.0158 (3)	BDL-0.029	0.0198 (3)	BDL-0.097	0.0351 (9)	BDL-0.06	0.025 (5)
Cs (ppm)	9.02-161	45.2 (13)	18.9-47	32.1 (18)	9.23-38.9	21.1 (20)	31.3-61.2	41.7 (18)	8.46-57.9	31.4 (22)	26.7-42.2	37.2 (14)	41.8-71.4	59.9 (19)	3.84-58.6	30.1 (11)	45.9-113	62.3 (18)	14.3-41.9	30.3 (13)
Ba (ppm)	2635-3316	3068 (13)	1217-2099	1805 (18)	2120-2837	2462 (20)	2360-3139	2819 (18)	1950-4183	2340 (22)	1121-1350	1240 (14)	1611-1884	1768 (19)	142-2085	1526 (11)	2843-3436	3142 (18)	1820-2336	2099 (13)
Pb (ppm)	0.249-1.04	0.518 (13)	0.265-0.791	0.465 (18)	0.27-1.12	0.471 (20)	0.247-0.978	0.515 (18)	0.263-1.08	0.578 (22)	0.205-2.4	0.76 (14)	0.169-0.666	0.31 (19)	0.194-3.64	0.891 (11)	0.329-4.71	1.33 (18)	0.391-8.8	2.75 (13)
Bi (ppm)	BDL-0.063	0.0189 (6)	BDL-0.0033	0.0033 (1)	BDL-0.116	0.0231 (14)	BDL-0.0218	0.00888 (4)	BDL-0.0173	0.006 (9)	BDL-0.59	0.117 (11)	BDL-0.0057	0.00495 (2)	BDL-0.033	0.0109 (7)	BDL-0.059	0.0113 (10)	BDL-0.327	0.0592 (10)

Quality control standard	BCR-2G (n=17) Average	1σ	Accepted value	NISTSRM612 (n=20) Average	1σ	Accepted value
MgO (wt%)	3.6	0.1	3.56	0.02	0.006	0.01
Al_2O_3 (wt%)	13.4	-	13.4	2.1	-	2.03
SiO_2 (wt%)	55	2.8	54.4	72	3.4	72.1
K_2O (wt%)	1.78	0.04	1.74	0.007	0.0003	0.008
TiO_2 (wt%)	2.29	0.06	2.27	0.007	0.0001	0.007
FeO (wt%)	12.8	0.2	12.4	0.01	0.002	0.007
Ca (ppm)	51607	2157	50464	93938	3219	85061
Cr (ppm)	15.3	0.94	17	37.1	1.1	36.4
Mn (ppm)	1581	47.5	1550	40.7	1.6	38.7
Co (ppm)	38.4	1	38	35.9	1.2	35.5
Ni (ppm)	12.5	0.9	13	39	1.4	38.8
Cu (ppm)	18.5	0.7	21	38.5	1.7	37.8
Zn (ppm	150	5.4	125	40.7	2.2	39.1
As (ppm)	0.77	0.12	-	26.4	1.4	35.7
Rb (ppm)	46.2	2.3	47	30	1.7	31.4
Sr (ppm)	346	5.5	342	84.8	1.2	78.4
Y (ppm)	34.9	1.6	35	44	1.5	38.3
Pd (ppm)	0.03	0.01	-	0.88	0.09	1.05
Ag (ppm)	0.63	0.06	0.5	22.1	1.5	22
Cd (ppm)	0.14	0.04	0.2	21.4	1.5	28.1
Sn (ppm)	1.72	0.09	2.6	31.4	1.8	38.6
Sb (ppm)	0.28	0.02	0.35	32.4	1.8	34.7
Cs (ppm)	1.15	0.06	1.16	41.4	2.4	42.7
Ba (ppm)	666	13	683	40	1.1	39.3
Pb (ppm)	10.8	0.45	11	40.3	2.7	38.6
Bi (ppm)	0.05	0.004	0.05	34.6	2.4	30.2

Notes: Abbreviation BDL stands for below detection limit. Major elements analyzed by EDS, trace elements by LA-ICPMS. Major element concentrations are slightly elevated since analyses are anhydrous. Average values were calculated excluding analyses below detection limits (the number of analyses, "n", are given for each calculation).

Dissolved concentrations of other economic and deleterious ore metals, such as Cu, PGE, As, Pb, Ag, and Sn were consistently low or below detection limits (Table 2), and showed no correlation to lithology or distance from sulfide ore (Figure 5). Diagrams of Cu concentration, and the ratio of dissolved Cu to bulk rock Cu, show that there are large ranges in Cu concentrations in biotite within individual samples (Figures 5 and 6). In order to understand these variations, LA-ICP-MS signals which gave the maximum and minimum Cu concentrations in samples with wide ranges were re-examined (Figure 7). It was found that in grains that contained relatively high Cu concentrations, there were anomalous peaks in the signal which may be interpreted as contamination by small (µm scale) sulfide inclusions, or as chemical zoning.

Using SEM-EDS measurements of biotite from each sample, the principle components of biotite were plotted by host rock type (Figure 8). The diagram shows that biotite found within the offset dyke have on average a slightly lower X_{Mg} (i.e. more Fe-rich) than biotite found within the Huronian country rocks (average X_{Mg} for QD, IQD, and Huronian country rocks are 0.52, 0.53, and 0.57 respectively), whereas biotite from the Sudbury diabase dykes (which occur both proximal and distal to the sulfide ore, and were emplaced post-sulfide mineralization) have the lowest average X_{Mg} (0.44 average). Therefore biotite found within the Worthington offset and Sudbury diabase dykes are closer to the ideal composition of annite than biotite from the country rocks.

4.2 Biotite petrography

Several distinct textural varieties of biotite were observed in the Totten mine area and surrounding country rocks (Figure 9). Biotite predominantly occurs as anhedral lathes intergrown with amphibole clusters (Figure 9, photos C, and E-F) in Huronian country

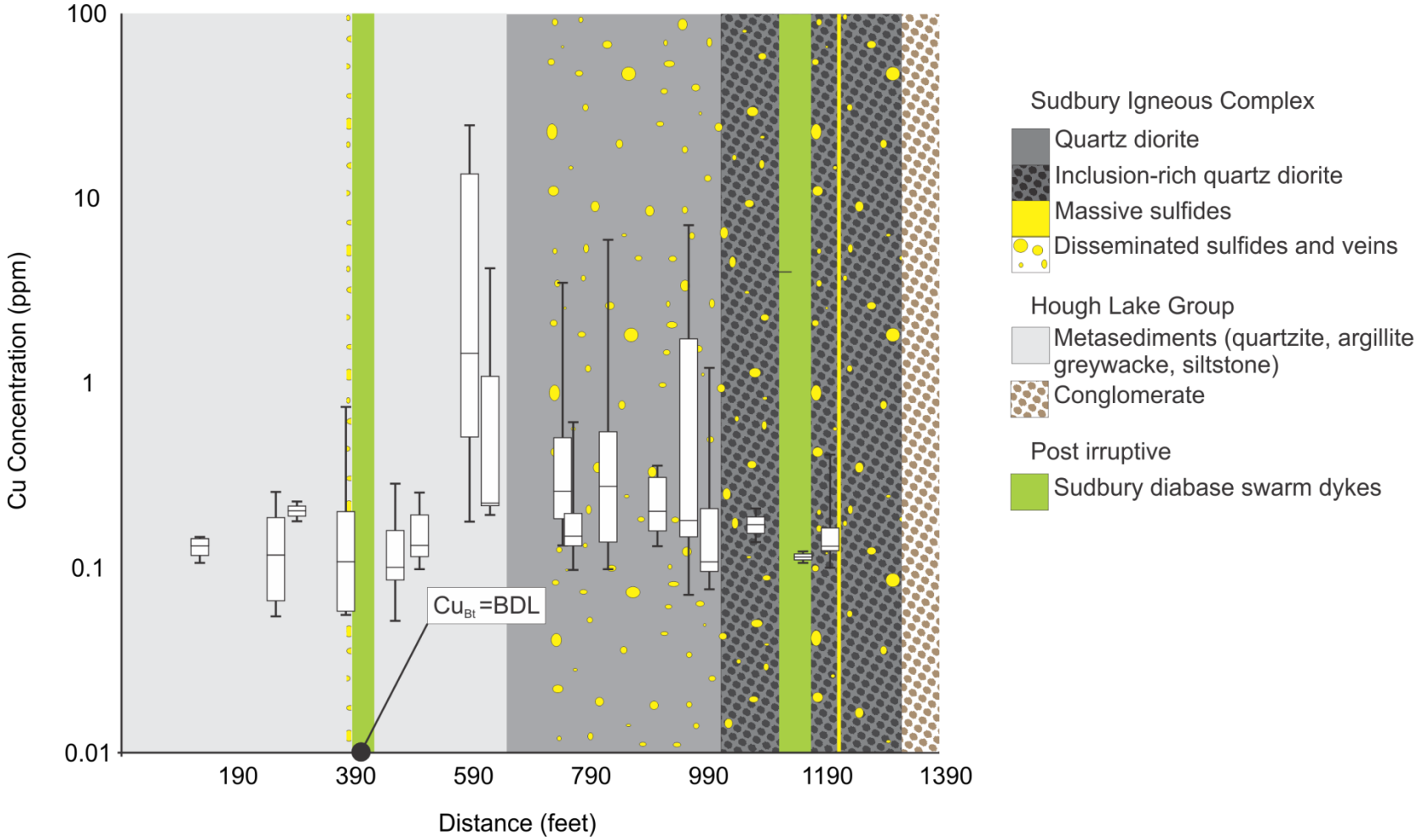
100
10
1
0.1
0.01
Cu Concentration (ppm)
190
390
590
790
990
1190
1390
Distance (feet)
Cu$_{Bt}$=BDL
Sudbury Igneous Complex
Quartz diorite
Inclusion-rich quartz diorite
Massive sulfides
Disseminated sulfides and veins
Hough Lake Group
Metasediments (quartzite, argillite greywacke, siltstone)
Conglomerate
Post irruptive
Sudbury diabase swarm dykes

Figure 5 (previous page). Box-plots of the Cu-concentration in biotite along Totten drill hole 1265980. For each sample the maximum, minimum, first quartile (upper box), third quartile (lower box), and mean (separation between quartiles) values are given. Lithological units were added using data from Vale drill logs. Altough sulfides are shown in both QD and IQD, the relative proportions of sulfide mineralization are not distinguished, and it is important to note that sulfides are more abundant in the IQD samples than in QD.

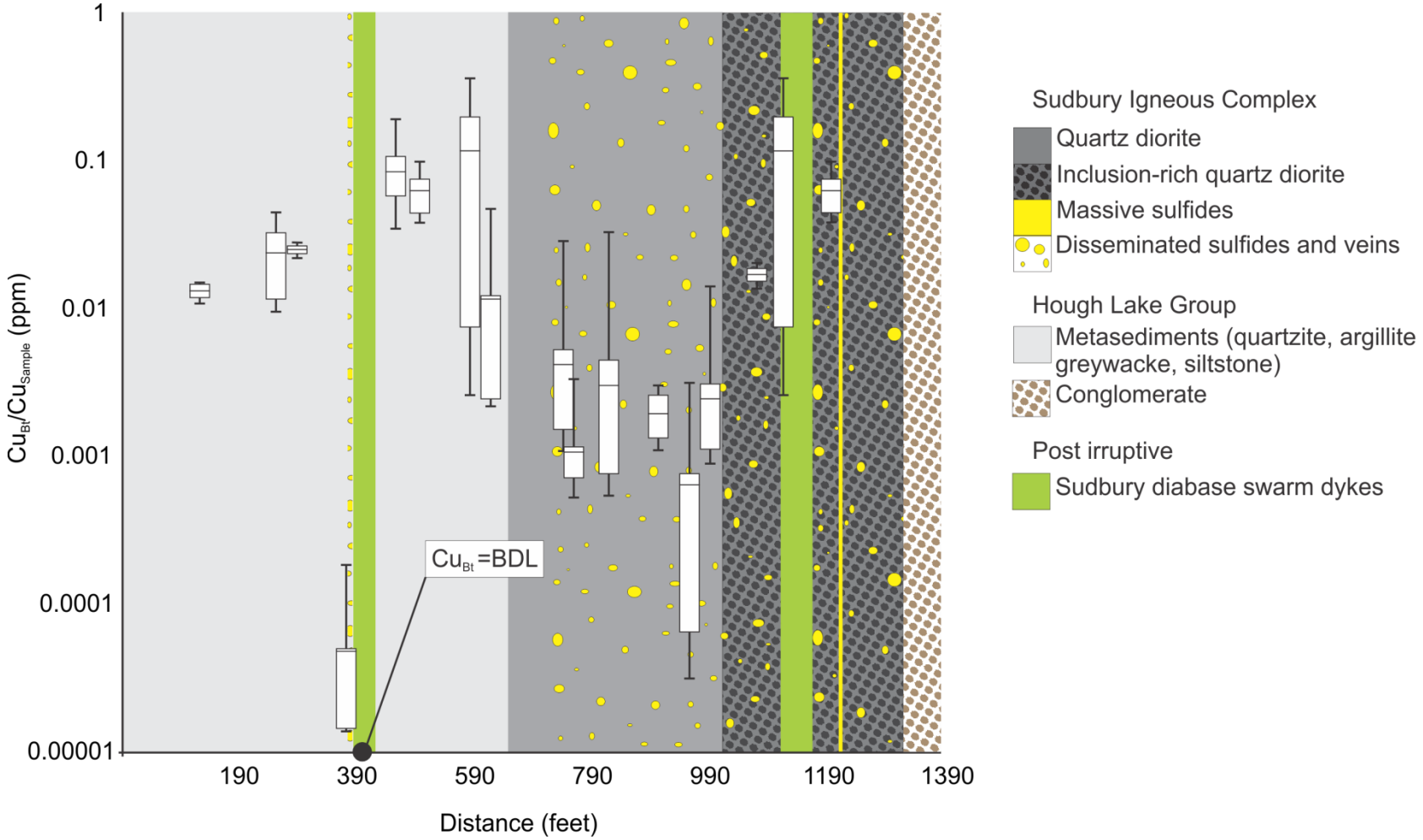
1
0.1
0.01
0.001
0.0001
0.00001
Cu_{Bt}/Cu_{Sample} (ppm)
Cu_{Bt}=BDL
190
390
590
790
990
1190
1390
Distance (feet)
Sudbury Igneous Complex
Quartz diorite
Inclusion-rich quartz diorite
Massive sulfides
Disseminated sulfides and veins
Hough Lake Group
Metasediments (quartzite, argillite greywacke, siltstone)
Conglomerate
Post irruptive
Sudbury diabase swarm dykes

Figure 6 (previous page). Box-plots of the ratio of Cu contained within biotite and the bulk rock concentration of Cu along Totten drill hole 1265980. For each sample the maximum, minimum, first quartile (upper box), third quartile (lower box), and mean (separation between quartiles) values are given. Lithological units were added using data from Vale drill logs. Altough sulfides are shown in both QD and IQD, the relative proportions of sulfide mineralization are not distinguished, and it is important to note that sulfides are more abundant in the IQD samples than in QD.

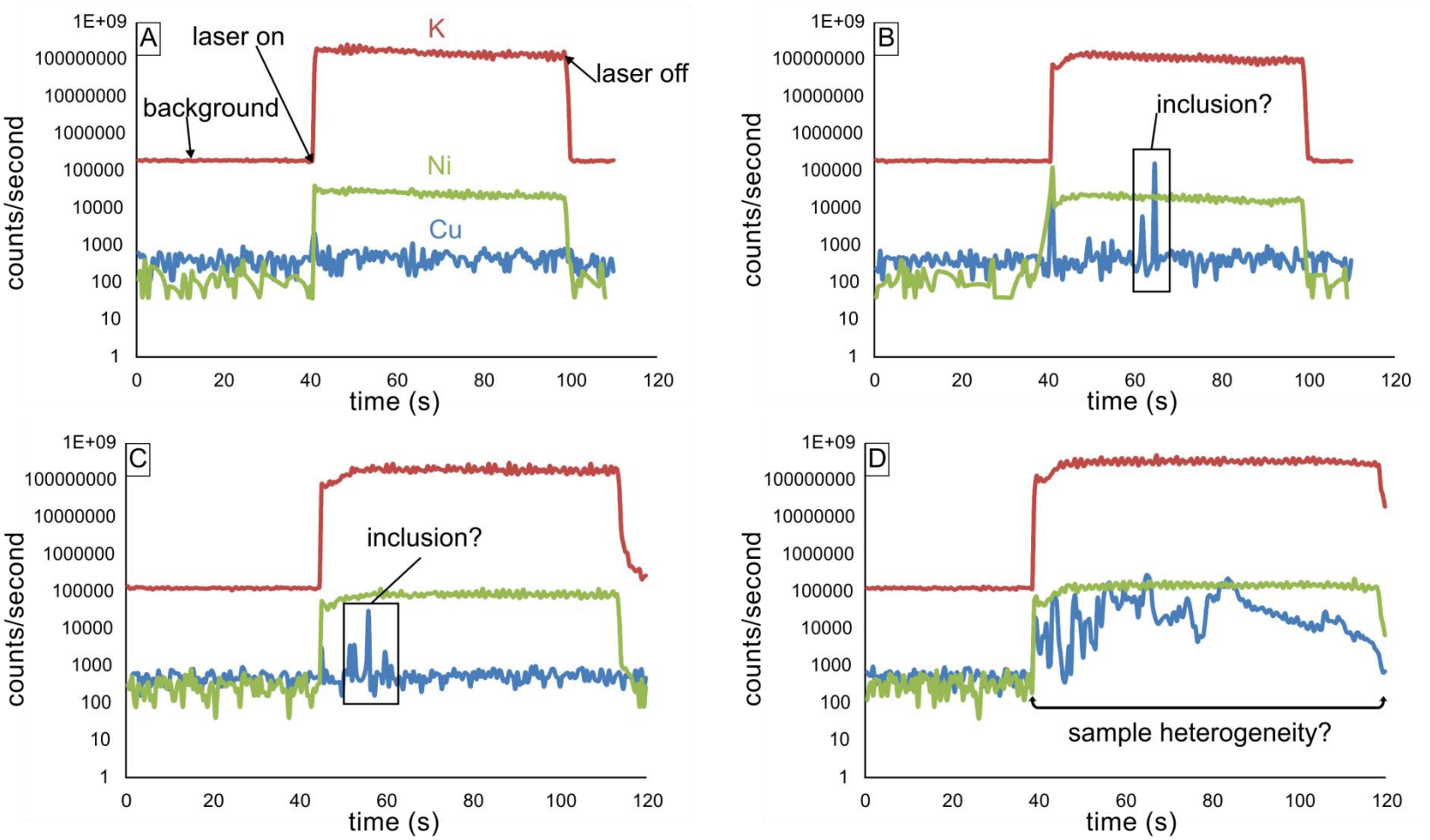

Figure 7. LA-ICP-MS signals from Totten biotite. These images indicate possible explanations for the wide range in Cu data seen in some samples. Image A shows a "clean" continuous signal. Anomalous peaks in other signals may indicate the presence of inclusions (B and C), and chemical zoning (D).

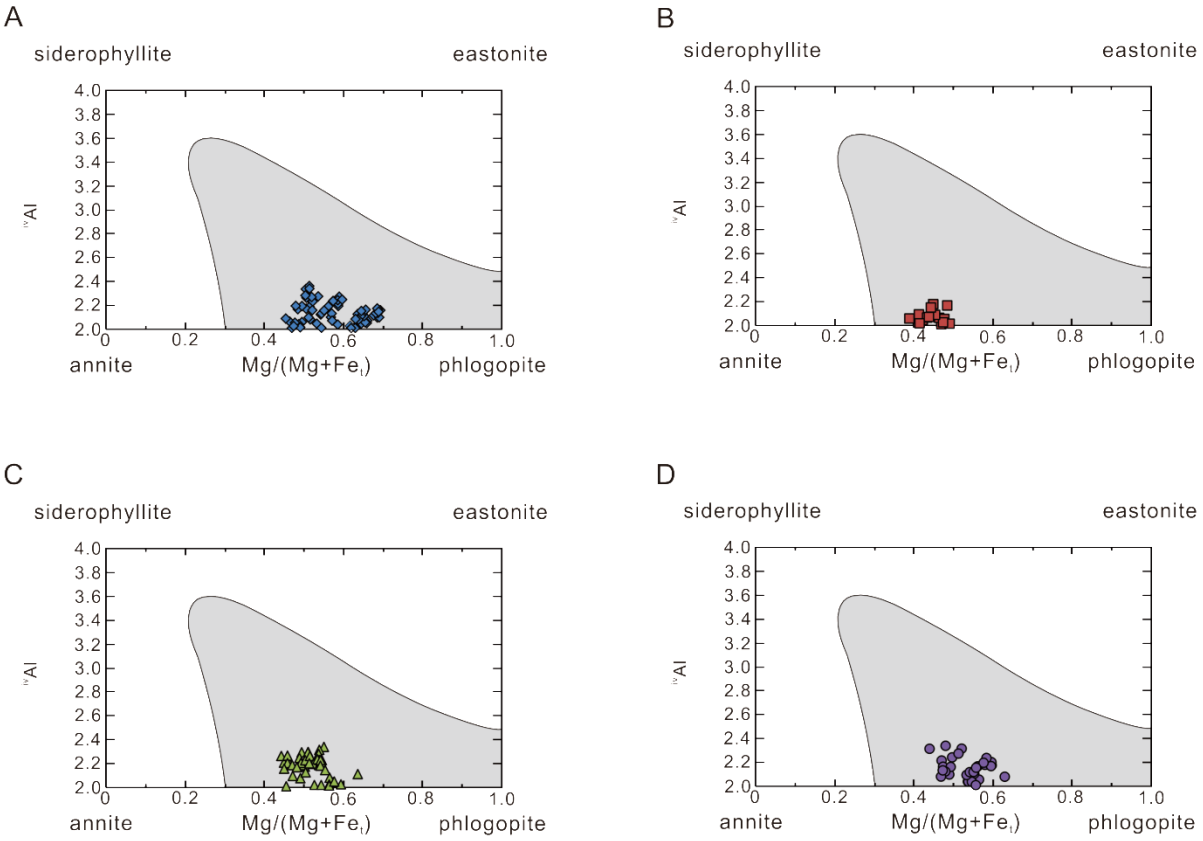

Figure 8. Totten mine biotite (n=190) plotted on diagrams showing the principle components of biotite, modified from Deer et al. (1966). Major element data was obtained by SEM from biotite hosted within (A) Huronian country rocks; (B) Sudbury diabase swarm dykes; (C) barren-low sulfide quartz diorite; and (D) sulfide-rich quartz diorite. Although the data fields of each lithology overlap, there is a general increase in Fe content of biotite approaching sulfide ore. The shaded field represents the compositional range of most natural biotite (Deer et al., 1966). Total Fe as Fe^{2+}

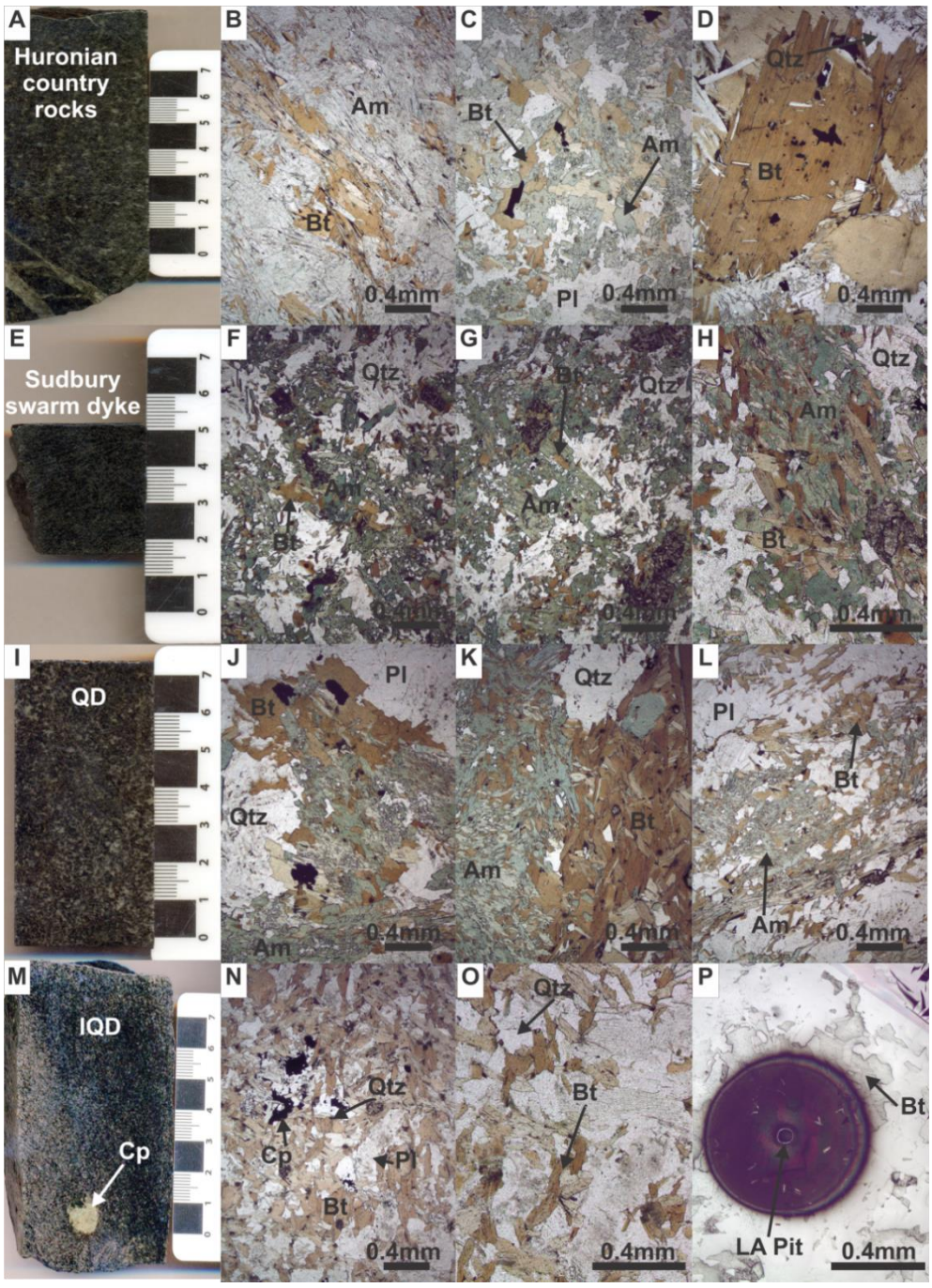

Figure 9. Photomicrographs of biotite (Bt) textures from Huronian country rocks (A), Sudbury swarm dyke (E), quartz diorite (I), and inclusion-rich quartz diorite (M). From these textures and biotite chemistry, three main groups are shown: (i) anhedral biotite intergrown with amphibole (Am) with low Ni and Cr concentrations (photos B,C, E-L), (ii) coarse grained biotite porphyroblasts with moderate Ni and elevated Cr (D), and (iii) euhedral coarse grained biotite clusters which show elevated Ni and moderate Cr in IQD samples (K, N-O). Image P shows an ablation pit from biotite analysis. Other abbreviations: chalcopyrite (Cp), quartz (Qtz) and plagioclase feldspar (Pl).

rocks, post-offset diabase dykes, and QD. Stewart (2002) describes similar biotite from the Totten deposit as an alteration of product amphibole, however the paragenetic relationship between amphibole and biotite is unclear in this study. These biotite generally display low (i.e. background) Ni and Cr concentrations (Table 2). Foliated biotite (Figure 9B) was also occasionally observed in country rocks (chemistry similar to other country rock biotite). Rare coarser grained subhedral to euhedral lathes were found in sample T69 (Figure 9D). These texturally distinct biotite demonstrate increased Ni and even higher Cr concentrations compared to background concentrations (Table 2). Another group of biotite was observed within both the QD and IQD. This group also consists of coarse grained euhedral lathes, however these are usually smaller than the biotite seen in T69 (Figure 9K, N-P). These biotite also occur in clusters (with or without amphibole). Those biotite hosted within QD demonstrate Ni and Cr concentrations similar to those found in country rock biotite (with the exception of T69), whereas IQD biotite show moderate Cr and elevated Ni (Table 2). Although texturally and chemically different, these groups of biotite are otherwise indistinguishable based on optical properties alone.

4.3 Comparison of Biotite composition to bulk rock analysis

Figure 10 is a scatter plot of bulk rock Ni *versus* the dissolved Ni in biotite by host rock lithology. Ideally, in order for biotite to be useful as a pathfinder mineral, this diagram would show a notable increase in the Ni content of biotite before elevated levels of Ni could be detected by bulk rock analysis. However, although the diagram does show the highest levels of Ni in biotite within IQD (a unit which is associated with the largest concentrations of sulfide ore at the Totten mine), biotite within the ore-proximal QD can show lower Ni concentrations than some of the surrounding Huronian country rocks

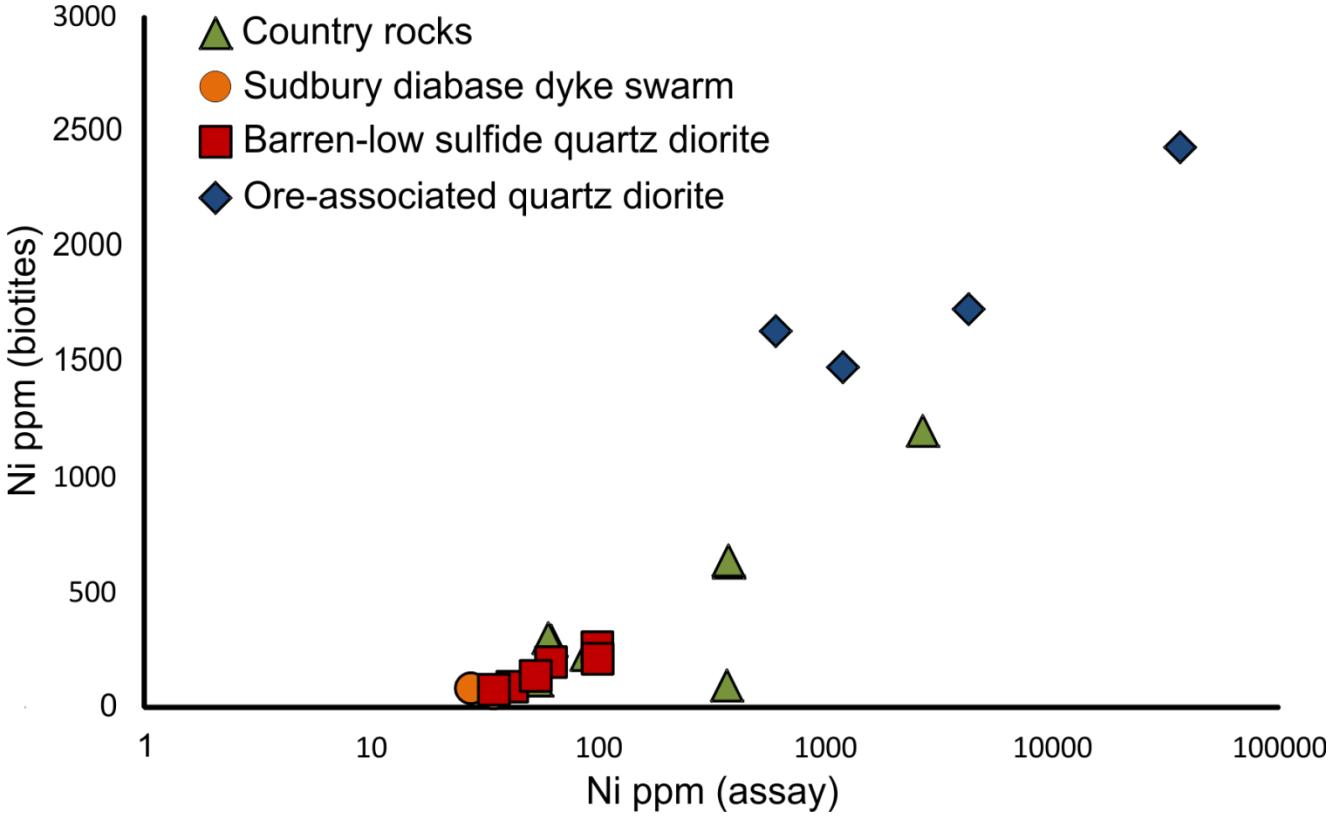

Figure 10. Scatter plot of bulk rock Ni versus the Ni content of biotite. The greatest levels of Ni in biotite are found within ore-associated IQD, however, there is not a systematic increase in biotite Ni relative to bulk rock Ni as a function of distance to ore. This is indicated by elevated Ni in biotite from country rocks that is greater than Ni found in offset hosted quartz diorite biotite (n=20).

(with which no sulfide ore is associated). Furthermore, anomalous Ni concentrations in Huronian biotite are associated with low levels of disseminated sulfides, whereas QD biotite do not show such elevated levels, even in the presence of disseminated sulfides. This result suggests that the control on the concentration of Ni in biotite is more complex than simply distance relative to sulfide ore.

5.0 Discussion

5.1 Comparison to other deposits

In order to demonstrate the reliability of biotite geochemistry as a pathfinder for mafic-ultramafic Ni-Cu-PGE deposits, the measured Ni content of biotite from this study (all rock types) have been compared to other barren and ore-forming environments at Sudbury as well as other layered mafic intrusions (i.e., Bushveld and Stillwater Complexes; Figure 11; Consequently, while PGE-rich, these deposits are Ni-poor by comparison to Sudbury). Elevated Ni was detected in biotite in close proximity to ore in all environments; however, no major distinctions can be made between systems using only the Ni content of biotite, due to the wide range in the Ni concentrations that is found within each environment. Since many of these measurements have focused mainly on samples within proximity to ore, the range in Ni concentrations also raises the question as to whether these analyses truly represent anomalous Ni concentrations. As an example, when comparing the Vermillion and McLennan offset deposits, the latter would not appear to contain elevated levels of Ni. Furthermore, the range in the McLennan Ni concentrations (as high as 508.4 ppm Ni, Figure 11) is much lower than that of the Huronian country rocks from the Totten mine area (as high as 1420 ppm, Figure 11). Without Ni analyses from biotite within the country rocks of the McLennan offset deposit, it is difficult to provide a geological context for the chemistry of biotite from ore

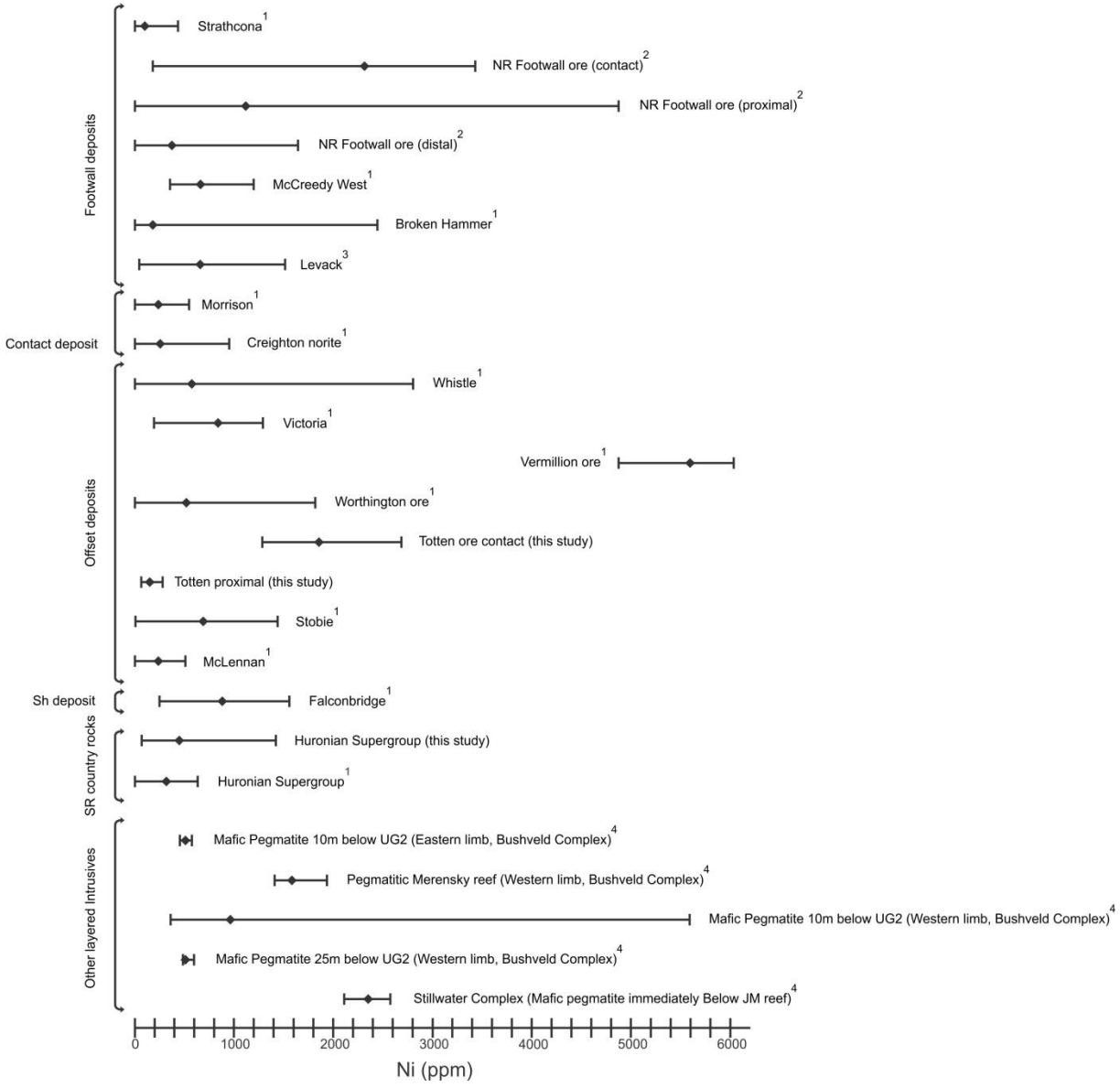

Figure 11. The range in dissolved Ni in biotite from different environments and lithologies associated with the Sudbury Igneous Complex, as well as some other mafic-ultramafic layered intrusions. Abbreviations: NR (North Range), SR (South Range), and Sh (shear hosted). Data were compiled from: (1) Ames and Kjarsgaard, 2013; (2) Hanley and Mungall, 2003; (3) Stewart, 2011; and (4) Hanley (personal communication).

hosting quartz diorite. Possible explanations for the range in Ni data could include: (i) contamination of the chemical analysis by sulfide minerals; and (ii) different populations of biotite which are defined by both their processes of crystallization (e.g. magmatic versus hydrothermal) and the local availability of metals due to the nature of the host rocks (such as the biotite populations which have been described in the results section of this thesis). The following sections of the discussion will examine these controls on biotite chemistry in order to identify potential exploration tools for magmatic Ni-Cu-PGE deposits.

5.2 The influence of sulfides on the trace metal content of biotite

As previously discussed in section 3, cleavage planes and visible inclusions of sulfides were avoided during LA-ICP-MS analysis in order to prevent sulfide contamination. Additionally, the Glitter^{TM} software package can be used to eliminate peaks in the LA-ICP-MS signal caused by the presence of inclusions within the biotite grains. Figure 12, demonstrates an additional complexity which is encountered by biotite in contact with sulfide phases. In this case, pyrrhotite locally provides Fe for the M-octahedral sites in biotite, which as we have discussed (section 2) affects in turn the incorporation of trace metals and halogens (e.g., Ni and Cl) into the crystal structure. Analysis of these localized zones in biotite would generate results that are unrepresentative of biotite chemistry in the sample, and could generate the wide ranges in biotite described in the previous section. To verify that the elevated Ni and Fe content of biotite in proximity to ore are not due to any form of contamination, compositional maps of biotite were produced using LA-ICP-MS. Sample TU11 represents biotite from a sample of

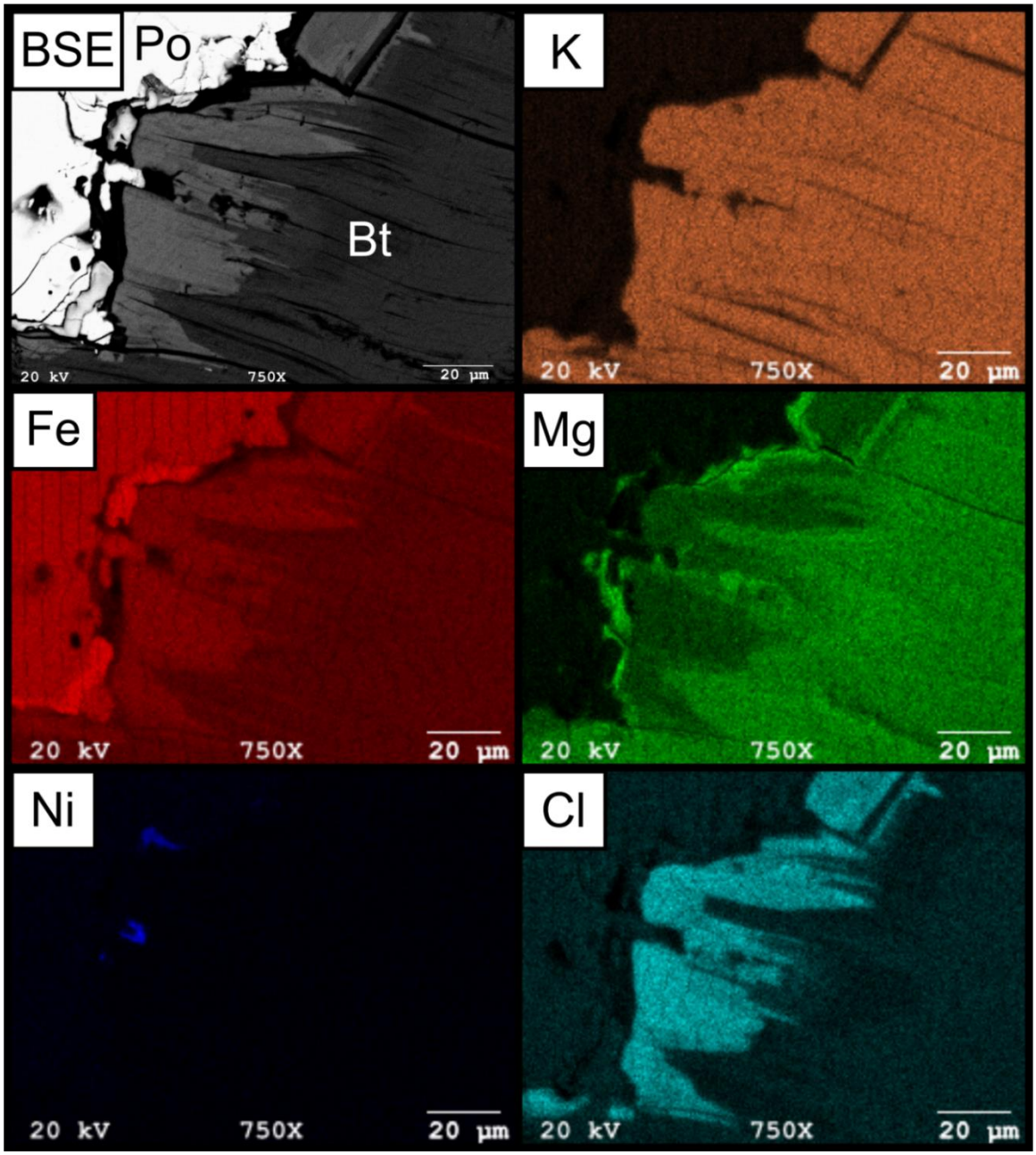

Figure 12. Photomicrographs showing X-ray intensities of biotite in contact with sulfide (images from Hanley, personal communication). The backscattered electron image (BSE) shows the grain of biotite (Bt) to be in direct contact with pyrrhotite (Po). The other images are compositional maps for potassium, iron, magnesium, nickel, and chlorine. The images demonstrate the effect of pyrrhotite on the composition of biotite along the contact of the two grains.

disseminated sulfide ore which consistently contained some of the highest levels of dissolved Ni measured in this study (Table 2). The compositional map of a biotite grain from sample TU11 illustrates that biotite is homogeneous with regards to its Ni, and Fe contents (Figure 13). The Ni content of the mapped grain is also in agreement with the elevated results found by LA-ICP-MS (see Table 2) which indicates that these values represent the true dissolved Ni content in biotite. However, these results cannot confirm that sulfide re-equilibration was not a factor in the analysis of biotite from other studies (Figure 11), and that the large ranges in Ni concentrations that were measured may have been the result of contamination. In future studies, it is important that the chemical homogeneity of analyzed grains be assessed, and that possible sources of contamination (such as sulfide inclusions, cleavages and fractures) are avoided during analysis.

5.3 Observations on biotite chemistry

In the literature, two major controls have been proposed for structural substitutions in biotite: (i) crystallography, including unit cell dimensions and avoidance/permissibility phenomenon (e.g., Volfinger and Robert, 1980; Volfinger et al., 1985), and (ii) environmental controls, such as the activity of substitutes within the fluid or melt phase with which the biotite equilibrated (Munoz, 1984; Munoz and Swenson, 1981; Finch et al., 1995; Coulson, 2001; Hanley and Mungall, 2003). As previously described in the results section, biotite from the Worthington offset contains slightly lower X_{Mg} than biotite from the surrounding Huronian country rocks. Furthermore biotite from the IQD contains elevated Ni and moderate Cr, whereas biotite from the Huronian country rocks with elevated Ni also contains elevated Cr (Table 2). In order to evaluate the trace metal signatures as a function of host lithology and changes in crystallography (i.e., substitution

PPL
Bt
K
0.178
0.323
0.584
1.06
1.91
3.46
6.26
11.3
20.5
37.1
67.1
121
220
398
720
1300
2360
4270
7720
14000
25300
45700
82800
150000
Ni
0.0199
0.0392
0.0773
0.152
0.300
0.590
1.16
2.29
4.51
8.89
17.5
34.5
67.9
134
264
519
1020
2010
3970
7810
15400
30300
59700
118000
Cu
0.0167
0.0301
0.0544
0.0984
0.178
0.322
0.582
1.05
1.90
3.44
6.22
11.2
20.3
36.8
66.5
120
217
393
711
1290
2320
4200
7600
13700
Fe
0.538
0.962
1.72
3.08
5.50
9.83
17.6
31.4
56.2
101
180
321
575
1030
1840
3290
5880
10500
18800
33600
60100
107000
192000
343000
Mg
0.0925
0.172
0.321
0.597
1.11
2.07
3.85
7.18
13.4
24.9
46.3
86.2
161
299
557
1040
1930
3590
6690
12500
23200
43200
80400
150000

Figure 13 (previous page). LA-ICP-MS compositional maps for biotite with elevated Ni. A plane polarized light image (PPL) is given for the analyzed biotite grain (Bt). Results demonstrate that the elevated levels of Ni are homogeneous and likely represent the true dissolved Ni content of biotite in this sample. Major metals also show no influence of sulfide grains or inclusions. Scales are in both ppm (Ni and Cu) and wt% (Fe, Mg, and K). Although several grains of biotite are present in this image, one grain has been outlined for the consideration of the reader.

of Fe and Mg) a scatter plot was generated for the MgO/FeO ratio compared to the Ni+Cr content of biotite analyzed by LA-ICP-MS (Figure 14A). From this diagram, two distinct compositional groups of biotite are observed: one has relatively low Ni+Cr (approximately ≤1000 ppm), and within an MgO/FeO ratio of 0.3-0.7; whereas the other group has relatively high Ni+Cr (approximately ≥1000 ppm), and within an MgO/FeO ratio of 0.5-1.0. The trend within the former group of biotite shows a positive correlation between Ni+Cr and the MgO/FeO ratio, which suggests that crystallography is a dominant control on the substitution of Ni and Cr within this range. Biotite with much higher Ni and Cr concentrations do not demonstrate the same correlation, indicating that at these concentrations there is a control other than mineral crystallography which determines the trace metal content of biotite. The evidence of this secondary control is shown by the narrow range in the MgO/FeO ratio of the Totten biotite (approximately 0.3-1), since there is an order of magnitude increase in the Ni+Cr content between the biotite groups without a concomitant increase in the MgO/FeO ratio. A similar diagram shows biotite geochemistry from a North Range Contact-style ore body (Figure 14B). Again there appears to be two groups of biotite, however, the overall range in the MgO/FeO ratio is greater than that seen at Totten. The group of relatively low Ni+Cr biotite in this diagram do not demonstrate the same positive correlation observed in South Range biotite; however this may be due to the difference in the number of analyses between the two diagrams. Furthermore, elevated Ni+Cr biotite (which are associated with sulfide ore) occur at higher concentrations of MgO than ore associated biotite from Totten.

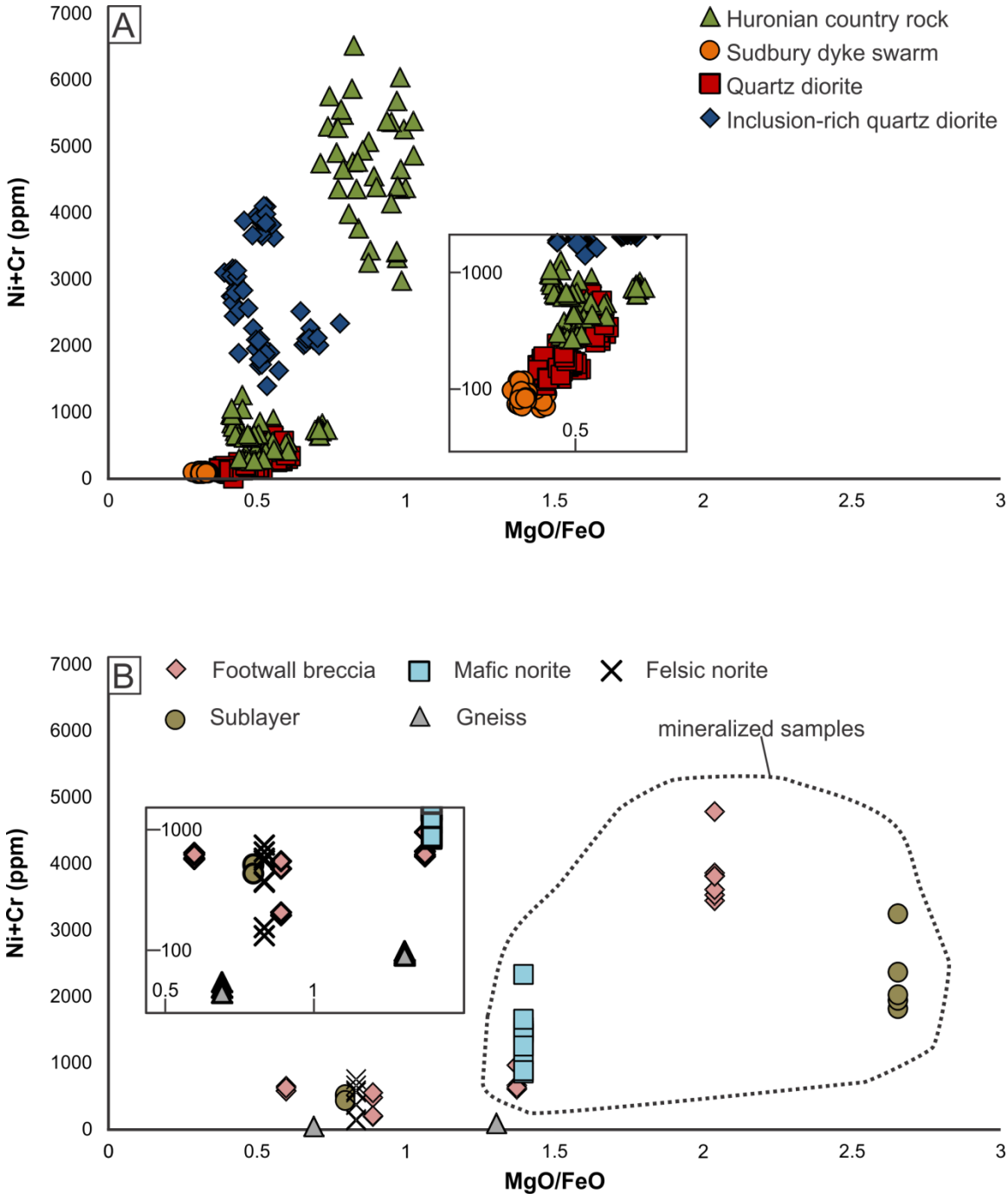

Figure 14. Scatter plots of the MgO/FeO ratio versus combined Ni and Cr in biotite from lithologies in (A) the Totten mine area (n=292 biotite analyses), and (B) North Range embayments (data from Stewart, 2011; n=52 biotite analyses). In both diagrams, two groups of biotite are distinguishable: (i) low Ni+Cr which may be controlled by crystallography (shown by a correlation to MgO/FeO), and (ii) elevated Ni+Cr samples which do not appear to be related to crystallography.

In order to identify potential pathfinder tools using biotite chemistry, it is essential to distinguish biotite that formed in ore-related environments from biotite the formed in barren environments. Unfortunately, in Figure 14A a group of anomalous biotite from the Huronian country rocks closely resemble biotite from ore-associated IQD. These anomalous country rock biotite are the group of moderate Ni and elevated Cr described in the results (section 4.2). Although the combined concentrations of Ni and Cr are similar to biotite from IQD, the ratio of Ni to Cr in the country rock samples is much lower. Therefore, a new diagram was constructed to show the Ni content of biotite against the Ni/Cr ratio for both the Totten offset and North Range Contact environment (Figure 15). In this diagram there is a clear separation of the high Ni and Ni/Cr biotite associated with the mineralized IQD (Figure 15A), which may represent a diagnostic tool for ore associated biotite. The distribution of the North Range biotite appears very similar, except for the absence of the high Ni and Ni/Cr field shown in the Totten data (Figure 15B). It is unclear if the Ni and Cr signature of the IQD biotite is unique to the relatively Ni-rich offset environment, or if a similar group of biotite in the North Range environment were not represented during sampling.

As demonstrated in section 2.1, the average composition of biotite from the Worthington offset is closer to the ideal composition of annite (biotite Fe endmember) than biotite from the Huronian country rocks (the respective X_{Mg} of biotite from the QD, IQD, and country rocks are: 0.44-0.64, 0.52 average; 0.44-0.63, 0.53 average; and 0.32-0.69, 0.57 average). This is similar to the observation of Stewart (2002), in biotite from the Totten mine area. The Cl content of Totten biotite was also discovered to increase in proximity to ore (Stewart, 2002). Although this cannot be confirmed by this study, the

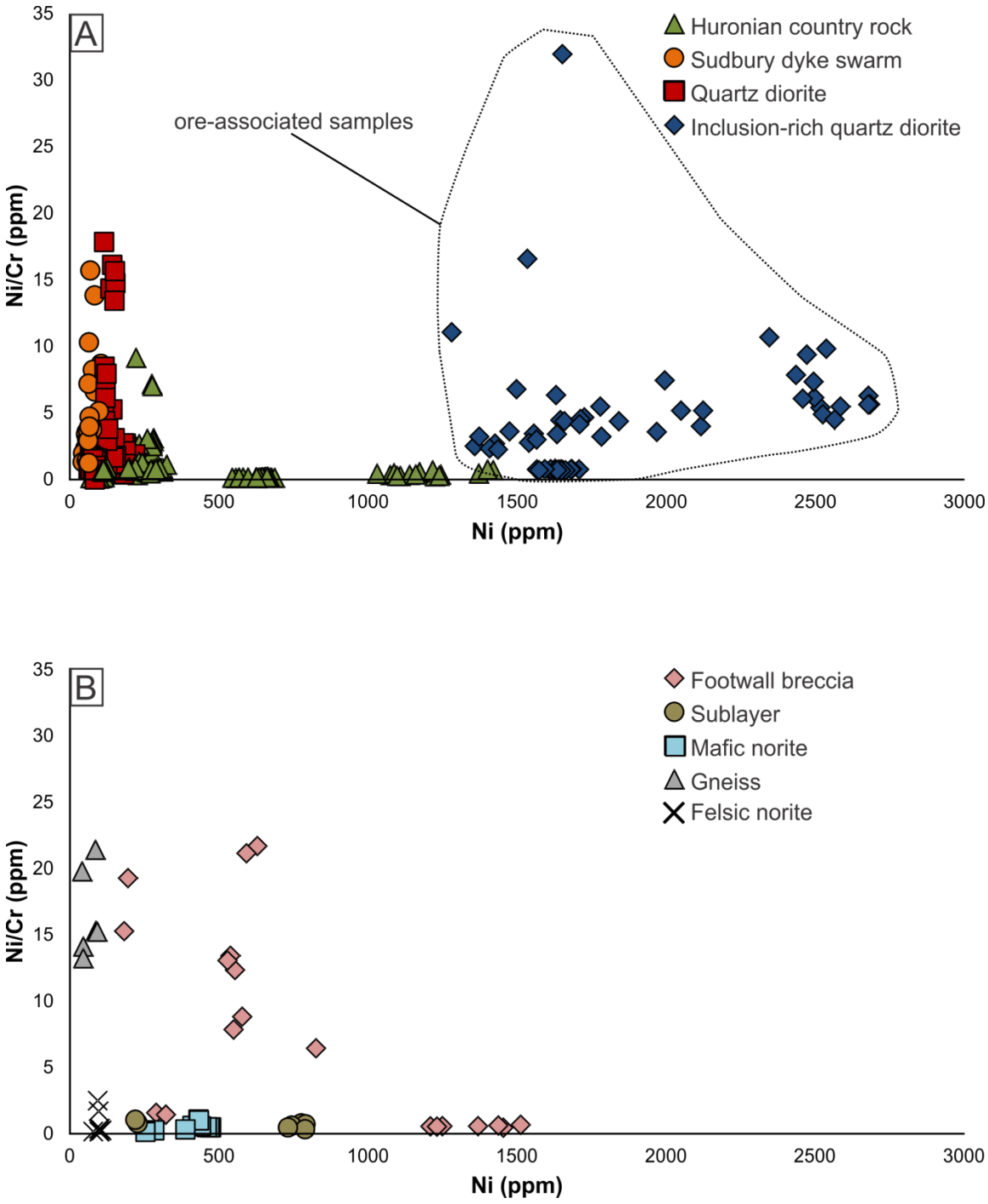

Figure 15. Scatter plots of Ni content versus Ni/Cr ratio in biotite from lithologies in (A) the Totten mine area (n=292 biotite analyses), and (B) North Range embayments (data from Stewart, 2011; n=52 biotite analyses).

trend seems unusual given both the increase in Ni content in IQD biotite, and the Ni-Cl avoidance phenomenon described by Volfinger et al. (1985). Hanley and Mungall (2003), also observed increased Ni, Fe, and Cl in biotite with proximity to Cu-Ni-PGE ore from the Fraser mine (North Range, Footwall deposit). Therefore the Ni-Cl avoidance phenomenon may only control the incorporation of Ni and Cl into biotite at low concentrations (such as in the distal lithologies; Hanley and Mungall, 2003). At higher concentrations, the ability of biotite to accommodate Ni and Cl could be more dependent on the species of biotite (such as Fe- and Mg-endmembers), and the availability of Cl and Ni in fluids with which the biotite equilibrate. This hypothesis is in agreement with Figure 14, which indicates a control other than crystallography (possibly composition of the host rock) influences Ni and Cr concentrations in biotite at elevated levels (approximately $\geq$1000 ppm).

5.4 The application of biotite analysis to routine exploration

In the previous sections, two chemical tools have been shown which can be used to distinguish biotite from the offset ore environment: (i) the Fe content of offset biotite is slightly greater than biotite from the Huronian country rocks; and (ii) there is a significant increase in both the Ni content and Ni/Cr ratio in ore-associated grains. However, as we have seen these variations are not systematic over great distances of either country rock or QD adjacent to mineralized IQD. This feature renders these tools inappropriate for drill core exploration, since the discovery of these chemical indicators would coincide with the discovery of sulfide ore in drill core. An alternative would be to consider the weathering products of a surface expression of sulfide ore. If ore-associated biotite and

their weathering products could be identified in regolith, then perhaps these could be used as a vector for undiscovered mafic-ultramafic Ni-Cu-PGE deposits.

Biotite readily alters at surface conditions and depending on the "strength" of chemical weathering, it may generate a variety of alteration products (e.g., vermiculite, chlorite, clay minerals, and Fe-oxides; Wilson, 2004; and references therein). The weathering of biotite may begin with vermiculation through the replacement of K by other cations (which may be controlled by the amount of K contained within external solutions; Martin and Sparks, 1985) as well as the loss of octahedral Fe through oxidation (Walker, 1949; Barshad 1948; Rausell-Colom et al., 1964; Newman and Brown, 1966). Despite these structural changes, Gilkes and Suddhiprakarn (1979) have shown that detectable levels of Ni and Cr are retained by both the altered biotite and its more advanced alteration products (clays). However, the extent to which the elevated concentrations of Ni and Cr in biotite are preserved in the weathering products of this mineral is unclear.

6.0 Conclusions

The study of biotite chemistry in the Totten mine area has led to new insights into its potential use as an exploration tool for magmatic Ni-Cu-PGE deposits. The key findings of this study are as follows:

(i) Dissolved concentrations of Ni in biotite from ore associated IQD is elevated (43.9-2684.1 ppm, 1644 ppm average) relative to biotite from the surrounding lithologies (43.9-687.4 ppm, 216.3 ppm average), with the exception of a small group of Ni-rich biotite from the Huronian country rocks (1031-1420 ppm, 1200 ppm average). No systematic

increase in the Ni content of biotite was detected in the country rocks approaching IQD. Other ore metals (e.g. Cu, PGE, As) are not present in elevated concentrations in biotite associated with sulfide ore.

(ii) Three distinct populations of biotite can be distinguished in the Totten mine area based on textures and chemistry: (i) anhedral biotite intergrown with amphibole clusters with low concentrations of Ni and Cr (average concentration of 216.3 ppm and 196 ppm respectively; Figure 9B, C, F-J, and L); (ii) coarser grained subhedral-euhedral lathes which contain elevated Ni and even higher Cr (average concentration of 1200 ppm and 3900 ppm respectively; Figure 9D); and (iii) euhedral-subhedral lathes which occur in clusters (with or without amphibole) with Ni and Cr concentrations that are consistent with the first biotite population, however similar grains in IQD contain elevated concentrations of Ni and moderate Cr (average concentration of 1644 ppm and 862 ppm average respectively; Figure 9K, N, and O).

(iii) In order to study the trace metal chemistry of biotite as a pathfinder for sulfide ore, it is imperative to establish local "background" concentrations of trace metals dissolved in this mineral. This is demonstrated by the wide range in Ni measured in biotite in close proximity to ore from Sudbury and layered mafic intrusions that do not contain Ni deposits (Figure 11). Without the context of local background trace metal concentrations in biotite, it is difficult to determine which analyses represent elevated measurements. Furthermore, this study has shown that elevated (relative to the local background level) concentrations of Ni can be found in biotite not associated with sulfide ore (however,

minor sulfides may be present), suggesting that the distance to ore is not the only parameter which must be considered (e.g. lithology and different biotite populations are other possible factors).

(iv) Sulfides may contaminate analyses of biotite either as discrete inclusions within biotite, or by inducing chemical zoning through the diffusion of metals (i.e. Fe) across mutual grain boundaries (which in turn may influence the trace metal and halogen content of biotite through structural avoidance and permissibility phenomenon; Figure 12). Compositional mapping of biotite grains (e.g. LA-ICP-MS or X-Ray mapping) with elevated concentrations of ore metals can be used to evaluate the possibility of sulfide contamination. In this study, IQD biotite were mapped by LA-ICP-MS and are homogeneous with respect to Ni (Figure 13), indicating that the measured concentrations are representative of the true dissolved Ni content of IQD biotite, and that they represent a chemically-distinct population of biotite. The presence of inclusions may also be detected and the final concentrations corrected by viewing the signal acquired during the analysis. This feature of Glitter^{TM} software is an advantage of using LA-ICP-MS over other analytical techniques for this investigation.

(v) Low concentrations (<1000 ppm) of Ni and Cr in biotite show a strong positive correlation to X_{Mg} (i.e. variations in the concentrations of Fe and Mg; Figure 14), which agrees with early experimental models in which the unit cell parameters of biotite control the incorporation of metal cations. However, at much greater concentrations of Ni and Cr (Ni+Cr $\geq$ 1000 ppm) there is no apparent correlation between trace metal content and

X_{Mg} (Figure 14), indicating that another parameter must influence the trace metal content of biotite. This is further shown by the narrow range in the X_{Mg} values of biotite in the Totten mine area, since there is a significant increase in the Ni+Cr content of biotite without a concomitant increase in the ratio of MgO to FeO. At these concentrations, it is more likely that the local availability of metals (e.g. host rock chemistry, or metal content of fluids with which biotite must equilibriate) is responsible for the trace metal content of biotite.

(vi) Two chemical indicators may be used to distinguish biotite in ore associated (QD/IQD) lithology from low to barren sulfide environments in the Totten area: (i) offset biotite have a slightly lower X_{Mg} (i.e. closer to the ideal composition of annite, 0.52 X_{Mg} average; Figure 8); and (ii) IQD biotite has high (>1000 ppm) dissolved Ni as well as high Ni to Cr ratios (Figure 15). Unfortunately, these indicators can only be detected in drill core and underground mining in close (decameter scale; Figure 3) proximity to sulfide ore, making it an impractical exploration tool in those conditions. An alternative might be to use the abundance of IQD biotite and its weathering products in soils as a vector towards surface exposures of ore bodies. Since biotite weathers readily under most surface conditions, it will be important to understand the ability of the advanced weathering products of biotite to preserve the chemical signature of the original biotite. Some experimental work on the effects of weathering on biotite chemistry show that Ni and Cr may be retained in the alteration products of biotite, however it is unclear if Ni and Cr concentrations as high as those measured in this study may be preserved in the alteration products of biotite.

7.0 References

Ames, D. E., Davidson, A. & Wodicka, N., 2008. Geology of the Giant Sudbury polymetallic mining camp, Ontario, Canada. Economic Geology, v. 103, pp. 1057-1077.

Ames, D.E. and Kjarsgaard, I.M., 2013. Sulphide and alteration mineral chemistry of low- and high- sulphide Cu-PGE-Ni deposits in the Footwall environment, Sudbury, Canada. Geological Survey of Canada, Open File 7331.

Barshad, I., 1948. Vermiculite and its relation to biotite as revealed by base exchange reactions, X-ray analysis, differential thermal curves and water content. American Mineralogist, v. 33, pp. 655-678.

Boudreau, A. E. & McCallum, I. S., 1985. Composition of Apatite and Biotite from the Stillwater Complex, Montana: Evidence for Hydrothermal Transport of PGE and REE in Cl-Bearing Solutions. Lunar and Planetary Science Abstract, v. 16, pp. 85-86.

Boudreau, A. E., Mathez, E.A., and McCallum, 1986. Halogen Geochemistry of the Stillwater and Bushveld Complexes: Evidence for Transport of the Platinum-Group Elements by Cl-Rich Fluids. Journal of Petrology, v. 27(4), pp. 967-986.65.

Brugger, J., Etschmann, B., Liu, W., Testemale, D., Hazemann, J.L., Emerich, H., Van Beek, W., and Proux, O., 2007. An XAS study of the structure and thermodynamics of Cu(I) chloride complexes in brines up to high temperature (400°C, 600 bar). Geochemica et Cosmochemica Acta, v. 71, pp. 4920-4941.

Card, K. D., Gupta, V. K., McGrath, P. H. & Grant, F. S., 1984. The Sudbury Structure: its regional geological and geophysical setting *in* Pye, E.G., Naldrett, A.J., and Giblin, P.E., eds., The Geology and Ore Deposits of the Sudbury Structure. Ontario Geological Survey, Special Publication v.1, p. 25-43.

Coats, C.J.A., and Snajdr, P., 1984. Ore Deposits of the North Range, Onaping-Levack Area, Sudbury *in* Pye, E.G., Naldrett, A.J., and Giblin, P.E., eds., The Geology and Ore Deposits of the Sudbury Structure. Ontario Geological Survey, Special Publication v.1, pp. 327-346.

Chon, C.M., Kim, S.A., Moon, H.S., 2003. Crystal structures of biotite at high temperatures and of heat-treated biotite using neutron powder diffraction. Clays and Clay Minerals, v. 51(5), pp. 519-528.

Cochrane, L. B., 1984. Ore Deposits of the Copper Cliff Offset *in* Pye, E.G., Naldrett, A.J., and Giblin, P.E., eds., The Geology and Ore Deposits of the Sudbury Structure. Ontario Geological Survey, Special Publication v.1, pp. 347-360.

Corfu, F., and Andrews, A.J., 1986. A U-Pb age for mineralized Nipissing diabase, Gowganda, Ontario. Canadian Journal of Earth Sciences, v. 23, pp. 107-109.

Coulson, I.M., Dipple, G.M., Raudsepp, M., 2001. Evolution of HF and HCl activity in magmatic volatiles of the gold-mineralized Emerald Lake pluton, Yukon Territory, Canada. Mineralium Deposita, v. 36, pp. 594–606.

Crowley, M.S., and Roy, R., 1960. The effect of formation pressure on sheet structures-a possible case of Al-Si ordering. Geochimica et Cosmochimica Acta, v. 18, pp. 94-100.

Della Ventura, G., Robert, J.-L., Raudsepp, M., and Hawthorne, F.C., 1993. Site occupancies in monoclinic amphiboles: Rietveld structure refinement of synthetic nickel-magnesium-cobalt-potassium-richerterite. American Mineralogist, v.78, pp. 327-346.

Dence, M.R., 1972. Meteorite impact craters and the structure of the Sudbury Basin *in* Guy-Bray, J.V., ed., New Developments in Sudbury Geology. Geological Association of Canada, Special Paper 10, pp. 7-18.

Deutsch, A., and Grieve, R.A.F., 1994. The Sudbury Structure: Constraints on its genesis from Lithoprobe results. Geophysical Research Letters, v. 21(10), pp. 963-966.

Dietz, R., 1964. Sudbury Structure as an astrobleme. The Journal of Geology, v. 72, pp. 412-434.

Dudás, F.O., Davidson, A., Bethune, K.M., 1994. Age of the Sudbury diabase dykes and their metamorphism in the Grenville province, Ontario: Radiogenic age and isotopic studies. Geological Survey of Canada, Report 6, Paper 1994-F, p. 97-106.

Farrow, C.E.G., 1994. Geology, alteration, and the role of fluids in Cu-Ni-PGE mineralization of the footwall rocks to the Sudbury Igneous Complex, Levack and Morgan Townships, Sudbury District, Ontario. Ph.D. thesis, Carleton University, Ottawa, Ontario, 373 p.

Farrow, C. E. G. & Lightfoot, P. C., 2002. Sudbury PGE revisited: Toward an integrated model *in* Cabri, L.J, ed., The Geology, Geochemistry, Mineralogy and Mineral Beneficiation of Platinum-Group Elements. Canadian Institute of Mining, Metallurgy and Petroleum, Special Volume 54, pp. 13-130.

Farrow, C.E.G., and Watkinson, D.H., 1992. Alteration and the role of fluids in Ni, Cu and platinum-group element deposition, Sudbury Igneous Complex, Onaping-Levack area, Ontario. Mineralogy and Petrology, v. 46, pp. 67-83.

Finch, A.A., Parsons, I., Mingard, S.C., 1995. Biotite as indicators of fluorine fugacities in late-stage magmatic fluids: the Gardar Province of South Greenland. Journal of Petrology, v. 36, pp. 1701-1728.

Frank, M.R., Candela, P.A., Piccoli, P.M., Glascock, M.D., 2002. Gold solubility, speciation, and partitioning as a function of HCl in the brine-silicate melt-metallic gold system at 800°C and 100 MPa. Geochemica et Cosmochemica Acta, v. 66(21), pp. 3719-3732.

French, B.M., 1967. Sudbury Structure, Ontario: some petrographic evidence for origin by meteorite impact. Science, v. 156, pp. 1094-1098.

French, B.M., 1970. Possible relations between meteorite impact and igneous petrogenesis, as indicated by the Sudbury Structure, Ontario, Canada. Bulletin of Volcanology, v. 34(2), pp. 466-517.

Gammons, C.H., 1995. Experimental investigations of the hydrothermal geochemistry of platinum and palladium: IV. The stoichiometry of Pt(IV) and Pd(II) chloride complexes at 100 to 300°C. Geochemica et Cosmochemica Acta, v. 59, 1655-1667.

Gammons, C.H., 1996. Experimental investigations of the hydrothermal geochemistry of platinum and palladium: V. Equilibria between Pt metal, Pt(II) and Pt(IV) chloride complexes at 25 to 300°C. Geochemica et Cosmochemica Acta, v. 60, pp. 1683-1694.

Gammons, C.H., and Williams-Jones, A.E., 1995. The solubility of Au-Ag alloy + AgCl in HCI/NaCI solutions at 300°C: New data on the stability of Au (I) chloride complexes in hydrothermal fluids. Geochemica and Cosmochemica Acta, v. 59(17), pp. 3453-3468.

Gilkes, R.J., and Anchalee Suddhiprakarn, 1979. Biotite alteration in deeply weathered granite. I. morphological, mineralogical, and chemical properties. Clays and Clay minerals, v. 27(5), pp. 349-360.

Grant, R. W. & Bite, A., 1984. Sudbury Quartz Diorite Offset Dykes *in* Pye, E.G., Naldrett, A.J., and Giblin, P.E., eds., The Geology and Ore Deposits of the Sudbury Structure. Ontario Geological Survey, Special Publication v.1, pp. 275-300.

Grieve, R.A.F., 1991. The Sudbury Structure: Controversial or Misunderstood? Journal of Geophysical Research, v. 95, pp. 22,753-22,764.

Gunow, A.J., Ludington, S., Munoz, J.L., 1980. Fluorine in micas from the Henderson molybdenite deposit, Colorado. Economic Geology, v. 75, pp. 1127-1137.

Hack, A.C., and Mavrogenes, J.A., 2006. A synthetic fluid inclusion study of copper solubility in hydrothermal brines from 525 to 725 °C and 0.3 to 1.7 GPa. Geochemica and Cosmochemica Acta, v. 70, pp. 3970-3985.

Hanley, J.J., and Mungall, J.E., 2003. Chlorine enrichment and hydrous alteration of the Sudbury Breccia hosting footwall Cu-Ni-PGE mineralization at the Fraser mine, Sudbury, Ontario, Canada. Canadian Mineralogist, v. 41, pp. 857-881.

Hanley, J.J., Pettke, T., Mungall, J.E., and Spooner, E.T.C., 2005. The solubility of platinum and gold in NaCl brines at 1.5 kbar, 600 to 800°C: A laser ablation ICP-MS pilot study of synthetic fluid inclusions. Geochemica et Cosmochemica Acta, v. 69, 2593-2611.

Hazen, R.M., and Burnham, C.W., 1973. The crystal structure of one layer phlogopite and annite. American Mineralogist, v. 58, pp. 889-900.

Hazen, R.M., and Wones, D.R., 1972. The effect of cation substitutions on the physical properties of trioctahedral micas. American Mineralogist, v. 57, pp. 103-129.

Jiang, S-Y., Palmer, M.R., Chunji, X., and Yanhe, L., 1994. Halogen-rich scapolite-biotite rocks from the Tongmugou Pb-Zn deposit, Qinling, northwestern China;

implications for the ore-forming processes. Mineralogical Magazine, v. 58(4), pp. 543-552.

Klein, C., and Ito, J., 1968. Zincian and manganoan amphiboles from Franklin New Jersery. American Mineralogist, v. 53, pp. 1264-1278.

Klingsberg, C., and Roy, R., 1957. Synthesis, stability and polytypism of nickel and gallium phlogophite. American Mineralogist, v. 42, pp.629-634.

Krogh, T. E., McNutt, R. H. & Davis, G. L., 1982. Two High Precision U-Pb Zircon Ages for the Sudbury Nickel Irruptive. Canadian Journal of Eath Sciences, v. 19, pp. 723-728.

Krogh, T.E., Corfu, F., Davis, D.W., Dunning, G.R., Heaman, L.M., Kamo, S.L., Machado, N., Greenhough, J.D., and Nakamura, N., 1987. Precise U-Pb isotopic ages of diabase dykes and mafic to ultramafic rocks using trace amounts of baddeleyite and zircon *in* Halls, H.C., Fahrig, W.F., eds., Mafic dyke swarms, Geological Association of Canada, Special paper 34, pp. 147-152.

Li, C., and Naldrett, A.J., 1993. High Chlorine Alteration Minerals and Calcium-Rich Brines in Fluid Inclusions from the Strathcona Deep Copper Zone, Sudbury, Ontario. Economic Geology, v. 88, pp. 1780-1796.

Lightfoot, P. C. & Farrow, C. E. G., 2002. Geology, geochemistry, and mineralogy of the Worthington Offset dyke: a genetic model for offset dyke mineralization in the Sudbury Igneous Complex. Economic Geology, v. 97, pp. 1419-1446.

Lightfoot, P. C., Keays, R.R., Morrison, G.G., Bite, A., and Farrell, K.P., 1997. Geochemical relationships in the Sudbury Igneous Complex: Origin of the main mass and offset dykes. Economic Geology, Volume v. 97, pp. 289-307.

Lightfoot, P. C., Keays, R.R., and Doherty, W., 2001. Chemical evolution and origin of the nickel sulfide mineralization in the Sudbury Igneous Complex, Ontario, Canada. Economic Geology, v. 96, pp. 1855-1875.

Lloyd, T. R., 2001. Totten Cu-Ni-PGE-Au Project Drury Township, Sudbury District. Inco Technical Services, internal report, 44p.

Magyarosi, Z., 1998. Metamorphism of the Proterozoic Rocks Associated with the Sudbury Structure. M.Sc. thesis, Carleton University, Ottawa.

Magyarosi, Z., Watkinson, D.H., and Jones, P.C., 2002. Mineralogy of Ni-Cu-Platinum-Group Element Sulfide Ore in the 800 and 810 Orebodies, Copper Cliff South Mine, and P-T-X Conditions during the Formation of Platinum-Group Minerals. Economic Geology, v. 97, pp. 1471-1486.

Martin, H.W., and Sparks, D.L., 1985. On the behaviour of non-exchangeable potassium in soils. Communications in soil Science and Plant analysis, v. 16, pp. 133-162.

Mohammad, B., Kazuo, N., and Lentz, D.R., 2010. The Sarcheshmeh porphyry copper deposit, Kerman, Iran: A mineralogical analysis of the igneous rocks and alteration zones including halogen element systematics related to Cu mineralization processes. Ore geology reviews, v. 38, pp. 367-381.

Mountain, B.W., and Wood, S.A., 1988. Chemical controls on the solubility, transport, and deposition of platinum and palladium in hydrothermal solutions: A thermodynamic approach. Economic Geology, v. 83, 492-510.

Mungall, J.E., Ames, D.E., and Hanley, J.J., 2004. Geochemical evidence from the Sudbury structure for crustal redistribution by large bolide impacts. Nature, v. 429, pp. 546-548.

Munoz, J.L., 1984. F–OH and Cl–OH exchange in micas with applications to hydrothermal ore deposits, *in* Bailey, S.W. (Ed.), Micas. Reviews in Mineralogy, Mineralogical Society of America, Washington, v. 13, pp. 469–493.

Munoz, J.L., Swenson, A., 1981. Chloride-hydroxyl exchange in biotite and estimation of relative HCl/HF activities in hydrothermal fluids. Economic Geology, v.76, pp. 2212–2221.

Murphy, A. J. & Spray, J. G., 2002. Geology, Mineralization, and Emplacement of the Whistle-Parkin Offset Dyke, Sudbury. Economic Geology, v. 97, p. 1399–1418.

Naldrett, A. J. & Hewins, R. H., 1984. The main mass of the Sudbury igneous complex *in* Pye, E.G., Naldrett, A.J., and Giblin, P.E., eds., The Geology and Ore Deposits of the Sudbury Structure. Ontario Geological Survey, Special Publication v.1, pp. 233-251.

Naldrett, A. J., Hewins, R. H., Dressler, B. O. & Rao, B. V., 1984. The Contact Sublayer of the Sudbury igneous complex *in* Pye, E.G., Naldrett, A.J., and Giblin, P.E., eds., The Geology and Ore Deposits of the Sudbury Structure. Ontario Geological Survey, Special Publication v.1, pp. 254-273.

Newman, A.C.D., and Brown, G., 1966. Chemical changes during the alteration of micas. Clay minerals, v.6, pp. 297-309.

Noble, S.R., Lightfoot, P.C., 1992. U-Pb baddeleyite ages of the Kerns and Triangle Mountain intrusions, Nipissing Diabase, Ontario. Canadian Journal of Earth Sciences, v. 29, pp. 1424-1429.

Owen, J.V., 2012. Double corona structures in 18th century porcelain (1st patent, Bow, London, mid-1740s) a record of partial melting and subsolidus reactions. The Canadian Mineralogist, v. 50, pp. 1255-1264.

Pattison, E. F., 1979. The Sudbury sublayer. Canadian Mineralogist, v. 17, pp. 257-274.

Peredery, W.V., 1972. Chemistry of fluidal glasses and melt bodies in the Onaping Formation *in* Guy-Bray, J.V., ed., New Developments in Sudbury Geology. Geological Association of Canada, Special Paper 10, pp. 49-59.

Rasmussen, Kristen, L., and Mortensen, J.K., 2012. Magmatic petrogenesis and the evolution of (F:Cl:OH) fluid composition in barren and tungsten skarn-associated plutons using apatite and biotite compositions: Case studies from the northern Canadian Cordillera. Ore Geology Reviews, v.50, pp. 118-142.

Rausell-Colom, J.A., Sweatman, T.R., Wells, C.B., Norrish, K., 1964. Studies in the artificial weathering of mica *in* Hallsworth, E.G., and Crawford, D.V. (eds) Experimental Pedology, Buttersworths, London, pp. 40-72.

Ritchie, N.W.M., Newbury, D.E., and Davis, J.M., 2012. EDS measurements of X-Ray intensity at WDS precision and accuracy using a silicon drift detector. Microscopy and Microanalysis, v. 18, pp. 892-904.

Russell, R.L., and Guggenheim, S., 1999. Crystal structures of near-end-member phlogopite at high temperatures and heat-treated Fe-rich phlogopite; the influence of the O, OH, F site. The Canadian Mineralogist, v. 37(3), pp. 711-720.

Rousell, D. H., Fedorowich, J. S. & Dressler, B. O., 2003. Sudbury Breccia (Canada): a product of the 1850 Ma Sudbury Event and host to footwall Cu–Ni–PGE deposits. Earth-Science Reviews, v. 60, p. 147–174.

Sassani, D.C., and Shock, E.L., 1990. Speciation and solubility of palladium in aqueous magmatic-hydrothermal solutions. Geology, v. 18, pp. 925-928.

Shelby, D., and Nesbitt, B.E., 2000. Chemical composition of biotite from the Casino porphyry Cu–Au–Mo mineralization, Yukon, Canada: evaluation of magmatic and hydrothermal fluid chemistry. Chemical Geology, v. 171, pp. 77-93.

Siahcheshm, K., Calagari, A.A., Abedini, A., and Lentz, D.R., 2012. Halogen signatures of biotite from the Maher-Abad porphyry copper deposit, Iran; characterization of volatiles in syn- to post-magmatic hydrothermal fluids. International Geology review, v. 54, pp. 11-12.

Sisson, V.B., 1987. Halogen chemistry as an indicator of metamorphic fluid interaction with the Ponder pluton, Coast plutonic complex, British Columbia, Canada. Contributions to Mineralogy and Petrology, v. 95, pp. 123-131.

Scribbins, B. R. & Naldrett, A. J., 1984. Mafic and Ultramafic Inclusions in the Sublayer of the Sudbury Igneous Complex. Canadian Mineralogist, v. 22, pp. 67-75.

Stewart, M. C., 2002. Petrology and mineralogy of Cu-Ni-PGE ore, Totten area, Worthington offset, Sudbury Igneous Complex. M.Sc. thesis, Carleton University, Ottawa.

Stewart, R.C., 2011. Halogen geochemistry of footwall breccia and associated units of the Main Mass of the Sudbury Igneous Complex, Ontario. M.Sc. thesis, Saint Mary's University, Halifax.

Volfinger, M., and Robert, J.-L, 1980. Structural control of the distribution of trace elements between silicates and hydrothermal solutions. Geochimica et Cosmochimica Acta, v. 44, pp. 1455-1461.

Volfinger, M., Robert, J.-L., Vielzeuf, D., and Neiva, A.M.R., 1985. Structural control of the chlorine content of OH-bearing silicates (micas and amphiboles). Geochimica et Cosmochimica Acta, v. 49, pp. 37-48.

Takeda, H., and Morosin, B., 1975. Comparison of observed and predicted structural parameters of mica at high temperature. Acta Crystallographica, section B, v. 31, 2444-2452.

Therriault, A. M., Fowler, A. D. and Grieve, R. A. F., 2002. The Sudbury Igneous Complex: A differentiated impact melt sheet. Economic Geology, v. 97, pp. 1521-1540.

Thomson, M.L., Barnett, R.L., Fleet, M.E., and Kerrich, R., 1985. Metamorphic assemlages in the South Range norite and Footwall mafic rocks near the Kirkwood mine, Sudbury, Ontario. Canadian Mineralogist, v. 23, pp. 173-186.

Tuchscherer, M. G. & Spray, J. G., 2002. Geology, Mineralization, and Emplacement of the Foy Offset Dyke, Sudbury Impact Structure. Economic Geology, v. 97, p. 1377–1397.

Tuba, G., 2012. Multiple hydrothermal systems in the footwall of the Sudbury Igneous Complex: Fluid characteristics, associated alteration, and the role in footwall-type "low-sulphide" Cu-(Ni)-PGE sulphide mineralization (North and East Ranges, Sudbury Structure, Canada). Ph.D. thesis, Eötvös Loránd University, Budapest. 183 p.

Walker, G.F., 1949. The decomposition of biotite in the soil. Mineralogical Magazine, v. 28, pp. 693-703.

Wilson, M.I., 2004. Weathering of the primary rock-forming minerals: processes, products and rates. Clay Minerals, v. 39, pp. 233-266.

Wood, S.A., 1987. Thermodynamic calculations of the volatility of the platinum group elements (PGE): the PGE content of fluids at magmatic temperatures. Geochemica et Cosmochemica Acta, v. 51, 3041-3050.

Xiong, Y., and Wood, S.A., 2000. Experimental quantification of hydrothermal solubility of platinum-group elements with special reference to porphyry copper environments. Mineralogy and Petrology, v. 68, pp. 1-28.

Zajacz, Z., Seo, J.H., Candela, P.A., Piccoli, P.M., Tossell, J.A., 2011. The solubility of copper in high-temperature magmatic vapors: A quest for the significance of various chloride and sulfide complexes. Geochemica et Cosmochemica Acta, v. 75, pp. 2811-2827.

Zaleski, E., 1989. Metamorphism, structure and petrogenesis of the Linda volcanogenic massive sulphide deposit, Snow Lake, Manitoba, Canada. Ph.D. thesis, University of Manitoba.

Zurbrigg, H. F., and geological staff, 1957. The Frood-Stobie Mine. *in* Structural Geology of Canadian Ore Deposits. Canadian Institute of Mining and Metallurgy, v. 2, pp. 341-363.

Chapter 4: Conclusions and future work

1.0 Significant findings

The comprehensive study of the Totten ores detailed in Chapter 2 revealed a diverse trace mineral assemblage exhibiting complex textural associations. Furthermore, mineralogical domains of residence for both economic (e.g. Ni, Cu, PGE, Ag, etc.) and deleterious (e.g As, Pb, Bi, Te, etc.) metals were quantified using a combination of high resolution chemical analyses (i.e. LA-ICP-MS) and exhaustive petrography (i.e. SEM-EDS point counting). In addition to our increased understanding of the genetic model of the Worthington offset, this research has potentially significant applications to the process of ore production at the Totten mine. The detailed information provided in this study on deleterious mineral (e.g., sulfarsenides, galena, nickeline) grain size and composition (which can be subdivided by ore type) may be used to isolate and remove the species from the ore during mineral processing. As a result, the penalties which are incurred by these minerals at the smelting stage may be greatly reduced. Furthermore, this study showed that the greatest concentrations of arsenides and sulfarsenides occurs along the margins of ore bodies (most likely due to the gravitational settling of these magmatic phases), which will allow Vale geologists to identify potentially problematic zones of an ore body. The detailed petrographic and chemical data reported in this study may also serve to isolate and retain precious metal carriers (e.g. PGM, electrum) which are otherwise lost during mineral processing (such as the loss of PGM hosted within pyrrhotite). However, it must be noted that the association of some PGM with arsenide and sulfarsenide phases may result in the reduction of PGE recovery during the removal of these deleterious phases. The comprehensive knowledge of the trace element

chemistry of major sulfide phases (pyrrhotite, pentlandite, chalcopyrite) can also prove to be important for ore processing. For example, mass balance calculations show that pyrrhotite contains up to 10% of the bulk rock concentration of Ni in massive sulfide ore, which would be lost if pyrrhotite was extracted from the ore (as well as any PGM hosted within pyrrhotite). The main findings of this study are as follows:

(i) The concentrations of deleterious metals (such as As and Pb) measured by LA-ICP-MS is low in pyrrhotite (As_{main}=0.05 ppm, n=30 analyses; As_{238}=0.07 ppm, n=60 analyses; Pb_{main}=0.52 ppm, n=30 analyses; Pb_{238}=0.88 ppm, n=60 analyses), pentlandite (As_{main}=4.87 ppm, n=30 analyses; As_{238}=5.93 ppm, n=62 analyses; Pb_{main}=2.33 ppm, n=30 analyses; Pb_{238}=16.7 ppm, n=62 analyses), and chalcopyrite (As_{main}=0.21 ppm, n=26 analyses; As_{238}=0.05 ppm, n=59 analyses; Pb_{main}=29.33 ppm, n=26 analyses; Pb_{238}=9.3 ppm, n=59 analyses), which indicates that these minerals do not significantly contribute to bulk rock concentrations of economically undesirable metals.

(ii) Nickeline (NiAs) and the cobaltite-gersdorffite-glaucodot solid solution [(Ni,Co, Fe)AsS] are the most important contributors to bulk rock As, even in abundances that are volumetrically insignificant (Chapter 2, Appendix A10). In both massive and semi-massive sulfide ores, these minerals are often hosted as inclusions fully encased in base metal sulfides (predominantly pyrrhotite, Chapter 2 Tables 4 and 5). However, in disseminated ore which represents the periphery of the ore environment, the arsenides and sulfarsenides are typically found along the margins of sulfide veins and disseminations, and do not appear to be related to any variations in host rock lithology.

Furthermore, the average volume (42305 μm^2 $average_{CGSS}$; 58256 μm^2 $average_{Nic}$) and abundance (n_{CGSS}=2885 grains, n_{Nic}=638 grains; Chapter 2 Table 6) of these As carriers is typically greater that what is found in massive and semi-massive sulfide ores (809 μm^2 $average_{CGSS}$, n=472 grains; 469 μm^2 $average_{Nic}$, n=80 grains), demonstrating a greater potential for bulk rock As in the disseminated ore environment. However, local As-contamination from wall rocks seems unlikely, therefore the association of As-minerals with these contacts may reflect locally low temperature, nucleation sites and sites for setteling of magmatic phenocrysts, and wall rock influence on sulfide flow dynamics.

(iii) The occurrence of sulfarsenides is well reported in the South Range deposits, however many authors consider them to be secondary (e.g. hydrothermal, metamorphic) in origin, whereas some more recent investigations favor a primary (magmatic) origin (Dare et al., 2010; Lefort, 2012). This study concluded that the magmatic genetic model seems far more likely given that: (i) in massive sulfides, sulfarsenides typically occur as euhedral crystals, that are fully encased by the *As+PGE depleted* base metal sulfides (i.e. they do not infill fractures and vugs which would have facilitated the propagation of secondary fluids); (ii) the occurrence of high temperature mineral inclusions (e.g. sperrylite, and irarsite-hollingworthite) at the core of sulfarsenide grains is the primary argument for the model of secondary origin (it is suggested that this zoning is representative of the evolution of fluid composition), however recent experimental studies have shown that these textures can also form by magmatic processes (i.e. the nucleation of sulfarsenides to the surface of higher temperature phases in the sulfide melt); (iii) the preference for larger and more abundant sulfarsenide grains in

disseminated sulfide ore (which form the peripheries of massive and semi-massive ore) may be explained by the settling of sulfarsenide crystals in a sulfide melt. This is further supported by the observation that annabergite [$Ni_3(AsO_4)_2 \bullet 8H_2O$, an oxidation product of Ni-arsenides] may preferentially occur along the lower margin (with respect to gravity) of a sulfide vein, providing a visual estimation of As distribution; and (iv) the model for the hydrothermal/metamorphic origin of the arsenides/sulfarsenides might be thought to require an association between As-carriers and the mineral assemblages of late (hydrothermal/metamorphic) veins, however no statistical correlation can be found between bulk rock As (controlled by nickeline and sulfarsenides) and Zn+Pb (which are controlled by sphalerite and galena, minerals common in the assemblages of late stage veins along the South Range).

(iv) Similar to other South Range offset deposits, the sulfarsenides from this study show a wide range in composition [$(Ni_{0.76}Co_{0.14}Fe_{0.11})_{\Sigma 1.00}As_{0.99}S_{1.01}$-$(Ni_{0.17}Co_{0.68}Fe_{0.15})_{\Sigma 1.00}As_{0.88}S_{1.12}$], possibly reflecting the range in temperature at which these crystals reached final equilibration (approximately 300-600°C, Chapter 2 Figure 12). The range in sulfarsenide composition may prove problematic for any floatation circuit if an ideal composition for the sulfarsenides is assumed, since even small abundances of sulfarsenides (e.g. 0.02 volume %) may still have a significant effect on bulk rock As (Chapter 2, Appendix A10).

(v) Using the results from the quantitative mass balances of Totten samples, it was possible to identify mineralogical trends on a scatter plot of bulk rock As *versus* the ratio

of Co/Ni: (i) for samples with Co/Ni > 0.06 and As < 0.1wt%, it was found that pentlandite controlled bulk rock Ni+Co and that grains of sulfarsenides were rare-absent (less than 0.3% by volume); (ii) samples with Co/Ni > 0.06 and As > 0.1wt%, the distribution of Ni-Co-As is dominantly controlled by sulfarsenides (demonstrated by the positive correlation between the two parameters in this field); (iii) in samples with Co/Ni < 0.06 and with increasing As, it was found that nickeline was the dominant carrier of As (whereas the dominant contributor to bulk Ni and Co could be either pentlandite or sulfarsenides, depending on their relative abundances); (iv) for samples with Co/Ni < 0.06 and with decreasing As (< 0.01 wt%) sperrylite, irarsite-hollingworthite, and base metal sulfides become the main carriers of As (once again the dominant carrier of Ni-Co varies between pentlandite and the sulfarsenides).

(vi) The average concentrations of dissolved Pt and Pd are consistently low in pyrrhotite [Pt_{main}=0.004 ppm (n=30 analyses); Pt_{238}=0.002 ppm (n=60 analyses); Pd_{main}= 0.097 ppm (n=30 analyses); Pd_{238}= 0.019 ppm (n=60 analyses)] and chalcopyrite [Pt_{main}=0.05 ppm (n=26 analyses); Pt_{238}=0.006 ppm (n=59 analyses); Pd_{main}=0.42 ppm (n=26 analyses); Pd_{238}= 0.38 ppm (n=26 analyses)]. Pentlandite is also poor in Pt [Pt_{main}= 0.021 ppm (n=30 analyses), Pt_{238}= 0.011 ppm (n=62 analyses)] but is enriched in Pd [Pd_{main}=1.31 ppm (n=30 analyses), Pd_{238}=1.24 ppm (n=62analyses)].

(vii) Sperrylite ($PtAs_2$) was the only discrete phase of Pt observed in this study, and mass balances indicate that this mineral is responsible for the majority of bulk rock Pt. Sperrylite typically occurs as euhedral-anhedral inclusions primarily hosted within

pyrrhotite in both massive and semi-massive sulfides (Chapter 2 Tables 4 and 5; average grain size 2183μm^2, n=41 grains). In disseminated samples, sperrylite commonly occurs as anhedral grains hosted within silicates at or near the boundary between silicates and sulfide blebs and veins (Chapter 2 Table 6; average grain size 150μm^2, n=4 grains). The well-formed nature of sperrylite grains in massive and semi massive ores; the occurrence of a sperrylite at the core of sulfarsenide grains; and experimental work done by others which shows sperrylite to be stable at high temperatures, indicates that sperrylite may have formed as an early magmatic phase, which depleted the melt in Pt and resulted in the Pt-poor base metal sulfides. In samples were calculated assays agreed with bulk rock assays nickeline and sulfarsenides may be responsible for as much as 0.00003% and 0.8% of the bulk concentration of Pt respectively.

(viii) Palladian michenerite (PdBiTe), froodite ($PdBi_2$), and ungavaite (Pd_4Sb_3) are the discrete Pd phases found in the Totten ore mineral assemblage. The dominant host minerals for michenerite are pyrrhotite in massive sulfides (Chapter 2 Table 4; average grain size 482μm^2, n=12 grains), pentlandite in semi-massive sulfides (Chapter 2 Table 5; average grain size 67μm^2, n=6 grains), and within silicates dispersed in disseminated sulfide ores (Chapter 2 Table 6; average grain size 607μm^2, n=33 grains). The main hosts for froodite are chalcopyrite in massive sulfides (Chapter 2 Table 4; average grain size 69μm^2, n=10 grains), pentlandite in semi-massive ores (Chapter 2 Table 5; average grain size 58μm^2, n=23 grains), and silicates dispersed within disseminated sulfide samples (Chapter 2 Table 6; average grain size 40μm^2, n=53 grains). Ungavaite is primarily hosted within pyrrhotite in massive sulfides (Chapter 2 Table 4; average grain size

54μm^2, n=1 grain), sulfarsenides in disseminated samples (Chapter 2 Table 6; average grain size 205μm^2, n=65 grains), and was absent in semi-massive samples. These Pd phases typically occur as anhedral grains within fractures and vugs in their host, but also occur along the boundaries of sulfide blebs and veins. Based on this textural information, the Pd minerals may crystalized from a late semi-metal rich melt, or have formed from secondary (e.g., hydrothermal, metamorphic) fluids. In samples were calculated assays agreed with bulk rock assays nickeline and sulfarsenides may be responsible for as much as 0.1% and 93% of the bulk concentration of Pd respectively.

(ix) Using bulk rock chemistry and mineralogical associations identified by quantitative mass balance (Chapter 2, Appendix A10); it is possible to predict PGE mineralogy using a scatter plot of Pt against Pd (Chapter 2, Figure 16). Increases in bulk rock Pt without a concomitant increases in Pd represents an increase in the modal abundance of sperrylite, whereas the converse represents an increase in the modal abundance of Pd-carriers (michenerite, froodite, and ungavaite). Corresponding increases in both bulk rock Pt and Pd indicate a spatial association of Pt and Pd carriers (mass balance calculations demonstrate that these metals have different dominant carriers), such as their mutual occurrence as inclusions in sulfarsenides.

(x) Galena (which is the dominant carrier of Pb) is typically hosted in pyrrhotite in massive sulfides (Chapter 2 Table 4; average grain size 240μm^2, n=535 grains), silicates dispersed within semi-massive (Chapter 2 Table 5; average grain size 117μm^2, n=405 grains) and disseminated sulfides (Chapter 2 Table 6; average grain size 401μm^2, n=625

grains). Altaite (which is a minor carrier of Pb) is mainly hosted in pyrrhotite in both massive and semi-massive sulfides (Chapter 2 Tables 4 and 5; average grain size 711μm^2, n=29 grains), and along the mutual grain boundaries of chalcopyrite and silicates in disseminated sulfide samples (Chapter 2 Table 6; average grain size 52μm^2, n=16 grains). Both Pb carriers infill vugs and fractures within their hosts, and occur as composite grains (two or more minerals as a conglomerated grain) with hessite (Ag_2Te, Chapter 2 Table 7), tsumoite (BiTe, Chapter 2 Table 7), and tellurobismuthite (Bi_2Te_3, Chapter 2 Table 7).

(xi) The sporadic distribution and trace abundances of the accessory phases (PGM, sulfarsenides, nickeline, galena, etc.) directly effects the representivity of these phases in thin section, which results in the under (and over) estimation of bulk rock concentrations (Chapter 2, Figure 10). This effect is present at all scales (hand sample, drill core, and stope; see Chapter 2 Figures 18-21); therefore in order to be representative of the ore mineral assemblage, multiple samples must be analyzed at regular intervals. Mineral liberation analyses (provided by Vale) of composite ore samples would therefore not be representative of the mineralogy of a stope. The MLA also did not detect arsenides, sulfarsenides, and PGM which were reported in this study. Since the scanning threshold of MLA is directly associated with the duration (and as a consequence, cost) of an analysis, it seems likely that the resolution was not high enough to detect the tiny accessory minerals. SEM-EDS analyses of multiple thin sections (as done by this study), was able to account for the carriers of deleterious (As, Pb) and economic (Ni, Cu, PGE) metals, and therefore may be a more cost/time effective alternative to MLA. Furthermore,

the in-situ textural detail of accessory phases is much greater using the SEM-EDS analyses of multiple thin sections.

The investigation of biotite chemistry in Chapter 3 highlighted important considerations which must be given in the study of biotite chemistry as a pathfinder for magmatic Ni-Cu-PGE deposits. The study also demonstrated that ore associated biotite in the Totten mine area have a distinct trace metal signature, which may be detected by modern analytical techniques (i.e. LA-ICP-MS). The main findings of this study and the implications of these findings to the exploration for magmatic Ni-Cu-PGE sulfide deposits are:

(i) The concentration of Ni dissolved inbiotite from the ore associated IQD (43.9-2684.1 ppm, 1644 ppm average) is much greater than that of biotite from ore proximal QD and the surrounding country rocks (43.9-687.4 ppm, 216.3 ppm average), except for a small group of biotite found within a localized package of country rocks (1031-1420 ppm, 1200 ppm average). No systematic changes were detected in biotite Ni leading up to IQD, and other ore metals (Cu, PGE, As) showed no increases in concentration in relation to sulfide ore.

(ii) Three texturally and chemically distinct populations of biotite were found in the Totten area: (i) anhedral grains intergrown with amphibole in clusters that contain low concentraions of both Ni and Cr (respective average concentrations of 216.3 ppm, and

196 ppm; Chapter 3 Figure 9B, C, F-J, and L); (ii) Larger euhedral-subhedral grains with elevated (relative to group "i") Ni and Cr (respective average concentrations of 1200 ppm and 3900 ppm; Chapter 3, Figure 9D); and (iii) euhedral-subhedral lathes occurring in biotite clusters (with or without amphibole), which when occurring in QD have a chemistry similar to group "i", and contain elevated Ni and moderate Cr in IQD occurrences (respective average concentrations of 1644 ppm and 862 ppm; Chapter 3 Figure 9K, N, and O).

(iii) Biotite within close proximity to ore in layered mafic intrusions can contain detectable concentrations of Ni; however there is a wide range in the relative enrichment of Ni in biotite between deposits (Chapter 3, Figure 11). For this reason it is essential that local normative (i.e. "background") concentrations of trace metals dissolved in biotite should be resolved in order to evaluate if the concentrations found in ore associated biotite truly represent elevated concentrations. Furthermore, high concentrations of Ni (relative to background concentrations) were measured in a distinct biotite population hosted within country rocks not associated with sulfide ore. This discovery indicates that distance to ore is not the only parameter which must be considered in evaluating biotite chemistry as a potential pathfinder for magmatic Ni-Cu-PGE ore (e.g. host rock lithology and the presence of multiple populations of biotite must also be considered).

(iv) Measurements of biotite chemistry of grains which contain tiny (µm scale) sulfide inclusions, or share a mutual grain boundary with sulfide minerals can be contaminated by those sulfides (Chapter 3, Figure 12). In order to evaluate whether the elevated

concentrations of Ni in IQD hosted biotite represent the true dissolved concentrations, or is the result of sulfide contamination, chemical composition maps (produced by LA-ICP-MS) were used to verify biotite chemistry. The results show that these biotite are indeed homogeneous with regards to their Ni content (i.e. the measured concentrations reflect the true dissolved concentrations; Chapter 3, Figure 13) and represent a population of biotite which may be a target for sulfide ore exploration. In addition to compositional mapping, discrete inclusions may be identified in measurements from LA-ICP-MS analyses of biotite by reviewing the signals acquired during analysis. Anomalous peaks resulting from inclusions may be isolated and removed from the final concentration, which is an advantage of using LA-ICP-MS for this investigation.

(v) At low (<1000 ppm) concentrations in biotite, Ni and Cr show a strong positive correlation with to X_{Mg} (i.e. variations in the species of biotite indicated by Mg and Fe), indicating that at these levels the capacity for biotite to accommodate Ni and Cr is controlled by the structural parameters of the unit cell (Chapter 3, Figure 14). At higher concentrations of Ni and Cr (≥1000 ppm) there is no apparent correlation to X_{Mg} suggesting that another parameter must influence the trace metal content of biotite (such as the local availability of Ni and Cr, Chapter 3 Figure 14). A secondary control (poosibly bulk rock chemistry) on Ni and Cr concentrations is also suggested by the observation that despite the wide range in Ni and Cr measured in biotite within the Totten area, the range in the X_{Mg} is quite narrow.

(vi) Two key features distinguish ore associated biotite from other biotite in the vicinity of the Totten mine area: (i) biotite hosted in offset quartz diorite are slightly enriched in Fe compared to biotite hosted within Huronian country rocks (Chapter 3, Figure 8); (ii) IQD biotite contain elevated (>1000 ppm) concentrations of Ni and have high Ni/Cr ratios compared to country rock biotite with anomalous concentrations of Ni (Chapter 3, Figure 15). In drill core and underground exploration, these chemical signatures can only be detected in close proximity to sulfide ore (decameter scale). Therefore, it could be more practical to search for eroded IQD biotite and its advanced weathering products in soils in order to locate surface expressions of a sulfide ore body. This is supported by some experimental work that has shown that detectable concentrations of Ni and Cr can be retained in the weathering products of biotite.

2.0 Future work

In order to better constrain the mineralogical domains and textural relationships in the Totten ores, further sampling of the main ore types (massive, semi massive, and disseminated) from varying depth within the ore bodies is required. Furthermore, it would be useful to include samples from other ore bodies in the Worthington offset not sampled in this study, in order to study the variations (or lack thereof) between these deposits. This work should be conducted using "manual" SEM-EDS techniques described in this study over the automated MLA-SEM analysis in order to ensure that the accessory phases have been well characterized, and to maximize the textural information obtained which may be used to increase our understanding of the relationships between the major and accessory minerals. These observations will be crucial to the development of visual indicators to assist with rapid grade assesments underground and within the core lab.

Additional work is also required to fully assess the potential for biotite chemistry as an exploration tool. Although nearly 300 LA-ICP-MS analyses were obtained in this study, these were produced from only 19 thick sections spread out over a distance of approximately 424 meters (not including underground samples). In order to for the results to be more representative, further sampling is required. Furthermore, similar robust investigations are required in order to fully evaluate the biotite trace metal chemistry of other Sudbury deposits. In these studies, several important considerations must be made: (i) analytical technique must be chosen carefully, although more expensive LA-ICP-MS offers excellent accuracy, precision, and the ability to detect and disregard small (µm scale) sulfide inclusions; (ii) contamination can be further minimized by avoiding cleavage planes and biotite grains in contact with sulfides during analysis; (iii) sampling must be representative of all local lithologies in order to establish normative metal concentrations in biotite (to evaluate if concentrations from ore associated grains are truly elevated), and also to establish any systematic variations in biotite chemistry with varying host lithology and distance to ore; (iv) multiple generations of biotite may be present, therefore it is important for analyses to be representative of all textural varieties of biotite found in thin section; and (v) compositional mapping (by X-Ray or LA-ICP-MS) may be useful to determine if measurements of anomalous grains represents the true dissolved trace metal content. In order to use biotite chemistry to distinguish ore associated grains and their alteration products in soils, it is essential that work be done to evaluate the ability of biotite and its alteration products to retain the chemical signature of the parent grain during weathering. Although some work has shown that detectable levels of Ni and

Cr are not modified significantly during weathering, it is not known if this applies to the elevated concentrations (>1000 ppm) that were measured in this study.